NASA CR-179496
RI/RD86-123

NASA

ANNUAL REPORT

COMPOSITE LOAD SPECTRA FOR SELECT SPACE PROPULSION STRUCTURAL COMPONENTS

by

J. F. Newell
R. E. Kurth
H. Ho

prepared for
NATIONAL AERONAUTICS AND SPACE ADMINISTRATION

March 1986

NASA-Lewis Research Center

Contract NAS3-24382

Dr. C. C. Chamis, Project Manager

NASA CR-179496
RI/RD86-123

ANNUAL REPORT

COMPOSITE LOAD SPECTRA FOR SELECT SPACE PROPULSION STRUCTURAL COMPONENTS

by

J. F. Newell
R. E. Kurth
H. Ho

prepared for
NATIONAL AERONAUTICS AND SPACE ADMINISTRATION

March 1986

NASA-Lewis Research Center

Contract NAS3-24382

Dr. C. C. Chamis, Project Manager

Abstract

The objective of this program is to develop generic load models with multiple levels of progressive sophistication to simulate the composite (combined) load spectra that are induced in space propulsion system components, representative of Space Shuttle Main Engines (SSME), such as transfer ducts, turbine blades, and liquid oxygen (LOX) posts. The approach will consist of using state-of-the-art probabilistic methods to describe the individual loading conditions and combinations of these loading conditions to synthesize the composite load spectra simulation. The methodology required to combine the various individual load simulation models (hot-gas dynamic, vibrations, instantaneous position, centrifugal field, etc.) into composite load spectra simulation models will be developed under this program. A computer code incorporating the various individual and composite load spectra models will be developed to construct the specific load model desired.

The objective of the first year's effort was to complete a sufficient portion of each task -- probabilistic models, code development, and validation, to have an initial operational code. This code was to have from its inception an expert system philosophy that could be added to throughout the contract and in the future. The initial code was to be restricted to turbine blade type loadings.

CONTENTS

APPENDICES

ILLUSTRATIONS

TABLES

1.0 INTRODUCTION

1.1 General

The ever-increasing demand for more performance and a lighter weight long-life rocket engine design leads to higher pressures, temperatures and mechanical and fluid vibration loads. These requirements combined with the need for man-rated systems result in stringent reliability requirements.

The use of engine cycles such as stage combustion result in engine operating pressures in the 3000 to 7000 psi regime. High performance turbomachinery operate at 30,000 to 100,000 RPM. These operational requirements result in complex high energy loading throughout the engine. The difficulty in installation, cost and the potential for destroying an engine has severely limited the required instrumentation and measurements to adequately define loads of key components such as turbine blades. Also, accurate analytical methodologies for defining internal flow related loads are just now emerging for rocket engines. The difficulty of obtaining measured data and verified analysis methodologies has led to the probabilistic load definition approach of this contract.

In the process of developing successful designs for SSME components, Rocketdyne has acquired state-of-the-art methods for defining loads and analyzing structural problems. At present, though, component loads are primarily derived by combining inputs from analytical studies, engine measurements, and expert opinions using deterministic methods. This methodology is consistent with the currently available elastic and inelastic methodology for structural analysis. The CLS (Composite Load Spectra) contract addresses the loads development and the associated PSAM (Probabilistic Structural Analysis Method) contract addresses the structural analysis methodology. A probabilistic analysis approach requires a total revamping of methodology.

The deterministic methodology and/or upper bound approach to loads results in conservative analysis. Means and standard deviations for loads are employed to formulate a limited number of SSME designs; however, the

probability of exceeding a particular load or its variation as a function of time are not usually defined. For loads composed of transient peaks super-imposed on steady state, additive models are employed to calculate resultant loads. In addition, power spectral density functions and shock spectra, when available for various parameters, are employed typically from an upper bound approach. These present techniques result in the manufacturing of components that may, in many cases, greatly exceed the design requirements but have no accurate method for assessing this excess margin. Thus, to formulate more effective designs, it is necessary that the loads on the components of rocket engine be derived by employing models that more accurately reflect the true risk. These loads can then be utilized in a probabilistic structural analysis as addressed in the PSAM contract.

Rocketdyne has the state of the art methods for defining loads and analyzing structural problems and has teamed with Battelle to utilize their expertise in the development of probabilistic models. Within the last few years, Battelle has expended a considerable amount of resources to develop a strong capability in the area of probabilistic modeling. Using these tools, it has conducted studies related to applications in the nuclear and transportation industries. The knowledge gained in this related work has greatly assisted the first years effort in this project.

This project will provide methods to combine technologies of analytical (deterministic) loads and probabilistic modeling. Since these methods will be approached from a generic approach, they will be applicable to current or advanced liquid rocket engines.

1.2 Project Objective

The objective of this program is to develop generic load models with multiple levels of progressive sophistication that simulate the composite (combined) load spectra that are experienced in space propulsion system components, representative of Space Shuttle Main Engines (SSME), such as transfer ducts, turbine blades, and liquid oxygen (LOX) posts. The approach will consist of using state-of-the-art probabilistic methods to describe the individual loading conditions and combinations of these loading conditions to synthesize the composite load spectra simulation.

The methodology required to combine the various individual load simulation models (pressure, temperature, aerodynamic, vibrations, centrifugal, etc.) into composite load spectra simulation models will be developed under this program. Results obtained from these models will be compared with available numerical results, with the loads induced by the individual load simulation models, and with available structural analysis results from individual analyses and tests. Developed theories will be further validated with respect to level of sophistication, predictive reliability and attendant level of confidence.

A computer code incorporating the various individual and composite load spectra models will be developed to construct the specific load model desired. The approach is to develop four incremental versions of the code. The initial code will address turbine blade steady state loading. Each subsequent version will add sophistication to the component probabilistic load definition and the decision making processes, as well as installing a new set of loads for an additional component, e.g., LOX post. This allows for ongoing evaluation and usage of the system by both Rocketdyne and NASA.

1.3 Program Overview

The development of probabilistic generic load models is a 3-year base program and a 2-year option program. Rocketdyne is responsible for the overall project. Battelle Columbus Laboratories is the major subcontractor for developing probabilistic load models and furnishing technical expertise in probabilistic modeling in general.

The effort is divided into three basic tasks (see Figure 1): the probabilistic model theory, code development and code validation and verification. The first task included a survey effort to review available LOX/LH_2 data on the components under study and a review and selection of appropriate probabilistic load methodologies for use in this contract. The effort evaluated the loads on four components. A LOX post, transfer duct, turbine blade and a fourth component to be selected and agreed on by the

contract monitor. The appropriate individual loads on each model will be simulated by a minimum of four shapes--nominal, random over nominal, random periodic over nominal, and random spike over nominal. Three probabilistic methods are required in the methodology development.

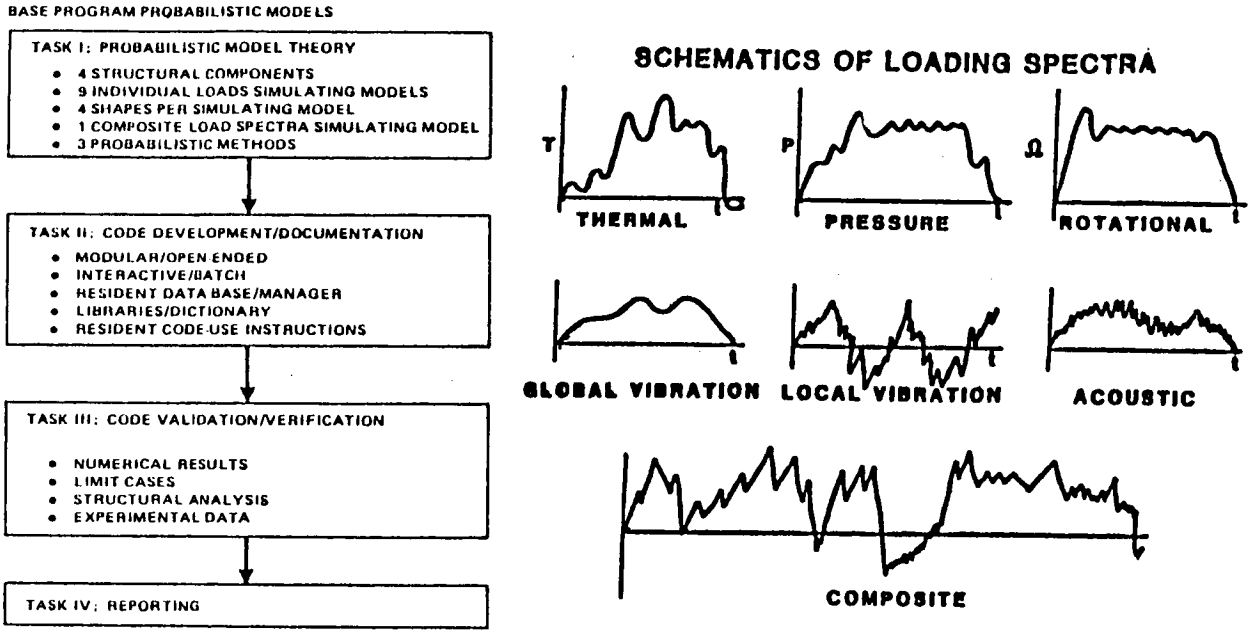

Figure 1 Task Summary

The code is an expert system specifically developed for this application. The code is to be developed in FORTRAN so that it can readily be modified by engineers and/or engineering programmers. A modular open-ended code is required with standard expert system elements such as a database, rule base and inferenced engine driver. The code validation will utilize standard techniques of numerical checks of each module and the overall code limit cases. Verification will use available analysis results and experimental data from engine tests.

1.4 First Year Objective

The objective of the first year's effort was to complete a sufficient portion of each task--probabilistic models, code development and validation to have an initial operational code. This code was to have from its inception an expert system philosophy that could be added to throughout the contract and in the future. The initial code was restricted to turbine blade type loadings. The survey effort was required as part of this task. The survey effort task addressed the loads and available information of the three components selected in the contract for study--turbine blades, LOX post and transfer duct--and a recommendation for the selection of the fourth component.

2.0 SUMMARY

The development of an initial probabilistic load expert system code has been completed. The initial code addresses limited turbine blade load components and types, but it has the main features required in the final expert system code. The intent of this initial code is to be a vehicle to test probabilistic methodologies and validate and verify the load information based on SSME engine data. Therefore, the loads simulated are limited to the SSME. The survey effort for both the engine component data and the probabilistic load methodology was completed. The approach used on the engine component survey was to compare the differences and commanalities between American made LOX/LH2 rocket engines. This allowed a more generic look at the engine components in question, e.g., LOX post, transfer duct, and turbine blades. The survey effort also included the search for probabilistic methodology applicable to the engine component loads.

For the fourth component, the MCC liner, nozzle steerhorn and HPOTP discharge duct were evaluated. The HPOTP discharge duct was recommended as the fourth component. Table 1 summarizes which type of load, and form of that load, that is applicable to the four components. One use of this table is to define the form of loads that have to be addressed by the probabilistic load model.

A probabilistic load model has been developed based on the complex requirements of rocket engines such as the SSME. A survey and assessment of available methods led to a probabilistic model structure with distribution fitting routines for loads that utilize a modified Discrete Probabilistic Distribution termed RASCAL, a barrier crossing method and a Monte Carlo method. An initial load model was developed by Battelle that is currently used for the slowly varying duty cycle type loading. The intent is to use the model and related codes essentially in the current form for all loads that are based on measured or calculated data that follow a slowly varying profile.

INDIVIDUAL LOAD	TURBINE BLADE	TRANSFER DUCT	LOX POST	HPOTPDD	LOAD FORM
.STATIC PRESSURE	X	X	X	X	DUTY CYCLE*
.DYNAMIC PRESSURE					
.CHUGGING(TRANSIENT)	-	X	-	-	AMS, STATOS
.TURBULENCE					
.SINUSOIDAL					
(REPEATED PULSE)	X	X			AMS, PSD, STATOS
.RANDOM	-	X	X	X	AMS, PSD
.CENTRIFUGAL	X	-	-	-	DUTY CYCLE*
.TEMPERATURE	X	X	X	X	DUTY CYCLE*
.STRUCTURAL VIBRATION					
.TRANSIENT					
.SIDELOAD	-	X	X	X	AMS, STATOS
.POPS	-	X	X	-	AMS, STATOS
.STEADY STATE					
.SINE	-	X	X	X	AMS, PSD, STATOS
.RANDOM	-	X	X	X	AMS, STATOS
.DEBRIS	X	X	X	-	HISTORY
.RUBBING	X	-	-	-	EXPERT OPINION
.INSTALLATION	-	-	X	X	EXPERT OPINION
.FAB	X	X	X	X	
.FRICTION	X	X	X	-	PSEUDO LOADS
.TOLERANCES	X	X	X	X	

*LOW FREQ. & TRANSIENT

Table 1 Summary Matrix of Individual Load vs Component

The use of an engine performance influence coefficient set was chosen as a practical method to generalize the loadings to significantly different engine cycles. In support of this effort, SSME influence coefficients have been extended to relate key engine variables to additional turbine and hot gas system related parameters. These coefficients are applicable to all four SSME components.

The example component chosen to start the Composite Load Spectra Code was turbine blade loads. Turbine blade loads including pressure and ΔP, centrifugal, dynamic loading and temperature were defined for the HPFTP blade first stage.

These are initial methodologies which are implemented to test the code and will be added to and improved in later versions of the code. (Note: The thermal loads were defined, but are yet to be added to the code.)

An expert system code has been started that is specific to the CLS effort. This code has primarily two parts. A rule base driver that controls the data base, allows the user to look at information in the database and contains the rules for developing the individual loads. The Battelle probabilistic load model is part of this module. The second part is the engine database code that enables the storage of the engine related deterministic and probabilistic information. The database information will be gradually added as the data is collected and developed for the components.

To support the probabilistic analysis effort next year, the transient load development (start and cutoff rapidly varying transient information) was collected and processed to define turbine related information for the HPFTP. Battelle currently has this information.

The first years effort concentrated on getting a baseline probabilistic code and expert system developed that can be used as a vehicle to upgrade and add in the rest of the development effort. The expert system is primitive with respect to user friendliness and overall capability. The probabilistic load module and data analysis code also have limited capability. Only the primary individual loads for a slowly varying duty cycle load are incorporated. The other individual loads will be added to the code in a phased fashion over the next two years. This is done in parallel with the load development efforts on the four components.

The technical features to be dealt with in the CLS code effort are summarized in Table 2. Similar methodologies are required to model the same type of individual load for any of the 4 components. As previously stated, in the first year the slowly varying duty cycle loads were implemented in the load module and expert system. Other individual loads will be phased into the probabilistic model and expert system in the indicated order. The next load type is the rapidly varying (transient) duty cycle load. This is followed by vibration and shock loading, then infrequent loading and a final upgrade of all the individual loads in the last 6 to 8 months of the project.

The more general technical issues will be worked on in parallel with the individual load developments. In the second years effort, the composite load development, generic loads formulation and further expert system development will be actively pursued. Battelle's efforts will support both the individual load development and composite loads work.

Table 2 Key Technical Features of Composite Load Code Effort

1. EXPERT SYSTEM
2. DATA ANALYSIS - STANDARD DISTRIBUTIONS AND DISCRETE DISTRIBUTIONS
3. PROBABILISTIC MODEL
   - .INDIVIDUAL LOADS
   - .COMPOSITE LOADS
4. INDIVIDUAL LOAD SHAPE SIMULATIONS
5. VARIOUS FORMS OF THE LOAD - SEE TABLE 1
   - A. DUTY CYCLE
     - .SLOWLY VARYING
     - .RAPIDLY VARYING TRANSIENTS
   - B. SHOCK
   - C. VIBRATION
     - .STEADY STATE
       - .PSD, AMS
       - .SINUSOIDAL - PSD, ISOPLOT
     - .TRANSIENT
   - D. INFREQUENT LOADS
     - .DEBRIS
     - .RUBBING
6. GENERIC LOADS
   - .DEFINITION
   - .IMPLEMENTATION IN EXPERT SYSTEM
   - .SCALING TECHNIQUES
7. VALIDATION AND VERIFICATION
8. ADDITIONAL COMPONENT IMPLEMENTED IN CODE
   - .TRANSFER DUCTS
   - .LOX POST
   - .4TH COMPONENT

3.0 SURVEY STRATEGY

3.1 General Information

The objective of the survey was to determine and select generic mission history profiles of individual loadings of four typical present and future rocket engine structural components. The components in question were turbine blades, transfer duct, LOX post, and a comparable component. The survey subtask was divided into five elements (Fig. 2).

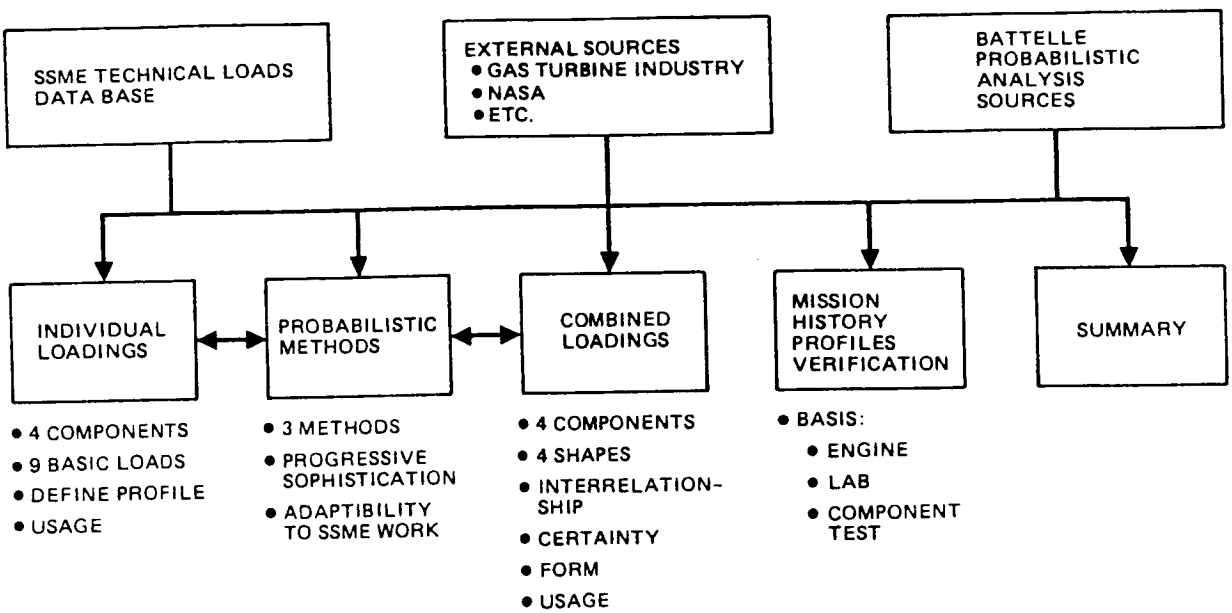

Figure 2 Survey Effort

Recommendations for the fourth component was made at the end of the survey. The three components were reviewed in this selection process: The main combustion chamber (MCC) liner, the nozzle feedlines and the high pressure oxidizer turbopump discharge duct (HPOTPDD).

A survey of available probabilistic methods applicable to the description of the individual and combined loadings was made. Three probabilistic methods were selected for use in the theoretical development described in the Simulated Individual Loading models and Simulated Composite Load Spectra model tasks.

A detailed description and summary of this effort was made. The next sections in this report and the appendices are the result of this overall effort. The survey task was a major effort since it is the basis for the technical work for the rest of this contract.

To provide a proper perspective of the survey effort, the approach used was to consider LOX/LH_2 engines which have been previously built, in fabrication or planning phases to define generic components, the resulting generic loads, and the considerations required to specify the loads. The J-2 engine, SSME, advanced expander cycle test bed engine (RS-44) and some aspects of the XLR129 engine were studied.

3.2 Generic Loads

In this contract effort, generic loads are defined as the following. Generic loads are a loads description of a component or element (like a LOX post) that considers all the potentially significant loads on this type of component. Loads on a specific engine component are a subset of this load set. The loads should be applicable to $LOX-LH_2$ engines such as J-2, SSME and potential variations and advance $LOX-LH_2$ engines such as OTV. The loads must be described such that they can be scaled, adjusted or modified by "key variables" that are correlated to engine tests and expert opinion when required. Typical key variables are power level, component mass, pump speed and velocity. An engine's packaging, component configuration, type of flow, etc. are often significant factors. Rocketdyne's overall engine experience and SSME test data will be used as a basis for the load distributions and mission history profile definition. These will be cast as probabilistic representations for both individual and combined loads. The results will be used in an expert system for the load determination.

3.3 Load Description

The formulation of the loads will be approached using the standard processing methodology that has been devised over the last 30 years of rocket engine to obtain "intelligence" from complex response measurements. This processing includes low frequency time dependent output, wide band high frequency (HF) output, narrow band HF output, amplitude sequence vs time plots, power spectral density plots (PSD), tracking filter, ISOPLOTS, and STATOS records. The combination of this processing allows a complete description of loads.

The loads for a specific structural analysis may use the data as formulated or defined in a form where they can be in other output formats more appropriate to the specific analysis methodology. For example, the current methodology for structural vibration analysis is based on elastic solutions where superposition of loads, statics and dynamics, are used. This may not be appropriate for a more general solution such as those specific in the PSAM contract.

3.4 Initial Load Database Philosophy

In order to utilize an expert system for defining component load spectra, certain key information is required. This data may be part of the expert systems knowledge base or added input, depending on the maturity of the computer code or the specific application. This discussion is an initial definition of some of the data required. The purpose of addressing the subject during the survey was in recognization that the expert system requirements can affect the characteristics of how the generic loads are defined and how the simulated individual models and composite load spectra are developed and utilized.

Information needed for generating loads (not in order of significance):

1) Engine cycle and characteristics. This will furnish data on engine operation, start and cutoff time interval, pumps and other component general characteristics.

2) Engine systems packaging and sizing. Engine and component weights and major component configurations can be load drivers or load absorbers; for example: a) nozzle expansion ratio is related to side loads, and b) mount configuration, supports and ducting can influence damping and transmissibility of loads between components. Closely coupled hardware do not act independently.

3) Engine data reduction analysis and transient model results. Basic steady state and transient operational temperatures, pressure, speeds, etc. are obtained from these models. Power level and power thrust profile are also obtained. These are basic indicators of duty cycle characteristics. Versions of these models are usually started in the proposal stage and gradually improved with the maturity of the program. Standard datasets for known engines like the SSME would be used as well as any new design data.

4) Vehicle mission history requirements. Flight conditions, engine ground test requirements and overall reliability requirements are usually specified by the customer.

5) Cooling cycles for the engine and/or local data within a component that affects thermal loads.

6) Key variables definition to allow for scaling and variations in operation conditions.

7) Mission history definition of the four components.

The information will be implemented such that new information can be readily added from on-going SSME tests, SSME development tests, future MSFC test bed engine tests and future engines. Optimumally, a direct interface to Rocketdyne's test data processing systems is desirable. This would provide the opportunity to capture data on a test-by-test basis and end up building an extensive database.

4.0 COMPARISON OF LOX/LH_2 ENGINES

For the development of generic loads, it is instructive to make a comparison of the differences and commonalities of the various LOX/LH_2 class of engines. There have been three American production LOX/LH_2 engines: RL10, J-2 and SSME. Other engines, either partially developed or designed in this class, include the XLR129 and the Rocketdyne RS-44 Advanced Expander cycle engine. These five engines will be used for this discussion. Table 3 summarizes selected features of the engines for an initial frame of reference. The engine configurations are shown in Figures 3-6.

Table 3 Selected Features of LOX/LH_2 Engines

ENGINE						TURBOPUMP ASSEMBLY	
Designation	Application	Thrust, lbf	Chamber pressure, psia	Combustion Chamber	Engine Cycle	Arrangement	Start System
RL10A-3-3	Centaur/OTV	15, 000	400	Tubular	Expander	Geared O_2 Pump	Tank Head
J-2	Saturn S-II and S-IVB	230, 000	787	Tubular	Gas Generator	Dual turbopump, series turbines	Pressurized-gas start tank
SSME	Space Shuttle	512, 000	3270	Channel Wall	Staged Combustion	Dual turbopump, parallel turbines	Tank head
XLR129	--	250, 000	2800	Transpiration cooled wafer	Staged Combustion	Dual turbopump parallel turbines	Tank head
RS-44	OTV Type	15, 000	1540	Channel Wall	Expander Cycle	Dual turbopump, series turbines	Tank Head

1. All engines have:

   (a) Regeneratively cooled nozzles
   (b) Coaxial injector elements
   (c) Axial turbines

The RL10 engine is of interest because it is a production engine and will be used as the initial engine for the OTV type of vehicle.

The RS-44 Advanced Expander Cycle Engine was designed by Rocketdyne as an advanced technology engine for OTV application. A breadboard version known as the Integrated Component Evaluator (ICE) has been completed and is ready for test.

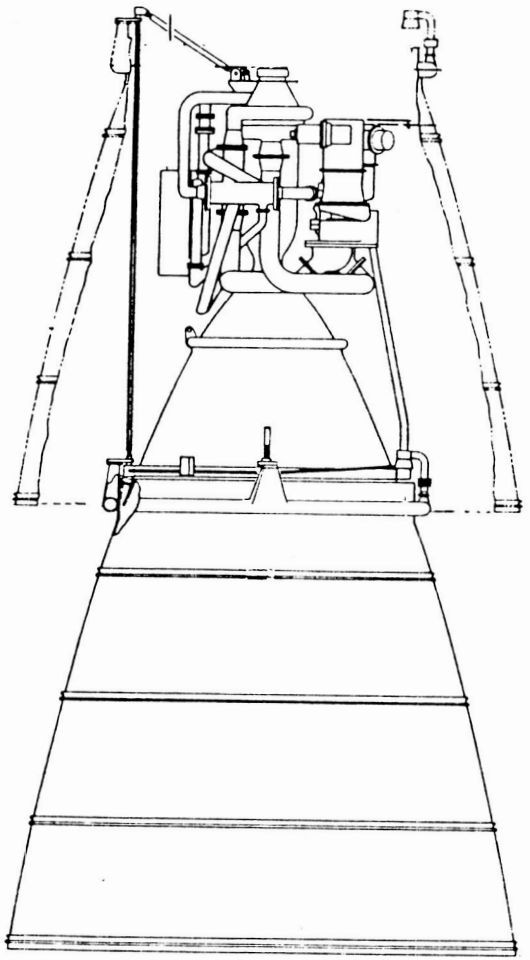

RL10 ENGINE

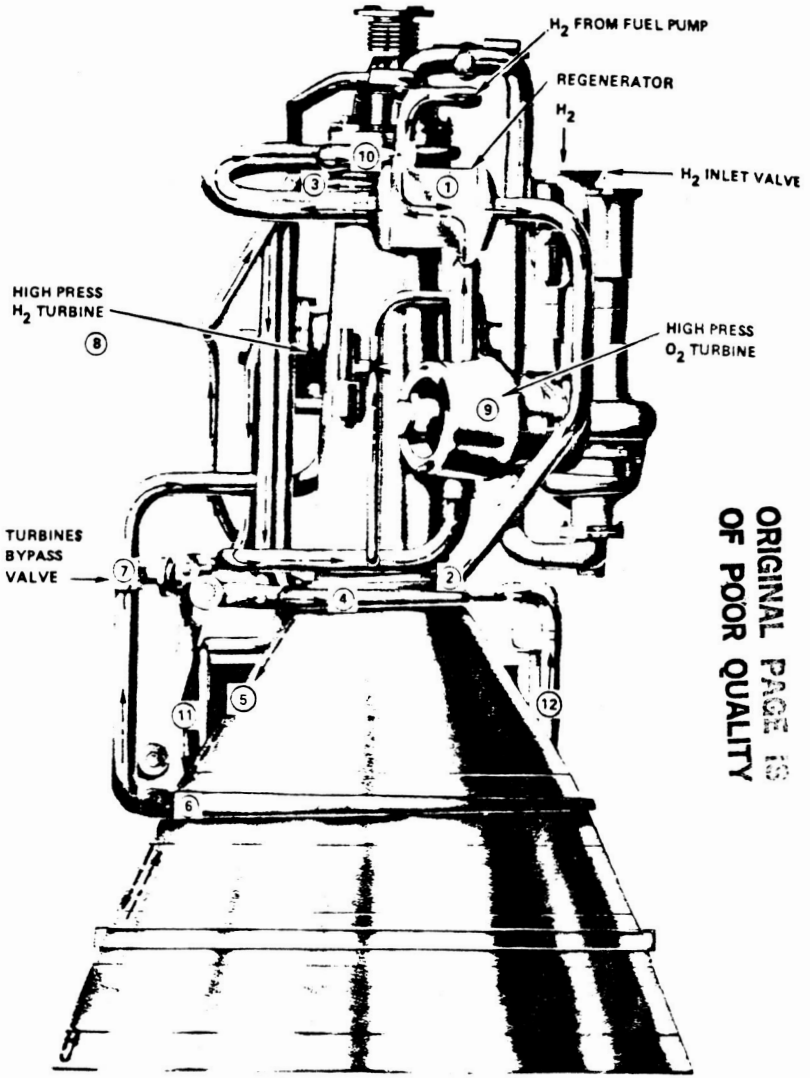

Hydrogen Flow in Advanced Expander Engine Point Desig

ADVANCED EXPANDER ENGINE

FIGURE 3 EXPANDER CYCLE ENGINES

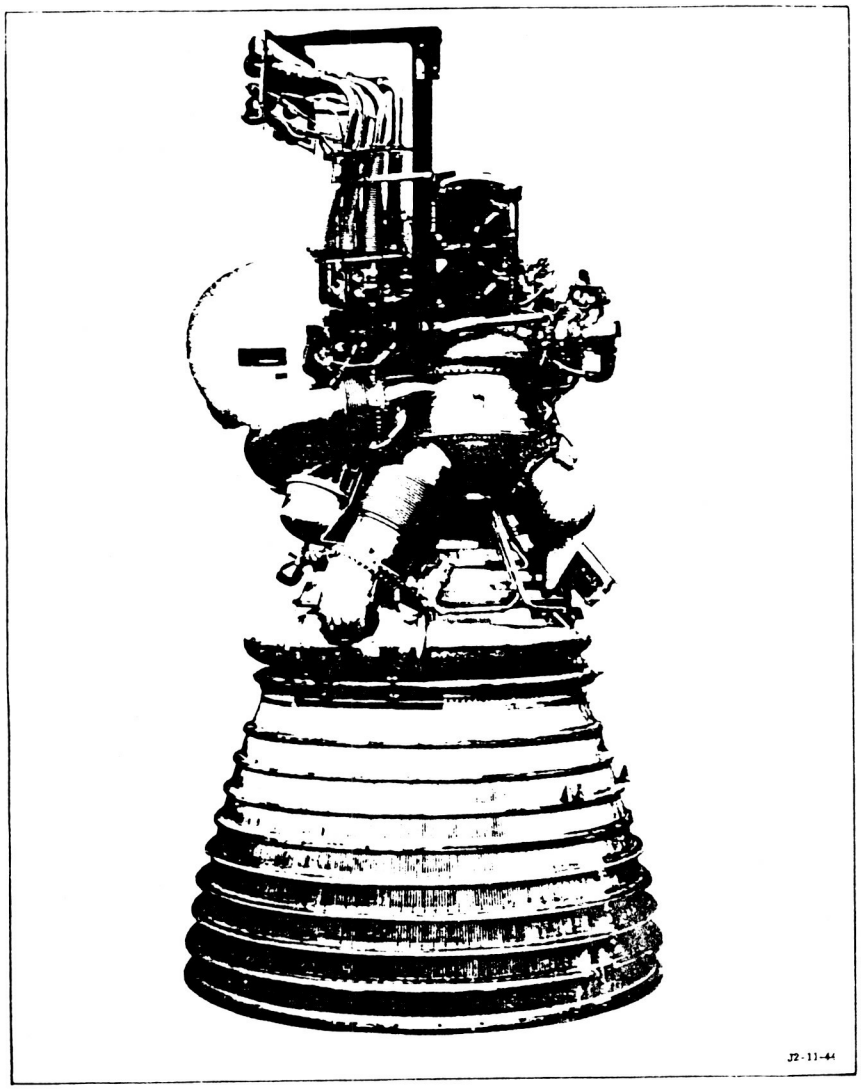

J-2 Rocket Engine

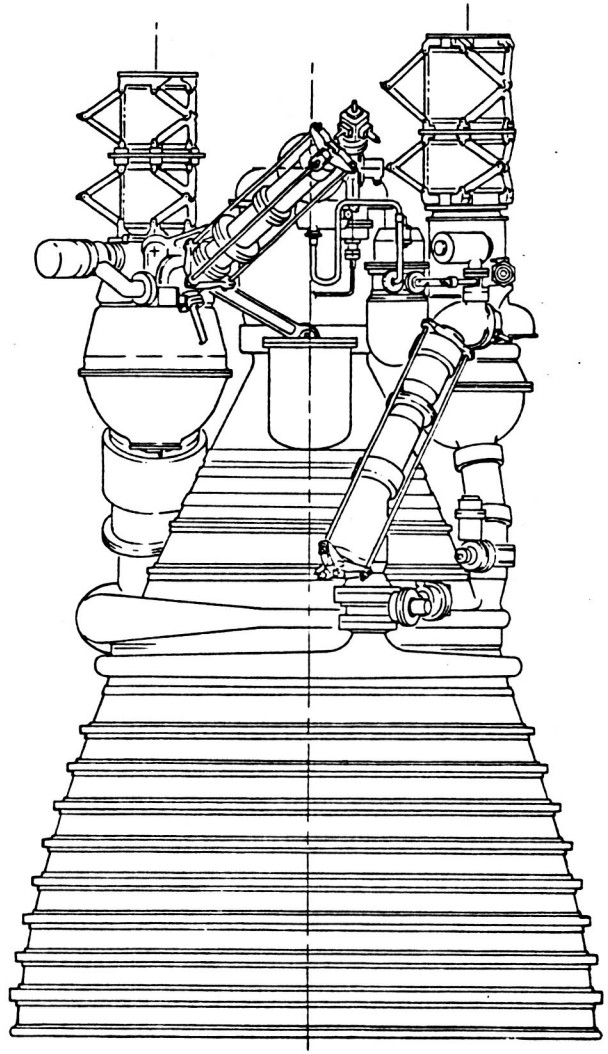

FIGURE 4 J-2 ENGINE

Figure 5 XLR129 DEMONSTRATOR ENGINE

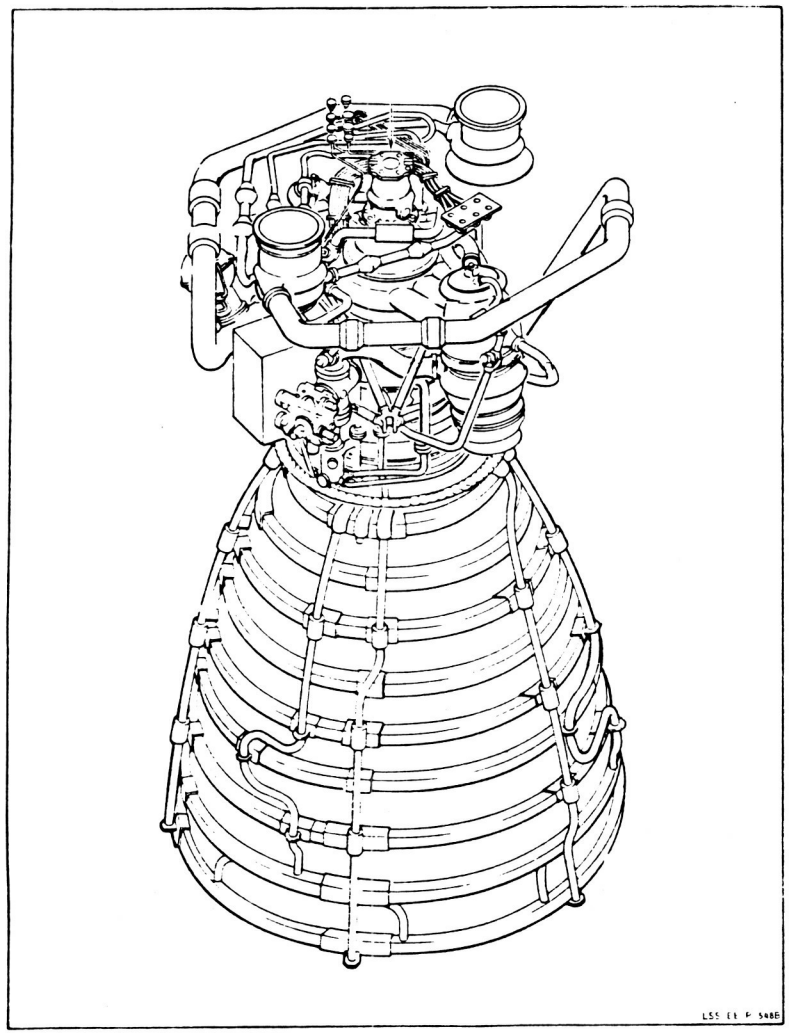

SSME Assembly

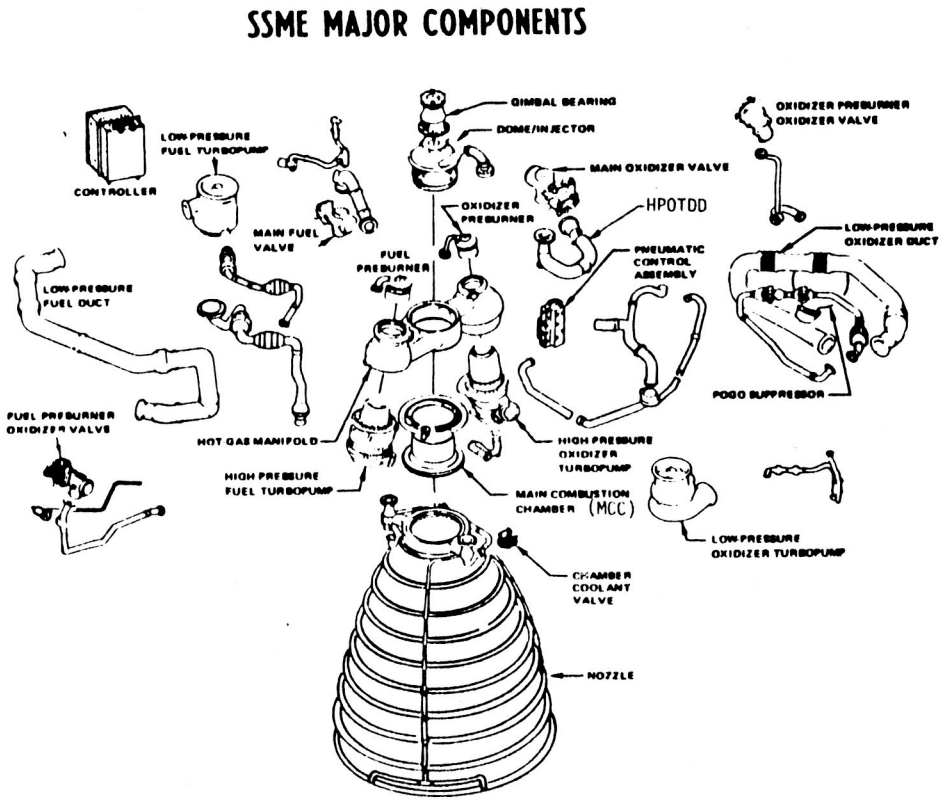

FIGURE 6 SPACE SHUTTLE MAIN ENGINE (SSME)

The J-2 was built by Rocketdyne and was part of the SATURN vehicle, so details of the engine are available for this study. The XLR129 was an Air Force engine where the development was carried through hot fire testing of certain key components such as the preburner injector, transition case and fuel turbopump (Ref. 1). The XLR129 concept was used in Pratt & Whitney's (P&W) proposal in the shuttle engine competition in 1970-1971. In a current study for NASA, P&W has been updating the powerhead design from a materials and technology standpoint for potential use in a future version of the SSME. The SSME is the shuttle engine and will be used in this contract for the test database for developing the composite loads spectra.

The engine configuration and packaging are part of the generic loads description because the individual component loads under study are not all self-generated or contained. The primary source for sinusoidal forcing functions in rocket engines is from turbopumps. The attachment or load path between a component and the turbopumps are a needed parameter for judging the load potential for the component. For example, the J-2 engine packaging concept was to use statically determinate mount systems and bellowed ducting for all primary lines. The turbopumps had a single ball or slide mount point on the thrust chamber and the other supports were bipod or strut mounts. Connections were through bolted joints that inherently have friction losses. The flexible ducts all had multiple bellows between primary structural supports. The combination of the mounts and lines help to uncouple the high frequency loads between engine components. The other four engines use a rigid line concept and may also use the lines as primary support structure, such as in the RS-44. Rigid lines have a higher potential for passing loads from the pump to other structures. The SSME and XLR129 carry these rigid attachments one step further with a powerhead construction where the preburners, pumps and injectors are closely grouped and rigidly tied together. The XLR129 is probably the most closely coupled and rigid system of the lot.

Measurements on the SSME preburners and main injector show high level high frequency (5KHz to 20KHz) sinusoidal vibrations that are readily traceable to both high pressure turbopumps. Larger components may be insensitive to these high frequencies, but they are a consideration in short stubby components as the SSME fuel preburner LOX post and a variety of instrumentation probes. This close coupling of major components ensures that the vibration, flow and other loads will interact.

The engine configuration defines the primary load paths for loads like thrust, gimbaling and engine side loads. For the J-2, RL-10, SSME and RS-44, the main injector is the primary load path of the thrust through to the gimbal attach point. For the XLR129, the transition case is the primary thrust load path to the gimbal bearing The turbopumps attachment to the case and the injector manifold are also part of this load path. This same load path is also used in reacting gimbaling loads and the sideload transients from start and cutoff. The SSME turbopumps and preburners are out of the primary load paths for thrust and sideloads.

Another example where engine packaging differences can readily affect loads is the flexible vs. hard line attachment. Misalignment loads for flexible lines are considerably less than for hard lines using the same misalignment deviation.

The above discussion is furnished to point out the need for including basic configuration information in defining the composite loads and the related expert system.

Another key variable from an engine standpoint is the turbine drive cycle used by the engine. The choice of turbine drive cycle affects all three components: lox posts, turbine blades, and transfer ducts, as well as some of the other components in the survey study. The choice of the staged combustion cycle for an engine (SSME & XLR129) ensures high pressures for the pumps, high temperatures for the turbines, high flow energies to drive vibrations, and a hot fuel for the main injector.

An excellent summary of the effects of the turbine drive cycle on an engine is furnished in Reference 2 and is edited in the following discussion to more specifically relate to the engines under discussion.

The method used to drive the turbine has a direct effect on the pump headrise and power requirements and on the pressure ratio and flowrate available to the turbine for supplying the necessary power. Thus, the turbine drive cycle used on a liquid rocket engine affects the design requirements of the turbine as well as those of the propellant pumps. Figure 7 shows typical flow schematics for the basic types of turbine drive cycles. If the turbine

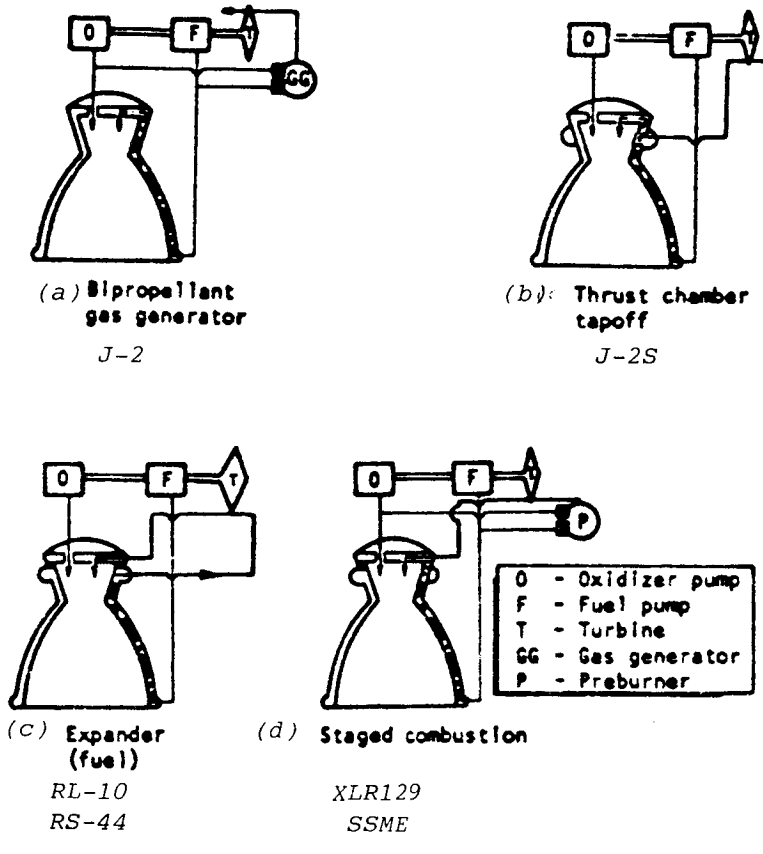

Figure 7 Basic Turbine Drive Cycles Used on LOX/LH_2 Engines

flow is in parallel with the combustion chamber (gas-generator and thrust-chamber-tapoff cycles), the pump head and power requirements are relatively low. However, if the turbine is in series with the combustion chamber (expander and staged-combustion cycles), the pressure drop across the turbine must be added to the pump discharge pressure and, therefore, the head and power requirements are high; in addition, the required pump discharge pressure is more sensitive to changes in the pump and turbine efficiencies.

The J-2 engine used the gas-generator (GG) cycle, in which the turbine working fluid is derived by combustion of the main propellants in the GG at a temperature below the turbine temperature limits. The J-2S development engine utilized a variation of the GG cycle called the tapoff cycle, in which the turbine working fluid is tapped off near the face of the injector at a location where a relatively cool gas is available.

In the expander (or hot-fuel tapoff) cycle, which is used for the RL10 engine and RS-44 Advanced Expander Engine, the hydrogen that is evaporated and heated in the thrust chamber regenerative jacket is used to drive the turbines. The turbine exhaust gas is fed to the main chamber for combustion.

In the staged-combustion cycle, which is used in the SSME and XLR129 engines, a preburner generates the turbine working fluid that is then discharged into the main combustion chamber where the second stage of combustion occurs.

The general advantages and disadvantages of the basic turbine drive cycles are available in Reference 2. For any cycle, the pump must meet the pressure and flowrate requirements of the engine, and the turbine must drive the pump within the pressure-ratio limitations imposed on the turbine by the engine system. The effects of cycle and chamber pressure on pump discharge

pressure are illustrated in Figure 8. In engines with GG and tapoff cycles, the chamber pressures generally are kept below 1500 psi in order to avoid the penalties of high turbine flowrates. In the expander cycle, the chamber pressure is relatively low on account of the limited amount of heating available for the turbine working fluid prior to entering the turbine. However, for the same chamber pressure, the expander cycle requires a higher pump discharge pressure because the turbine is in series with the combustion chamber. For the staged-combustion cycle, the chamber pressure can be as high as 3000 psi because the preburner provides high-energy fluid for the turbine; 3000 psi is an approximate upper limit for this cycle because for given values of turbine inlet temperature and turbopump efficiency, the required pump discharge pressure rises steeply at higher values. Allowing for pressure drops in the lines, regenerative jacket, preburner, turbine and injector, the resultant required discharge pressures can be as high as 7000 to 8000 psia.

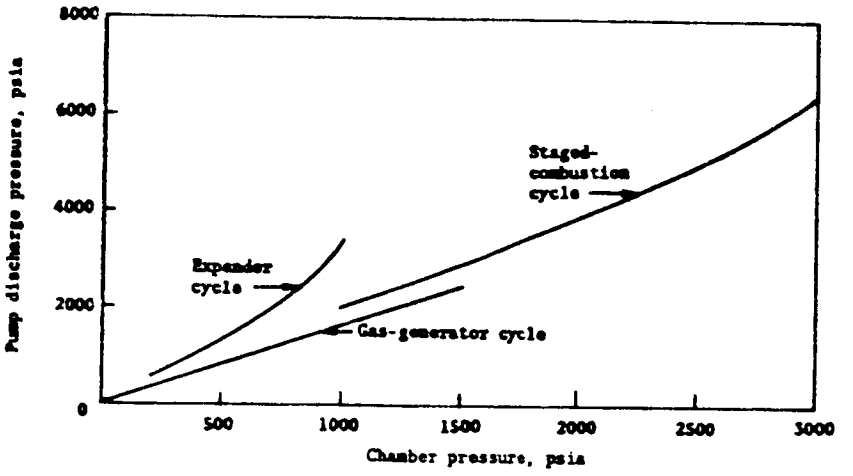

Figure 8 Effect of Drive Cycle & Chamber Pressure on Pump Discharge Pressure (Oxygen/Hydrogen Engine, Mixture Ratio = 6)

For the GG and tapoff cycles, turbine pressure ratios of approximately 20 are required to minimize the flowrate of turbine working fluid and thereby maximize the engine specific impulse. For the expander and staged-combustion cycles, the optimum turbine pressure ratios are generally less than 1.5 because of the large quantities of turbine working fluid available. In design, expander and staged-combustion cycle turbine pressure ratios are minimized in order to maximize chamber pressure and minimize turbopump weight, thereby minimizing engine weight.

Relative to GG cycles, turbopump weight and horsepower generally are somewhat greater for expander cycles and are much greater for staged-combustion cycles. These differences result from the pump discharge pressure requirements. To meet the high efficiency requirements, pumps in expander and staged-combustion cycles must either operate at higher speed or have more stages than those in GG cycles. To meet the turbine pressure-ratio requirements, GG and tapoff cycles generally incorporate two-row velocity-compounded turbines, and expander and staged-combustion cycles generally incorporate either two-stage pressure-compounded or reaction turbines. The high horsepower and pressure requirements for the stage-combustion cycle produces a high level of mechanical and flow vibrations.

5.0 SSME OVERVIEW

The orbiter vehicle main propulsion system includes three Space Shuttle Main Engines (SSMEs). An SSME is a reusable, high-performance, liquid-propellant rocket engine with variable thrust. All three engines are ignited on the ground during launch, operating in parallel with the solid rocket boosters during the initial ascent phase, and continue to operate for approximately 550 seconds total firing duration. Each engine operates at a mixture ratio (liquid oxygen/liquid hydrogen) of 6:1 and a chamber pressure of approximately 3,000 psia to produce a sea level thrust of 375,000 pounds and a vacuum thrust of 470,000 pounds. The engines are throttleable over a thrust range of 65 to 109 percent of the rated power level. This provides a higher thrust level during lift-off and the initial ascent phase, and allows orbiter acceleration to be limited to 3 g's during the final ascent phase. The engines are gimbaled to provide pitch, yaw, and roll control during orbiter boost phase.

A typical flight profile is shown in Figure 9. This basic profile is characteristic of a majority of the pressure, flow and pump characteristic parameters.

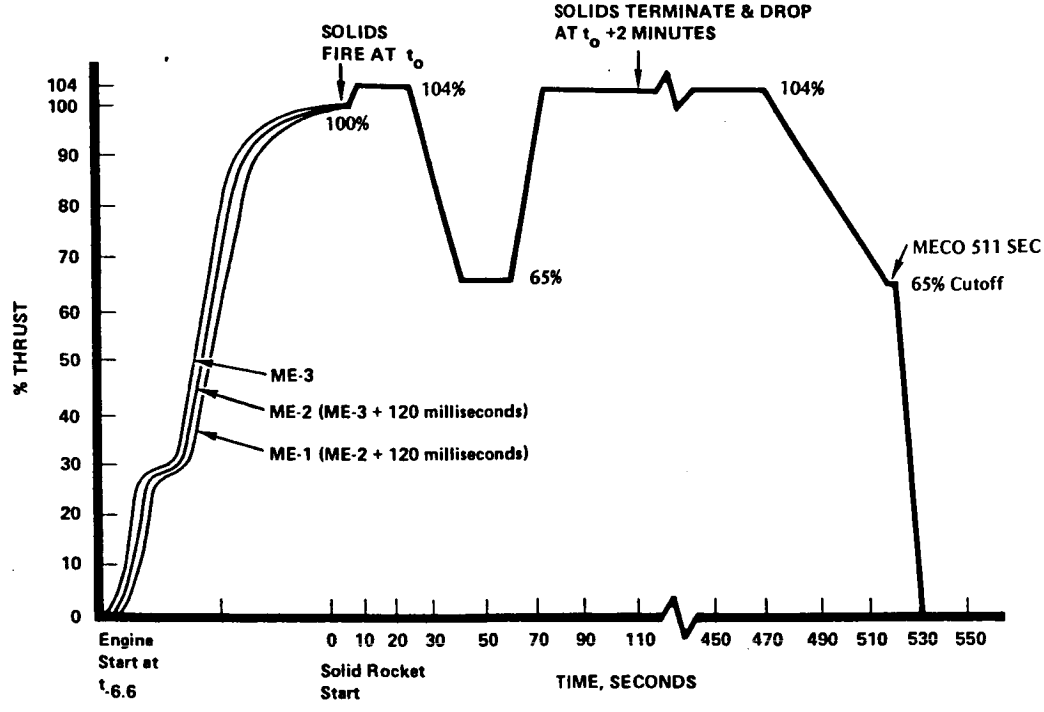

Figure 9 Typical SSME Thrust Profile

A brief description of the engine operation and propellant flow schematic is in order to furnish an overall perspective of the engine and its loads. Figure 10 is a simplified flow schematic with the main engine components and flows shown.

A description of the start sequence follows.

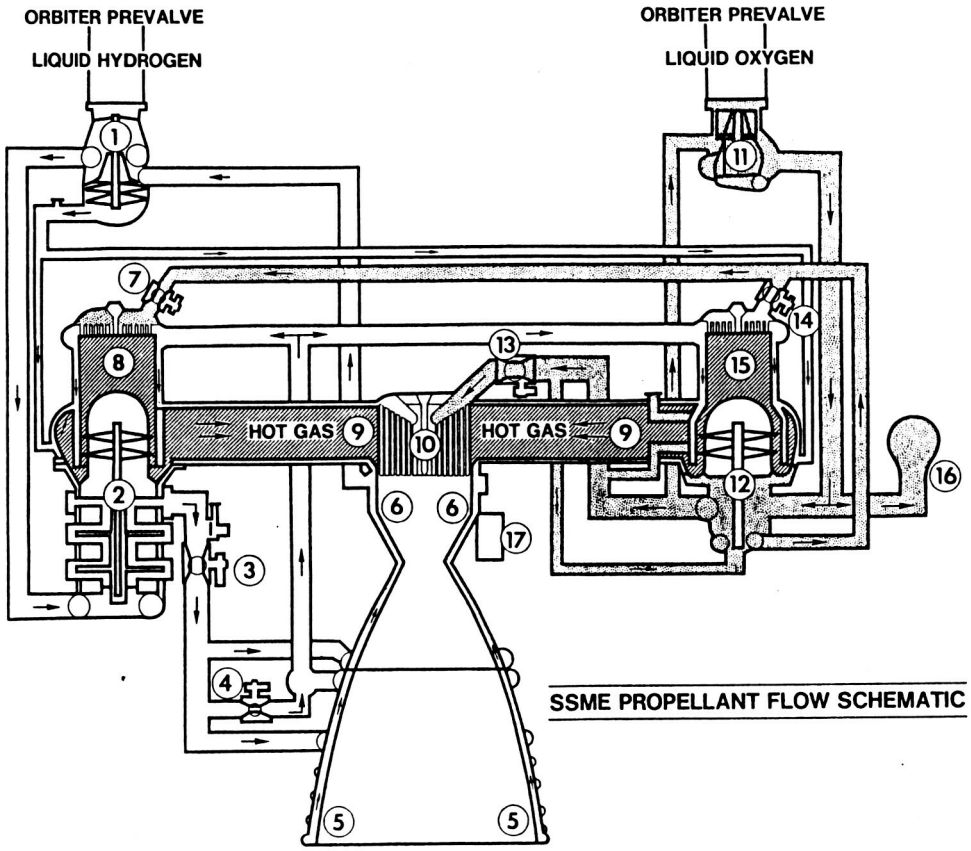

Figure 10 SSME Propellant Flow Schematic

Components

1. Low Pressure Fuel Turbopump
2. High Pressure Fuel Turbopump
3. Main Fuel Valve
4. Chamber Coolant Control Valve
5. Nozzle
6. Main Combustion Chamber
7. Fuel Preburner Oxidizer Valve
8. Fuel Preburner (LOX Posts)
9. Hot Gas Manifold (& Transfer Tubes
10. Main Injector (LOX Posts)
11. Low Pressure Oxidizer T/P
12. High Pressure Oxidizer T/P
13. Main Oxidizer Valve
14. Oxid. Preburner Control Valve
15. Oxidizer Preburner
16. Pogo Suppressor
17. Controller

The flow of liquid hydrogen (or fuel) and liquid oxygen (or oxidizer) from the Space Shuttle External Tank is restrained from entering the engine by prevalves (or isolation valves) located in the orbiter above the low pressure turbopumps (1 and 11). Approximately one hour prior to firing, the prevalves are opened to allow propellants to flow through the low pressure turbopumps (1 and 11), and through the high pressure turbopumps (2 and 12), and then to the main propellant valves (3 and 13). On the liquid oxygen side, the system also fills two preburner valves (7 and 14). The cryogenic propellants are held in the ducts for sufficient time to chill the engine and attain liquid conditions in the respective propellant systems. The chill process is aided by bleedlines which remove gaseous propellants as they are formed.

In the start sequence, the hydrogen and oxygen sides operate almost simultaneously. The hydrogen (or fuel) side is explained first.

Upon receipt of the ignition command from the orbiter, the main fuel valve (3) is opened. This permits hydrogen to flow into the coolant loop, through the nozzle tubes (5), and through channels in the main combustion chamber (6). Part of this coolant loop flow is diverted by the coolant control valve (4) to the preburners (8 and 15), for combustion and cooling of the preburner walls. Some of the hydrogen used in the coolant loop is warmed in the process to virtually ambient conditions and is tapped off at the main combustion chamber (6) for routing back to the low pressure turbopump (1) to drive the turbine for that pump. This flow passes through the turbine and is returned to the walls of the hot gas manifold (9), and the main injector (10) to provide cooling.

On the oxygen (or oxidizer) side, the ignition command opens the main oxidizer valve (13). The liquid oxygen flows through the two turbopumps (11 and 12) to the main injector (10) and also (through valves at 7 and 14) to the two preburners (8 and 15). Oxygen, tapped off downstream of the high pressure oxidizer turbopump (12), is routed to the low pressure turbopump (11) and to serve as the turbine-drive fluid for that pump. This flow continues through the low pressure oxidizer turbopump (11), thus re-entering the circuit.

Spark igniters located in the dome of both preburners (8 and 15) and the main chamber (10) initiate combustion.

After the engine is signaled to start, the initial combustion occurs in the preburners. There are two preburners: one provides power to the high-pressure fuel turbomachinery (8), and the other provides power to the high pressure oxidizer turbomachinery (15). Proper sequencing of these two preburners allows the engine to start repeatedly regardless of the engine inlet conditions. Each of the two preburners operates at a low mixture ratio of less than one part oxygen to hydrogen to produce hot gas (or hydrogen-rich steam) to provide low-temperature gases for turbomachinery operation. Each temperature can be varied by moving a single valve. The two preburners thus provide a convenient method of controlling engine thrust and mixture ratio. The preburners operate over a broad range of pressure and temperature to achieve the full range of engine operating conditions.

As the fuel-rich gases leave the preburners, they immediately enter the high-pressure turbomachinery. The gases are expanded in a turbine and the expansion reduces the temperature. After the gases leave the turbomachinery, they enter the hot-gas manifold. This manifold transports and distributes the gases to the main injector. The hot-gas manifold serves multiple functions. It supports the two preburners and two high-pressure turbopumps, and also forms a portion of the thrust chamber structure. The compactness of the hot-gas manifold allows the powerhead diameter to be minimized, and its orientation permits access for the removal and inspection of turbomachinery and preburners.

After the gases are routed through the hot-gas manifold, they enter the thrust chamber. The thrust chamber consists of three major parts: the main injector (10), the main combustion chamber (6), and the nozzle (5).

The fuel-rich gases from the hot gas manifold enter the thrust chamber through the injector and are distributed in the injector. Liquid oxygen from the high pressure oxidizer turbopump (2) enters at the top of the injector, is uniformly distributed within the oxidizer "dome", and then

enters the center tube of each of the injector coaxial elements. The fuel-rich hot gas enters the large annular tube of the coaxial element. The coaxial elements are designed and optimized so that the hot gas plus the oxygen are uniformly distributed throughout the combustion chamber. This is achieved by proper matching of gas and oxygen velocities and uniform spacing of elements across the injector face. Some of the injector elements are extended into the combustion chamber to form acoustic baffles. These elements, quite similar to the ones used on the injector face, inject hydrogen and oxygen at the same mixture ratio as the elements on the injector face and maintain uniform distribution and high performance.

The propellants injected into the main chamber are combusted rapidly at a mixture ratio of six parts of oxygen to one part hydrogen. The gases are accelerated to sonic velocity and supersonically expanded in the aft portion of the main combustion chamber and the nozzle.

6.0 SSME LOADS DATABASE

A standard set of engine measurements are taken on each SSME engine ground test and are used for calculating engine performance; measuring critical levels of vibration, temperature, etc. for engine redlines and measuring general engine operation. A subset of this information that is applicable to the composite loads contract is shown in Figure 11. These measured data relate to LOX posts, turbine blades and transfer ducts. Most of the measurements are low frequency digital data. The accelerometer data are all high frequency analog measurements.

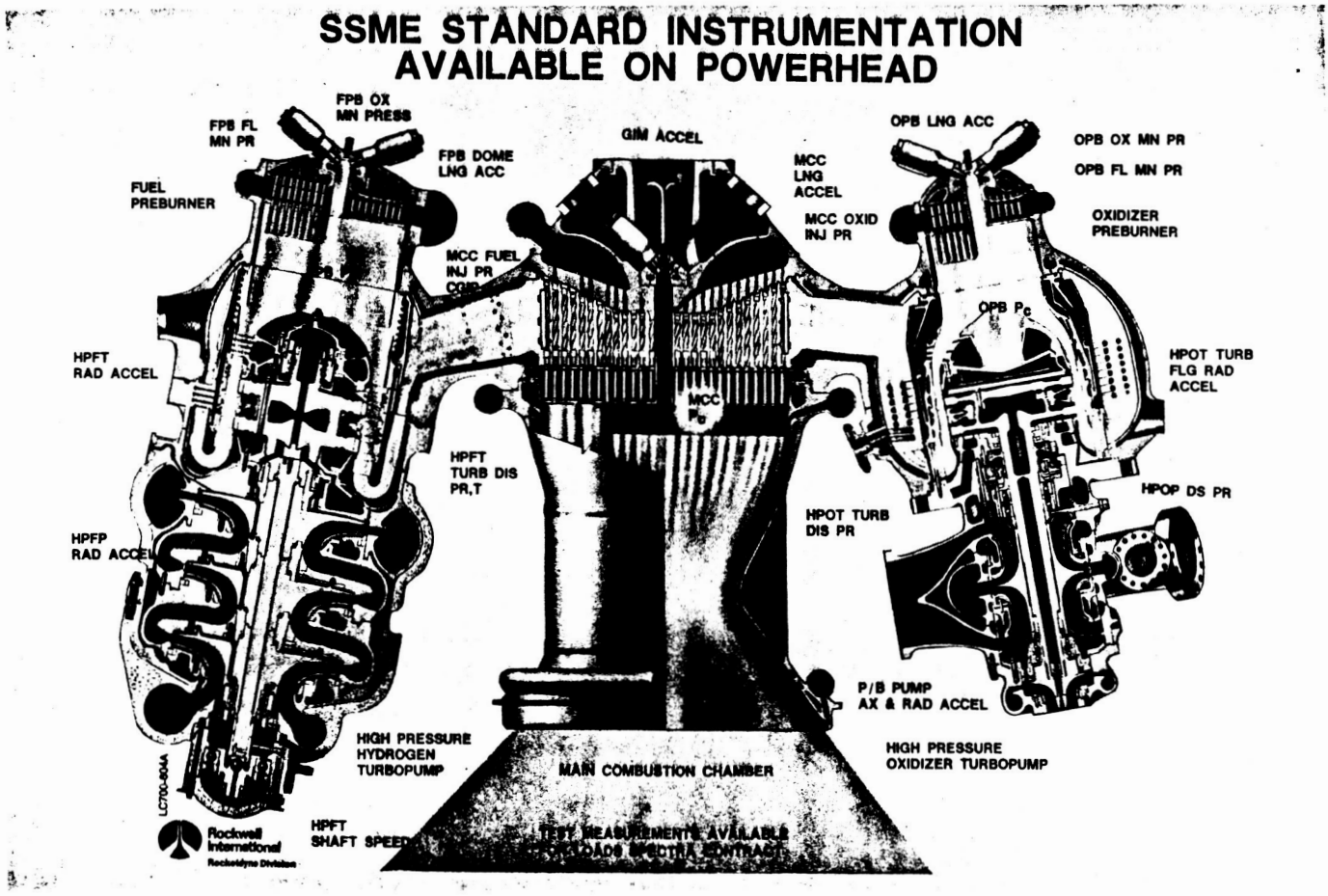

Figure 11 SSME Standard Instrumentation Available on Powerhead

Figure 12 shows the standard flow of engine test data processing for the SSME engine. The low frequency data is processed through a data reduction code and either plotted or further processed to provide steady state performance calculations that include both measured and calculated flows, temperatures, pressures, torques, speeds, power level, etc. The analog data passes through a high frequency data processing facility records. These data are all reviewed for each test firing of the engine and are collected in various databases for later use and review. Datatapes are saved from all engine tests and information is recoverable at any time.

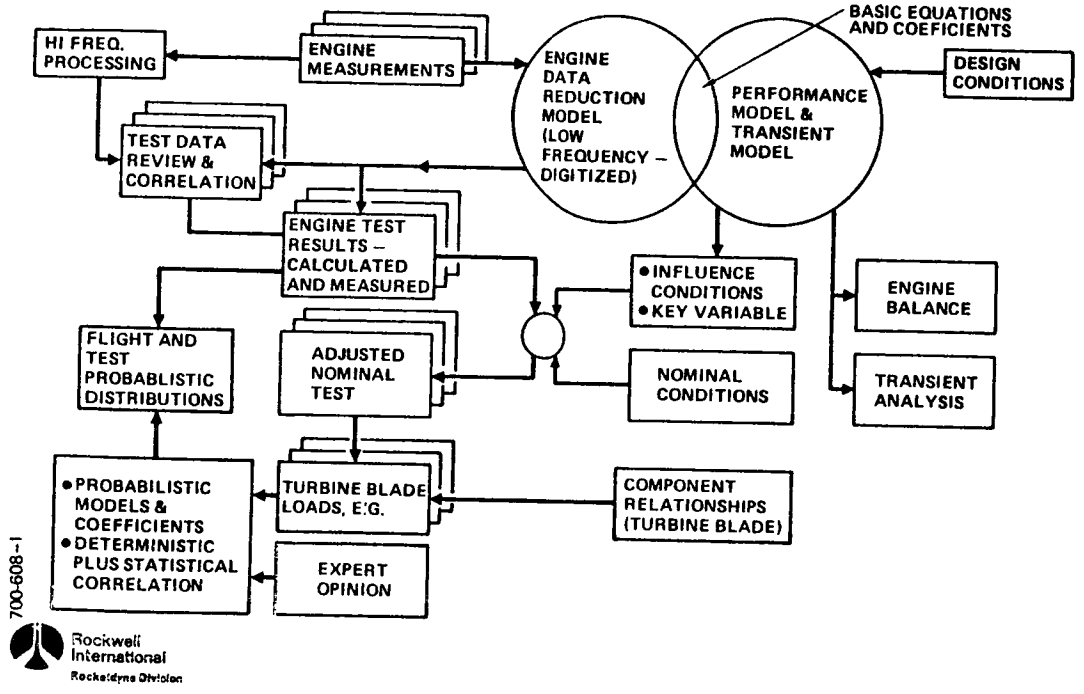

Figure 12 Data Analysis

The right hand side of Figure 12 depicts the interrelationship of the engine performance model and the engine data analysis. The engine data reduction model and the performance model are essentially the same code. For the data analysis, engine measurements are used as the independent variables. For the performance model, design conditions are used for the independent variables. The coefficients for these models have been adjusted based on empirical measurements on over 1000 engine tests. The difference for a new design vs a production engine is essentially the accuracy of the equation coefficients--assuming similar overall accuracy in modeling the physics of the problem.

The influence conditions or coefficients and nominals are a set of equations with coefficients that are varied as a function of power level to accurately represent the performance model at specific power levels between 65 and 109% power level. The influence coefficients and nominals are a cost effective method of determining engine parameters for a limited set of independent and dependent variables.

These measurements form the best ready database for developing at least a portion of the probabilistic loads. Since they are all time phased together, it is a convenient method to obtain some of the combined load effects. In the development of the individual loads, key variables, such as power level, torques and flow rates are available to aid in developing correlations so that the generic loads can later be scaled using these parameters.

Table 4 provides an overall perspective of where information is obtained for detail analysis of components. The first two items relate to the direct engine measurements and analysis just discussed.

The engine balance and engine transient model have similar simulation codes for modeling engine components. The engine balance model furnishes higher accuracy steady state quantities, whereas the transient model depicts the full range of engine test conditions. Both models project standard engine

Table 4 Classification of Data Available for Use in Probabilistic Load Determination

DATA/ANALYSIS	AVAILABILITY	EXAMPLES
1) ENGINE TEST MEASUREMENTS . LOW FREQUENCY (DIGITAL) . HI FREQUENCY (FM TAPE)	. EVERY ENGINE TEST . VARIOUS TYPES OF PROCESSED DATA AND RECORDS	. TURBINE DISCHARGE TEMP, P_C, . TURBOPUMP OR INJECTOR ACCELEROMETERS
2) ENGINE TEST CALCULATED VARIABLES . LOW FREQ (DIGITAL) . STEADY STATE ONLY 1 sec, 3 sec, 10 sec AVG . MAJOR COMPONENT LEVEL	. EVERY ENGINE TEST	. PUMP TORQUE, FLOW RATES
3) ENGINE TRANSIENT SIMULATION MODEL . LOW FREQUENCY DIGITAL ANALYSIS . MAJOR COMPONENT LEVEL	. SPECIFIC SIMULATIONS FOR UNDERSTANDING START & CUTOFF . NOT TEST SPECIFIC, BUT CORRELATED TO TEST RESULTS	. ENGINE VALVING & SEQUENCING OF OVERALL ENGINE. START & CUTOFF . MAJOR COMPONENT VARIABLES
4) ENGINE BALANCE MODEL . STEADY STATE ANALYSIS . SPECIFIC OPERATING CONDITIONS . NOMINALS, MAX, MINS	. SPECIFIC ENGINE OPERATION CONDITIONS	. RPL, FPL, 111% AND OTHER POWER LEVELS . VARIOUS ENGINE CONFIGURATIONS . MAJOR COMPONENT VARIABLES
5) SHOCK & VIBRATION ENVIRONMENTS . DESIGN & TEST ENGINE ENVIRONMENTS	. SPECIFIC ZONES ON ENGINE . EXPECTED MAX CONDITIONS . DIFFERENT THRUST LEVEL & ENGINE CONFIGURATIONS . HISTORICAL DATABASE FOR ENGINE	. ZONE A, MAIN COMBUSTION CHAMBER ZONE . ZONE E, FUEL PREBURNER
6) SPECIAL MEASUREMENTS	. LIMITED DATABASE . CRITICAL HARDWARE . FEW MEASUREMENT . DIFFICULT TO OBTAIN	. INSTRUMENTED TURBOPUMPS . STRUCTURAL & VIBRATION TESTS . INSTRUMENTED INJECTOR . SWHGM COLD FLOW . ENGINE 0110 TESTS
7) INDIVIDUAL COMPONENT ANALYSIS . STEADY STATE BASIS . ENGINE BALANCE CONDITIONS . VIBRATION ENVIRONMENT . TRANSIENT ANALYSIS . ENGINE TRANSIENT MODEL . SHOCK ENVIRONMENT . EXPERT OPINION	. SOME INFORMATION FOR ALL COMPONENTS . LEVEL OF DETAIL DEPENDENT ON - CRITICALITY OF COMPONENT, ACCURACY OF MODEL AND KNOWLEDGE OF LOADS . STEADY STATE PRIMARILY . LIMITED DUTY CYCLE ANALYSIS . LIMITED ENGINE & LAB TEST MEASUREMENTS	. LOX POST . TURBINE BLADES . TRANSFER DUCTS

or typical engine operating conditions. Engine test results are not directly used as input, but are used as correlation data to compare with engine testing. In general, the engine balance data and to a lesser extent the engine transient simulation model results are used for component analysis.

The structural vibration loads are based on the shock and vibration environment definitions rather than individual engine measurements. Detail structural analyses are usually based on limit or maximum conditions that occur within the load duty cycle of the component, rather than a detailed time dependent analysis of a mission-history profile. Most of the loads are not readily available in the proper format for the CLS contract.

The following discussion is furnished to give a perspective of the form of the available engine data and some of its characteristics. Figure 13 is the processed data of the fuel preburner chamber pressure (FPB Pc) for a typical test. This trace mirrors in form the thrust profile trace in Figure 14. The thrust profile trace also notates when venting of the run tanks occurs in the tests, since pressure and temperature changes at the engine propellant inlets affect engine performance.

The high frequency sample data processing examples include AMS, PSD, ISOPLOTS, Tracking Filter and STATOS. Figure 15 shows the power level profile of the test. This test was chosen since it varies the power level in 1% decrements from 109% to 90%. Each step has a steady state response of 3 seconds. This incremental change is easily noted in the high pressure fuel pump speed profile in Figure 16. Figure 17 is a typical AMS plot that furnishes a composite level squared time history of the variables noted. These traces show transient effects during start and cutoff, as well as the variation caused by changes in steady state power level. Figure 18 is a power level spectral density plot (PSD) of a selected time interval of the test (14 to 24 seconds from start). The variable is the fuel preburner longitudinal acceleration. This plot shows the HPFTP sinusoidal harmonics

at 12N, 18N, 24N and 30N that stand out above the average RMS level of the signal. The HPOTP sinusoidal harmonic at 16N is also annotated. The same HPFTP sinusoidal frequencies are easily seen on the ISOPLOT in Figure 19. The ISOPLOT also shows how these harmonics drop off (since they are pump speed dependent) as the power level is decreased from 109%.

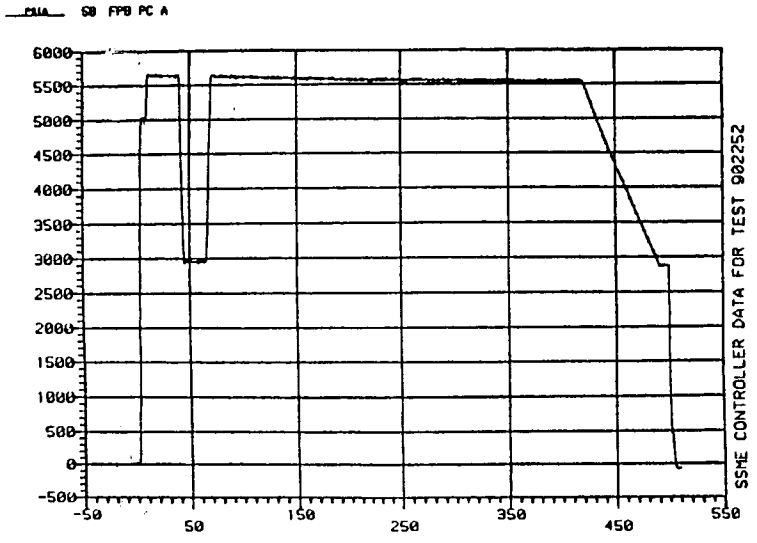

Figure 13 Time from Engine Start, Secs

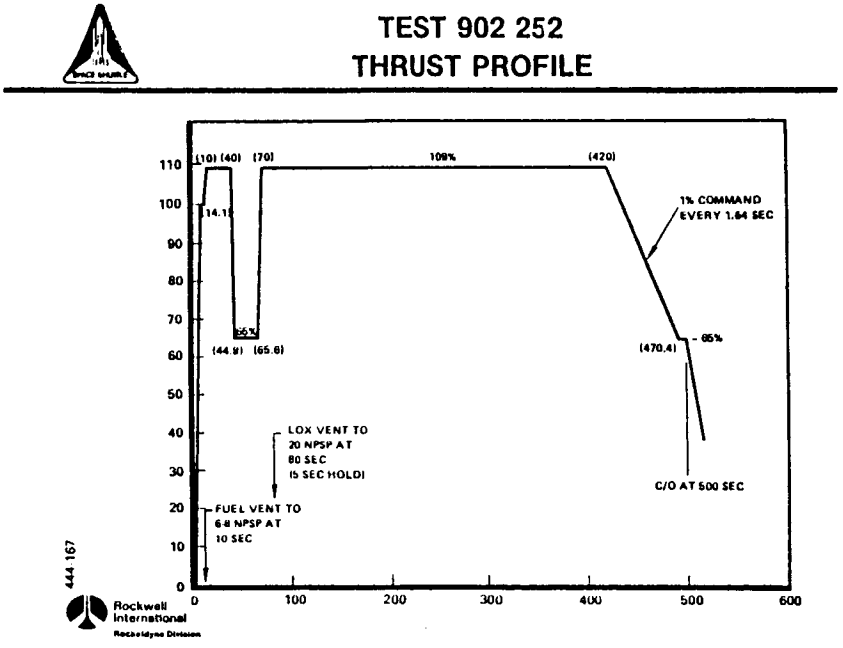

Figure 14 Thrust Profile

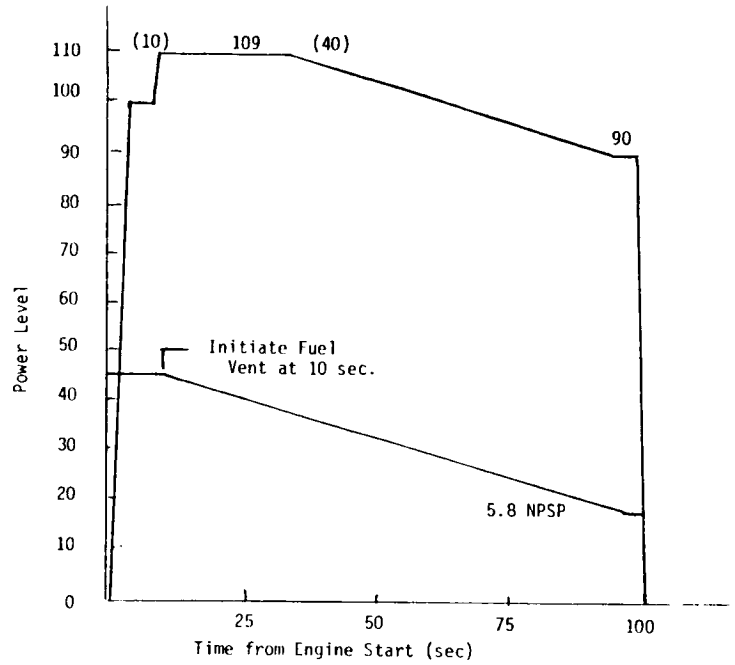

Figure 15 Pump Signature Test

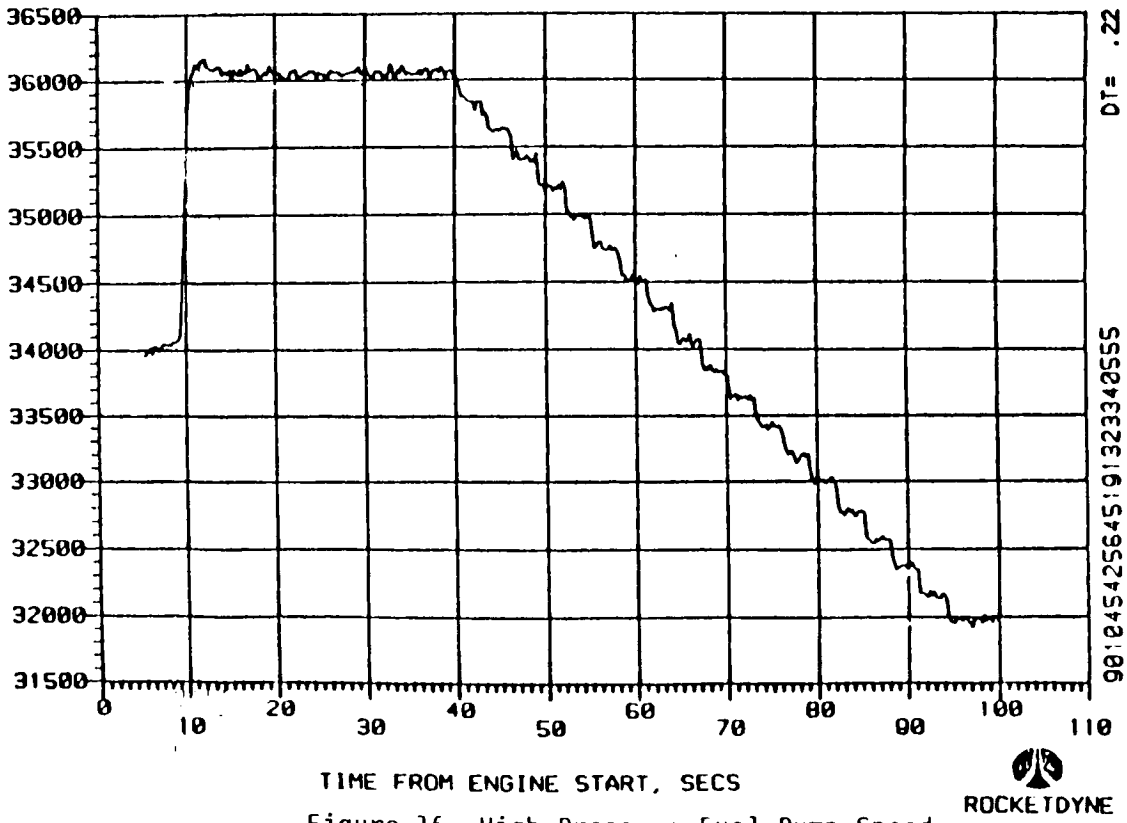

Figure 16 High Pressure Fuel Pump Speed

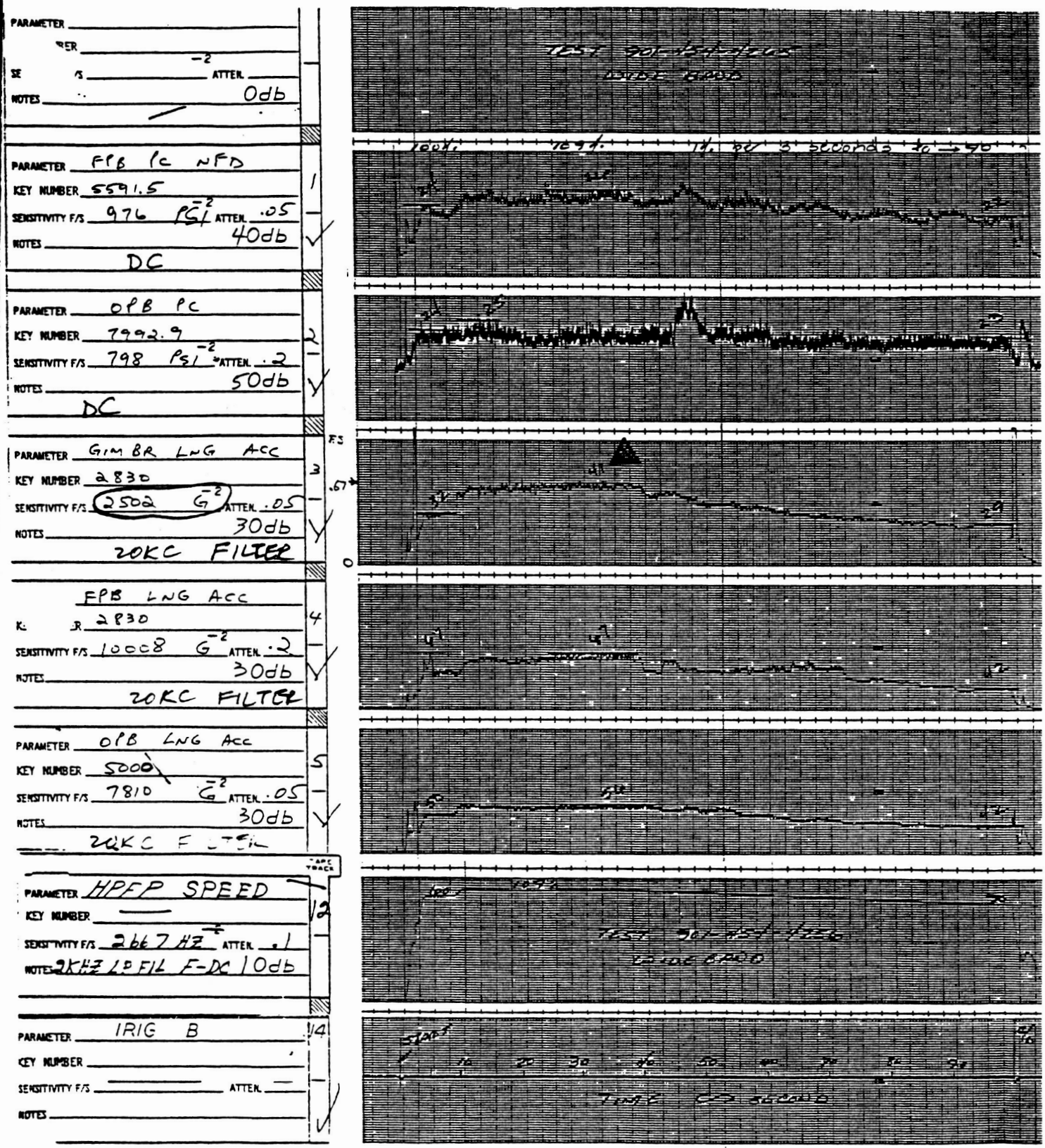

Figure 17 AMS Fuel Preburner Pc

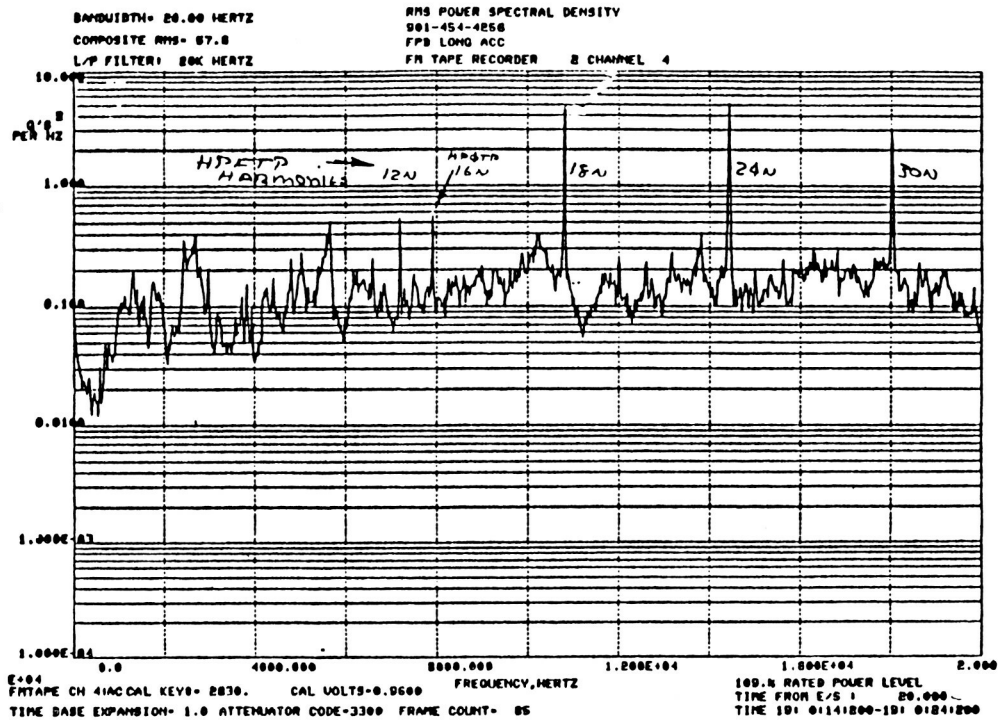

PSD

FUEL PREBURNER LONGITUDINAL ACCELEROMETER PDS

Figure 18 PSD Fuel Preburner Longitudinal Accel.

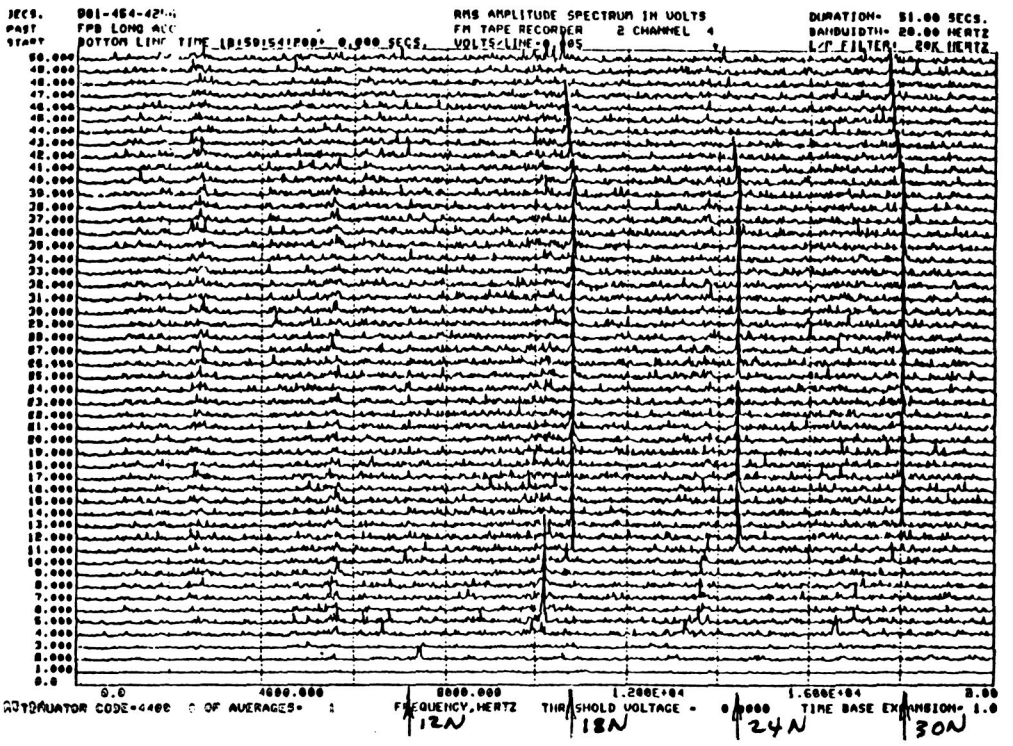

ISOPLOT

Figure 19 Isoplot Fuel Preburner Longitudinal Accel.

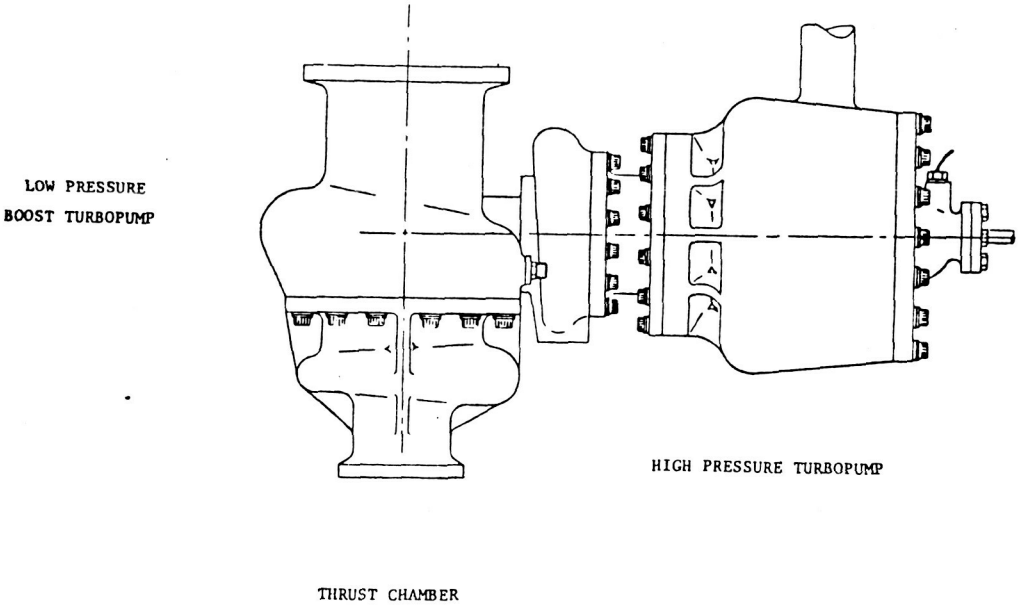

Figure 20 Expander Cycle Liquid Oxygen Turbomachinery

The PSD shown demonstrates that high frequency inputs from both pumps are carried through the powerhead and drive the fuel preburner accelerometer. Similar responses are found in the main injector accelerometer. Interaction of loads such as vibrations should be expected in any rigidly tied, closely-coupled components, whether it is the SSME or RL129 powerheads, or advanced expander cycle engine "T" mount oxidizer turbopumps, Figure 20.

The STATOS record, Figure 21, is included to show that the accelerometer response is of such a wide spectrum that the special (standard) processing shown in the previous figures is required to gain intelligent information from the data.

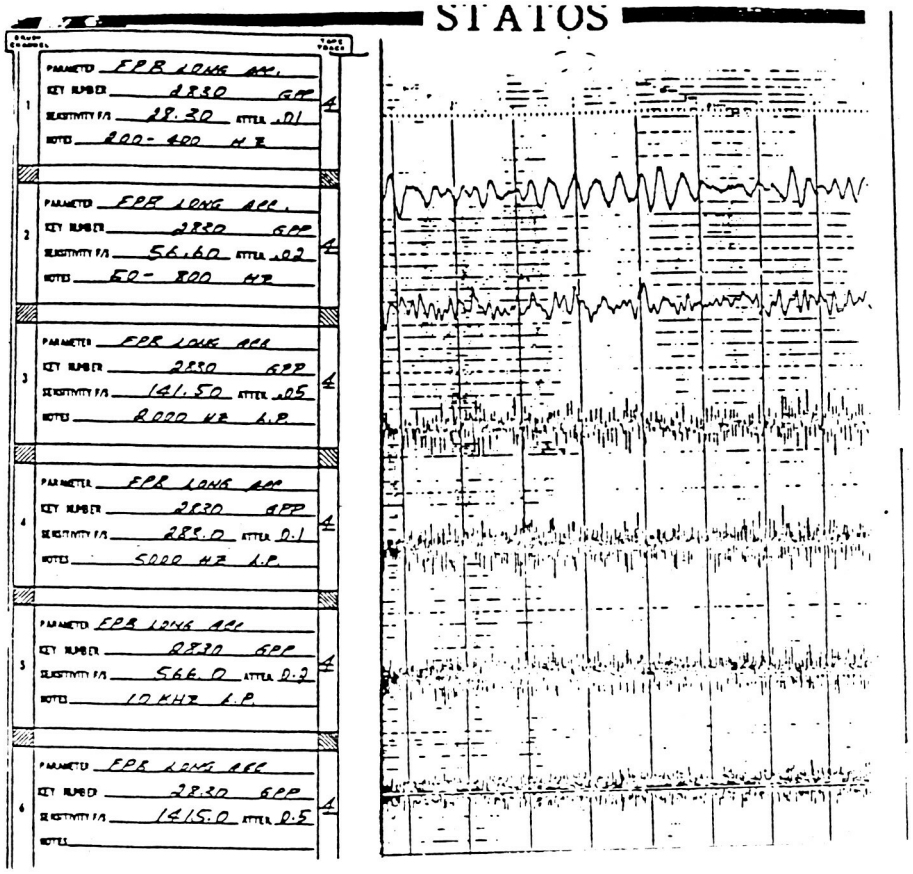

Figure 21 Statos Record

7.0 PROBABILISTIC LOADS SURVEY

7.1 Introduction

The development of a generic load model capable of addressing not only the loads typical in current space propulsion engines but also the loads which may result as a consequence of design modifications to the engine requires a probabilistic technique which is flexible, yet provides the accuracy necessary to model such a complex environment. The probabilistic load model which is to be developed must not only be capable of simulating the loads of a generic engine but also be able to allocate accuracy dynamically, i.e. the user specifies the accuracy desired and the computer code provides results which satisfy this requirement.

The probabilistic load model must be capable of addressing two load types: individual and composite. Sources of individual loads include pressures, temperatures, acoustics, vibrations, and debris. The composite load model will require that a probabilistic 'synthesis' of the individual loads be made. In this program the composite loads will be obtained by the combination (based on deterministic information, simple rules or expert opinion) of the individual loads so that the probabilistic content of the individual loads is correctly contained in the composite load description.

This model is to be included in an expert system code which will use the results of the probabilistic analysis to predict what effect design changes or changes in the mission requirements will have on the overall loads as seen in a space propulsion engine. This further constrains the problem from a practical standpoint since the operation of an expert system would not be efficient or useful if each individual load analysis required significant computer time.

To develop a model which satisfies each of these qualitative constraints required that the first step to be taken was a survey of the available literature and an assessment of the techniques which could potentially be

useful in the probabilistic load model analysis. This section presents the results of this survey and assessment. The remainder of this section describes the following topics. First, a detailed quantitative description of the problem is given with an overview of the kinds of loads which need to be modeled. Next, a brief description of the probabilistic problem is given. The major probabilistic techniques which could be applied to the current analysis are given, and recommendations are made for the appropriate choice of probabilistic methods which should be used in the probabilistic load model development.

7.2 Probabilistic Load Model Requirements

Introduction. The types of loads which are seen in the space shuttle main engine (SSME) have been grouped into two broad categories: individual and composite. These categories were developed based on the physics of the engine operation rather than any mathematical concepts. However, as will be seen later, these categories can become confusing when some of the calculations are being made since some of the individual loads (in the physical sense) are obtained from calculations based on the measurement of other loads. For example, the high pressure fuel turbopump (HPFTP) discharge pressure, usually not directly measured, is obtained via computer analysis from other engine parameters, such as the power level, mixture ratio, inlet pressure, and so on. While this situation has been encountered early in the program, while the SSME is the primary focus, it is anticipated that the definition of the terms will be similar for all LOX type engines. Therefore, for clarity of the discussion throughout this report, the following definitions are made.

Individual Loads. The term individual load shall refer to those loads which are typically grouped together in engineering analysis and for which direct experimental measurements are available. For the probabilistic load model development, the individual loads will be limited to the following list, which may be modified as the program develops:

- temperatures
- temperature gradients
- gas pressures
- static loads (other than gas pressures)
- centrifugal forces (turbine blades only)
- periodic excitations
- structural dynamic excitations
- acoustic excitations
- impulsive excitations

Calculated Loads. The term calculated load shall refer to any of the individual loads which must be determined by the combination of two or more engine parameters, at least one of which has a random variable component. These loads are still individual loads but they have been separately identified for two reasons. First, the development of the probability density function (PDF's) for individual loads will be based on measurements and, therefore, will introduce only two sources of variability into the composite load calculation: the random behavior of the load and measurement error. Calculated loads will introduce a third source of variability, which in many instances cannot be quantified, which is due to modeling error. Secondly, the use of these calculated loads will involve a two-step process that requires the probabilistic model to be applied twice. In the first step, the individual load PDF is constructed from other individual loads and engine parameters (which are not loads). The second step requires combining these resulting distributions into the overall composite load signature. Therefore, while each of these load types are individual loads in the context of this program, the crucial distinction is that calculated loads involve the combination of non-load parameters and composite loads involve only the combination of individual loads.

Composite Loads. The term composite load shall refer to the combination of two or more individual (measured or calculated) loads which are of a like type, i.e. their units of measurement match in a physically meaningful manner. The composite load calculation provides the probabilistic time behavior of the engine loads. These composite loads are then combined

through a probabilistic "synthesis" into an overall load signature. This load signature is not a physical load, but rather is an indication of the state of the engine. This does not imply that an actual physical model is needed to accomplish this combination.

While these definitions seem almost trivial, their use will enable a clearer discussion of the available probabilistic methods to be made.
To best understand the requirements for the probabilistic load model it is worthwhile to review the random features of each type of load. The following discussions will briefly outline the type of data that can be expected for each type of load, as defined above, and what special concerns must be kept in mind when one is examining the type of probabilistic technique which can be used to model each of the load types. After this discussion, a summary will be given which highlights the special requirements of each load type in the selection of a probabilistic model. The features of the probabilistic models as they relate to the loads is examined in the following section.

Individual Loads. The key feature of the individual loads is that they only require a specification of the magnitude of the load, its probability of occurrence, and its frequency. For later analysis it will be necessary to define dependencies among variables, for example, does the variation in the vibration at the turbine blade depend on the current magnitude of the pressure. However, it is not necessary at this time to define these dependencies since they will not affect the type of probabilistic model to be used in a description of the individual load.

The best description of a random variable is provided by a probability density function (PDF). The determination of the individual variable's PDF can be done either by the replication of experiments, by fitting a standard PDF form to the available data, or by developing PDF's from expert opinion. The generation of the PDF can be made using standard statistical methods. These techniques have been programmed in a computer code for use in generating the generic PDF description of individual load variables. This program has been applied to selected measurements of the SSME to test its

applicability for this program. It has been found to work well and will be used to assist in developing the generic distributions for each individual load. Further explanations of this program are given in the following section.

In defining the probabilistic content of the individual load variables rarely occurring events are included in the PDF describing the variable. This is appropriate for these individual measurements since the effect of their inclusion will be to increase the 'tails' area of the distribution. However, when there are no direct measurements of the load, care must be taken in including such rarely occurring events since they can introduce a bias into the distribution (see below and later discussions). When direct measurements are made, the artificial shift of the PDF as discussed will not occur, since the measurements provide a direct reading of the true load distribution and no special precautions need to be taken.

The overriding question throughout the probabilistic load model development will be: Is the load stationary? Because of the importance of this topic the following definition is made.

Stationary Stochastic Process. For a stochastic process, [L(t)], of random variables L(t) where t is the index, the stochastic process is said to be stationary if all of the distributions of the random variable are invariant to a translation of the index origin.

Normally the index t represents a time increment and for this model development t will always represent time. In this case the load is stationary if it is invariant to a translation of the time origin, that is if the nature of the randomness of the load does not change with time. If the load is stationary then

$$L \stackrel{=}{=} L(t)$$

and the stochastic process is equivalent to a random variable. If the load is stationary then one only needs to specify the distributional type and its

parameters to have defined the individual load model. If the process is nonstationary then these parameters must be specified for each of the index values t, or their functional relationship to t must be defined. Once this is done, the probabilistic model for the individual load has been defined given that the current index (time) t is known.

Calculated Loads. The only relevant difference between calculated loads, denoted C, and the individual loads, L, is that the calculated loads must be calculated, i.e. they are not directly measured. Mathematically,

$$C(t) = V(L_1(t), \ldots, L_M(t), p_1(t), \ldots, p_N(t))$$

where V represents the functional relationship between the individual loads, L, and the other engine parameters, p_1 through p_N to the load which is desired, C. Therefore, once all of the individual loads and the basic engine variables have been probabilistically characterized then the next step is to identify an appropriate method for combining distributions.

The handling of rarely occurring loads for the case of calculated loads must be done in such a way that a bias is not introduced into the analysis. If the rarely occurring load is included in the data analysis of the steady state load, then the tails of this distribution will be changed since the load will add 'weight' to these values. This is undesirable for several reasons. First, and most importantly, by placing the transient load effect in the base load distribution the entire distribution is shifted, (although near the mean or modal values this shift will be slight) and therefore the distribution will have a bias introduced to it that is artificial. An example has been constructed to illustrate how this shift can occur.

An example. Assume that the steady state loading of a structure has been measured and is given by the data in Table 5. This data is plotted in Figure 22 in the form of a histogram. Also shown in Figure 22 is the Rayleigh distribution fit to this histogram as a solid line. If two additional points are added, which represents the transient data, as shown in Table 5 then the probability mass increases in the tails as pictured by

Table 5

Load Data For Example To Demonstrate Transient Bias

Base Load Interval	Number of Occurrences
10-18	5
18-26	12
26-34	17
34-46	20
46-52	18
52-58	16
58-66	13
66-74	9
74-82	5
82-98	3
98-122	1
Rarely occurring Data	
118	1
142	1

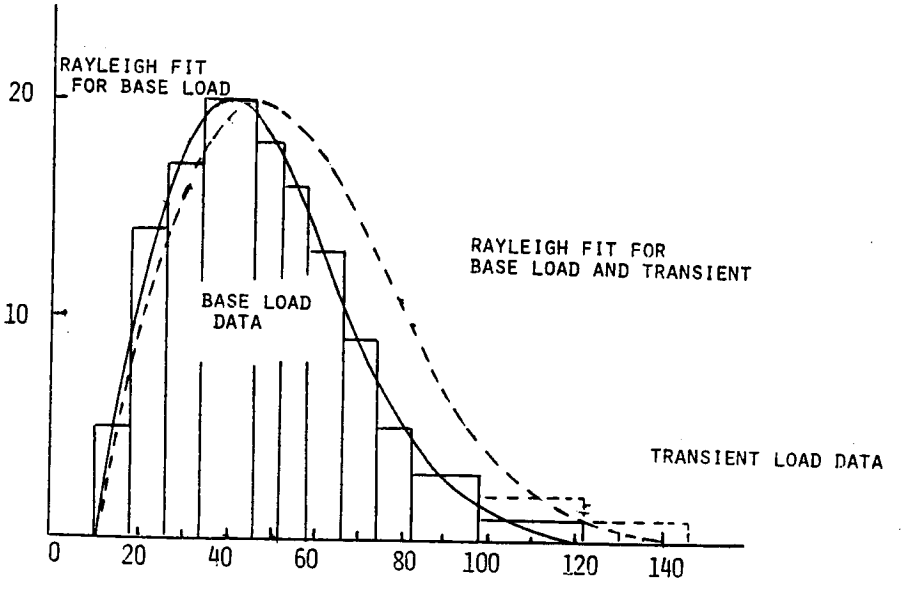

Figure 22 Bias Introduced by Transient Data Addition

the dashed lines on the histogram. The change in the Rayleigh distribution parameters has been calculated and are given in Table 6. As these values show the modal value of the Rayleigh distribution has been changed by approximately 17%. While this is not a large change it is significant and can lead to either overly conservative or nonconservative results.

There are other reasons for not wanting to include the rarely occurring data in the base load data base. If the rarely occurring data were included in the steady state data base then each time the frequency of occurrence changed the entire data analysis must be redone, not just the transient data analysis. Additionally, the amount of 'bookkeeping' that would need to be done would dramatically increase if such data were included with the steady state data base since a new distribution must be defined each time a portion of the mission history is entered in which a new transient is introduced. If a new distribution is not needed then probabilistic coefficients can be used to turn on or turn off the rarely occurring events. Therefore, for all of these reasons the rarely occurring load data base will be kept seperate from the steady state data base.

Table 6

Rayleigh Distribution Parameters

Parameter	Base Load	Base and Rarely occurring
Modal	40.0	46.86
Minimum	10.0	10.0

Composite Loads. The composite load and calculated load models are similar in the context of probabilistic modeling since they require the combination of two or more random variables. In the composite load case, there are no engine parameters that enter the modeling since these effects have all been included in the individual and calculated load modeling. Because many of the inputs to the composite load model will be the results of the calculated load analysis, it is important that the composite load model be capable of handling non-standard distributions, e.g. bimodal. This can severely limit the types of probabilistic techniques that can be used in the composite load analysis since some assume that the underlying distributions are one of the standard distributional types, e.g. gaussian (normal).

Rarely occurring loads for the composite model should be addressed in the same manner as the calculated load model discussed previously. The question of stationarity will also be of concern for the composite load analysis, just as in the individual and calculated load models.

Summary Of Probabilistic Load Model Requirements. The discussion for each of the three type of loads has indicated that the probabilistic model must satisfy several criterion in addition to the contractual requirements of the probabilistic load model: availability of numerical solution algorithms, ability to estimate reliability and confidence levels, and non-proprietary software availability. These additional criterion are:

(Unless specifically addressed, it will be assumed for the sake of simplicity in the discussion that the loads are stationary.)

Criterion 1. Distribution fitting capability must be available so that the individual load data can be properly represented by a PDF if that is required for subsequent analysis.

Criterion 2. Tests for stationarity must be available so that the appropriate methods can be employed for stationary loads. For nonstationary loads a bookkeeping method or a method for transforming nonstationary loads to stationary loads must be available.

Criterion 3. A method for including rarely occurring load events must be included in the overall model so that artificial bias is not introduced into the calculated and composite load description.

Criterion 4. The combination and dependencies among the various loads must be able to be performed efficiently since the overall probabilistic model must operate in the framework of an expert system code.

These are the requirements of the probabilistic load model which are imposed by the nature of the loads which are currently encountered in the SSME. It must be implicitly assumed throughout the model development that these criteria must be updated or changed whenever conditions unique to the SSME are controlling the selection of the probabilistic technique in order to insure that the probabilistic load model is generic to the maximum extent possible. The criteria developed above were used to screen the list of references presented in Appendix A. Many of the references in the Appendix, while developing sound mathematical foundations, use assumptions in obtaining the solutions to the load combination, or similar problem under study, that the applicability of the study was limited to a special class of loadings (e.g., normally distributed variations) or physical situations (e.g., stationary or time independent loads). In such instances, these models would not be appropriate for this program because of the need to address generic engines. Because it is difficult to anticipate what kinds of distributions (normal, bi-modal, and so on) will be included and how they behave probabilisticly (e.g. stationary versus non-stationary, dependent variables, etc.) models which severely restrict the range of application are less desirable than those that accept a wider variety of problems. Rather than providing a long list of references with a rationale for each as to whether or not it is acceptable for use in this program a composite description of those methods which are best able to satisfy the needs of this program is provided. The information obtained from the survey effort was screened according to the criteria established in this chapter. The results of this screening are discussed in the following section.

7.3 Probabilistic Methods Survey

Several probabilistic models emerged from the technical literature survey as viable methods for taking random combinations of various loads and forming a composite load at some point of interest. The models discussed, based on certain assumptions and boundary conditions, provide a means of producing probability functions for loads and load spectra for components of an engine like the SSME. Each method is adaptable to a probabilistic model which is governed both in terms of the specific piece of equipment being studied and in the context of some rule or law describing a physical load process. The remainder of this chapter describes the distribution fitting technique to be used for the individual load model, and the probabilistic methods found in the literature survey which are believed to be relevant to the current program. Finally, a recommendation for the methods to be used for the probabilistic load model is given.

Distribution Fitting Method. Given data (or a histogram summarizing data) generated by either N experimental tests or Monte Carlo simulations, the problem is to fit a suitable analytic distribution. For the purpose of illustration, formulas for three analytic distributions will be developed here: Normal, Lognormal, and Uniform. Formulas for additional distributional families are available, however, the inclusion of such formulas would only encumber the discussion. The basic fitting procedure is moment matching, though, in some cases, matching of percentiles works better. Let X be a random variable with a probability density (PDF) denoted f(X),

The moments of X are

$$\mu_i = E(X^i) = \int_{-\infty}^{\infty} X^i f(x)dX \qquad i = 1, 2, 3, \ldots$$

while the central moments are

$$m_i = E((X - \mu_1)^i) = \int_{-\infty}^{\infty} (x - \mu_1)^i f(x)dx, \quad i = 1, 2, 3, \ldots$$

Given a set of data X_1, X_2, ..., X_N, sample statistics furnishing estimates of the moments and central moments can be calculated by

$$\mu_i = \frac{1}{N} \sum_{j=1}^{N} X_j^i \qquad m_i = \frac{1}{N} \sum_{j=1}^{N} (X_j - \mu_1)^i$$

In fitting distributions to the data, it is sometimes necessary to shift the theoretical distribution by an amount Δ, i.e., to replace X by $X + \Delta$. The shifted density is $f(X - \Delta)$, but there is no change in the central moments. (But there is a shift in the mean.)

In choosing the distributional family to be used during the fitting procedure, higher order moments of the sample are used to guide the choice. The coefficient of skewness, b_1, and the coefficient of kurtosis, b_2, are defined as

$$b_1 = m_3 / (m_2)^{3/2}$$

$$b_2 = m_4 / (m_2)^2$$

Caution must be exercised in reading the literature because these definitions are not standardized. Skewness and kurtosis are dimensionless quantities, invariant under transformations of the form $cX + d$ where c is greater than zero.

The procedure for choosing the distributional family is to first estimate the skewness and kurtosis . The b_1 and b_2 points thus obtained are then plotted and the point (or line in case of the lognormal) closest to the theoretical is chosen as the correct family. For cases in which the (b_1, b_2) point is in between two distributional families, the choice is based on two statistical tests: Chi-square and the Kolmogorov-Smirnov test. A plot of the (b_1, b_2) pairs for several standard distributions is shown in Figure 23.

Probabilistic Analysis And Load Combination Models. Probabilistic analysis in general is a vast and growing field of mathematical study. It is not the purpose of this section to provide an overview of the area but rather to discuss probabilistic analysis in the context of load combination when those loads are stochastic processes. This discussion is of a qualitative nature and relates the desired qualities of the probabilistic method to the engine loads. To simplify this discussion it is assumed that there are two loads, L_1 and L_2, that are represented by the stochastic processes, $\pm L_1(t)x$ and $\pm L_2(t)x$, over the time interval [0, T]. Since the indices for both these processes are the same the shorter notation $\pm L_1 x$ and $\pm L_2 x$ can be used. The basic load combination problem can be stated as: What is the probability that the process

$$\pm L(t)x = \pm L_1(t)x + \pm L_2(t)x$$

exceeds a value larger than B(t) during the reference period?
This probability is given by:

$$P[\max(L(t)) > B(t),\ 0 \leq t \leq T] = P[L(0) > B(0)] + P_U \qquad (1)$$

where P_U is the conditional probability that there is one or more upcrossings of B(t) given that L(0) is less than B(0).

In order to calculate the probability given by equation (1) barrier crossing methods are employed. To obtain such formulas it is necessary to perform multiple integrations of the product of the joint density function of the load process and its derivative process, denoted L'(t). If the probability of L(0) exceeding B(0) is much less than the product of the probability of one or more upcrossings of a fixed load level and the time interval T and this product is much less than one then this probability
can be well approximated by

$$F_L(B^*) \doteq 1.0 - T \cdot \int_{\dot{x}=0}^{\infty} \dot{x} \int_{x_1=-\infty}^{\infty} \int_{\dot{x}_1=-\infty}^{\infty} f_{x_1 \dot{x}_1}(x_1, \dot{x}_1) f_{x_2 \dot{x}_2}(B^* - x_1, \dot{x} - \dot{x}_1)\, d\dot{x}_1\, dx_1\, d\dot{x}$$

where x represents the derivative process. This derivation is given in Thoft-Christensen and Baker. Because this is such a complex formula no

analytic solution exists for this equation for an arbitrary joint density function. In addition it must be recalled that this formula is only applicable for the case in which there are two loads - if there are three or more the complexity increases dramatically.

To deal with such complex modeling it is necessary to introduce some simplifying assumptions if one wishes to have an analytic formulation for dealing with this situation. Perhaps the most well known of the load combination models which are of this type is the Ferry Borges-Castanheta model. One of the major drawbacks to the use of this model is that it must be assumed that the loads are independent. In such a situation rectangular pulses are used to represent the fluctuations of the loads and an approximation to the probability that a load exceeds a prescribed level can be determined. If the load level of interest is a function of time, B(t), rather than a fixed value, B*, then the load combination model must be applied at every time step and the error can increase with an increase in the index for time if the current level has any history dependence. In actual calculations these types of models are only reasonable in bounding calculations because of their approximate nature.

Analytic approximations to the solution, such as fast probability integrator (FPI) methods, are capable of dealing with more complex probability density functions (PDF's) but suffer from the drawback that they must be reapplied if the process is nonstationary or if the load level is varying with time. The actual benefit of the FPI technique is lost in many instances in which the load level of interest changes rapidly since these techniques require an approximation to the true PDF near the level of interest. If this level B(t) is changing rapidly very small time steps may be required in order to accurately represent the probability of exceeding this level. Of course, since the FPI method must be reapplied each time a new load level is desired even if the time index remains the same then this method can become not only inaccurate but slow in its prediction of the probability of exceeding the specified range of load levels.

The use of simulation techniques bypasses almost all of these problems. When a simulation method is used the entire distribution of the desired load is obtained. By grouping these results into a histogram form it is possible to obtain the output of any level being exceeded. Of course the drawback to simulation methods is their cost. Thus, it is critical to have defined the problem which one wishes to solve in order to rationally select the appropriate type of probabilistic method upon which to build a model.

There are two problems which are of importance in probabilistic modeling:

Problem 1 The probability of a stochastic process or random variable exceeding a specified, fixed level is desired.

Problem 2 The probability of a stochastic process or random variable exceeding any, arbitrary level is desired.

Problems of type 1 are best handled by barrier crossing or FPI methods. Type 2 problems are best addressed by simulation methods. Since this program is to develop a probabilistic model which will be used in an expert system set of computer programs to predict the load in space propulsion units it is a type 2 problem being studied. Thus, simulation techniques are the preferred methods. Barrier crossing techniques will be employed to provide bounding calculations. Such bounding analysis can then be used in the expert system model to determine if further analysis is required by the more time consuming simulation techniques.

The current data being generated from the test stands and mission history profiles of the SSME indicate that many of the load variables are non-stationary - i.e. the mean, variance, and/or autocovariances of the load process are time dependent. These type of processes are inherently difficult and expensive to model. The final probabilistic load model must have some method for dealing with these processes so that the final model can be used in an expert system type analysis.

While the simulation techniques will form the basis for the probabilistic model, some cases may call for faster solution algorithms even if it implies a reduction in the accuracy. The use of FPI methods may be useful for screening calculations (for example if the probability of a load coincidence

is very low that part of the calculation may be bypassed without significant loss in accuracy) or in the composite load model development. In addition, if the Monte Carlo analysis must be used to obtain the desired accuracy then it is worthwhile to have a Markov chain model available for sensitivity studies so that a costly Monte Carlo analysis can be replaced by a Markov analysis. Thus, not only are the Monte Carlo, DPD, and barrier crossing analysis methods planned for the probabilistic load construction but also the FPI and the Markov chain models will be available.

The literature surveyed during this task produced additional techniques which are not planned to be used in the load model. These techniques are not discussed any further here since they are not believed to be capable of adding any additional capability to the probabilistic load model that cannot be obtained from the methods previously listed. However, for the sake of completeness, references which are believed to be relevant to the program but not directly used are abstracted in Appendix A. The following section describes in more detail each of the probabilistic methods which are to be included in the final probabilistic load model.

Relevant Probabilistic Analysis Methods From The Literature Survey. The results of the literature survey produced six major techniques which have promise for the development of a probabilistic load model: Monte Carlo, Markov Chain, Barrier Crossing, Limit State, Discrete Probability Distribution, and Response Envelopes. Each of these methods is briefly described below. Appendix A contains the summaries of relevant literature as well as a bibliography of general sources for this material. The discussions provided below will form the basis for the recommendations for the probabilistic methods to be used for the load model development.

Monte Carlo. The Monte Carlo technique is a method for solving problems by constructing for each problem a random process. This random process is devised in such a way that parameters and quantities of interest may be calculated from random samples from a given distribution. In effect, it is simply a method for adding a probabilistic structure to a deterministic model.

As an example, consider a specific piece of equipment in the SSME. Suppose the composite load, denoted by $L_c(t)$, is related to the individual load $L_i(t)$, by a general function

$$L_c(t) = f(L_1(t), L_2(t), \ldots, L_n(t))$$

Consider, for instance, $L_c(t)$ for the turbine blades where the $L_i(t)$ are loads due to the effects of temperature, pressure, vibrational modes, and so forth. If each individual load has been characterized by a probability distribution function (PDF), then the following procedure is used during a Monte Carlo simulation:

1. The cumulative distribution function (CDF) of each individual load is generated by integrating the PDF.

2. Invert the CDF.

3. Generate a random number, r_1, between the values of 0 and 1.

4. Let $F(L_j(t_1))$ represent cumulative probability of realizing a load $L_j(t_1)$ at time step t_1. From the inverted CDF, the value of $L_j(t_1)$ is uniquely determined, where $F(L_j(t)) = r_1$.

5. Let N be the total number of individual loads. Let M be the total number of time steps, ti. Repeat Steps 3 and 4 for each $L_j(t_i) : 1 \leq j \leq N$, for a given t_i. A value of $L_c(t_i)$, where

$$L_c(t_i) = f(L_1(t_i), L_2(t_i), \ldots, L_N(t_i))$$

is calculated. The entire process is repeated until the number of times steps exceeds M (or insufficient computer time terminates execution.

The result is an M-dimensional vector of composite loads: ($L_c(t)$, $L_c(2)$, ..., $L_c(M)$). This vector is used to construct a histogram of the composite load. This histogram can now be analyzed statistically to obtain estimates of the mean, kurtosis, probability of the load being exceeded, and so on. By the law of large numbers, the vector described above approaches the continuous distribution in the limit as M tends to infinity. In order to achieve accurate results, however, the value of M must be so large that alternate sampling schemes must be utilized.

The Monte Carlo technique has been included in the probabilistic methods for the load model construction because of the accuracy which can be obtained from the model. Classical statitical estimates of the confidence level can be obtained. If the N responses calculated by the Monte Carlo simulation method are ordered from smallest to largest then the αth percentile of the load can be bounded by

$$L_u = INT[N\alpha + \Phi\,(0.5(1+\beta))(N\alpha(1-\alpha))^{1/2}]+1$$
$$L_L = INT[N\alpha - \Phi\,(0.5(1+\beta))(N\alpha(1-\alpha))^{1/2}]+1$$

where α is in fractional form, Φ is the cumulative distribution function of the standard normal variable, INT[...] is the truncated integer part of a real number and β is the desired confidence level. For example, if β is equal to 95% then

$$L_u = INT[N\alpha + 0.83525(N\alpha(1-\alpha))^{1/2}]+1$$
$$L_L = INT[N\alpha - 0.83525(N\alpha(1-\alpha))^{1/2}]+1$$

The major disadvantage to the Monte Carlo method is the cost. Because it is a 'brute force' method, the number of simulations which must be performed to estimate low probability loads grows very quickly. While there are methods available for estimating with greater confidence, these low probability events for relatively low values of N (for example, importance or stratified sampling methods) the accuracy must necessarily decrease elsewhere. Thus, if the entire range of loads must be determined, then importance sampling methods are not very useful.

Markov Chains. In contrast to the Monte Carlo technique, the Markov chain method is a deterministic model based on given initial conditions. Loads are defined by discrete states with time measured by duty cycles. During the course of the calculation, the Markov assumption is made, i.e., the probability that the load which is currently in state i will be in state j in the next duty cycle is only dependent on its present state and not on the previous load history. Consider

$$t = 0, 1, 2, 3, \ldots\ldots$$

which need not be of equal duration. The load is defined by variable states

$$L = 0, 1, 2, \ldots, N$$

where L = 0 implies no load and L = N may be defined as the limit state. The initial distribution of the loads is defined by

$$I = (i_1, i_2, \ldots, i_n)$$

where, for instance, $i_1 = 3$ means the load labeled number 1 is in state three. The transition probabilities, Pij, are defined as the probability that given the load is currently in state i, it will exist in state j after the next duty cycle. The evolution of the load process is given by

$$P_t = IM^T$$

where

M = matrix of transition probabilities P_{ij}

T = number of duty cycles during the elapse of time t.

$P_t = (P_t(1), P_t(2), \ldots, P_t(N))$, PDF of loads at time t.

Using the Markov assumption, an upper bound on the mean lifetime of the system may be obtained. Denote by $q_i(t)$ the probability that in time t the system passes from the state i into one of the absorbing states. It can be shown that in the case of the SSME there exists a value $t = t_o$ such that for all i we have $q_i(t_o) > 0$. This implies that every state in the system, with nonzero probability, can pass into an absorbing state in time t_o.

In order to represent the nonlinear load time dependency in the composite load spectra, however, some modification to the Markov model would be necessary. Such modifications may include such items as

1. More parameters added to the definition of the load state so that history dependencies are included in the present state of the system.

2. Use of a multiple Markov Chain model. Here, the future states of the system are allowed to depend not only on the present state but on a fixed number of past states.

In addition, there is ongoing research in the use of Martingales for incorporating time dependencies in the general Markov model. Finally, there has been work done in refining the Markovian approximation of the amplitude response of an oscillator to a random excitation with an evolutionary broad-band power spectrum.

The Markov model provides the advantage that complex systems can be represented by a mathematical model which is linear and involves only matrix multiplaction. Of course, the major disadvantage is that some of the load processes are not Markovian processes and thus, this model is not generally applicable. It does have the ability to act as an inexpensive sensitivity analysis method when Monte Carlo analysis is performed. If the Markov model is used in this way, then the transition probabilities are calculated during the initial Monte Carlo analysis. Subsequently, the Markov model can be used to determin the load's sensitivity to changes in the initial conditions.

Limit State Methods.[5] The limit state model is an approximate analytic solution to the probabilistic modeling of composite load spectra, since it used a fast probability integration technique. It computes the probability of failure for a component whose design factors are modelled as random variables. The basic goal of this type of probabilistic model is to calculate, or at least bound, the probability that a level or barrier is

[5] Also known as fast probability integrator methods

exceeded or that the limit state (a surface in the multi-dimensional sense) is entered. To examine how various rules or models are used, an example with the individual component load effects are represented by $L_1(t)$, $L_2(t)$, ..., $L_N(t)$ is used. Assume that the probability of failure, denoted P_F, is desired. The limit state condition can be written as

$$q(RQ) = R - Q$$

where R is the measure of the structural strength, and Q is the measure of the combined load. The limit state probability P_F can be determined as

$$P_F = P(R < Q) = \int F_R(x) f_Q(x) dx = \int [1 - F_Q(x)] f_R(x) dx$$

provided the cumulative distribution functions (CDF) $F_R(x)$ and $F_Q(x)$, respectively, of R and Q and the corresponding probability density function (PDF) $f_R(x)$ and to $f_Q(x)$ are obtained. It should be noted that if more than one of the component loads $L_i(t)$ must be regarded as a random (stochastic) process rather than a random variable, then the calculation of $F_Q(x)$ becomes difficult. Therefore, for this discussion, assume that only one of the $L_i(t)$, say $L_N(t)$, is truly a random process, while all others are random variables. Then finding the distribution of $F_{QT}(x)$ is equivalent to either the problem of evaluating the probability that the random process $Y_N(t)$ will exceed a specified level $x(> 0)$ in a given time interval $[0, T]$ or to the problem of deriving the CDF $F_T(t)$ of the time T at which the process crosses the level for the first time and from below. The first problem is referred to as a level crossing problem while the latter is a first passage time problem. Clearly,

$$F_{QT}(X) = 1 - F_T(T).$$

Therefore, once the CDF of Q_T is found, the limit state probability, i.e., the probability of failure, can be determined.

Due to the nonlinear behavior of the loads in the SSME, however, fast integration techniques can only be used for estimating limit state probabilities. In these instances, no exact solutions are available for first excursion probabilities such as those outlined above.

Additional accuracy can be obtained through the use of response surface methods: a statistically based tool for obtaining a polynomial approximation to a complex function.

Barrier Crossing Computations. The barrier crossing method provides a quick and relatively simple method for estimating the probability that a random variable exceeds a specified value, commonly called a barrier or limit state. The basic concept of the barrier crossing technique has been derived for normally distributed random variables and is discussed in Thoft-Christensen and Baker. This technique has been extended by Battelle to include non-normally distributed variables by a moment transformation technique. In order to compute the probability of a specified load level, i.e. barrier, being exceeded the process must be described by the proper peak distribution function, characterized by the parameter, α,

$$\alpha = \frac{\text{expected number of mean crossings}}{\text{expected number of peaks}}$$

In the case of a stationary process with zero mean, it can be shown that the general expression of the density function, $f(\delta)$, for the peak magnitude with barrier δ is given by

$$f(\delta) = \frac{1}{\sqrt{2\pi}} \frac{\sqrt{1-\alpha^2}}{\sigma_x} e^{\frac{-\delta^2}{2\sigma_x^2(1-\alpha^2)}}$$

$$+ \frac{\alpha\delta}{2\sigma_x^2}\left[1+\text{erf}\left(\frac{\delta}{\sigma_x}\left(\frac{2}{\alpha^2}-2\right)^{\frac{1}{2}}\right)\right] e^{\frac{-\delta^2}{2\sigma_x^2}}$$

where erf denotes the error function. This function can be adapted for the situation in which the mean is not zero. The adaptation itself involves a transformation of variables in the above expression specific to the type of distribution being modeled. These transformations have been derived and are currently incorporated into the model.

Recall that the goal is to predict the response of a probabilistic function with inputs for the load levels and its associated probability of occurrence. Therefore, it is necessary to compute the probability that a peak value, δ, exceeds the specified barrier, δ_p. To perform this calculation it is necessary to integrate equation (2) from the barrier level to infinity. Due to the complex form of equation (2) not all of the terms can be integrated analytically. However, a solution to this equation has been developed at Battelle which involves partial sums of an infinite series expansion of the equation. In the case where the number of summation terms necessary to obtain convergence becomes large a numerical integration using a variable time step Simpson integration can be used.

The derivation of the method for obtaining the cumulative distribution function for the peak distribution has been based on the assumption that the underlying process is stationary. Some of the other available techniques also make this assumption. Therefore, the next topic discussed is a method for transforming a non-stationary process into a stationary process.

Non-stationary Process Transform. A non-stationary process is one in which the mean, variance, and autocovariances of the process are time dependent. These types of processes are inherently difficult and expensive to model. In particular, portions of the SSME mission history have variable responses, such as the high pressure fuel pump speed and the main injection chamber pressure, which exhibit non-stationary behavior. An investigation has been conducted into transforming such a non-stationary process into a stationary process where the mean, variance, and autocovariances are invariant under time translations.

The non-stationary behavior found in the SSME data falls into the category which is known as homogeneous non-stationary. These are processes where the observations are described by random trends where, apart from local level and/or local trend, one part of the spectrum behaves like the others.

Mean Stabilizing Transformations: It has been shown that homogeneous non-stationary sequences can be transformed into stationary sequences by taking successive differences of the discrete spectrum.
Thus, let

$$[X(t):t \in T]$$

be a non-stationary stochastic process where T is the index set for the time period of interest. The transformation is performed by considering the series $\Delta x(t)$, $\Delta^2 x(t), \ldots$ where
Δ is the difference operator,

$$\Delta = 1-B \quad .$$

B is called the backshift operator given by $Bx(t) = (x(t-1))$, and in general $B^m x(t) = x(t-m)$. The difference method can be employed with three trend models.

Model 1: The first model is the deterministic trend model

$$X(t) = \beta_0 + \beta_1 t + a_t$$

where a_t is a zero-mean stationary process. In this model,
$\mu_t = E(x(t)) = \beta_0 + \beta_1 t$ increases as a linear function of time.

Model 2: The second model involved the first differences of the series and a constant trend parameter β_1. It is given by

$$(1-B)\ x\ (t) = \beta_1 + a_t$$

Model two also leads to a linear trend. The conditional expectation of x(t) given x(t-1), x(t-2), ... is $\mu_t = x(t-1) + \beta_1$. In this case, the level depends on the constant slope parameter β_1 and the previous observation x(t-1). The trend changes stochastically since x(t-1) is subject to random shocks.

Model 3: The third model involves the second differences of the data

$$(1-B)^2\ x\ (t) = a_t$$

where

$$x(t) = 2x(t-1) - x(t-2) + a_t$$

Since X(t-1) and x(t-2) in the level $\mu_t = 2x(t-1) - x(t-2)$ are subject to random shocks, both the intercept and the slope of the trend, which passes through x(t-1) and x(t-2), change stochastically, Figure 24 illustrates the general behavior of each model. Model 1 is characterized by a deterministic trend, models two and three by stochastic trends.

Note that in model two only the intercept in the trend model is subject to change, whereas in model three the slope parameter also varies randomly.

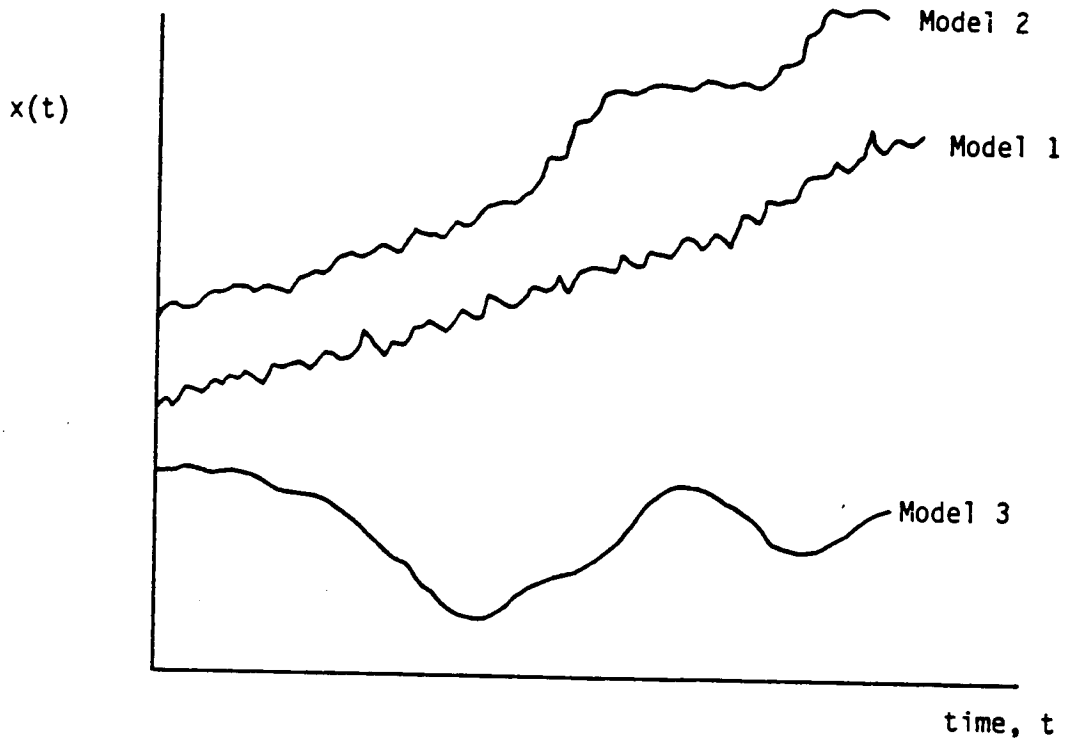

Figure 24 Sample Paths for Three Non-Stationary Processes

Variance - Stabilizing Transformations. The variance, as well as the mean, may exhibit a time dependent behavior. Many times the variation in the data increases with the level. In these cases it is necessary to use transformations to stabilize the variance.

In its most general form, the regression model can be written as

$$y_t = f(X_t; \beta) + \varepsilon_t$$

where $f(x_t; \beta)$ is a function of the p independent variables $x(t) = [x(t_1),\ldots,x(t_p)]$ and unknown parameters $\beta = [\beta_1,\ldots, \beta_m]$. ε_t is the associated error term. Let

$$y_t = f(x_t; \beta) + \varepsilon_t = n_t + \varepsilon_t$$

where

$$f(x_t; \beta) = n_t.$$

Assume that the variance of the errors is related to the mean level n_t by

$$V(y_t) - V(\varepsilon t) = h^2(n_t)\,\sigma^2$$

where h is some unknown function. The goal is to find a transformation of the data $g(y_t)$ that will stabilize the variance.

Expand $g(y_t)$ in a first-order Taylor series around n_t:

$$g(y_t) \simeq g(n_t) + (y_t - n_t)\, g'(n_t) \quad .$$

The variance of the transformed variable can then be approximated as

$$V[g(y_t)] = [g'(n_t)]^2[h(n_t)]^2\,\sigma^2 \quad .$$

Thus, in order to stabilize the variance, $g(y_t)$ must be chosen so that

$$g'(n_t) = \frac{1}{h(n_t)}$$

Thus, a knowledge of the functional relationship between the variance and the level provides the needed transformation function.

Discrete Probability Distribution Method. Discrete Probability Distributions (DPD's) are a tool in risk analysis to simplify the computations necessary to determine failure probabilities. DPD's may be used to investigate probabilistic functions, i.e., functions whose exact form is uncertain, and the calculation of quantities where there is significant uncertainty in the numerical values of the parameters. It follows, then, in these calculations, numerical quantities should be replaced by probability distributions and mathematical operations between these quantities should be replaced by analogous operations between probability distributions.

Suppose the initial values of the loads are discretized into M values. Each value of each variable is then assigned a probability of occurrence. Additionally, the various forms of any probabilistic function are assigned a probability of being correct. If these discrete values are paired with their probabilities, the following vectors of ordered pairs result for two loads X and Y:

$$X = (X_1, p_1), (X_2, p_2), \ldots, (X_m, p_m))$$
$$Y = (Y_1, q_1), (Y_1, q_2), \ldots, (Y_m, q_m)).$$

The number of discrete points in each of these vectors has been chosen to be the same, although it is not necessary to do so. The additional of two discrete vectors is defined by

$$Z = Y + X$$
$$Z = (Y_i, p_i) + (X_j, q_j), \text{ and}$$
$$Z = (X_j + Y_i, P_i * q_j) \text{ for all i and j.}$$

Therefore, the addition of two vectors containing m ordered pairs each results in a vector which has m^2 ordered pairs. The multiplication of DPD's is similarly defined:

$$Z = X * Y$$
$$Z = [X_j * Y_i, p_i * q_j)] \text{ for all i and j}$$

For the combination of a large number of loads, the amount of computer storage increases very quickly. If there are k loads, each described by M discrete points, then the vector will contain M^k ordered pairs. Since, even for relatively small values of M and K (on the order of 20), the computer storage capability will quickly be exceeded, it is necessary to examine some procedure for reducing this vector's size. This leads to the introduction of a condensation or aggregation procedure.

The condensation operation must preserve the total probability and mean within each vector, while ensuring that the residual error afterwards is as small as possible.

The DPD method provides accuracy close to the Monte Carlo method in less computational time. In addition, if a given region of the input variable's range needs to be examined more accurately, the DPD method provides a means for doing so by input rather than requiring coding changes. The DPD method does not provide any way to estimate the confidence level of the result such as is available with the Monte Carlo analysis. However, the true result can be approached asymptotically by increasing the number of data points used in the individual DPD's.

Response Envelopes. Response envelope statistics is a method for determining the nonstationary response statistics of randomly excited nonlinear second-order systems. This method is an improvement over the first crossing methods and up crossing techniques. Consider, for example, a random variable which reflects whether the present load in a structure is below or exceeds a specified level called a barrier. Then the response envelope is the most direct method for providing information on the following items.

1. Determine the expected time at which the barrier is reached (barrier and first crossing).
2. Determine the probability that the barrier is exceeded (upcrossing).
3. Describe the buildup of the response.
4. Determine the maximum response which will be obtained for a given duration of excitation.

The mathematical foundation for this method is rather advanced and will not be provided here. It has one constraint in that it is applicable only to lightly damped weakly nonlinear systems.

Summary and Recommendations of Probabilistic Loads Survey. The five methods described above are the ones which are believed to be the most promising for fulfilling the criteria and requirements of the probabilistic load model. As the bibliography in Appendix A shows there are a variety of other investigations which deal with the combination of random and randomly occurring loads. However, most of the other methods are very mathematical in nature and either require or use many assumptions about the load types or distributions. In the development of a generic probabilistic load model it is necessary to limit the number of assumptions so that the widest possible spectrum of load types can be handled by the model.

Based on the discussion previously made the following recommendations for the probabilistic methods are made.

Individual Load Model	Distribution fitting method based on skewness-kurtosis plots.
	Barrier crossing methods.
Calculated Load Model	Barrier crossing method
	Discrete probability distribution
	Monte Carlo
Composite Load Model	Barrier crossing method
	Discrete probability distribution
	Monte Carlo

The selection of the distribution fitting scheme based on the skewness-kurtosis plots is made because it is believed to be more important to select the family of the distribution based on the shape of the data than by simply matching moments. While it is true that the use of such a distribution fitting scheme will sometimes lead to slightly higher values for Chi-square than if a simple moment matching scheme is used the difference is slight and the overall shape of the data is better represented. In addition, there is a software program available that has been linked to other probabilistic analysis programs. An example of such an analysis is given in the following section.

Barrier crossing methods were selected over the fast probability integrator (FPI) techniques because they are simpler. For non-standard distributions (bimodal) the barrier crossing methods are faster, albeit less accurate, than the FPI methods and only need a single parameter, the ratio of mean crossings to peak values, to provide an estimate of the probability. Again this method is available in a software package at Battelle. The FPI model of Wirsching is also available and can be used if the results of the barrier crossing method prove to be too gross of an approximation to the true results.

The discrete probability method has also been selected because it is a relatively fast and accurate method for combining two or more random variables. The method is also available at Battelle.

Finally, the Monte Carlo method will be used to accurately approximate the true integral of the joint probabilities. Since in almost all cases that will be examined by the probabilistic load model no analytic solution will be available the Monte Carlo method will be the only means available for validating some of the load models. This is sufficient reason to include this technique in the overall probabilistic model.

7.4 Probabilistic Methods - Sample Calculations

The development of a generic probabilistic load (GPL) model requires the integration of many facets of statistical and deterministic analysis. Because the ultimate model must be generic in nature the generic probabilistic load model must be capable of addressing several important types of stochastic behavior including nonstationarity, physical dependence, and rarely on (transient) behavior. This discussion focuses on the development of the generic probabilistic load model in the context of combined loads (as opposed to composite loads) to address the topic of physical dependency. To review the definitions of these loads, by combined loads it is meant that the individual load variable currently being analyzed

has not been directly measured but is rather derived from expert opinion, calculations, or both. This is in contrast to the composite load which is a load that is the combination of two or more loads.

To illustrate the important features of the calculation model a simplified example has been constructed to illustrate these features. The example is based on the type of analysis which will be performed for the final model but is not meant to represent the absolute value of the physical numbers, or distribution of numbers expected in the actual analysis. It is believed that the use of such an example will clearly illustrate the requirements of the probabilistic techniques without adding the complexity of the nonstandard distributional shapes which can be seen in some of the data.

The following section briefly describes the physical model to be used in the example, after which the results of a sample probabilistic calculation will be described to illustrate the probabilistic concepts introduced earlier.

Physical Model. The physical model used in these calculations relates turbine inlet and outlet pressures and temperatures to the mass flow rate and the power level and mass flow rate to the turbine speed.

The following equations are used in this study:

$$M_f = I_1(P_L).P_o/T + I_2(P_L).P_2/T \qquad (1)$$

$$S_T = I_3(P_L).M_f + I_4(P_L).P_L^2 \qquad (2)$$

where

M_f: mass flow rate
P_L: power level
P_o: turbine outlet pressure
P_i: turbine inlet pressure
T_o: turbine outlet temperature
T_i: turbine inlet temperature
S_T: turbine speed
I_j: influence coefficients for j=1,2,3,4

In determining the influence coefficients expert opinion or computer codes are employed. Ultimately, these coefficients will be expanded to include transient terms, nonstationary processes, and so forth. These coefficients will then be driven by the expert system to set the values of the Ij's or to turn on or off additional terms. However, this discussion is limited to the available probabilistic analysis methods and therefore no further examination of the interfacing of the expert system and the probabilistic model is undertaken at this time.

In equations (1) and (2) there are five independent inputs and two dependent variables being calculated. It is assumed for this example that the five independent variables have been statistically characterized by data analysis. In the actual model turbine inlet and outlet conditions will most likely have to be calculated, however, they are assumed to be measured quantities for this example. The mass flow rate is a dependent variable because it is calculated from an influence equation but it is also an input to the influence function for the calculation of the turbine speed. Therefore if the model can handle this set of equations then it should be straightforward to generalize to the case when there are multiple dependent variable inputs to an influence function.

The distributional type and associated parameters are shown in Table 7 for each of the independent variables. These values were input to the probabilistic model to determine the distribution of the mass flow rate and turbine pump speed. The results of these calculations are contained in the next section.

Table 7 Statistical Parameters For The Five Independent Variables

Variable	Distributional	Parameter 1[1]	Parameter 2[1]
P_i	Uniform	6950	7050
T_o	Normal	1500	30
P_o	Uniform (30%)	4980	5020
	Normal (70%)	5060	10
T_i	Rayleigh	50	100
P_L	Uniform	.650	.007

[1]For the uniform distribution parameter 1 is the lower bound and parameter 2 is the upper bound, while for the normal distribution it is the mean and standard deviation, respectively, and for the Rayleigh they are the minimum and the modal, respectively.

Sample Calculations. The example calculations using equations (1) and (2) must first have the random nature of the five variables included. To keep the example straightforward it is assumed that the only time at which the analysis is to be performed is for the steady state 65% power level. Therefore, no dependency of the influence coefficients, I_j's, on the power level is included in the current calculations.

The first calculation is performed with the discrete probability distribution (DPD) method. In this calculation fifty discrete intervals were used to obtain a high degree of accuracy. The two response variables, mass flow rate and turbine shaft speed, were also calculated using fifty discrete points.

Table 8 summarizes the results of these calculations for both of the response variables, and Figure 25 furnishes a sample histogram of the mass flow rate. This information will provide the basic probabilistic load model for individual loads at its greatest level of sophistication.

The Inclusion Of Transient Data In The Current Load Model. To handle the transient data a change is made to the COMBIN routine in the generic probabilistic load model. Given that transient, L_i, occurs with a frequency, f_i, then the steady state load is changed, on the average by:

$$B_j = B_j + f_1 . L_1 + \ldots + f_K . L_k$$

where there are K transients. The transient loads could also be given by a distribution, i.e. they are also random variables rather than the fixed values L_i, in which case they are handled as are all other variables except they are normalized by their frequency of occurrence.

Table 8 Results of DPD Calculations for the Mass Flow Rate And Turbine Shaft Speed

Percentile	Mass Flow Rate Value	Turbine Shaft Speed Value
5	177	28,450
10	193	31,050
50	240	38,000
90	271	42,310
95	277	

Here a transient load has been added to the mass flow rate that occurs 5% of the time and is normally distributed with a mean value of 260 and a standard deviation of 10. The same example that was discussed previously was run with the transient analysis added. Because of the infrequent occurrence of this load no significant effect on the mean value is seen, however, there is a second 'bump' in the probability density function which is developing in the tails of the distribution as shown by the data and dramatically seen in the histogram plot, Figure 26.

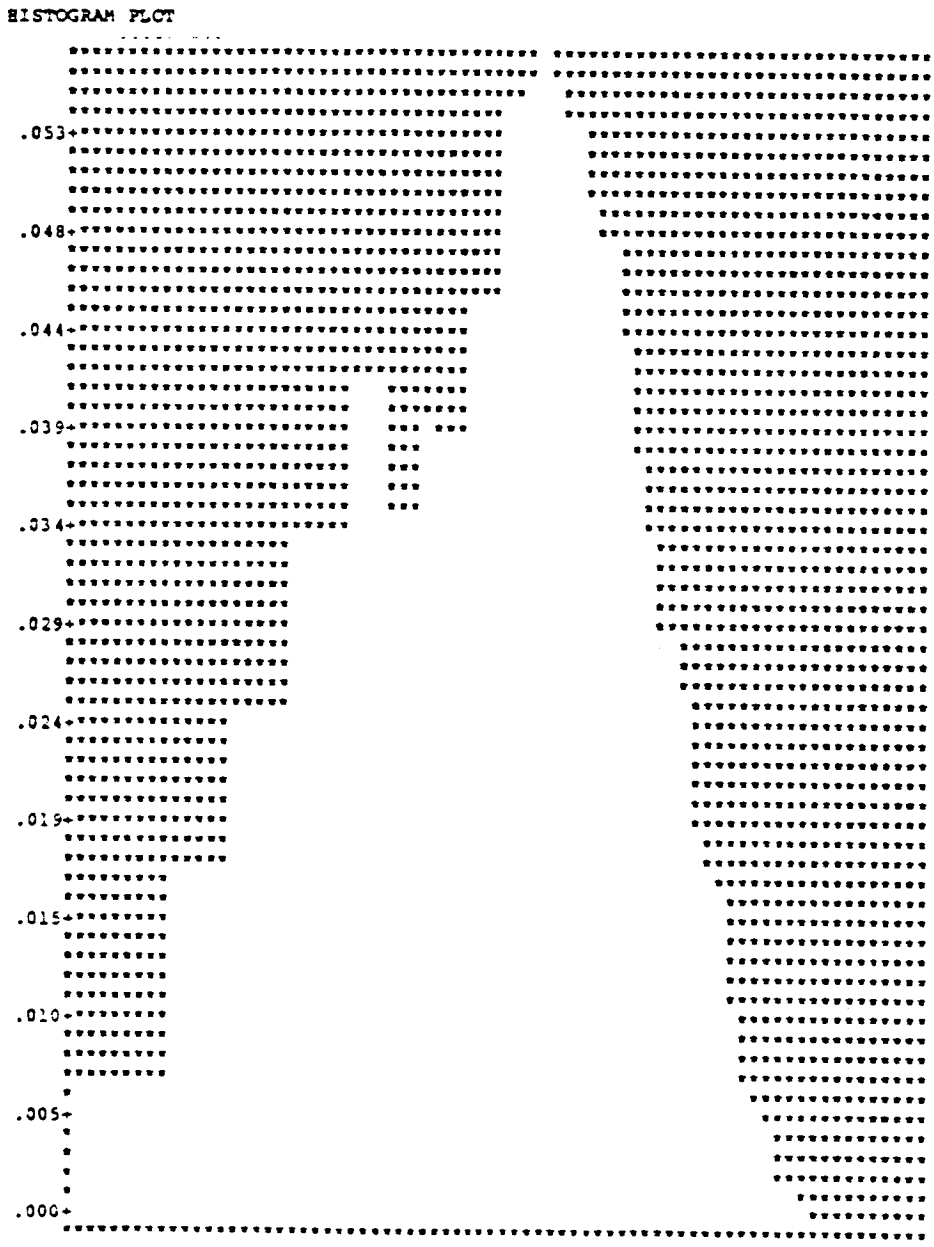

Mass Flow Rate

Figure 25 Histograms of Response Variables

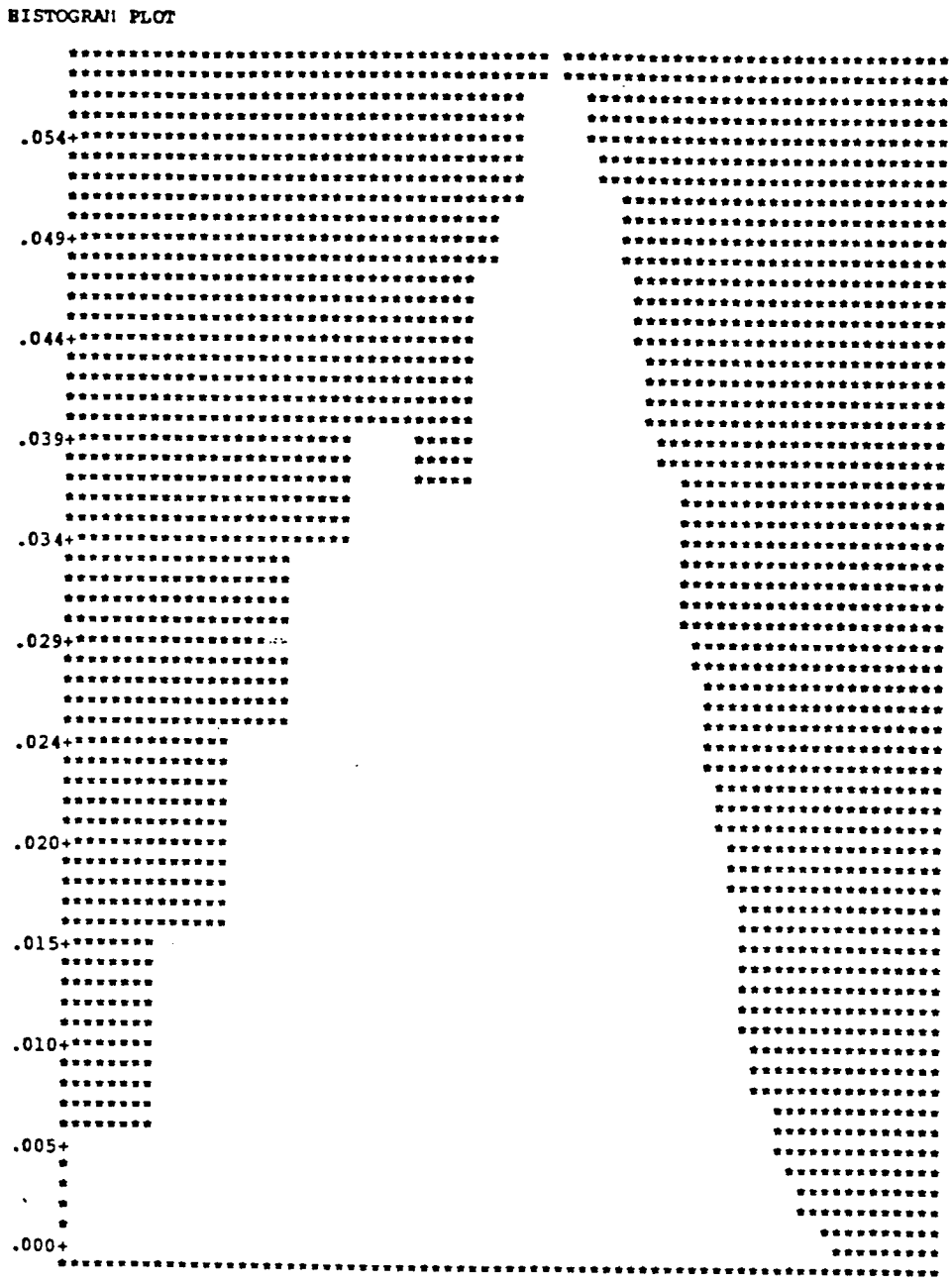

Turbine Shaft Speed

Figure 25 (contd.) Histograms of Response Variables

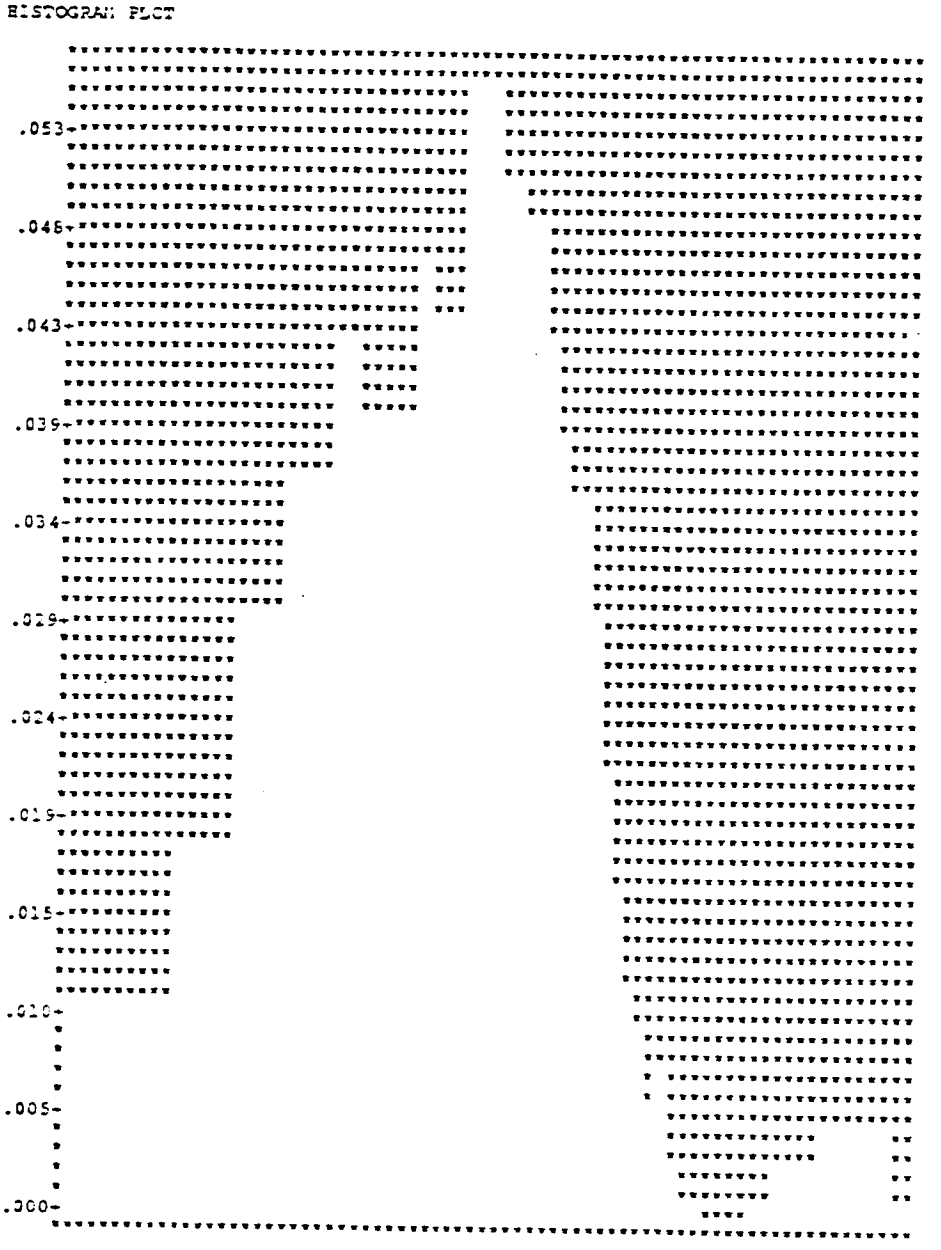

Figure 26 Turbine Shaft Speed with Transient Added

7.5 Summary

The literature of available probabilistic methods for developing a probabilistic load model for the space shuttle main engine has been reviewed and an assessment of the ability of each method to perform the task required for such a complex environment has been made. There are four important considerations in the development of this model: (1) the ability of the model to handle nonstandard distributional forms, (2) the treatment of nonstationary processes, (3) the handling of physical dependencies in the model, and (4) the ability of the method to operate efficiently so that it will be able to be included in an expert system computer code.

The proposed structure for the probabilistic model is to have a distribution fitting routine for the individual loads with a barrier crossing method, Discrete Probability Distribution (DPD) method, and a Monte Carlo method for the combined and composite load models. A transformation method for changing non-stationary load processes into stationary processes will also be included in the model so that the barrier crossing techniques can be used for a broader spectrum of problems. Because these models are based on the probability density function representing the frequency of the various load levels occurring, all forms of load shape curves can be handled including nominal (rectangular pulse), periodic, periodic over nominal, and random over nominal. The case of spike (transient) loads occurring will be handled with a simulation method, or, if appropriate, the barrier crossing method.

Because these calculations must be performed in the context of an expert system they must perform efficiently. Since two of the proposed techniques, DPD and Monte Carlo, are simulation methods which are usually slow relative to the classic load combination models a sample calculation was performed to demonstrate their viability. Calculations of the mass flow rate and turbine speed were performed on an IBM PC-XT with the 8087 co-processing chip and found to be limited by the printer speed, i.e. there was no discernible lag in the time at which the input to the code was completed and the output began.

Therefore, the development of a probabilistic load model based on these recommendations appears to be the most efficient one to address the problem of a generic space propulsion component. Since the feasibility of using such techniques has been demonstrated and they can be used either on a mainframe computer or a personal computer the development will continue to use these techniques unless new models are developed which improve on the current state-of-the-art.

8.1 Introduction

Turbines receive working fluid at a high temperature and pressure, extract energy that is transformed to torque and exhaust the fluid at lower temperature and pressure.

Turbines, which are the drive mechanism for turbopumps, provide the required shaft power for the pump. Key elements of the turbine are shown in Figure 27.

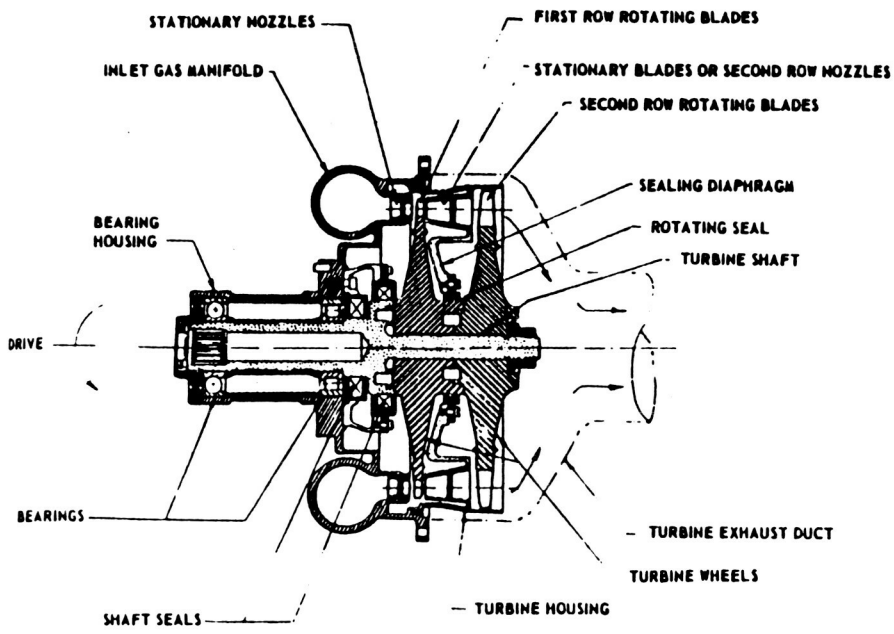

Figure 27 Elements of a Turbine

A comparison of turbine flow rate and horse power for various Rocketdyne turbopumps is shown in Table 9.

1 OF 2

MODEL	TYPE	NO. STGS	ENGINE	FLUID	HP	RPM	D_m INCH.	U_m FT/SEC	T_{t1} F	P_{t1} PSIA	PR	U_m/C_o	η_t (T-S) %
MARK 3	PC	2	H-1	O_2/RP-1	4,007	32,800	9.00	1290	1200	800	17.7	0.42	62.5
MARK 4	PC	2	ATLAS	O_2/RP-1	1,680	38,000	6.00	995	1075	760	25	0.39	46.3
MARK 8	VC	1	E-1	O_2/RP-1	14,860	8,900	22.06	857	1400	650	25	0.20	62.0
MARK 10	VC	1	F-1	O_2/FP-1	54,359	5,490	34.90	840	1550	929	16.3	0.20	60.5
MARK 14	VC	1	H-2	O_2/FP-1	7,650	14,300	16.07	1000	1700	525	11.5	0.21	58.9
MARK 15-0	VC	1	J-2	O_2/H_2	2,604	8,650	15.50	585	740	62	3.18	0.11	48.4
MARK 15F	VC	1	J-2	O_2/H_2	8,749	26,052	12.50	1448	1200	620	6.35	0.18	60.1
MARK 19-0	IMPULSE	1	X-8	O_2/H_2	750	32,800	8.00	880	1200	450	9.0	0.102	19.7
MARK 19F	PC	2	X-8	O_2/H_2	4,000	27,000	9.00	1160	1200	410	16.4	0.116	40.7

NOTES.

VC = VELOCITY COMPOUNDED, 2-ROW
PC = PRESSURE COMPOUNDED

D_m = PITCH DIAMETER
U_m = PITCHLINE VELOCITY

PR = PRESSURE RATIO
U_m/C_o = VELOCITY RATIO

Table 9a Design Parameters of Rocketdyne Turbines

2 OF 2

MODEL	TYPE	NO. STGS	ENGINE	FLUID	HP	RPM	D_m INCH	U_m FT/SEC	T_{t1} F	P_{t1} PSIA	PR	U_m/C_o	η_t(T-S) %
MARK 29F (MOD MK-15/F)	VC	1	J-2H	O_2/H_2	12,700	28,050	12.50	1535	1050	920	7	0.191	54.1
MARK 29F	VC	1	J-2S	O_2/H_2	10,810	28,000	10.5	1288	1200	889	7.30	0.161	56.1
MARK 29-0 (MOD MK-15/O)	VC	1	J-2S	O_2/H_2	3,263	9,050	15.5	613	740	100	2.68	0.119	48.0
H-1/O	VC	1	H-1	O_2/H_2	24,665	3,530	33.0	508	763	194	1.62	0.13	54.0
H-1/F	VC	1	H-1	O_2/H_2	74,138	12,961	23.18	1310	1000	904	3.87	0.19	65.0
MARK 38 (HPOTP)	REACT.	2	SSME	O_2/H_2	26,700	31,200	10.09	1374	1107	5848	1.552	0.309	0.768 (T-T)
MARK 38 (HPFTP)	REACT.	2	SSME	O_2/H_2	76,700	38,000	10.19	1689	1468	5916	1.58	0.357	0.791 (T-T)
MARK 48-0	IMPULSE PARTIAL ADMISS.	1	ASE	O_2/H_2	856	70,000	4.7	1435	1414	3368	1.424	0.343	0.698
MARK 48F	REACT.	2	ASE	O_2/H_2	2,543	95,000	3.5	1451	1400	3420	1.443	0.483	0.74 (T-T)

NOTES.

VC = VELOCITY COMPOUNDED, 2-ROW
PC = PRESSURE COMPOUNDED

D_m = PITCH DIAMETER
U_m = PITCHLINE VELOCITY

PR = PRESSURE RATIO
U_m/C_o = VELOCITY RATIO

Table 9b Design Parameters of Rocketdyne Turbines (Contd.)

Distinguishing factors of rocket engine turbine include:

a) Comparatively short but severe service life
b) Strict limitations on size and weight
c) High energy content of fluids
d) High specific work output
e) Rapid start and short run duration
f) Severe thermal shock conditions
g) High stage loading and stresses

Because of emphasis on high performance and weight requirements rocket engine turbines run at a very high speed. Advances in bearings and seals have resulted in direct drive turbopump systems with no need for reduction gears. Liquid rocket engine turbopumps have one of the highest power to weight ratio in the entire field of turbomachinery.

Of the two major types of turbines, impulse and reaction, reaction turbines have been used extensively in oxidizer and fuel turbopumps in rocket engines. Other design options in turbine design include single vs. multistage, full vs. partial admission and axial vs. radial flow. Actual turbine installation used in a rocket engine is very dependent on the engine system used.

All the high pressure turbines herein considered are axial turbines. All the low pressure pump turbines are axial except for the XLR129 and the Rocketdyne Advanced Expander engine (RS44) low pressure LO_2 pumps which are radial inflow hydraulic turbines. The turbines and blades of these engines will be described later.

Turbine working fluids can be a) combustion products (LOX/RP1, LOX/LH2, LOX/CH4) b) compressible fluids (ambient hydrogen or nitrogen) c) mono propellants (Hydrogen peroxide) and d) for hydraulic turbines, liquid oxygen or liquid fuel.

C-2

The major geometrical features in a turbine blade include (Figure 28) the shroud, airfoil, platform, shank, firtree, damper pockets, land and hollow core.

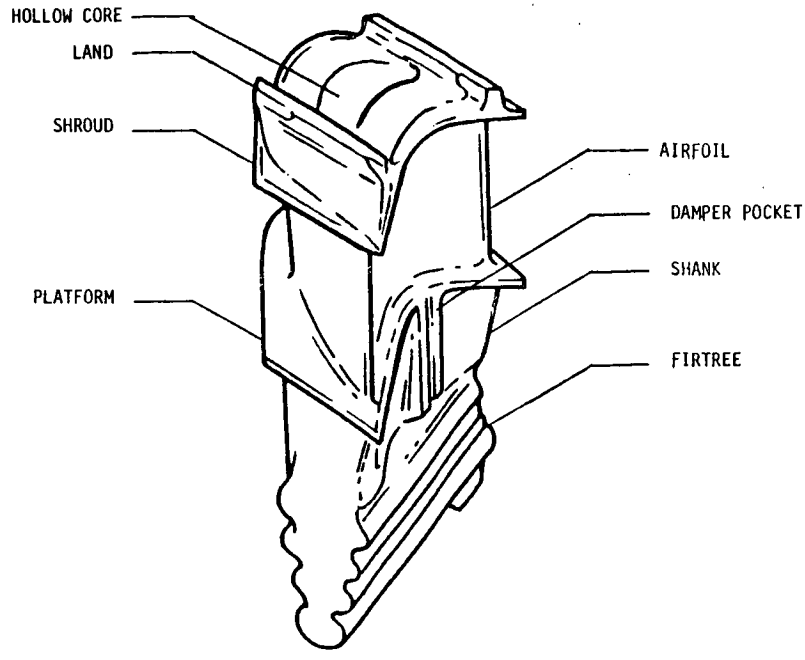

Figure 28 Turbine Blade Geometry Description

All the features may or may not be present in a single blade. The airfoil design deals with the development of the blade profile that defines the required gas path vector diagram relationships and pass the working fluid mess flow at design operating conditions. Numerous geometrical design parameters are used to evolve design blade profiles. Circular arcs and straight lines can be used to define the airfoil shape as was the case with rotors of the Mark 3, Mark 4, and Mark 15 turbines. Turbine airfoils are also designed with tangent parabola curves which introduce more gradual curvature change thereby lessening the potential for suction surface separation. Elliptical leading edges and conic curves were used in SSME and other subsequent designs.

The J-2 engine turbines are shown in Figure 29. The fuel turbine was attached to the gas generator (GG), and its exhaust was directed to the oxidizer turbine. All four turbine blades (lox & fuel turbines) were uncooled, fir-treed, and had platforms at the blade root & tip. Honeycomb tip seals were used on the oxidizer blade. The fir trees were directly connected to the platform with no transition shank. No dampers were utilized. No cooling was utilized for the disks or blade roots.

The M-1 turbine is illustrated in Figure 30. This one million pound thrust engine had turbine blades electron-beam welded to the rotors. Like the J-2, it was a multistage velocity compounded turbine.

The two expander cycle engines, the RL10 and the RS44 both have partial admission turbines to drive their pumps. The partial-admission turbine is used in applications that, because of limitations imposed by design horsepower, mass flowrate, and required flow area, would require excessively small blade heights for full-admission nozzle configurations. Pitch diameters cannot be reduced to accommodate larger blading in these designs because of velocity-ratio considerations. Blading heights, however, can be increased to practical design limits under the circumstances by adjusting the nozzle arc of admission. The RL10 has an integral disk and blades made of aluminum. The blading is fully shrouded and labyrinth seals are used to minimize leakage. The turbine is a pressure compounded design. Exit guide vanes are utilized to minimized discharge losses (Reference 2).

The RS44 engine has four turbopumps - two high pressure pumps and two inducer pumps, see Figures 31 and 32. Three of the four turbines are axial flow turbines, and the low pressure oxidizer pump has a radial inflow hydraulic turbine. The three axial turbines - the high pressure fuel and lox and low pressure fuel - have integrally machined disks and turbine blades. These three turbines are partial admission turbines. The high pressure fuel turbine has two stages (Reference 3).

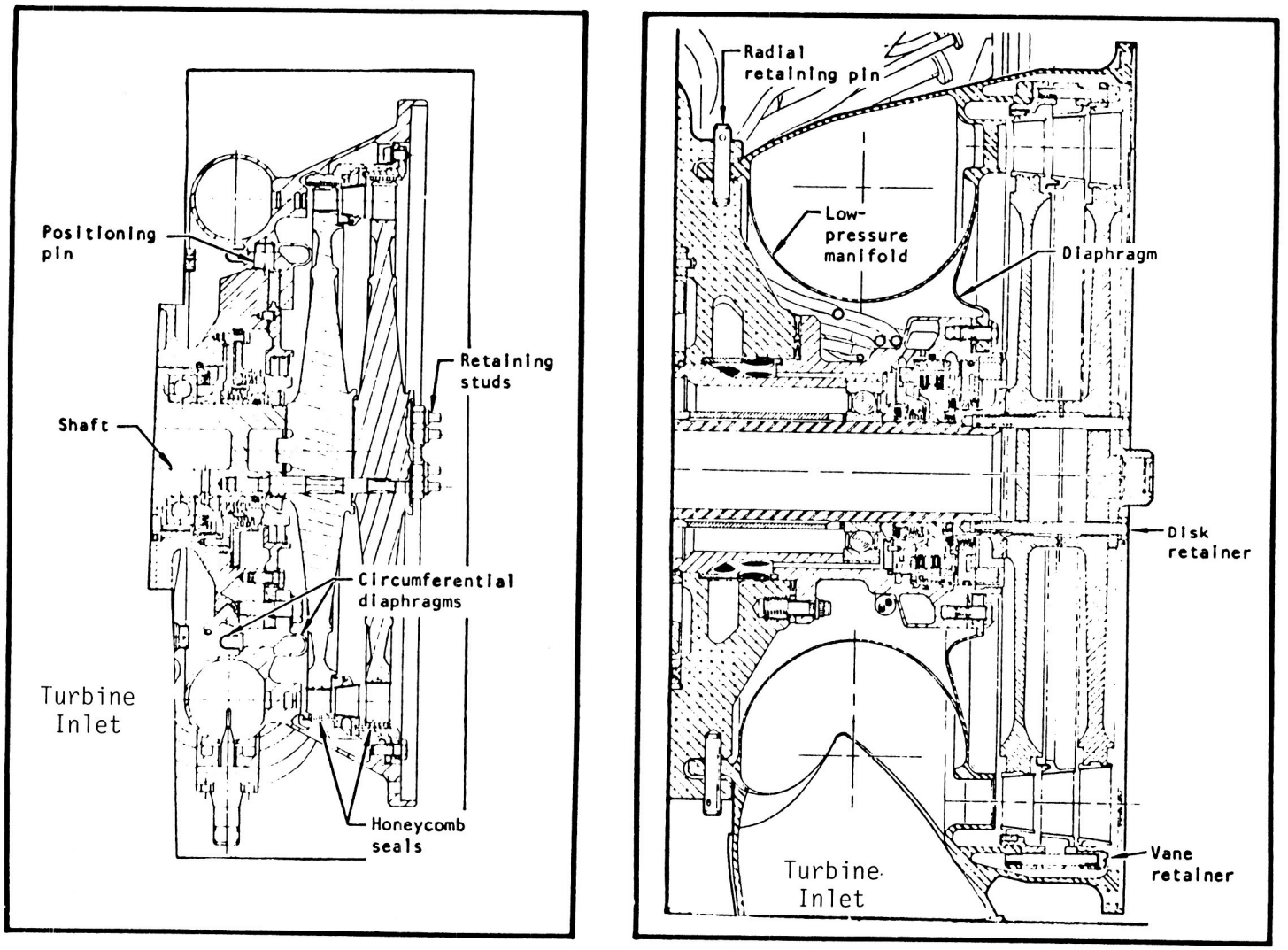

MARK 15 F

MARK 15 O

Figure 29 J-2 Turbines

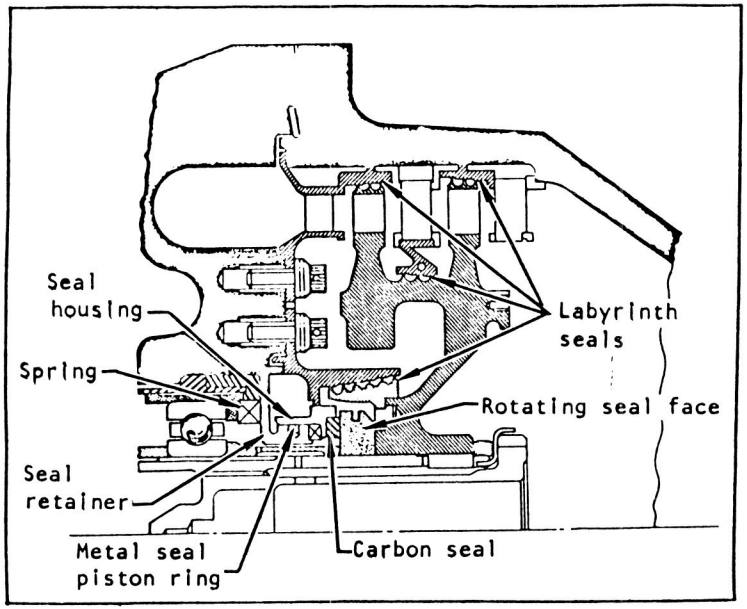

RL10 A3-3 turbine assembly.

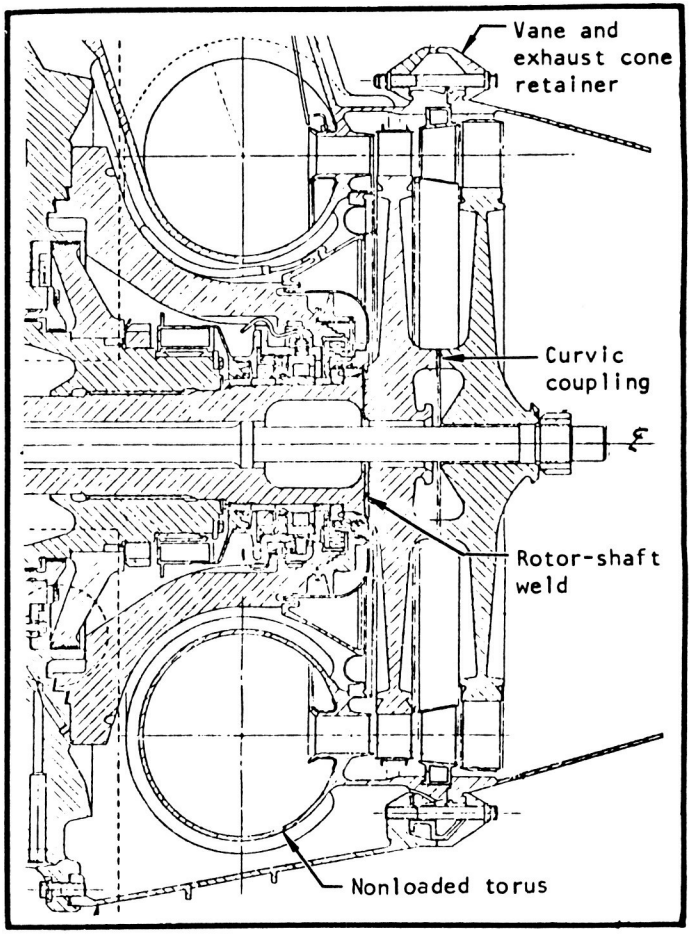

M-1 fuel turbine assembly.

Figure 30 RL10 & M1 Turbines

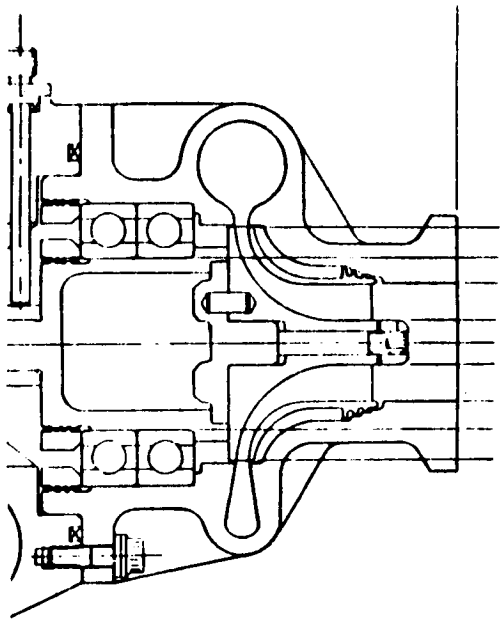

Oxidizer - Low Pressure Turbopump

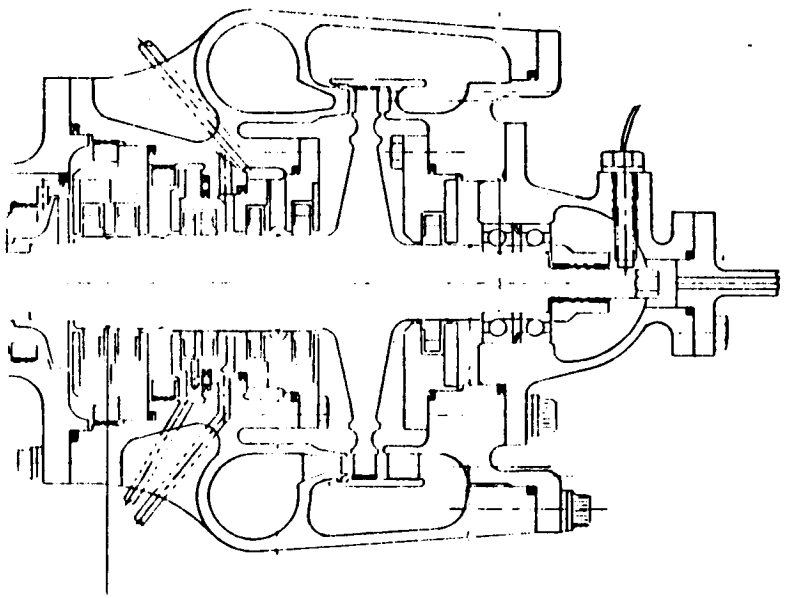

Oxidizer - High Pressure Turbopump

Figure 31 RS44 Oxidizer Turbines

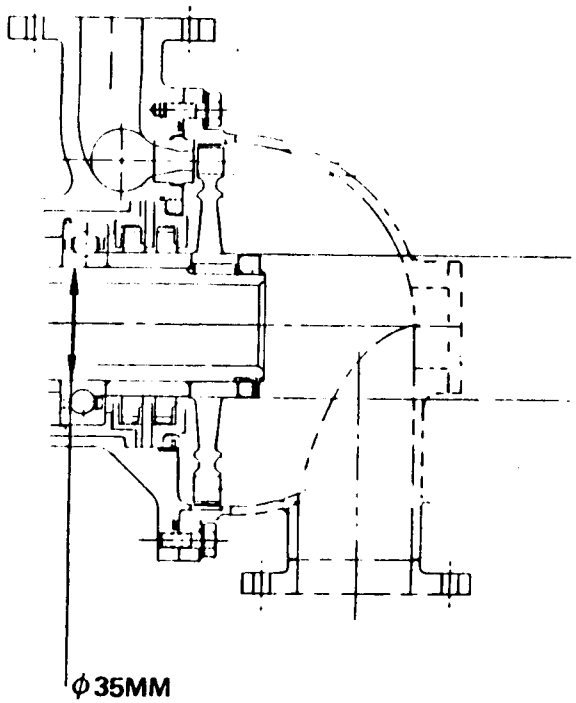

Fuel Low Pressure Pump

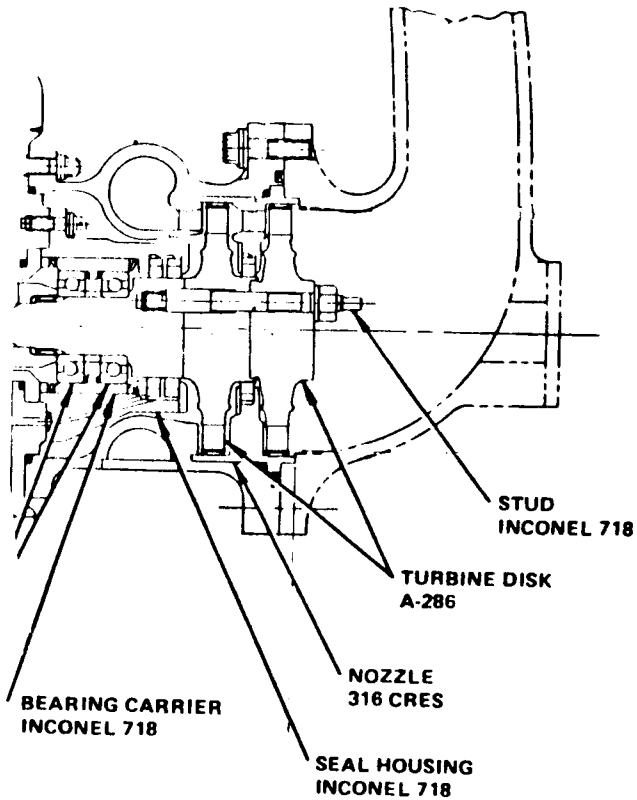

Fuel - High Pressure Turbopump

Figure 32 RS44 Fuel Turbines

The XLR129 was a partially developed expander cycle engine that had four turbopumps - two high pressure pumps and two inducer pumps. Similar to the RS44, three of the turbines were axial turbines and the low pressure oxidizer pump had a variable admission, radial inflow, hydraulic turbine, Figure 33 and 34. Only the high pressure fuel turbopump was fabricated and tested in a hot turbine test rig. Both high pressure turbopumps had two stage turbines. The fuel turbine was fir treed to the disk and had a platform between the shank and blade. The damper was attached to a sealing strip between blades. The oxidizer turbine blades were uncooled solid airfoils with integral tip shrouds, preloaded to contact adjacent shrouds and damp blade vibrations (Reference 1).

Figures 35 to 38 are data sheets on the four SSME turbopumps (Reference 4). Like the XLR129 it is a staged combustion cycle with two low pressure and two high pressure turbopumps. The probabilistic distributions for the generic loads will be developed primarily from SSME test data.

The low pressure fuel turbopump, Figure 35, has a partial admission, two stage impulse turbine driven by the main combustion chamber hydrogen coolant flow. The turbine rotors are A286 material with integrally machined turbine blades. The outer shroud is brazed to the blades.

The low pressure oxidizer turbopump, Figure 36, has a full admission, six stage impulse turbine driven by the HPOTP discharge. The blades are integrally machined to the rotor and do not have an outer shroud.

The high pressure fuel turbopump has a two stage reaction turbine, Figure 37, that is driven by partially combusted propellants from the fuel preburner. Each blade produces 700 horsepower per blade.

The turbine drive gases are high pressure hydrogen enriched steam. This requires hydrogen environment embrittlement consideration for the turbine components. Active hydrogen gas cooling is used to keep the turbine disk and turbine blade roots and shanks at below the strength drop off temperatures of the materials. The blades are fir treed into the disk.

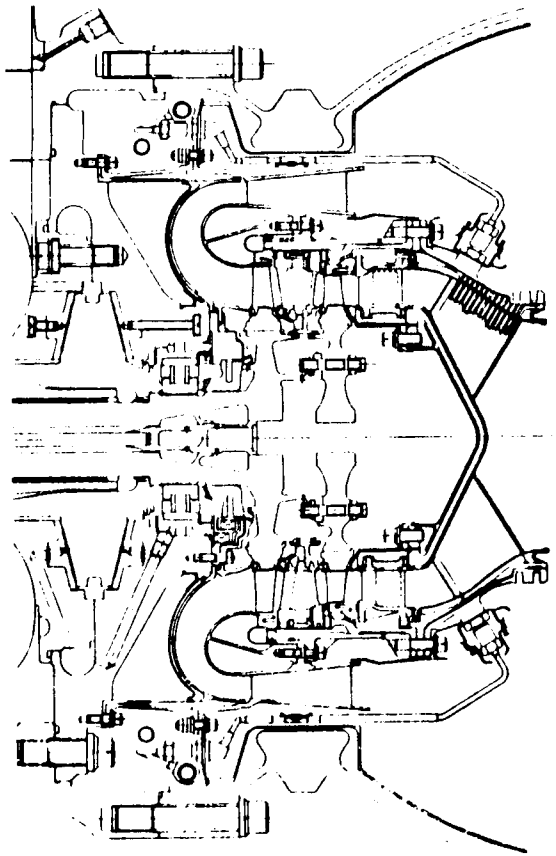

XRL129 HPFTP TURBINE

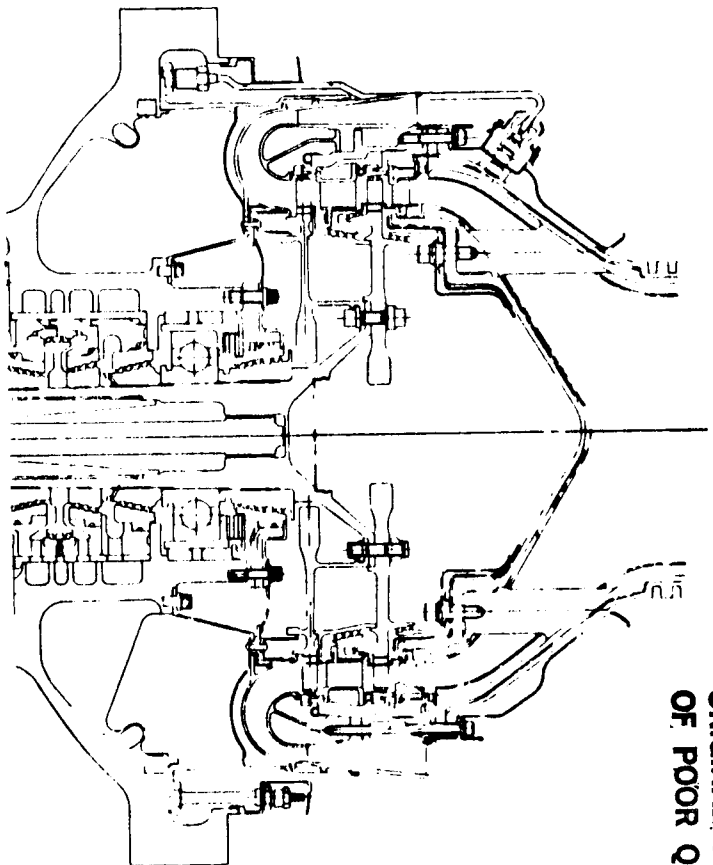

XRL129 HPOTP TURBINE

Figure 33 XLR129 High Pressure Turbines

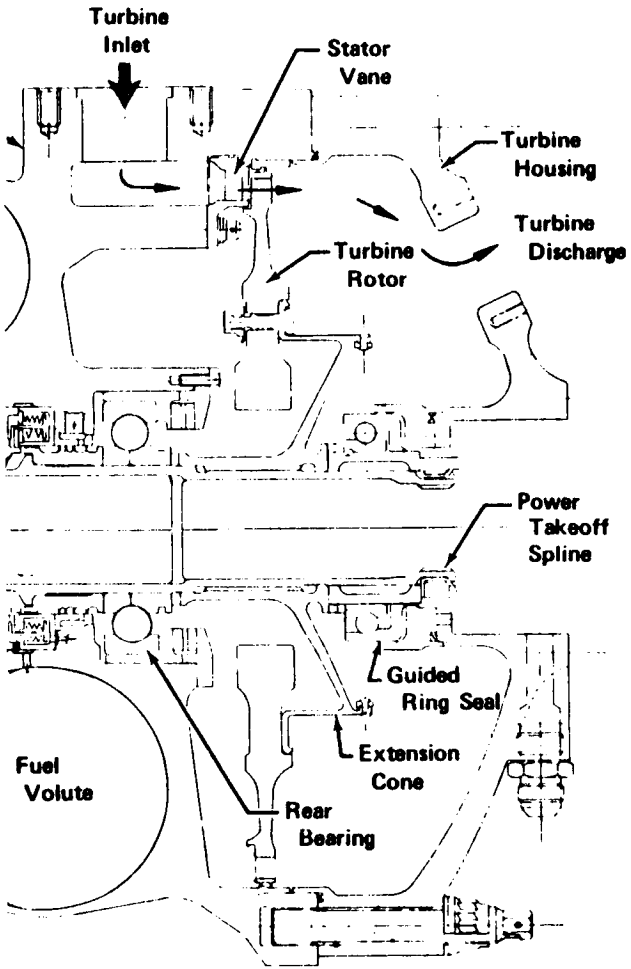

XLR129 LOW PRESSURE FUEL TURBINE

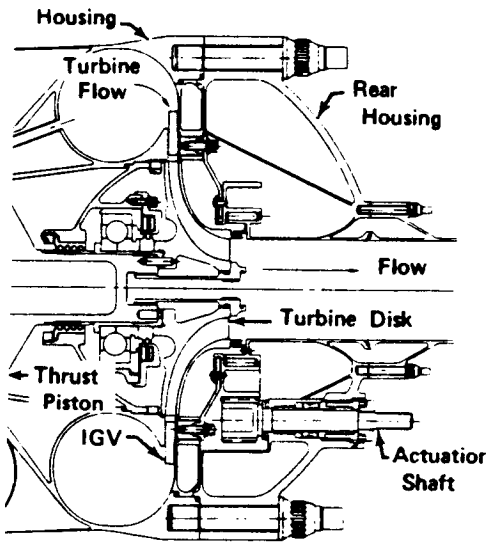

XLR129 LOW PRESSURE OXIDIZER TURBINE

Figure 34 XLR129 Low Pressure Turbines

The low-pressure fuel turbopump (LPFTP) is an axial-flow pump directly driven by a two-stage turbine that uses gaseous hydrogen (GH_2) as the power medium. During engine start and mainstage operation, the LPFTP maintains sufficient pressure to the high-pressure fuel turbopump (HPFTP) to permit the HPFTP to operate at high speeds. The turbine is powered by GH_2 from the main combustion chamber (MCC) coolant outlet manifold.

The inducer and shaft are supported by three liquid hydrogen-cooled (LH_2) ball bearings. The bearing coolant is the leakage across the inducer discharge labyrinth seal. The coolant flows through the pump end bearings and turbine bearing and is returned to the pump inlet through passages in the shaft, bearing bearing spacer, and inducer.

Before engine start, leakage from the pump into the turbine is prevented by a spring-loaded-closed, propellant pressure-actuated-open, lift-off seal. During engine start the seal nose is separated from its mate ring when increasing fuel pressure overcomes the spring force. A positive separation between the seal nose and mate ring is maintained until engine shutdown when fuel pressure decreases below spring force. During operation, leakage from the turbine into the pump is minimized by the pump and turbine seals.

A redundant-element, magnetic-type speed transducer is installed in the pump volute to monitor shaft speed.

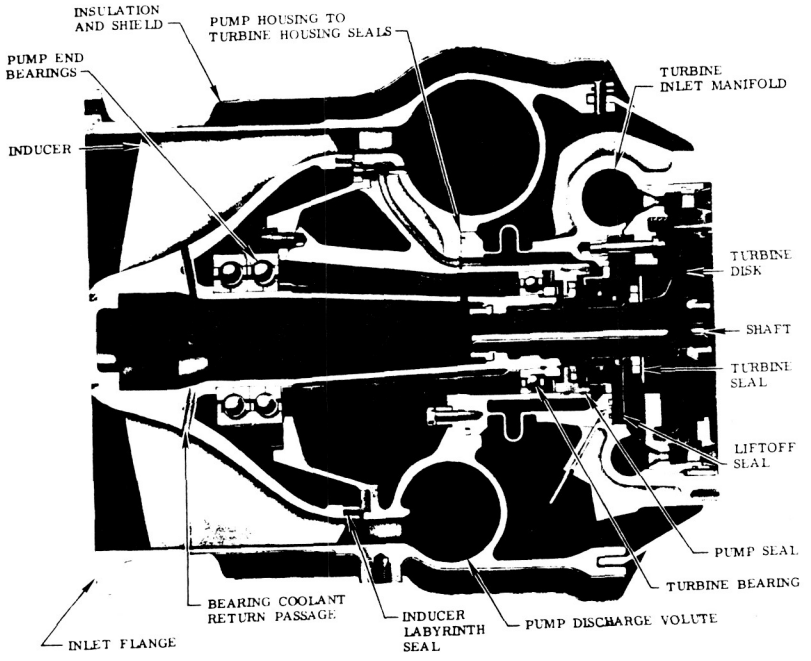

Figure 35 Low Pressure Fuel Turbopump

The low-pressure oxidizer turbopump (LPOTP) is an axial-flow pump directly driven by a six-stage axial flow turbine that is powered by liquid oxygen. During engine start and mainstage, the LPOTP maintains sufficient pressure to the high-pressure oxidizer turbopump (HPOTP) to permit the HPOTP to operate at high speeds. Turbine-drive fluid is tapped from the HPOTP discharge and, after powering the turbine, is injected into the pumped fluid through a port between the turbine discharge and pump discharge volutes. The combined flows are then routed to the HPOTP inlet. Since the pumped fluid and turbine drive fluid are both liquid oxygen and the LPOTP is located upstream of the oxidizer valves, the requirement for dynamic seals, purges, and drains has been eliminated.

The rotor is supported by two liquid oxygen-cooled ball bearings. The turbine-end bearing coolant flow path is from the last stage of the turbine, through the bearing, hollow rotor, radial holes in the rotor, and to the inducer discharge. Coolant for the inducer-end bearing is from the turbine inlet, through the rotor labyrinth seal, through the bearing, and to the inducer discharge.

A redundant-element, magnetic-type speed transducer is installed on the turbine end of the turbopump housing.

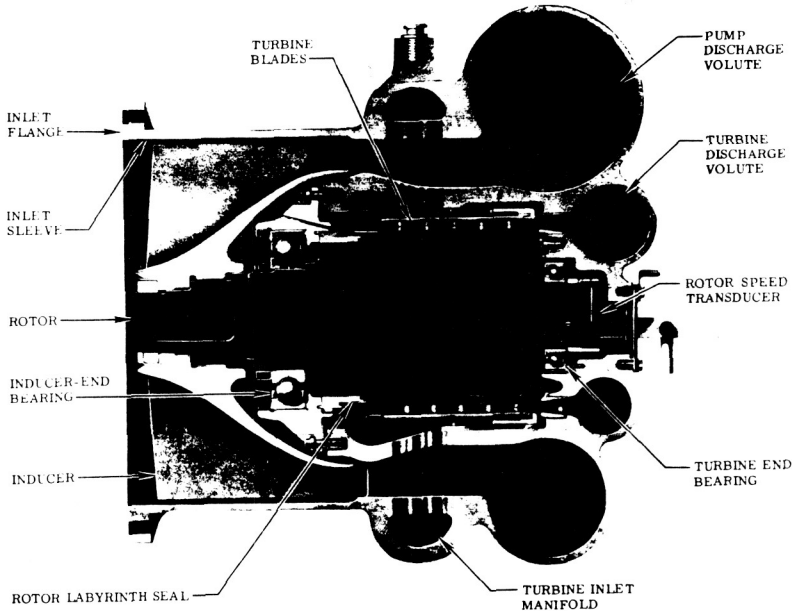

Figure 36 Low Pressure Oxidizer Turbopump

The high-pressure fuel turbopump turbine is powered by hot-gas (hydrogen-rich steam) generated by the fuel preburner (FPB). Hot gas enters the turbine and flows across the shielded support struts, through the first- and second-stage nozzles and blades, and is discharged into the hot-gas manifold (HGM). The turbine disks are mated through a curvic coupling and are held together with a circle of bolts. The two-stage turbine transmits torque to the pump by a splined coupling between the second-stage wheel and the pump third-stage impeller.

Bearing and turbine coolant is supplied through the shaft static lift-off seal when the seal is lifted at engine start. The turbine coolant flows over or through the hot-gas components and is then exhausted into the hot-gas flow stream.

Turbine-to-FPB sealing is accomplished by a bellows that loads a Naflex seal against the FPB flange.

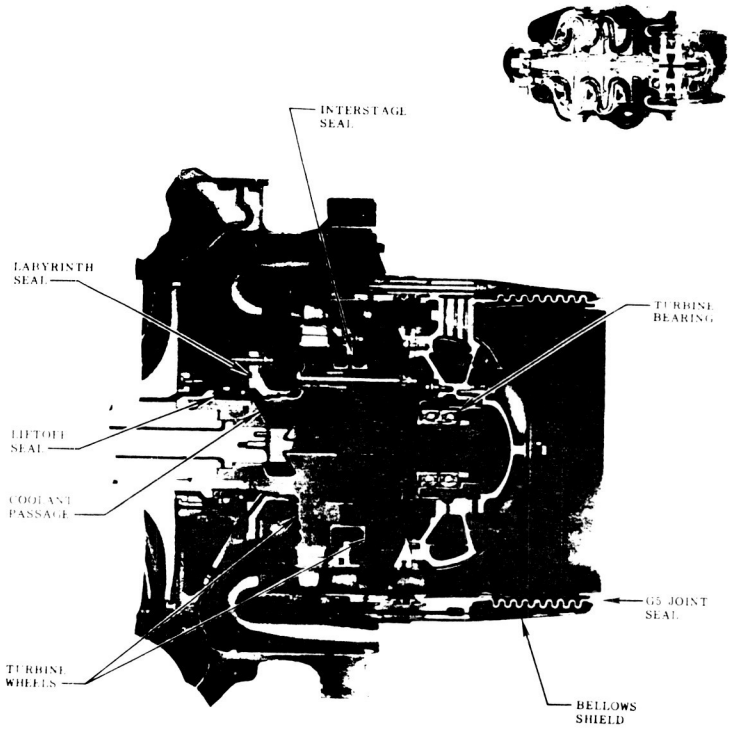

Figure 37 High Pressure Fuel Turbopump Turbine

The high-pressure oxidizer turbopump turbine is powered by hot gas (hydrogen-rich steam) generated by the oxidizer preburner (OPB). Hot gas enters the turbine and flows across the shielded support struts, through the first- and second-stage nozzles and blades, and is discharged into the hot-gas manifold (HGM). The turbine rotors are mated through a curvic coupling and are held together with a circle of bolts. The second-stage rotor is integral with the pump shaft. Turbine blade-to-housing leakage is minimized by lands on the outer perimeter of the blade shrouds that run against seals in the turbine housing.

All components of the turbine are cooled by gaseous hydrogen flowing over or through them. Coolant is supplied from the OPB coolant jacket. After cooling the turbine components, the coolant is exhausted into the hot-gas flow stream.

Turbine-to-OPB sealing is accomplished by a pair of concentric bellows that load dual seals in the turbine inlet flange to the OPB. The diameter of the turbine rotors with blades is approximately 11 inches.

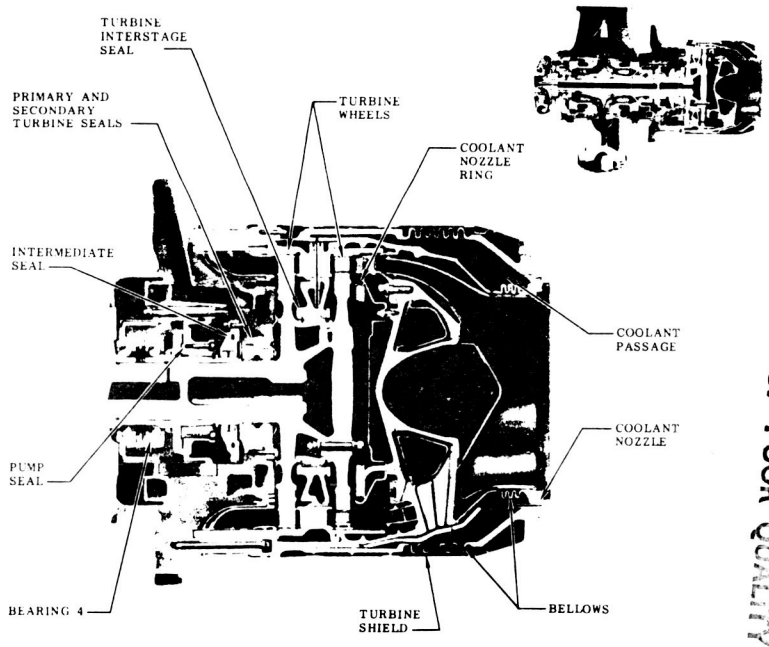

Figure 38 High Pressure Oxidizer Turbopump Turbine

A transition shank is used between the fir tree and inner shroud to distribute the load from the airfoil into the shank and to allow for proper geometric considerations for the damper. The separate damper is inset under the shroud and is captured between adjacent blades. No outer shroud is used on the solid blade, see Figure 39.

The high pressure oxidizer turbopump, Figure 38, has a two stage reaction turbine with similar hot gas flow and design constraints. This turbine is driven by a separate preburner with similar hot gas considerations. The turbine blades are similar in that they are fir treed to the disk, have a transition shank and lower platform and a damper. The current damper blade is a single piece captured radial between the shanks. A two piece damper that adds an additional horizontal damper to provide damping in all modes of vibration is designed and planned testing is in the current development schedule, see Figure 40.

8.2 Generic Configurations

A review of the above discussed turbines indicates that they typically have turbine rotors with upstream stator nozzles or vanes and often downstream vanes. The upstream elements cause variations in the flow field that result in the primary dynamic excitation on the blade airfoil. The downstream vanes or nozzles may also affect the flowfield but their effect is not well understood. For engines with coolant flow, there is also a potential for dynamic excitation from the coolant flow. The SSME HPOTP is an example of this condition where a coolant nozzle ring has 19 jets that impinge on the first stage turbine blade shanks.

Tip seals are a generic design feature used on most turbines to minimize leakage. Rubbing of the seals can load the blades. A seal design variation that can increase tip rubbing is used on the SSME HPFTP. The turbine housing has a circumferential pressure gradient that deflects the housing into a slightly elliptical shape during operation. To account for this, the seal is designed to be elliptical in the fabbed condition so that it is round during operation. Under transient conditions, the tip of the blades may rub the seal.

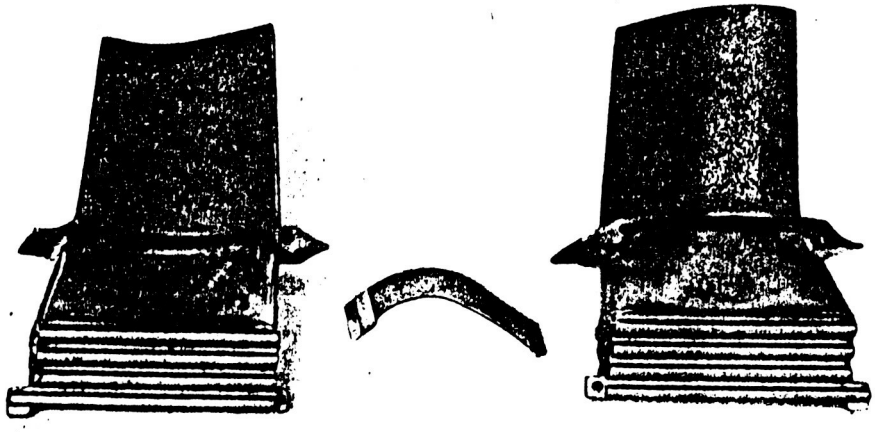

Figure 39 High Pressure Fuel Turbopump Turbine Blade Damper

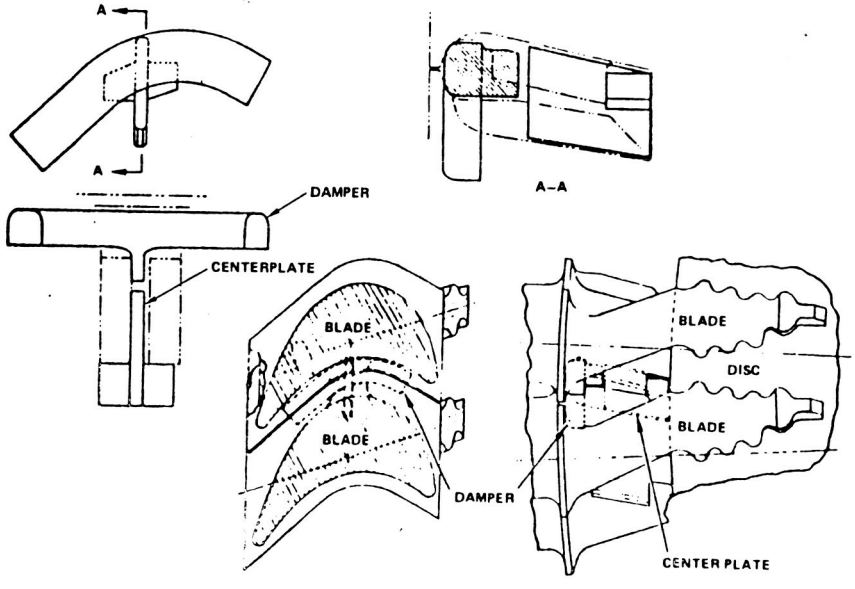

Figure 40 HPOTP First Stage Two-Piece Damper Design

A practical design consideration is debris loads from fractured pieces of upstream structure or contamination items that can be injected into the turbine blades.

The dominant steady loads on the turbine blading are centrifugal load from speed, thermal and differential pressures across the airfoil.

The thermal loads on the rocket engine turbine blades are important in both transient and steady-state portions of the duty cycle. The transient conditions result in large thermal gradients and the steady-state operation has constant temperature in the airfoil with thermal gradients across the platform, shank and fir tree. The fabrication or assembly method can influence residual stresses or loads on a part. The brazed shroud on the LPFTP rotor blades are an example of residual load conditions. Other conditions that can be considered related to loads are: damper weight variation, friction between blades and dampers or platforms and blade stacking axes tolerances and criteria. These variables are best approached from a probabilistic standpoint and are needed as input to a structural analyses. The inclusion of these variables into the database and codes will be an objective, but are not considered as part of the required loads.

Figure 41 summarizes these loads and their primary influence from an engine key parameter standpoint. Each load is discussed in detail in the appendix. During steady-state operations with slow variations of power level, the individual loads typically mirror the thrust profile. There are, of course, test to test, engine to engine and component variations that will be used in developing the probabilistic distributions. The transient conditions for the HPF turbine show both general oscillations and two variable level peaks that occur on the fuel turbine side of the SSME engine - the ignition spike and a fuel side oscillation. These type of loads are generic to rocket engine turbines, but their importance may change from turbine to turbine.

TURBINE BLADE LOADS

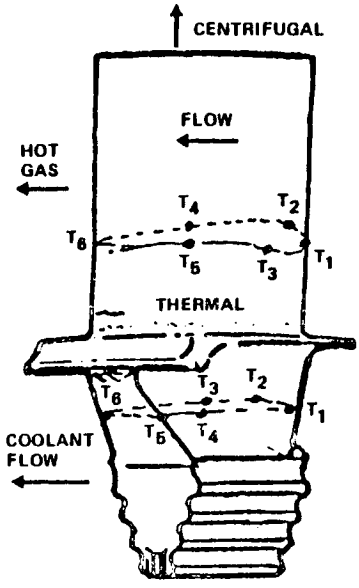

- AIRFOIL
  - CENTRIFUGAL
  - PRESSURE
  - BLADE TEMPERATURE
  - DYNAMIC ΔP
  - IMPINGEMENT LOADS
  - DAMPER/FRICTION
  - TIP RUBBING
- SHANK
  - PRESSURE
  - METAL TEMPERATURES
  - DYNAMIC ΔP
- EXPERT OPINION INPUT REQUIRED
  - LACK OF MEASURED DATA

KEY VARIABLES
SPEED
TURBINE ANALYSIS
TURBINE/THERMAL ANALYSIS
SPEED, INTERRUPTIONS
UPSTREAM DEBRIS POTENTIAL
GEOMETRY, WHIRLIGIG TEST
DESIGN
COOLANT FLOW AND THERMAL ANALYSIS
SPEED, INTERRUPTIONS

Rockwell International
Rocketdyne Division

Figure 41 Turbine Blade Loads

The engine test duty cycle measured and calculated quantities available for use in the developing the probabilistic loads include:

1. Turbine speed (SSME measured quantity)
2. Torque
3. Flowrate
4. Inlet pressure and temperature
5. Outlet pressure and temperature (SSME measured quantity)
6. Mixture ratio

8.3 Individual Loads Summary

Details of the individual loads are covered in Appendix B and a summary of the information is furnished for an overall perspective. The summary in Table 10 covers how the load is determined, form available, an engineering estimate of the degree of certainty and how the load is used. A review of the chart shows that the majority of the loads are predicted. Only very limited data is available of actual turbine blade or turbine nozzle hot fire test measurements of temperatures or strain gage responses. The predictions are based on both analysis of engine operation and visual examination of hardware post test either in the assembled or disassembled condition. Detail mission history profiles are also not available for some of the loads. The current deterministic analysis approaches have normally addressed limit conditions during the duty cycle rather than a detail analysis of the duty cycle. Current SSME plans are to perform a detail duty cycle analysis of the first stage HPFTP turbine blade. The results of this analysis will be available for use in this program. The structural model is currently being developed.

The degree of certainty of some loads has to be down rated since they have not been verified from instrumented tests. Confidence in the analysis procedure has been gained from extended overall engine testing. The probabilistic approach will better quantify these loads and scaling techniques and more exactly assign confidence limits.

INDIVIDUAL LOADS	HOW DETERMINED	FORM AVAILABLE	DEGREE OF CERTAINTY	HOW USED
CENTRIFUGAL	MEASURED	DUTY CYCLE & LIMITS	HIGH	INPUT TO STRUCTURAL ANALYSIS AS VALUES, LIMIT CASES OR DUTY CYCLE
STATIC PRESSURE AND ΔP	PREDICTED FROM TURBINE ANALYSIS	PRESSURE PROFILES AT STREAMLINES ON AIR FOIL (*)	TOTAL MAGNITUDE HIGH (TORQUE) DISTRIBUTION MODERATE	INPUT TO STRUCTURAL ANALYSIS AS LIMIT CASES OR DUTY CYCLE
DYNAMIC PRESSURE	PREDICTED FROM TURBINE ANALYSIS AND CASCADE ESTIMATES OR TESTS	PRESSURE PROFILE SCALED TO FORCING FUNCTION SHAPE (*)	MODERATE TO LOW	INPUT TO FORCED VIBRATION ANALYSIS, CAMPBELL DIAGRAM LIMITS
TEMPERATURE	PREDICTED FROM TURBINE PLUS THERMAL ANALYSIS	TEMPERATURES AT LOCATION THROUGHOUT BLADE (COMPUTERIZED DATASET) (*)	STEADY STATE-HIGH, TRANSIENT-LOW	INPUT TO STRUCTURAL ANALYSIS
DEBRIS	PREDICTED, BASED ON HISTORY OF INCIDENTS	PARTICLE SIZE AND VELOCITY	LOW	SENSITIVITY ANALYSIS OR INCIDENT INVESTIGATION

Table 10 Individual Load Summary

INDIVIDUAL LOADS	HOW DETERMINED	FORM AVAILABLE	DEGREE OF CERTAINTY	HOW USED
RUBBING AT SEALS	PREDICTED, BASED ON OBSERVED MARKS ON BLADES & SEALS	LOAD RANGE	LOW	SENSITIVITY ANALYSIS
FABRICATION	PREDICTED/ MEASURED		LOW	
DAMPER	MEASURED	SAMPLE LOT WEIGHT DISTRIBUTION	HIGH	INPUTS TO STRUCTURAL ANALYSIS, FATIGUE ANALYSIS,
FRICTION	MEASURED/PREDICTED BASED ON WHIRLIGIG TESTS AND DYNAMIC ANALYSIS	RANGE OF VALUES	MODERATE BASED ON MEASUREMENTS	DYNAMICS ANALYSIS FORCED VIBRATION
TOLERANCE OF BLADE AND CROSS-SECTION	MEASURED/PREDICTED BASED ON LOT BLADE MEASUREMENTS	RANGE OF VALUES	MODERATE TO HIGH	STATIC ANALYSIS FORCED VIBRATION

Table 10 Individual Load Summary (Contd)

The individual loads are used as part of a structural analysis -- either static or dynamic. For steady state analysis maximum conditions are utilized for determining responses and stresses.

8.4 Combined Load Assessment

Combined turbine blade loads are obtained from deterministic solution methods. Table 11 summarizes this assessment. For steady state loads, the maximum engine balance values are used. Analysis is approached from non-compatible limit conditions that are furnished in the engine balance. Engine test data is available from each hot-fire test and for use in this project to obtain actual variations in the combined loads assessment.

The transient dynamic model results are available and can guide the combined loads determination. Processed test data can be plotted, such as multivariable information, and related to the same time scale. The transient conditions are much more difficult to address from exact timing of related turbine blade loads. Test results are tracked on turbine discharge temperatures and can be used for statistical purposes.

The analyst typically needs combined data to perform structural analysis. Individual loads maybe useful for perturbation or sensitivity analysis, but proper combined loads are needed for static and dynamic analysis. Typically, a static analysis is performed for all non-dynamic loads. A time dependent analysis or a steady-state analysis is performed depending on the criticality of the transient effects the information available on the loads and the potential for inelastic effects. Dynamic analysis of the forced vibration is obtained as a separate analysis or as an estimated factor times the pressure load influences. The static and dynamic load solutions are then combined to obtain mean and alternating stresses.

Table 11 Combined Load Assessment

- HOW COMBINED LOADS DETERMINED
  - STEADY-STATE
    - TEST DATA REDUCTION MODEL
    - ENGINE PERFORMANCE MODEL
      - DESIGN POINT AND LIMIT CASES
      - PRIMARY ANALYSIS METHOD
  - TRANSIENT
    - TEST DATA MULTI-VARIABLE VS TIME
    - ENGINE TRANSIENT MODEL
  - DETERMINISTIC MODELS ADJUSTED FOR TEST RESULTS
  - RELATED BY TIME PHASED ANALYSIS
  - DEGREE OF CERTAINTY
    - STEADY-STATE-MODERATE TO HIGH
    - TRANSIENT - LOW TO MODERATE
      - HIGH VARIABILITY IN LOAD MAGNITUDES TEST TO TEST
      - TIME PHASING CHANGES TEST TO TEST
  - FORM AVAILABLE
    - TABLE DATA FOR STEADY STATE
    - DATATAPES OR TABLE DATA FOR TRANSIENTS
  - USAGE BY ANALYST
    - INPUT TO STRUCTURAL ANALYSIS CODES
  - DEBRIS, RUBBING, FABRICATION-ADDED AS PERTURBATIONS TO ANALYSIS

1516e

9.0 LO_2/LH_2 INJECTOR AND LOX POST CONFIGURATION

9.1 Introduction

The function of an injector is to introduce and meter the propellant flow to the combustion chamber after atomizing and mixing the propellants. There are several methods for injecting (combining the oxidizer and fuel to obtain combustion), but the one used for LO_2/LH_2 engines is coaxial injection. This has proven to provide favorable combustion performance and stability.

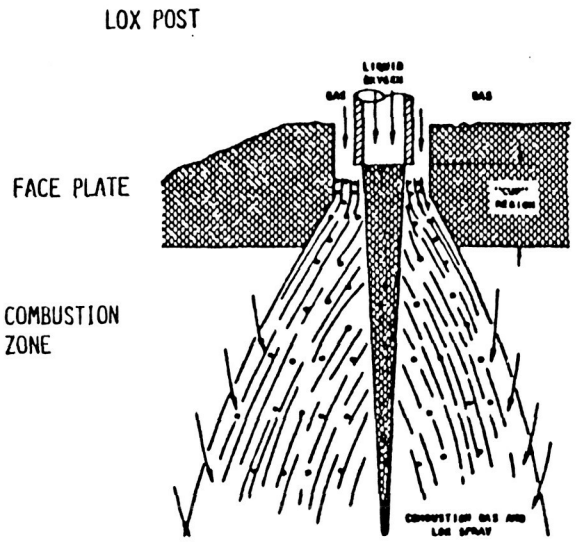

- FAVORABLE DESIGN FEATURES
  - HIGH DIFFERENTIAL GAS-LIQUID INJECTION VELOCITIES
  - RECESS CUP
  - THIN LOX POST TRAILING EDGE
  - UNIFORM ELEMENT SPACING

Figure 42 Typical Gas-Liquid Coaxial Element Model

A qualitative description of the coaxial element design is shown in Figure 42. The coaxial elements are particularly adapted to mixing of gaseous propellants such as hydrogen, with liquid propellants such as oxygen. Coaxial elements consist of tubes or drilled posts that provide the flow area for the oxidizer, and the concentric annuli provide the flow area for the fuel. Proper propellant atomization and mixing which is central to combustion efficiency is promoted by momentum exchange due to high differential velocities between the fuel and oxidizer. The recess cup region where the LOX Post stops short of being flush with the face plate and a thin LOX post trailing edge have definite positive influences on the combustion performance of the injector.

The SSME injector configuration can be seen in the powerhead cross-section, Figure 43. Both preburners and the main injector use coaxial LOX posts. Typical injectors have inlets for the propellants, manifolds to distribute the flow to the individual LOX posts, a face plate as a barrier to the combustion gasses in the combustion chambers, and baffles to inhibit combustion instability. Another primary variable in injector design is the pattern that the LOX posts are distributed within the cross-section of the combustion zone. A uniform distribution of LOX posts promotes a uniform combustion process and better overall performance.

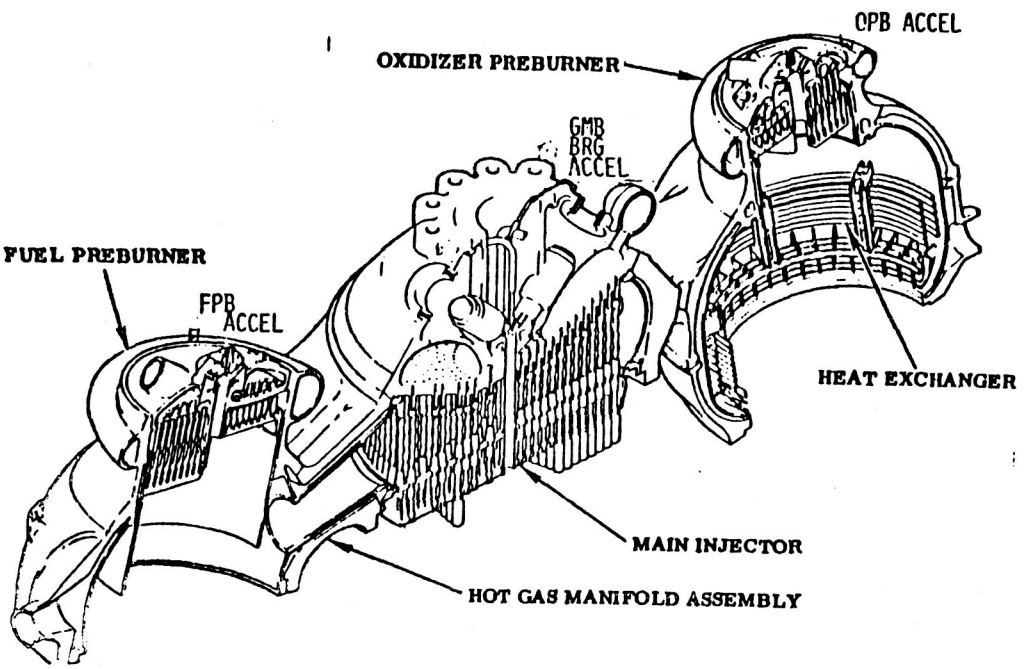

Figure 43 Cutaway View of Hot Gas and LOX Manifolds

9.2 SSME Injectors Configuration

The basic configuration and names of the elements of the SSME LOX posts for the main injector and both preburners are furnished in Figures 43 to 47. These terminology will be utilized for the discussion of loads.

9.3 Generic Configuration and Loads

The SSME configuration (Fig. 44) utilizes a uniform coaxial pattern in the face of the injector similar to many other injectors, see Figure 48. The XRL129 design utilized a coaxial spray bar pattern. Other injectors are shown in Figures 49 thru 54 and include the J2, M1, XLR129 and advanced expander cycle. A summary of their design geometry is furnished in Table 12. All the injectors except the XLR129 main injector have: 1) interpropellant plates where the LOX posts are attached on one end and a face plate attached at the injector face, 2) LOX flow from the interpropellant plate through the post and, 3) cross flow of fuel inward from a circumferential manifold at the outer diameter of the injector. The XLR129 wagon-wheel, spray-bar injector is different in that the spray bars are connected to a LOX manifold at the external diameter. The LO_2 is distributed to the tapered spray bar with attached LOX posts extended like teeth in a comb. The fuel approaches axially from a plenum and flows around the spray bars and LOX posts through slots in the face plate.

Because of the wide variation in thrust for these engines - 1 million to 15K or less - the number of elements and other parameters such as combustion chamber pressure, thrust per element and fuel temperature also have wide variations as indicated in Table 12. The LOX temperature of 200°R is constant. Most posts have relatively small Δt's - 400° max., with the exception of the SSME and XLR129 main injectors.

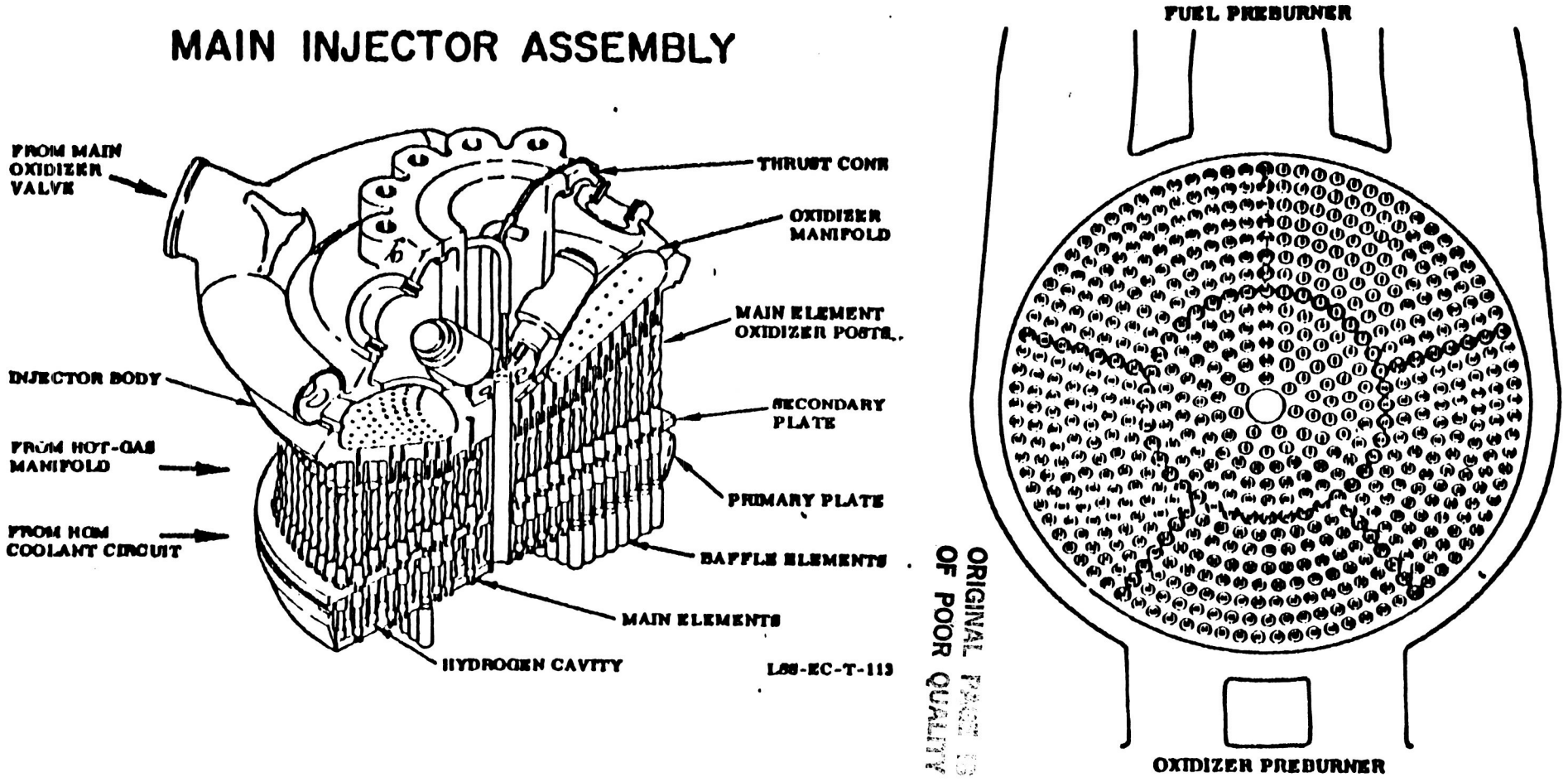

Figure 44 SSME Main Injector Assembly

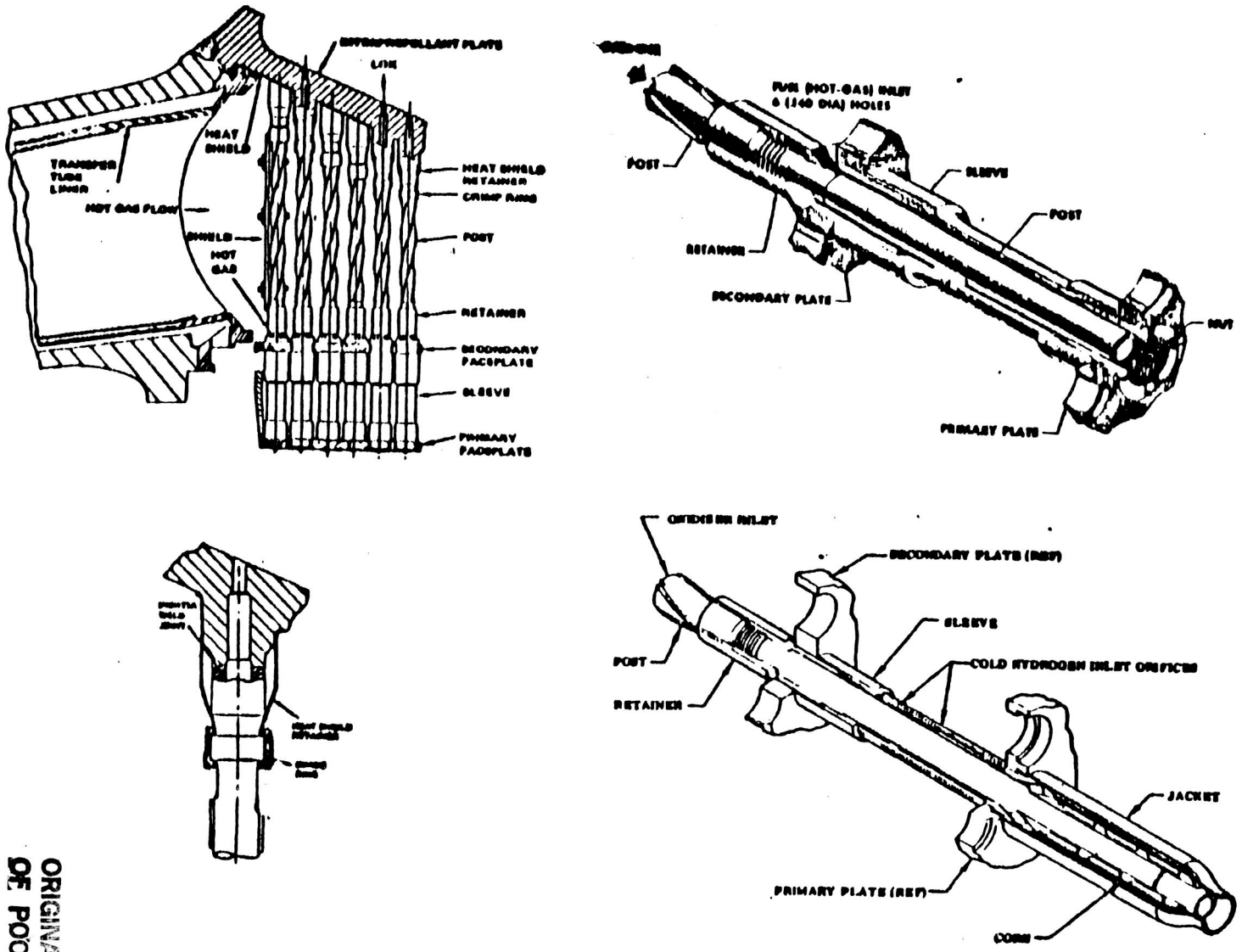

Figure 45 SSME Main Injector LOX Post Details

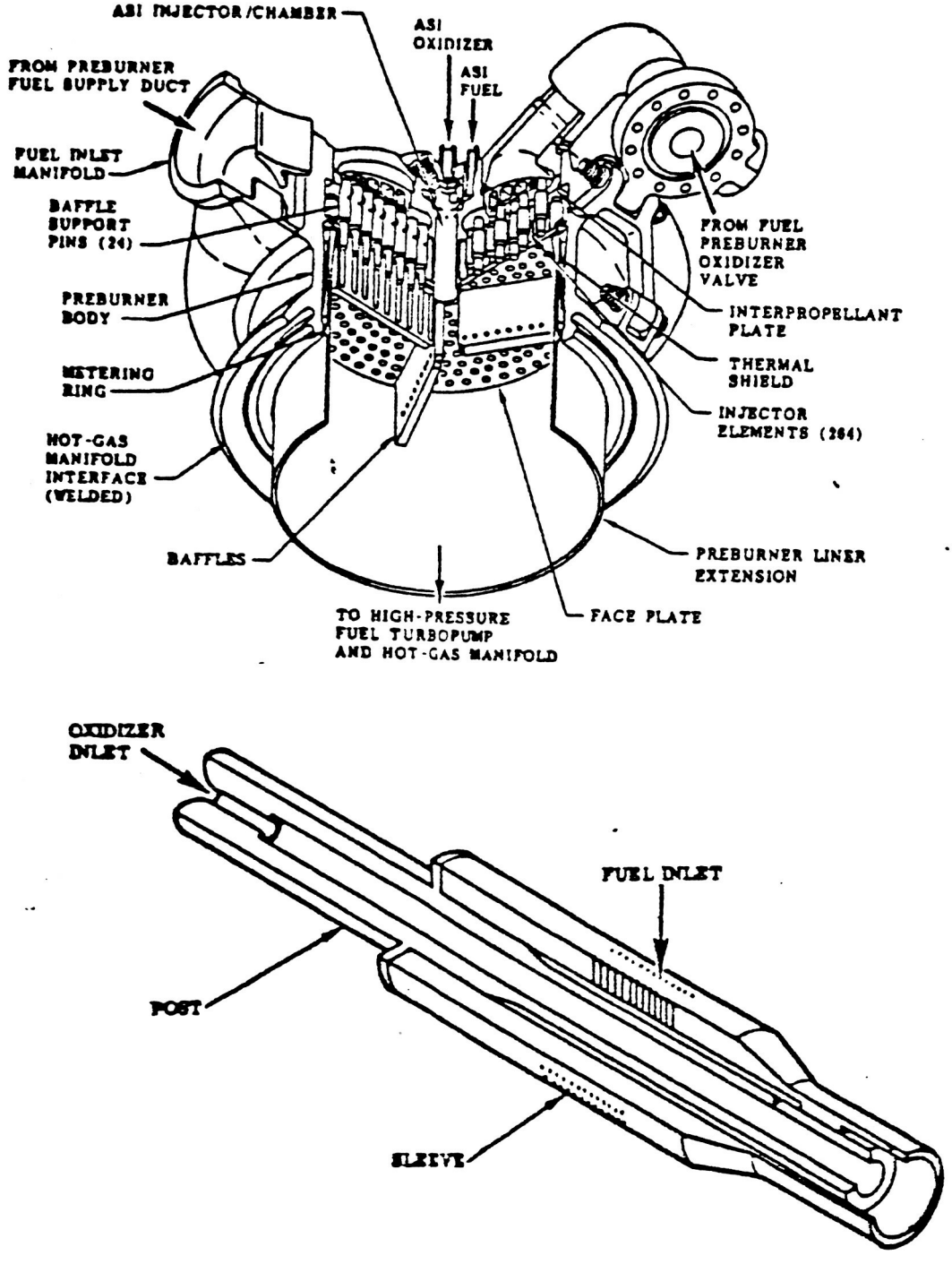

Figure 46 SSME Fuel Preburner

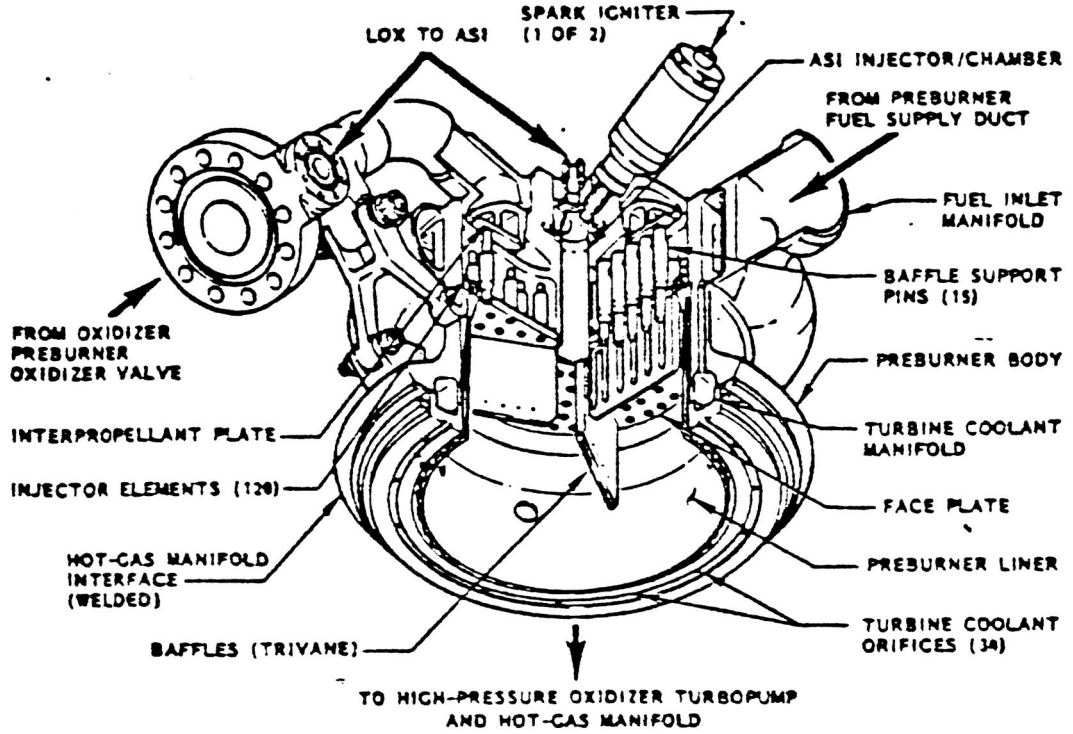

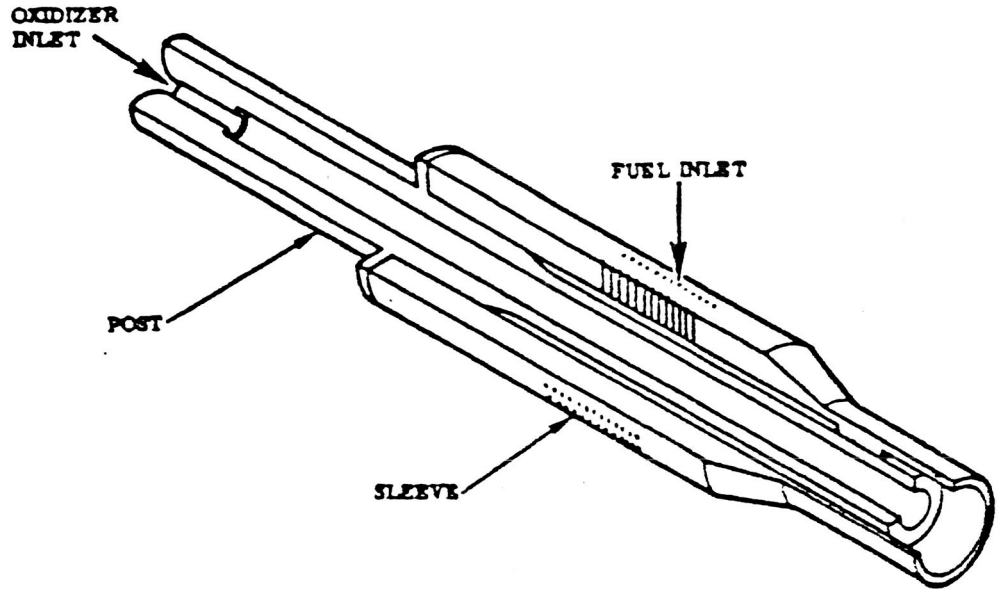

Figure 47 SSME Oxidizer Preburner

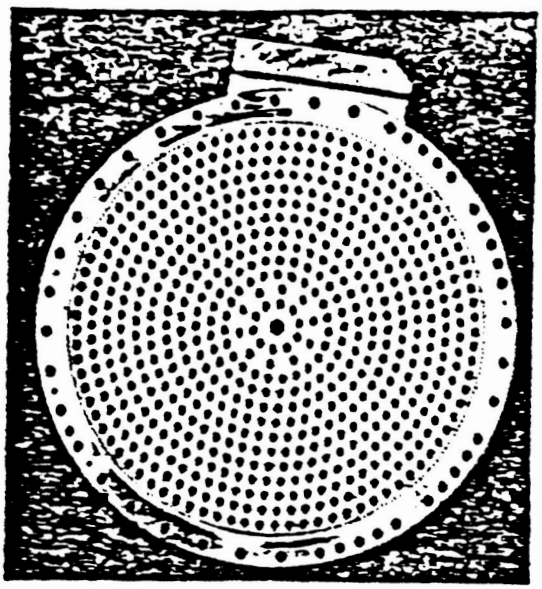

J-2 Injector Assembly

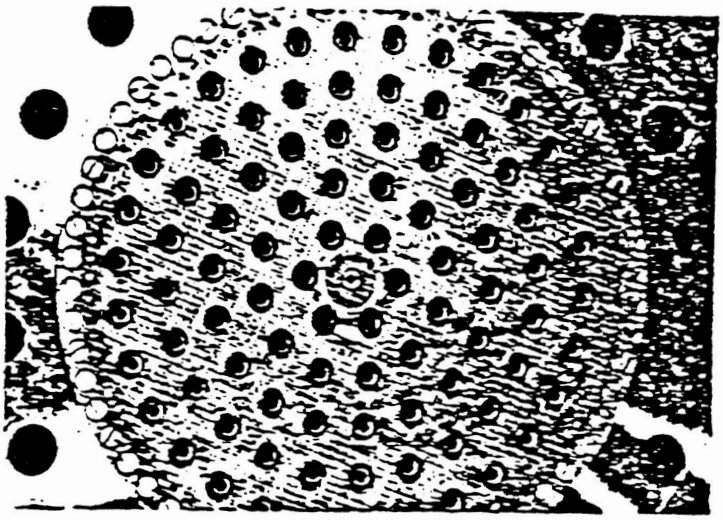

BORD I Injector Assembly

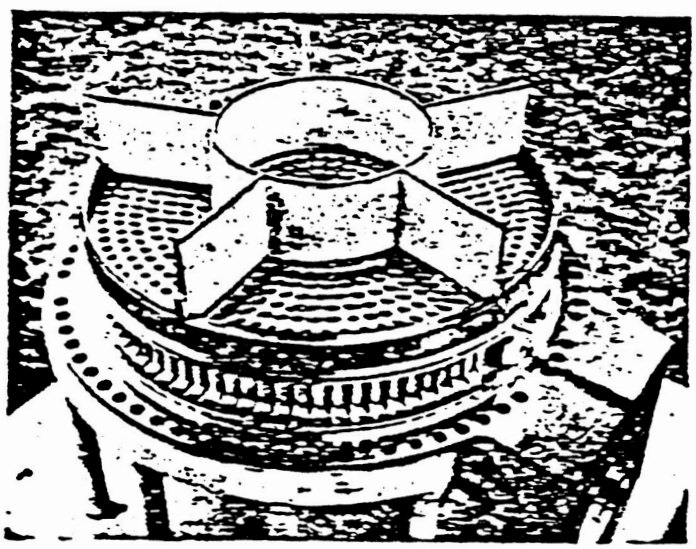

J-2S Baffled Injector Assembly

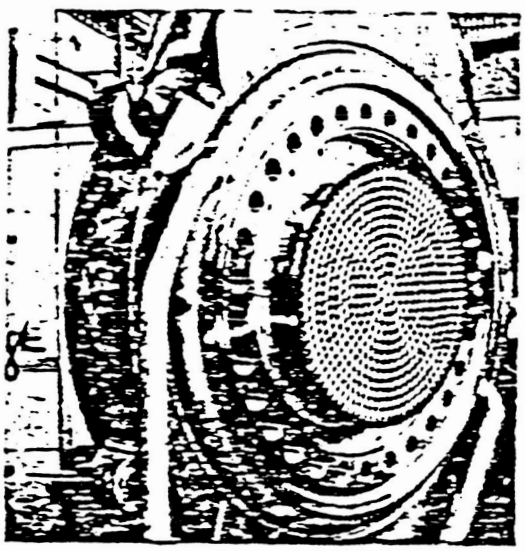

SSME Full-Scale Test
Injector Assembly

Figure 48 Examples of Uniform Coaxial Injector Patterns

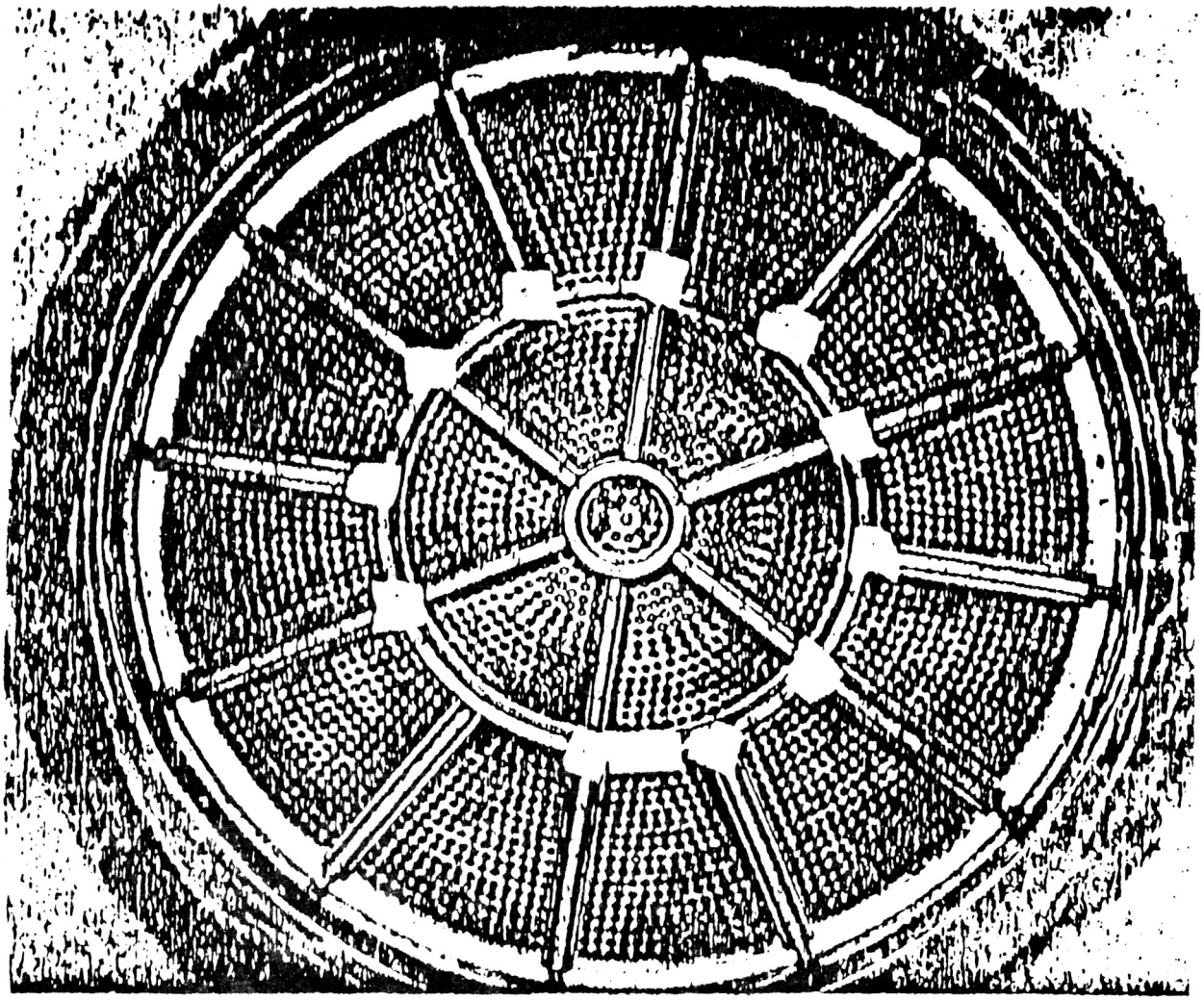

Million Pound M1 Engine Coaxial Injector Pattern

Figure 49 Examples of Uniform Coaxial Injector Patterns

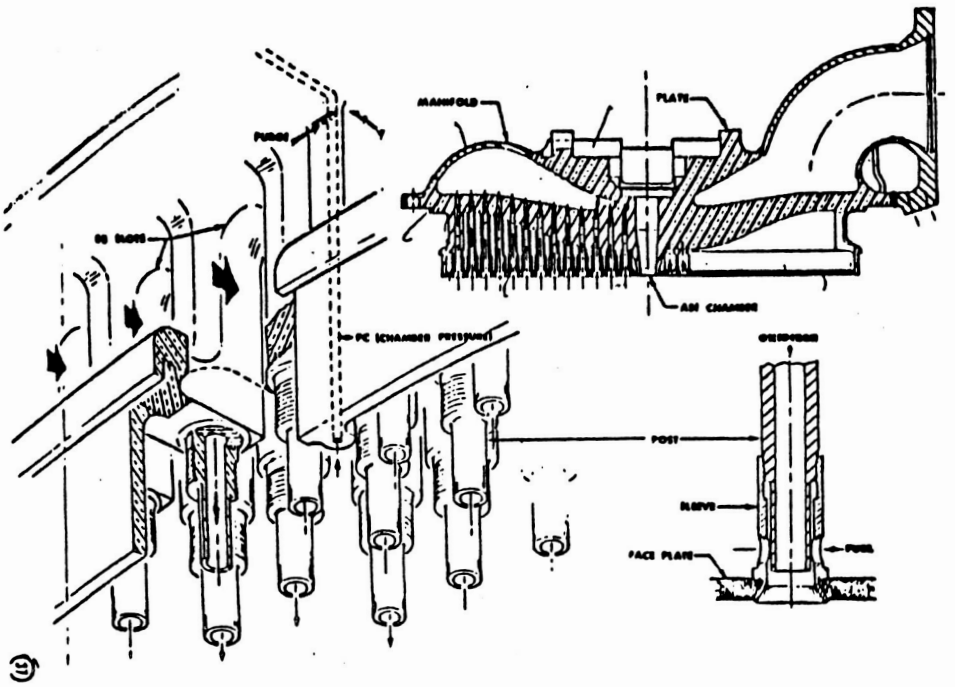

Figure 50 J-2 Injector

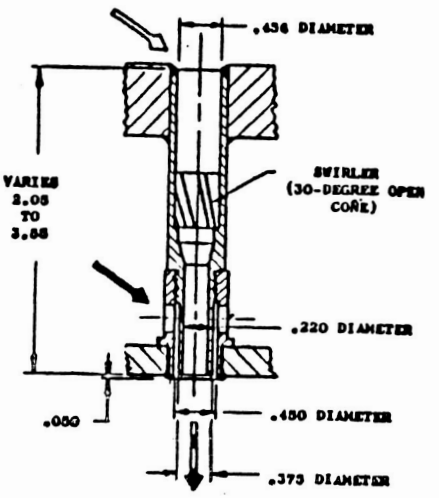

Figure 51 M1 Injector Post Configuration

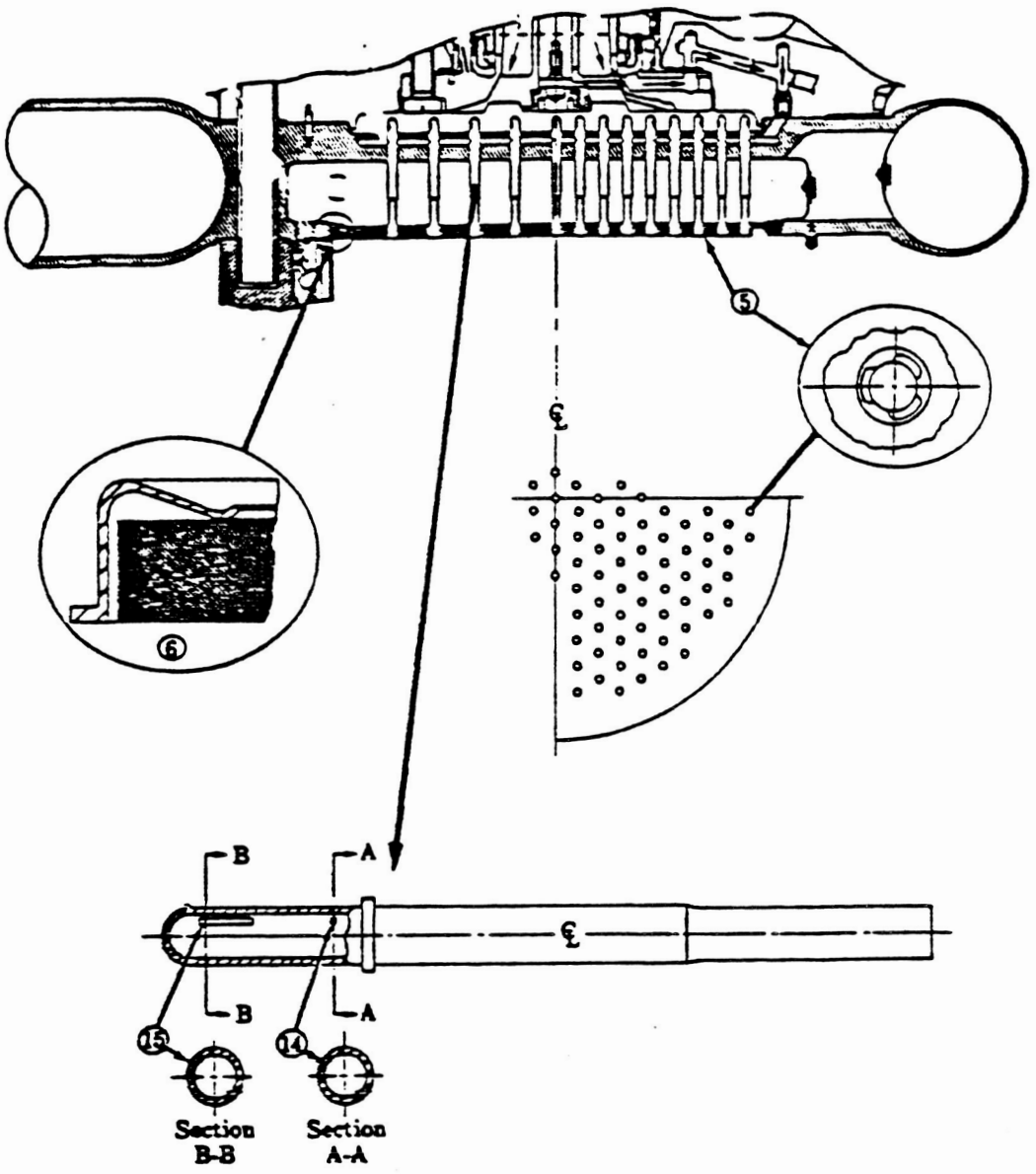

Figure 52 Demonstrator Engine Preburner Injector

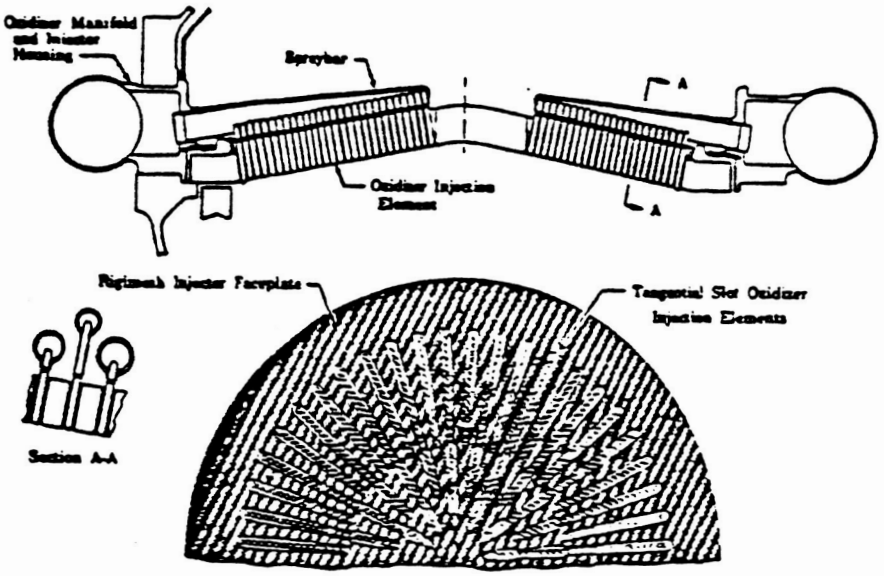

Main Burner Injector

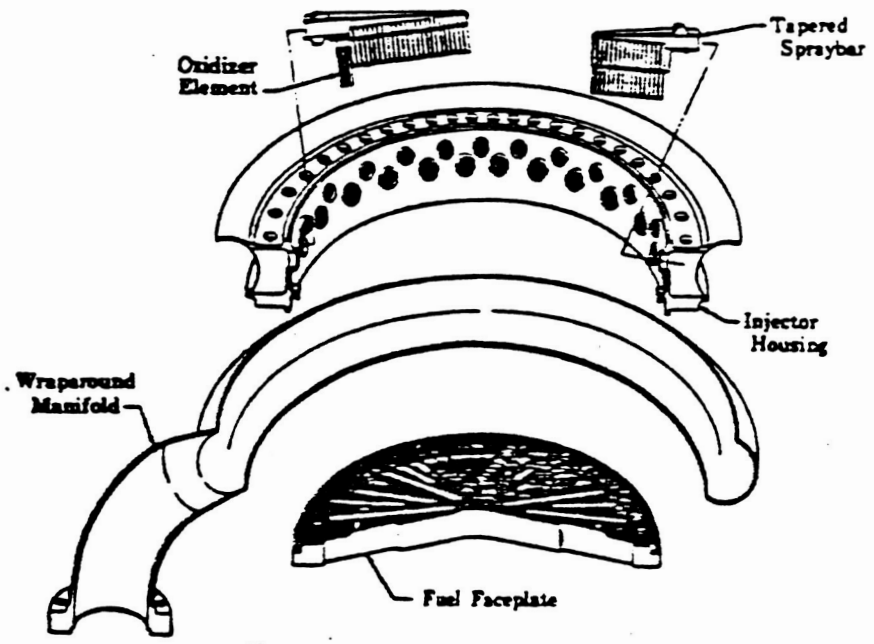

Segmented Injector Concept

Figure 53 XLR129 Main Injector Configuration

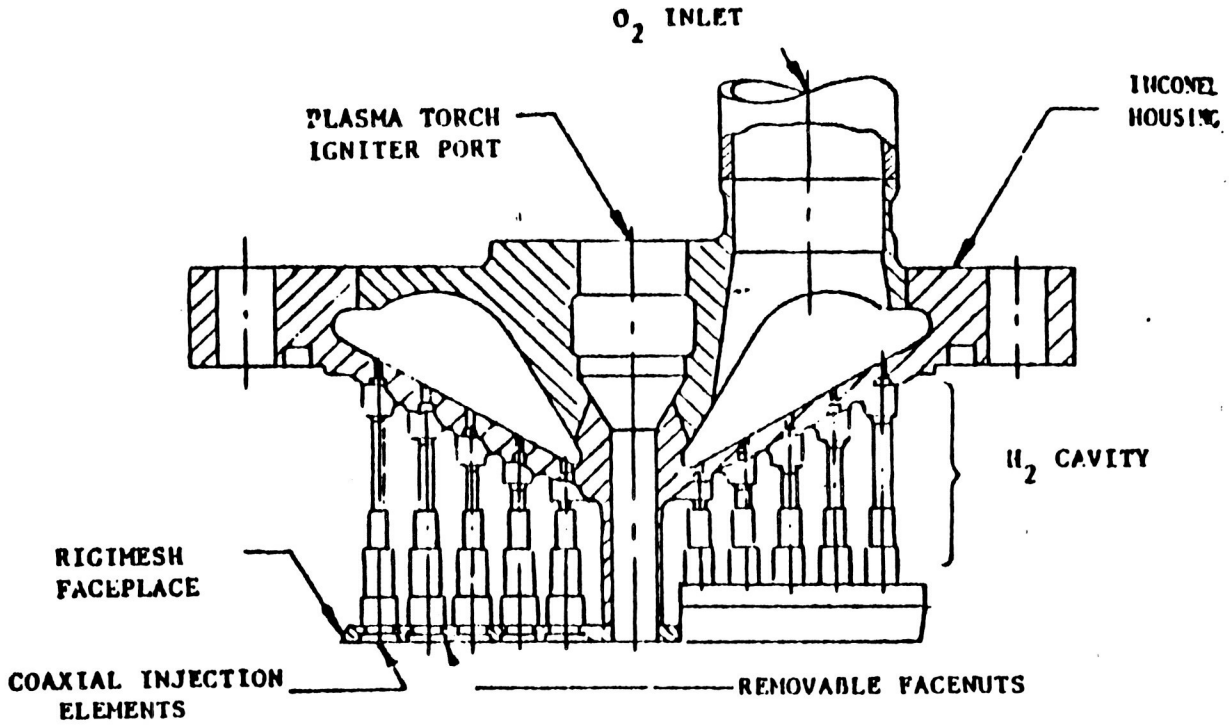

Figure 54 Advanced Expander Cycle Injector Concept (RS44)

DESIGN GEOMETRY OF CO-AXIAL ELEMENTS (GH_2/LO_2) FOR VARIOUS ROCKET ENGINES

TABLE 12

ENGINE	#COAX ELEMENTS	(IN) FUEL SLEEVE DIA. (O.D.)	(IN) OX. POST DIA. (I.D.)/O.D.	(IN^2) AREA OX/FUEL	LB/S FLOWRATE PER ELEMENT OX/FUEL	LBS. THRUST/EL	CUP RECESS	ΔP_{OX}	ΔP_{FUEL}	P_C	INJECTOR DIA. (IN)	INJECTOR FACE TO THROAT LENGTH	CONTR. RATIO	ΔT THERMAL LOX TEMP	ΔT THERMAL FUEL TEMP
J2	614	.332	$.182/.244$	$15.97/25.26$	$.741/.118$	325.0	.200	207	102	787	18.50	17.926	2.30	180°R	195°R
M1	3248	.334	$.210/.290$	$159.5/70.15$	$.831/.153$	300.0	.231	335	175.0	1000.0	42.17	30.0	1.74	180°R	140°R
SSME M.C.C. (FPL)	600	.389	$.188/.220$	$16.66/46.38$	$1.42/.4298$	783.0	.255	641.7	251.2	3000.0	17.74	14.0	2.96	191	1444
J2S	614	.323	$.119/.254$	$19.10/19.20$	$.849/.132$	431.0	.200	210	130.0	1245	18.50	17.926	1.57	180	257
RL-10	216	.186	$.014/.120$	$.9289/3.426$	$.130/.024$	70.3		52.4	77.6	395.0	10.30	15.0	4.0	167	451
ADV.EXP. CYCLE	.108	.190	$.094/.126$	--	$.247/.0357$	--	.093	--	--	1540	5.0	20.0	3.85	183	660

The large Δt observed in the SSME and XLR129 injector post results from the staged combustion process providing hot gas fuel (hydrogen rich steam) -- whereas other engines use cold hydrogen gas as the fuel. The common features of injectors from the J2, M1 and SSME include having brazed, welded or integral connection at the LO_2 dome and a threaded connection at the injector face for the fuel sleeve. High hot gas flow rates and pressures like in the SSME require large cavities to accommodate the flow. This results in the longer LOX posts - up to 9 inches - of the SSME main injectors and the wagon wheel spray bar design of the XLR129.

The design of the injector and the importance of the thermal loading is a direct function of the engine cycle. For a staged combustion engine that uses a preburner(s) to drive the turbines and whose exhaust is then used for the combustion chamber fuel, there is inherently a high Δt between the fuel and oxidizer. Other turbine drive cycles (gas generator, expanders, thrust chamber tapoff, etc) do not use combustion products as a fuel and, therefore, have relatively low Δt's in the LOX posts.

9.4 Individual Loads Summary

Details of the individual loads are covered in Appendix C. A summary of these loads is furnished in Table 13 to provide an overall perspective. The summary has categories of the individual load, how it is determined, the form available, the degree of certainty and how it is used. The loads that can be easily measured external to the pressure systems or in manifolds etc., are mechanical vibration, manifold pressures, chamber pressure, and static loads. The more difficult to measure quantities, such as LOX post temperature and flow loads, are predicted from analysis and/or analysis plus model measurements. Most loads used in the current deterministic analysis are approached from a maximum or limit view point for critical portions of the start, steady state or cut off portion of the duty cycle.

INDIVIDUAL LOADS	HOW DETERMINED	FORM AVAILABLE	DEGREE OF CERTAINTY	HOW USED
. STRUCTURAL DYNAMICS . TRANSIENT: . POPS, SIDELOADS . RANDOM VIBRATION . STEADY STATE . RANDOM VIBRATION . RANDOM PERIODIC (COMBUSTION INSTABILITY) . STEADY STATE SINUSOIDAL	ACCELEROMETERS (MEASURED)	TIME TRACES, PSD'S ISOPLOTS, AMS, TRACE SUMMARIES OR PLOTS	HIGH	INPUT TO DYNAMIC ANALYSIS
. FLOW LOADS . FLUID EXCITATION (SINUSOIDAL) . TURBULENCE (RANDOM) . VORTEX SHEDDING (RANDOM) . JET IMPINGEMENT (SINUSOIDAL)	. INSTRUMENTED FLOW TESTS . ENGINE PRESSURE MEASUREMENTS . LIMITED STRAIN GAGE RESPONSES	PSD, SPECTRUM OF LEVELS (GGIP), ANALYTICAL MODEL'S WATER TABLE TEST PICTURES	LOW TO MODERATE	INPUT TO DYNAMIC ANALYSIS

Table 13a Individual Load Summary

INDIVIDUAL LOADS	HOW DETERMINED	FORM AVAILABLE	DEGREE OF CERTAINTY	HOW USED
. TEMPERATURE LOADS	PREDICTED FLOW TEST MEASUREMENTS	TEMPERATURE FIELD ON GEOMETRY CROSS-SECTION(S)	MODERATE	INPUT TO STRUCTURAL ANALYSIS
STATIC PRESSURE	MEASURED AND CALCULATED	DISTRIBUTED VALUES ON POST SURFACE	MODERATE TO HIGH	STRUCTURAL ANALYSIS
DEBRIS	PREDICTED, BASED ON HISTORY OF ENGINE	DEBRIS SIZE AND VELOCITY	LOW	SENSITIVITY ANALYSIS OR INCIDENT INVESTIGATION
STATIC	ENGINE LOADS ANALYSIS	TABLE	MODERATE	STRUCTURAL ANALYSIS
FABRICATION	PREDICTED	ANALYSIS RESULTS	LOW	STRUCTURAL ANALYSIS
DAMPING	CORRELATE FROM STRAIN GAGES PREDICTED-ROW 13, LIFE COMPARISON OTHER ROWS	TABLE	MODERATE	DYNAMICS ANALYSIS

Table 13b Individual Load Summary (Contd)

The degree of certainty is downrated for the loads that have either limited or no actual engine test verification of calculated conditions. In some cases, analysis confidence is based on engine test results. The fleet leader SSME injector was on engine 2010 that had almost 20,000 seconds of hot fire testing. Over 8400 seconds of this testing was at FPL conditions. The powerhead from this engine is currently being disassembled and disected for engineering data. Typically, the individual loads are used in a combined structural analysis of an individual LOX post.

9.5 Combined Load Assessment

The combined loads for the LOX post are treated in a similar fashion as the turbine blades, see section 8.5. The LOX posts have additional loads such as mechanical vibration that are developed from high frequency measurements using accelerometers. The engine vibration measurements are used to develop a dynamic environment that is used for a mechanical vibration analysis. The dynamic analysis is an elastic solution that considers shock and transient loads separate from steady-state conditions. The dynamic analysis results are combined with the static analysis results for the strength and life analysis.

10.0 TRANSFER DUCTS

10.1 Introduction

The need for hot gas manifold transfer ducts like those used on the SSME is dependent on the overall engine cycle and packaging. The high pressures, temperatures and systems requirements of a staged combustion engine have led to a close coupled powerhead packaging of turbopumps, preburners, injector and main combustion chamber. The complexity and interaction of loads from this type of packaging adversely affects other engine systems goals such as fabrication and accessibility requirements. Both the SSME and XLR129 staged combustion engines utilize this integrated powerhead approach.

The other three LOX/LH_2 engines used in the generic loads evaluation use different packaging concepts. The GG and expander cycle engines have lower pressures and temperatures in the hot gas systems. This allows for simpler packaging and ducting systems. Ducting on these engines are single wall structures that take both the pressure and thermal loads from the hot gases. The concept used in the staged combustion engines has been to separate the pressure and thermal loads. The outer structural shells are kept at low temperatures and support pressure and mechanical external loads. The transfer ducts (liners) are cooled on one side or have stagnant hot gases behind them to absorb the system heat load and have a small differential pressure load. This separation of loading adds complexity, but markedly reduces the weight of the structural shell.

The SSME engine packaging concept is shown in Figure 55 and Figure 56. Figure 55 shows the manifold configuration and Figure 56 indicates how the component integration with the manifold is achieved. Hot gas from preburners is ducted directly to high pressure turbines which then discharges the gas to a toroidal manifold. The high pressure, high flow rate, high temperature hydrogen rich gas then enters the hot gas transfer ducts; three on the fuel side and two on the oxidizer side. The gas is then routed to the main injector torus manifold where it is radially directed into the hot gas cavity of the main injector.

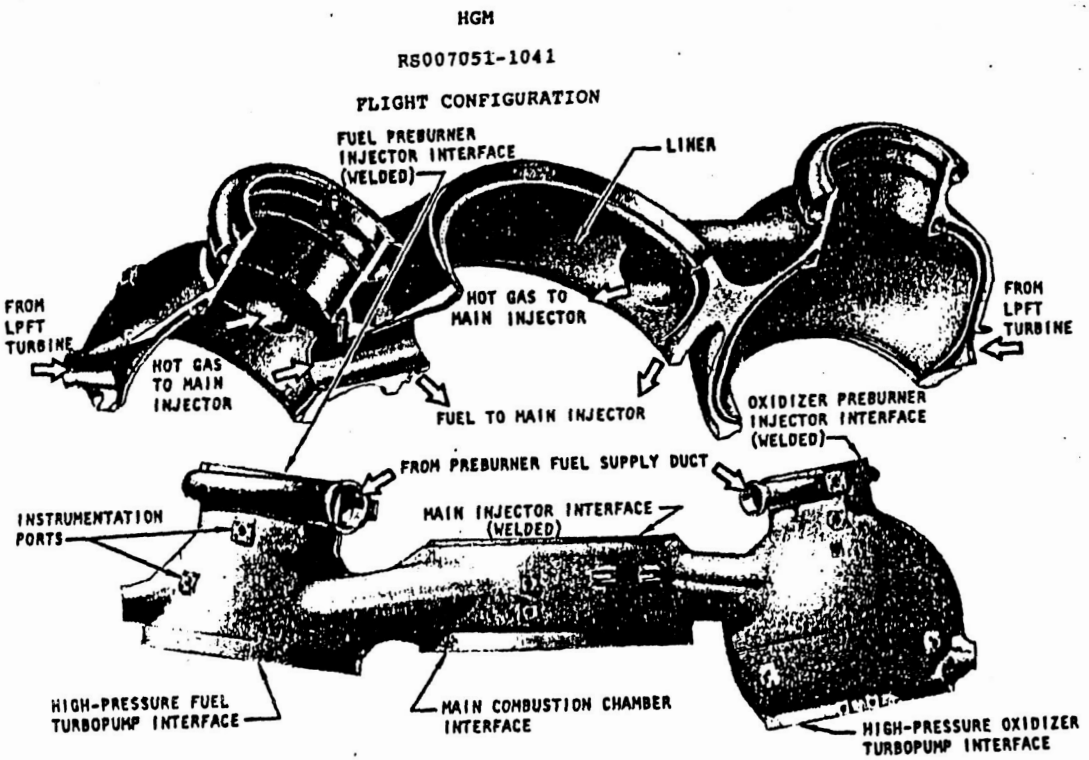

Figure 55 SSME Hot Gas Manifold

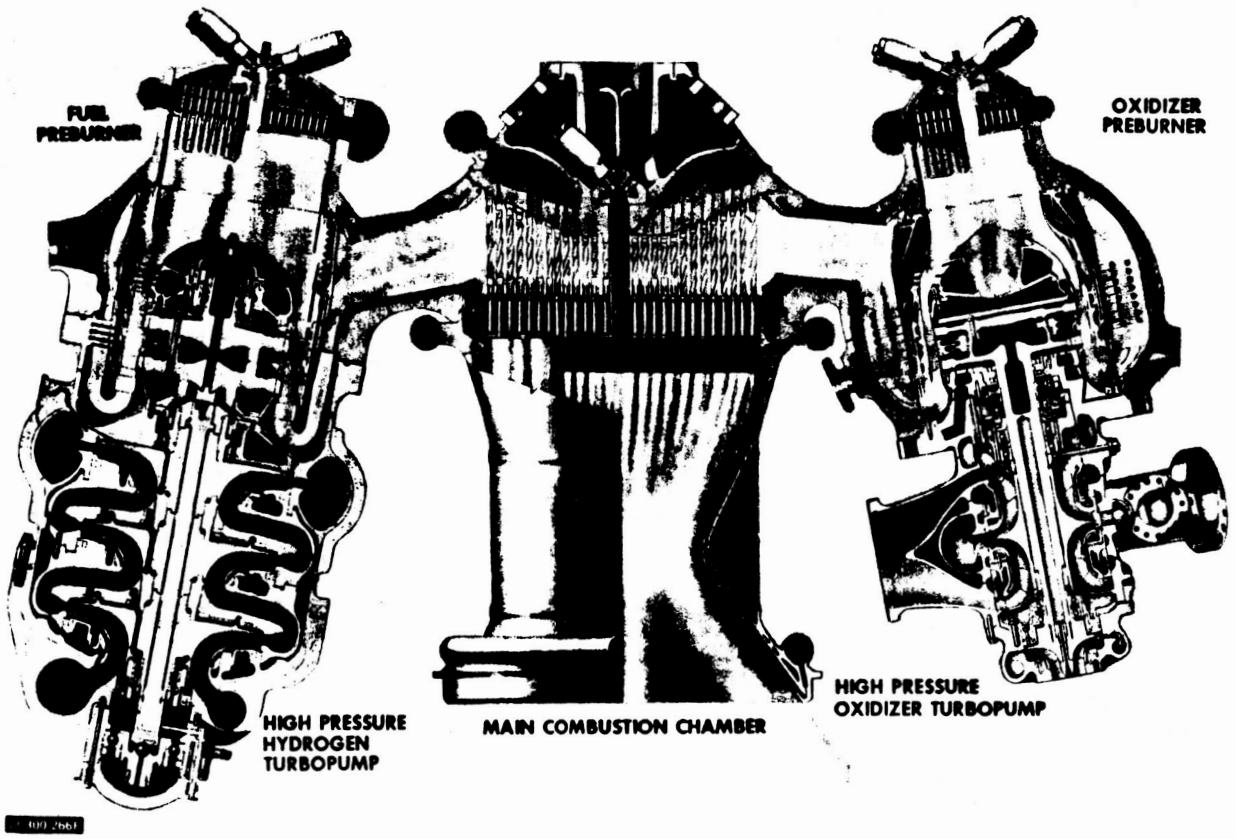

Figure 56 SSME Powerhead Component Arrangement

A somewhat different engine packaging concept was utilized in the XLR129 reusable rocket engine which had very limited component testing. Figure 57 shows the transition case relationship between the preburner and turbopumps. Figure 58 shows how the components were attached or plugged into the transition case. Similar to the hot gas manifold of SSME, the transition case served as the mounting structure for major components - the preburner, oxidizer pump, fuel pump, injector and main combustion chamber. It contained internal ducting that routed preburner discharge gases through the fuel and oxidizer turbines and to the main injector. This ducting in the transition case center body is equivalent to the SSME transfer ducts.

The liner was hydrogen transpiration-cooled and limited the case external skin from temperatures to 540°R. The inside of the outer case preburner segment was gold plating (0.0001 inch) which reduced preburner flow duct radiation effect on the temperature of the outer case structure in this area.

The liner took the shape of the outer case and was assembled into the outer case by welding together preformed spherical segments fabricated from sintered wire mesh, creating a porous metal barrier between the outer case and turbine exhaust products. Hydrogen passed through the liner forming an insulating boundary.

Design studies indicated that a spherical Rigimesh liner that uniformly follows the outer case contour is optimum for providing the best flow properties. This ensured there was no severe maldistribution of coolant caused by the quantity or location of coolant supply points. The liner was set at a liner-to-outer-shell proximity of 0.170 to 0.190 inch to minimize the volume. The volume behind the Rigimesh strongly affects liner pressure differential during a transient. The selected liner was designed for a 10 psi pressure differential under design conditions, providing a Rigimesh liner differential pressure of 4 psi at minimum thrust and maximum mixture ratio conditions. The liner was 0.057 inch thick. The liner was flame sprayed in local areas as required to ensure the proper flowrate (Ref. 1).

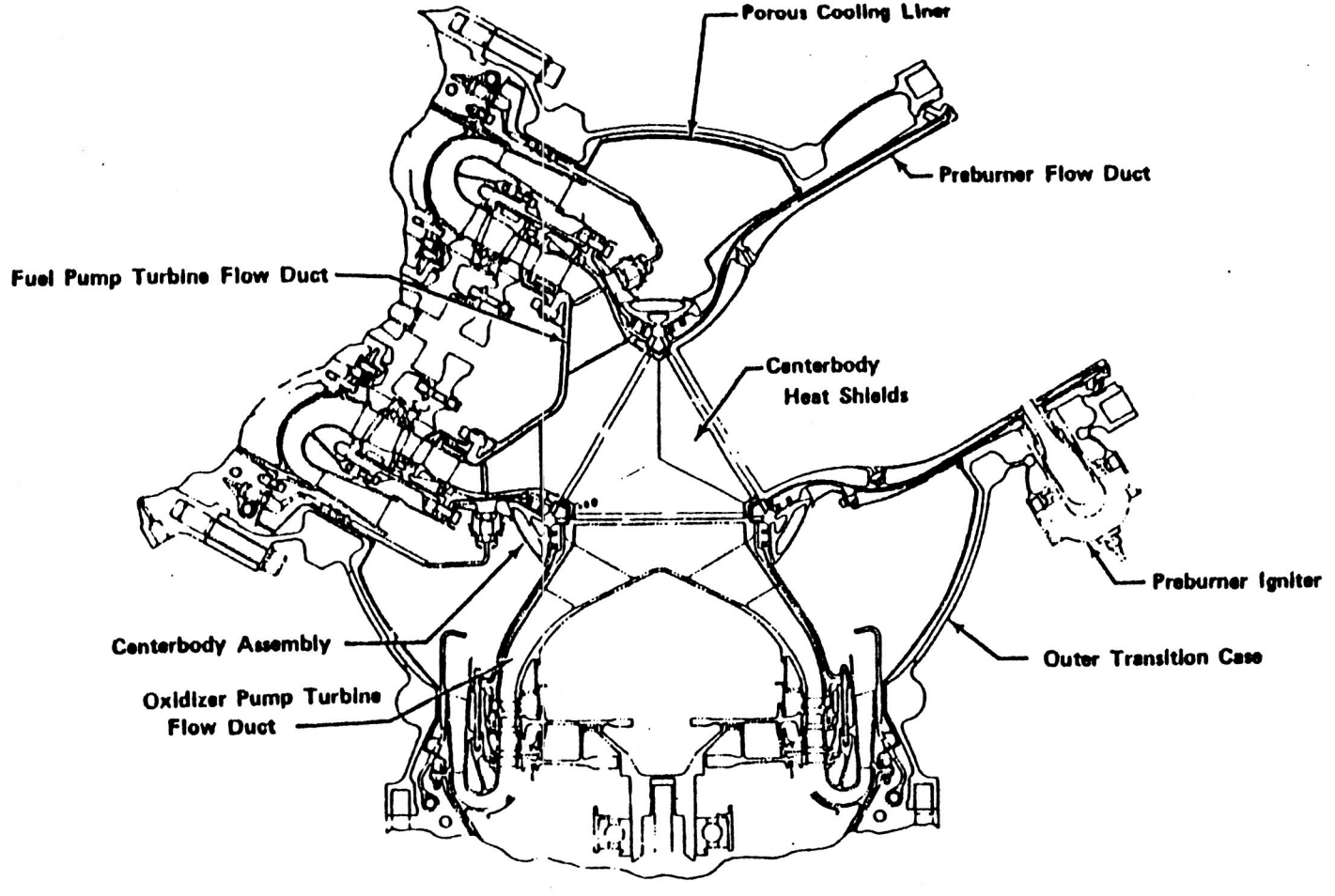

Figure 57 Transition Case Assembly

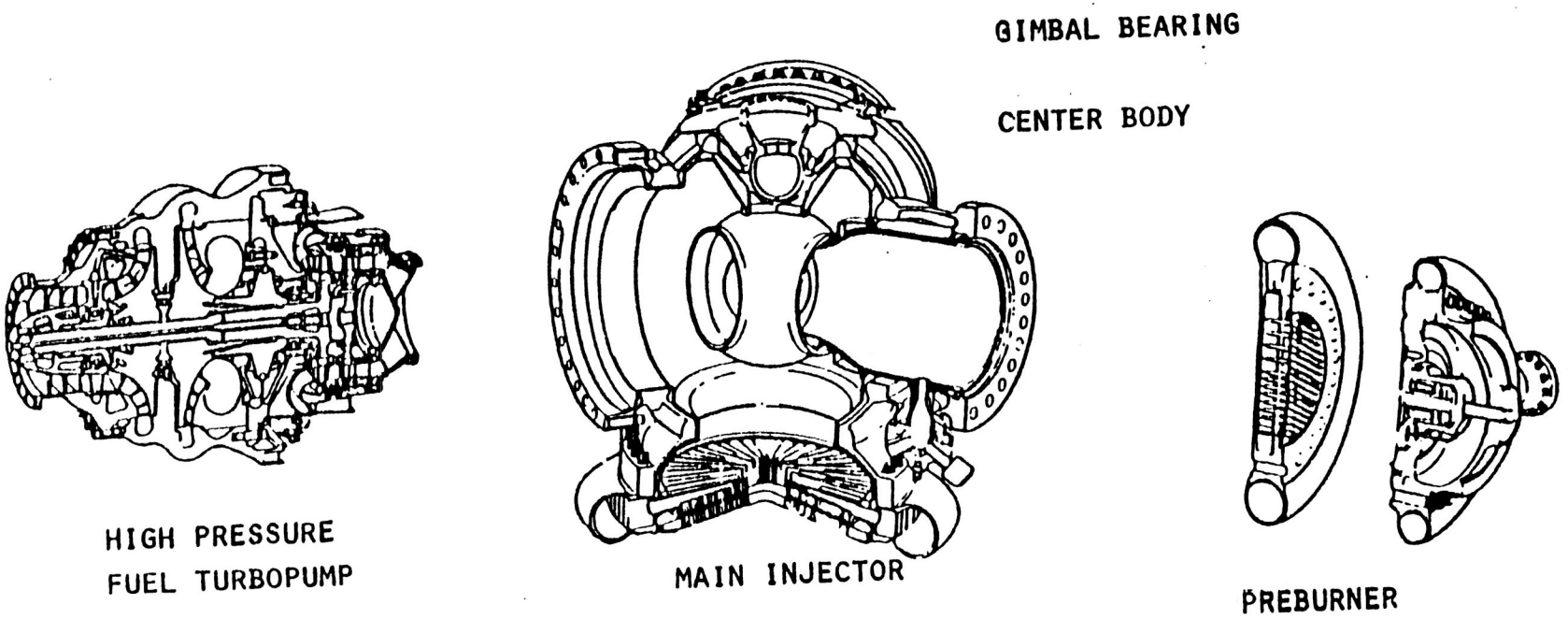

Figure 58 XLR129 P-1 Engine Packaging Concept

Thus a manifold design for a stage combustion engine consists of structurally efficient spheres and cylinders. Cooled structural shell concepts are invariably used to minimize the system weight. This is achieved by having a structural thermal liner which forms anular passages between the liner and the outer casing, through which the cold hydrogen flows. Integrity of the structural thermal liner is important for satisfactory engine operation. It must be emphasized that the internal environment is very severe having high temperature, high flow rate, high velocity and gases.

A second scrub liner can be used in part of the flow path to act as an additional barrier against hot gas impinging on the structural liner. This minimizes the structural liner temperature and thermal expansion. The scrub liner can also be used as a flow guide. Usually, stagnant gas is present in the gap between the liner elements. Such scrub liners are used in both the SSME and the XLR129 hot gas system.

Extensive engine experience has indicated few problems with the outer case structural shell of the hot gas manifold. However, the inner liners are subjected to environments and forces that are not well understood. For purposes of this contract, the transfer duct component analysis is limited to the analysis of structural and scrub liners.

10.2 SSME Transfer Ducts

The shape of the transfer tube liners is determined by the geometry of the outer structural shell of the transfer tube and the integration of the liner tubes into the toroid or spherical shell shapes that line the preburners (PB) and main injector . Figure 59 shows the overall liner configuration within the hot gas manifold on the SSME production engine and delineates the transfer duct liner configuration.

In addition to the production configuration, there is a modified HGM development configuration that has two tubes on the fuel pump side rather

than the current three tube design. This design incorporates smoother fairings between the inlet to the transfer duct and the preburner liner. The smooth fairing to the bowl liner reduces stress concentrations as well as providing a better flow geometry (Figure 60). These doubly curved complex shell regions can be stress or buckling critical.

The cross-section of the production transfer duct is circular and the axial length varies as a function of the transition length between the preburner and injector liner bowls. The crossectional shape of the tube is determined by the area needed to transport the given amount of gas and simultaneously satisfying envelope, structural strength and flow requirements. The development HGM fuel side transfer duct are elliptical in shape because of packaging limitations. A round shape of sufficient area would require a longer powerhead which was a design constraint.

The coolant flow bathes the outside surfaces of the HGM liners and is nominally 100 to 200 psi greater than the hot gas pressure. This is a design requirement to insure any cracking or damage to the liner will leak coolant into the hot gas rather than the hot gas into the coolant. This results in an external pressure load on the liner and transfer duct.

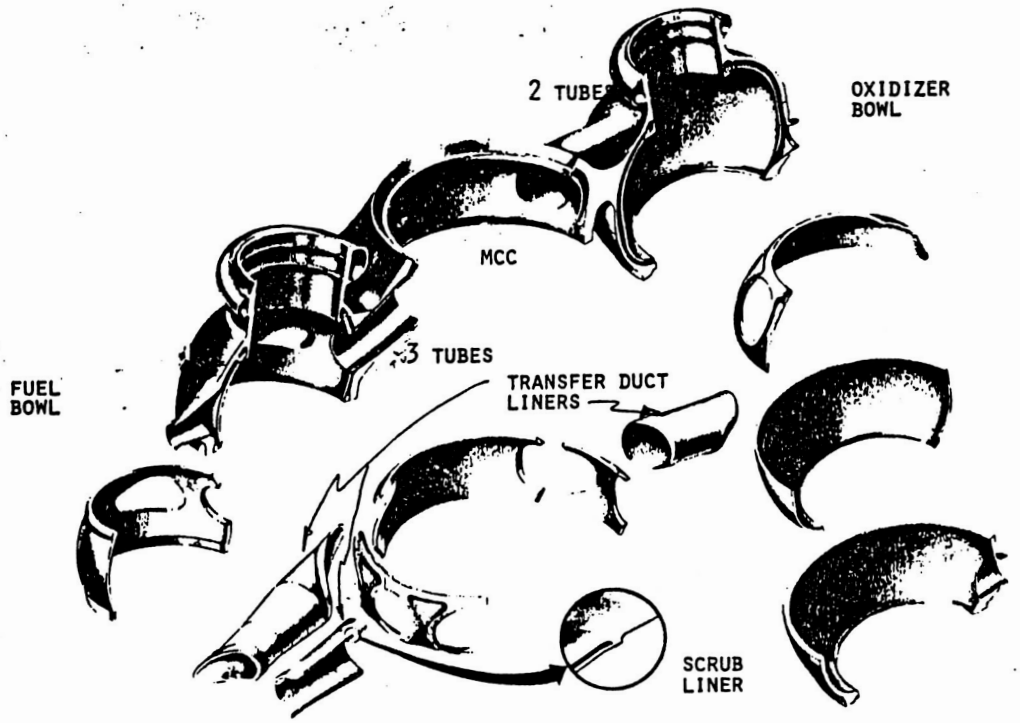

Figure 59 Hot Gas Manifold Line Production Engine

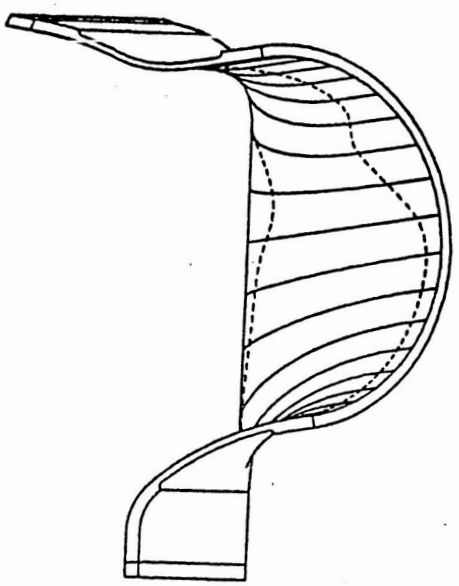

Figure 60 Inlet Fairing to the Fuel Transfer Tube of the Two-Duct HGM

The liners are joined by welds at the main injector liner bowl and the respective fuel or oxidizer liner bowl. The integral attachment results in large thermal restraint loads at the liner to shell intersections and axial loads in the liner. The basic concept of the transfer duct is shown in Figure 61. Typical weld joints are shown for the liner and the scrub liner. The cooled structural liners are thermally protected by the scrub liners such that the ends of structural liners incur less axial growth than without the scrub liners. The uncooled scrub liners run at gas temperatures and are cantilevered from the inlet side to allow for free expansion.

Evidence of unsatisfactory structural performance of the transfer tube scrub liner, resulting from FPL (full power level) testing operations, was first noted in mid 1980. The failures were the scrub liner cracking in the central fuel tube of many engines and were attributed to high cycle alternating stresses. The conditions started on all of the engines after a relatively short test period at full power level (FPL, 109% rated power level). The initial design was adequate for RPL operations as no transfer duct problems were experienced at that power level. The cracking occured at the junction of the transfer tube to the fuel transfer tube liner inlets (Figure 62). The cracking was attributed to the liner first bending mode and shell bending mode combination and was restricted to the center fuel transfer tube. This failure mode was eliminated by adding motion limiting support spacers (buttons Figure 63) to the thermal protection liners. These devices are welded to the thermal protection liner and limit relative radial motion between the thermal protection and structural liners. Failures persisted in some engines even with the spacer configuration. However, the failures occurred when the support spacer installation allowed excessive initial gap between the support spacer ends and the structural liner. The gap increased due to support spacer deterioration by impacting of the structural liner, eventually allowing the thermal protection liner to fail in a similar manner to the earlier unsupported liner assemblies. Support spacer installation criteria was established to preclude service deterioration and doublers have also been added to locally increase the strength of the liner. These are only interim solutions. All new designs incorporate integrally machined deflection limiting supports on the liner (Figure 64).

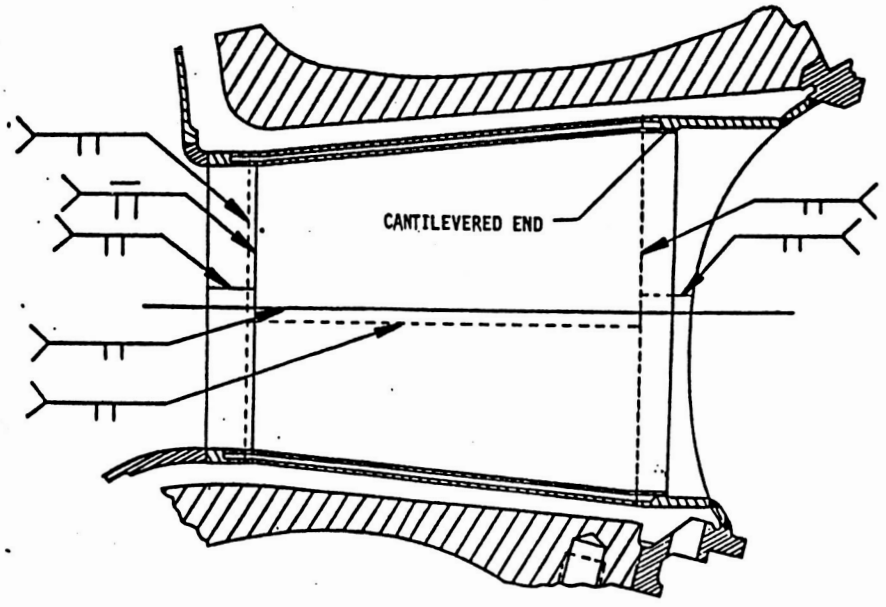

Figure 61 Scrub Liner & Structural Liner Concept Used in HGM Transfer Tube Design

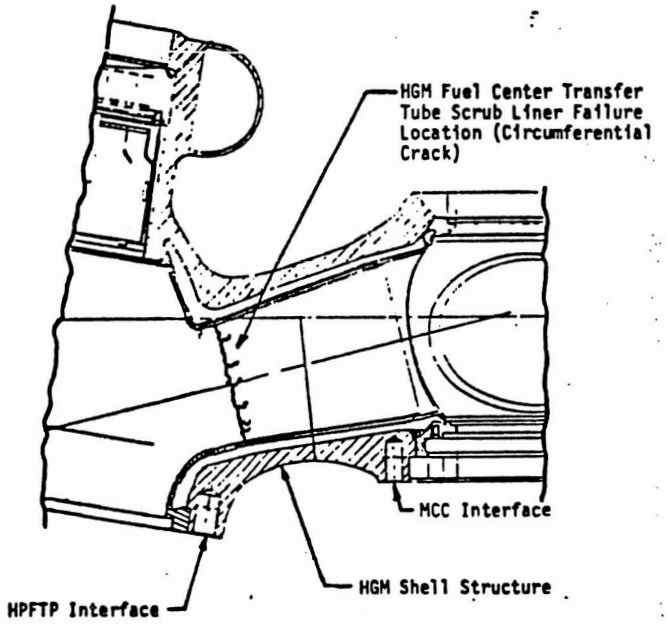

Figure 62 Center Transfer Tube Liner Failure

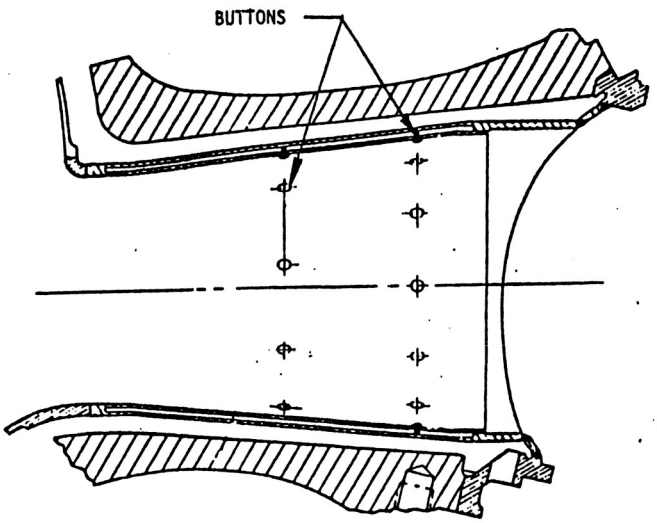

Figure 63 Center Transfer Tube Liner with Motion Limiting Buttom Configuration

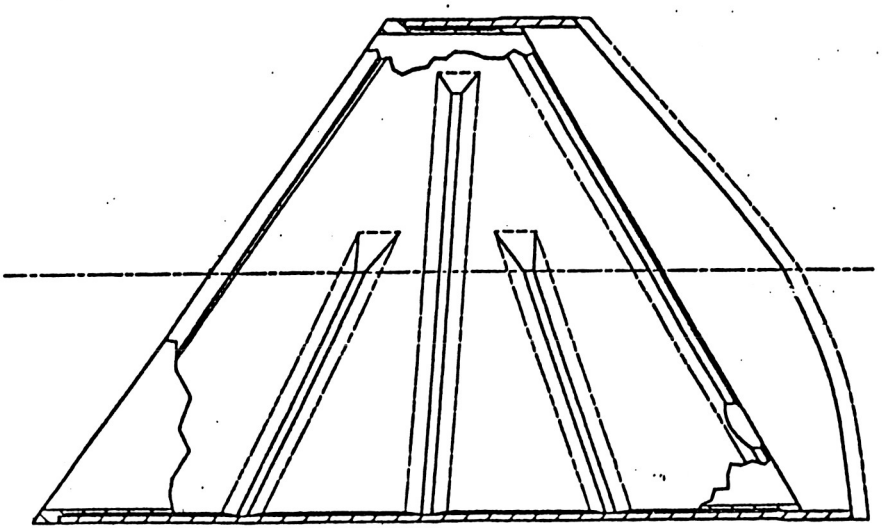

Figure 64 New HGM Liner Design with Integrally Machined Motion Limiters

10.3 Loading Environment

The current design procedure includes duty cycle analysis for static pressure, random pressure, temperature, temperature gradients and mechanical loading. The flight configuration has three ducts on the fuel side. A development configuration has only two ducts on both fuel and lox sides of the HGM. The two duct configuration has had only water table and air flow testing to date. Due to the severe environment in the transfer tubes, no measurements of static or dynamic pressure in the transfer tubes itself are available from hot fire engine tests. The pressure loading that is used in analysis is a combination of engine balance, scaled values from extensive airflow tests and the nearest available instrumentation to the point of interest from hot fire engine tests. In most cases, the HGM port in the injector zone is the closest instrumented pressure. An accurate determination of the flow field in the hot gas manifold is a difficult task due to intricacy of the flow passages. The flow exits the turbine at a high velocity and the tight turnaround ducts leads to separation of flow on the inner wall. Figure 65 shows two design configurations and the difference in flow conditions. The swirling action of the gas at the turbine exits to a one sided discharge. The compactness of the manifold leads to a transverse pressure differential. The flow in all the transfer tubes is not equal. Typical mass flow splits for the three duct system are 52, 9 and 39% and for the two duct system are 52% in the transfer duct favored by the swirl direction and 48% in the other duct. The maximum engine scaled mach number observed in the three duct configuration is 0.26, while the two duct HGM exhibits a maximum mach number of 0.16.

One of the primary objectives of the current SSME development program is to make design changes that improve the flow field in the hot gas manifold. In support of these design changes, data from extensive air flow tests, computational fluid dynamics model results and water flow test data are available for both the two and three duct configuration.

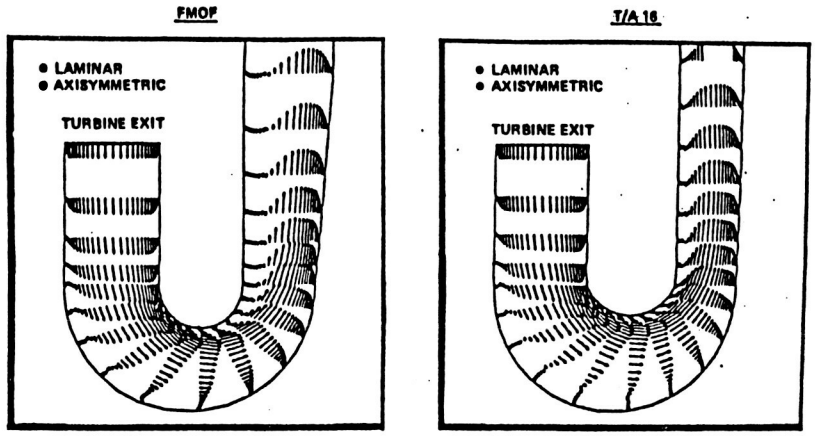

Figure 65 CFD Velocity Vector Results for Two Turnaround Duct Configurations

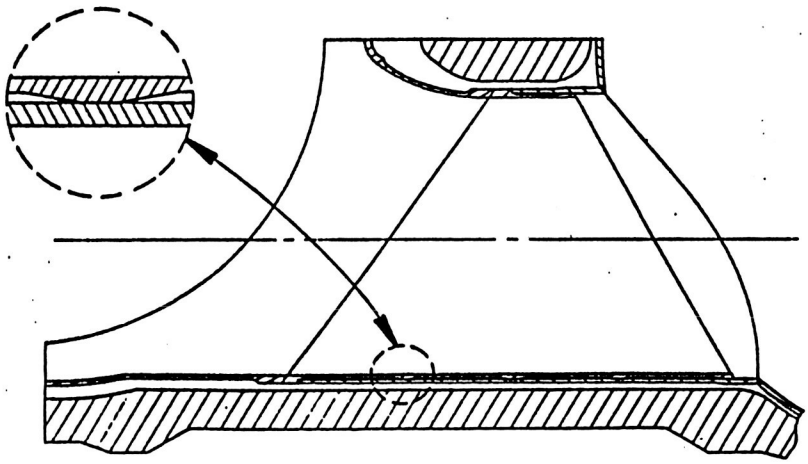

Figure 66 Integrally Machined Motion Limiters in the Two Duct Tube Liner Designs

The transfer duct geometry is characterized by a short length compared to its diameter (Figure 66). Thus simulating flow in the transfer ducts as flow through a long duct can be a gross error. The static pressure flow field in the transfer duct is affected by the geometry of the turnaround duct and the details of the inlet fairing to the transfer duct, where the variation in static pressure in the thirteen zones has been observed. The measurements were made using two dimensional probes. The flow rate used in the model testing is more than 100 lbm/sec. of ambient air, which is equivalent to 60% of the Reynolds number of the hot fire engine operating of RPL. Previous testing has shown this simulation to be a sufficiently accurate modeling of the hot fire engine.

In a transfer duct liner design, scrub liners are not designed for any significant pressure differential. Pressure relief passages are provided to avoid any pressure differential. On the other hand, the structural liners are designed for pressure differential between coolant pressure and the gas pressure. Measurements of coolant pressures in the transfer tube liners are not available. These values are obtained from engine balance and transient simulation models. The differential pressures are evaluated for both steady state and transient conditions. The maximum differential pressure is of the order of 200 psi between the coolant and hot gas.

10.4 Individual Loads Summary

To provide an overall prospective, the individual loads are covered in the following sections. A summary of these loads is furnished in Table 14. The summary has categories of the individual load, how it is determined, the form available, the degree of certainty and how it is used. The loads that can be easily measured external to the pressure systems are mechanical vibration and manifold pressures. The more difficult to measure quantities are predicted from analysis and/or analysis plus air flow model measurements. Most loads used in the current deterministic analysis are approached from a maximum or limit view point for critical time slices of the start, steady state or cut off cycles.

INDIVIDUAL LOADS	HOW DETERMINED	FORM AVAILABLE	DEGREE OF CERTAINTY	HOW USED
. DYNAMIC PRESSURE . TURBULENCE . FLOW OPERATION	CALCULATED FROM AIRFLOW TESTS AND SCALED TO ENGINE OPERATION	PSD'S	MODERATE TO LOW	INPUT TO DYNAMIC ANALYSIS
. TEMPERATURE LOADS	PREDICTED	TEMPERATURE FIELD ON GEOMETRY CROSS-SECTION	MODERATE	INPUT TO STRUCTURAL ANALYSIS
. DEBRIS	PREDICTED, BASED ON HISTORY OF ENGINE	DEBRIS SIZE AND VELOCITY	LOW	SENSITIVITY ANALYSIS OR INCIDENT INVESTIGATION
. FABRICATION	PREDICTED	--	LOW	STRUCTURAL ANALYSIS

TABLE 14 INDIVIDUAL LOAD SUMMARY - Transfer Ducts

INDIVIDUAL LOADS	HOW DETERMINED	FORM AVAILABLE	DEGREE OF CERTAINTY	HOW USED
. STRUCTURAL DYNAMICS . TRANSIENT . SIDELOADS . RANDOM . STEADY STATE . RANDOM . SINUSOIDAL	ACCELEROMETERS (MEASURED)	TIME TRACES, PSD'S, ISOPLOTS & SUMMARIES OF PLOTS	HIGH, ALTHOUGH MEASUREMENT ON HGM SHELL NOT DIRECTLY ON COMPONENT	INPUT TO DYNAMICS ANALYSIS
. STATIC PRESSURE . AVERAGE CROSS SECTION . TRANSIENT WITH CHUGGING . STEADY STATE . COOLANT FLOW AND LINER ΔP . CIRCUMFERENTIAL VARIATION	CALCULATED FROM ENGINE MODELS AND AIRFLOW TESTS	LOCAL VALUES THAT ARE THEN DISTRIBUTED ON LINER.	MODERATE	STRUCTURAL ANALYSIS

TABLE 14 INDIVIDUAL LOAD SUMMARY - Transfer Ducts (Contd.)

The degree of certainty is downrated for the loads that have either limited or no actual engine test verification of calculated conditions. In some cases, analysis confidence is based on engine test results. The fleet leader hot gas manifold was on engine 2010 that had almost 20,000 seconds of hot fire testing. Over 8400 seconds of this testing was at FPL conditions. The powerhead from this engine is currently being disassembled and disected for engineering data. The individual loads are used in a combined structural analysis of an individual transfer duct.

10.5 Combined Load Assessment

The combined loads for the transfer duct are approached in a similar fashion to the LOX posts and turbine blades, see sections 9.5 and 8.5. There is more emphasis on the dynamic flow loads and how they are integrated in the analysis since they are a primary driver in the high cycle fatigue life assessment.

11.0 FOURTH COMPONENT

11.1 Introduction

The survey effort to determine a fourth component included three components: the HPOTP discharge duct, the MCC liner and the nozzle feedlines. These components were chosen for evaluation as they have had extensive analysis as part of the SSME development. At the start of this effort a selection criteria was established to aid in the evaluation. The selection criteria considerations were that the component has:

1. Received a lot of attention--failures, limited life, NASA interest.
2. Available hot fire test data
   a. Current database
   b. New test data planned
3. Data on multiple configurations/load history changes
4. Typical mission history profiles of a large number of engine components
5. Importance structural contract (PSAM)
7. Loading extends the probabilistic formulation methodology

The following three subsections furnish the generic survey and individual and combined loads summary. The details of the fourth component survey are found in Appendix E.

11.2 High Pressure Oxidizer Turbopump Discharge Duct

Introduction. The high-pressure oxidizer turbopump discharge duct (HPOTPDD) transfers propellant from the high pressure oxidizer turbopump discharge to the main oxidizer valve, and (through a branching duct) to the preburner boost pump inlet. Key loads that affect the duct performance and structural capability are pressure, installation misalignment, and mechanical and flow induced vibration loads. Loads affecting the duct design are both static and dynamic. The steady-state loads dictate the design of the duct and the loads from the start transient have a negligible effect.

This duct is one of 24 interconnecting lines on the engine that include 1) articulating main propellant ducts, 2) fluid interface lines - articulating, flexhose and hard lines and 3) component interconnects - hard lines and flexhoses. These ducts are summarized in Table 15. Figures 67 to 69 show some of these lines and their routing and packaging.

The major difference between articulating ducts, fluid interface ducts and hard lines is that the former lines are flexible to angular and translational deflections. The main angular deflections and translations are caused by gimbaling of the engine. Added deflection capability is necessitated by the engine alignment requirement for the engine thrust vector to be within 30 minutes of arc to the engine center line and laterally within 0.6 inch of the gimbal center. In order to permit conformance with the lateral alignment requirement, an adjustment capability of ± 0.50 inch was designed into the gimbal bearing thrust chamber interface. The duct design must also be capable of absorbing torsional deflections caused by gimbal bearing torsional flexibility and Hooke's joint effect.

Table 15 Summary of Interconnects

ARTICULATING MAIN PROPELLANTS	FLUID INTERFACE LINES	COMPONENT INTERCONNECTS
LPFTP PUMP DISCHARGE	ARTICULATING	HARD LINES
LPFTP TURBINE DRIVE		
LPFTP TURBINE DISCHARGE	FUEL BLEED	HPFTP DISCHARGE
LPOTP PUMP DISCHARGE	OXIDIZER BLEED	PREBURNER FUEL SUPPLY
LPOTP TURBINE DRIVE	OXIDIZER TANK PRESSURANT	HPOTP DISCHARGE
		PREBURNER OXIDIZER SUPPLY
	FLEX HOSES	HEAT EXCHANGER SUPPLY
	HYDRAULIC SUPPLY	HGM COOLANT DUCT
	HYDRAULIC RETURN	PREBURNER PUMP SUPPLY
	ENGINE GASEOUS NITROGEN	
	SUPPLY	FLEX HOSES
	ENGINE HELIUM SUPPLY	PNEUMATIC SHUTDOWN CONTROL
		FUEL PUMP LIFTOFF SEAL
		CONTROL
	HARD LINES	
	FUEL TANK PRESSURANT	

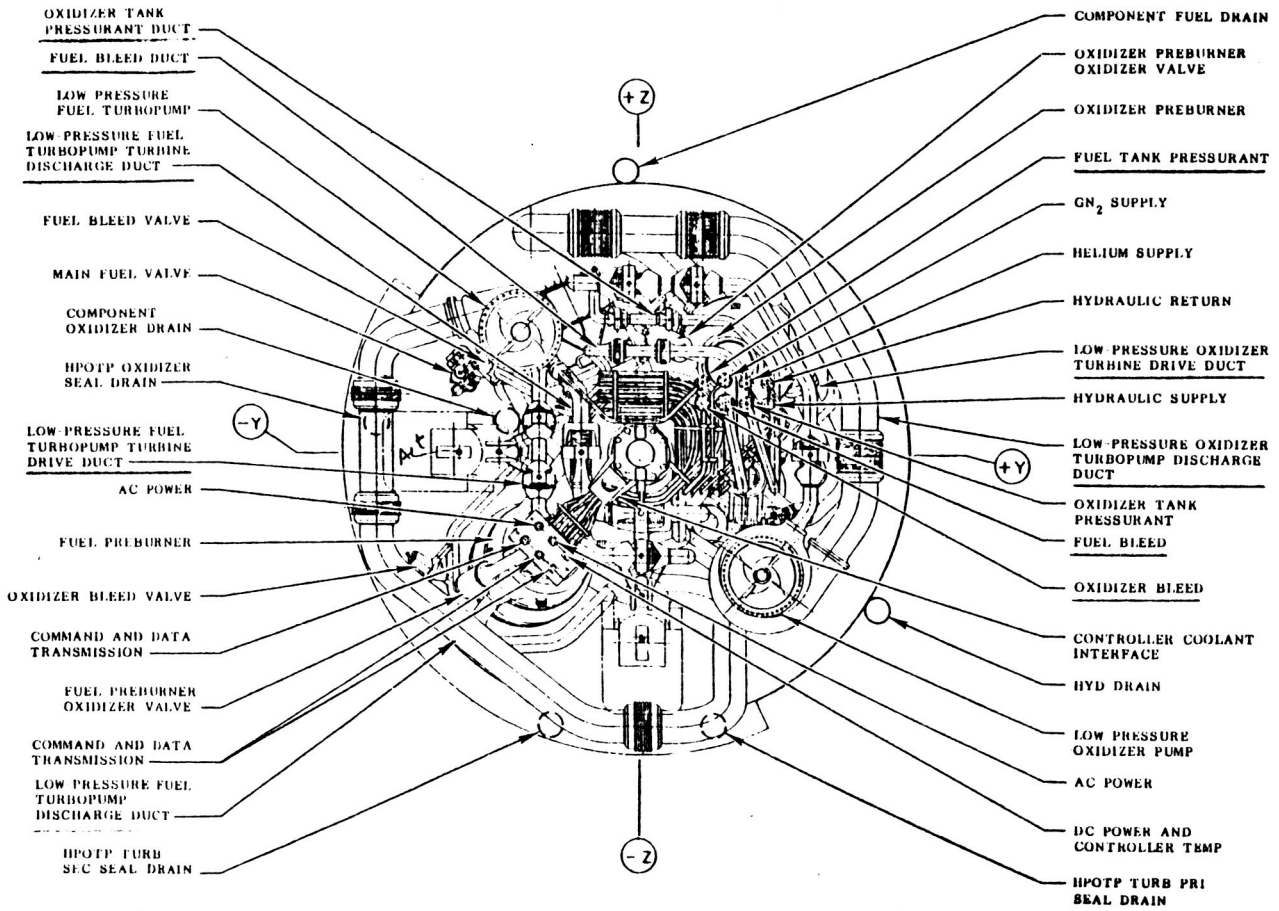

Figure 67 SSME Propellant Ducts

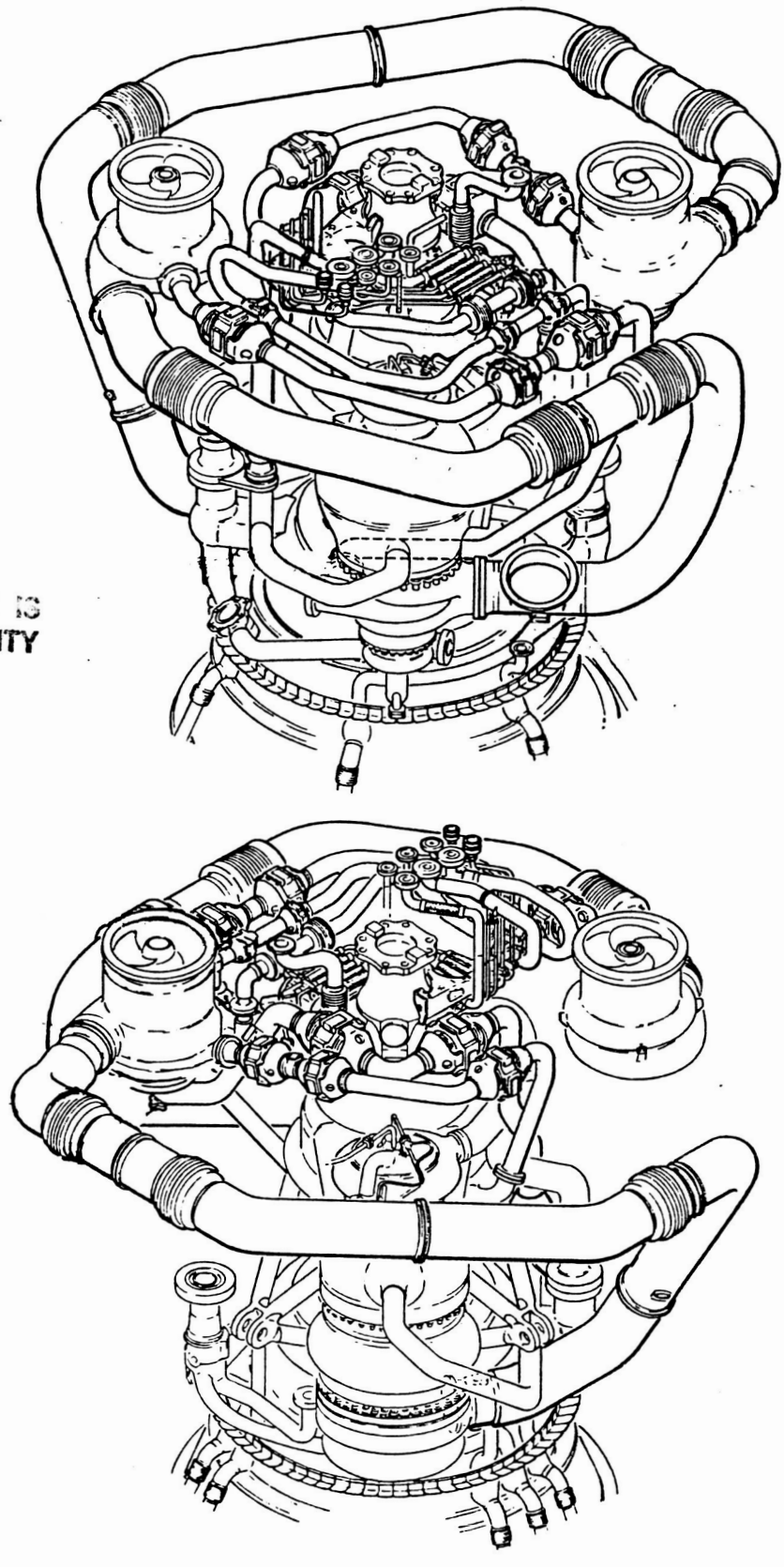

Figure 68 Typical SSME View

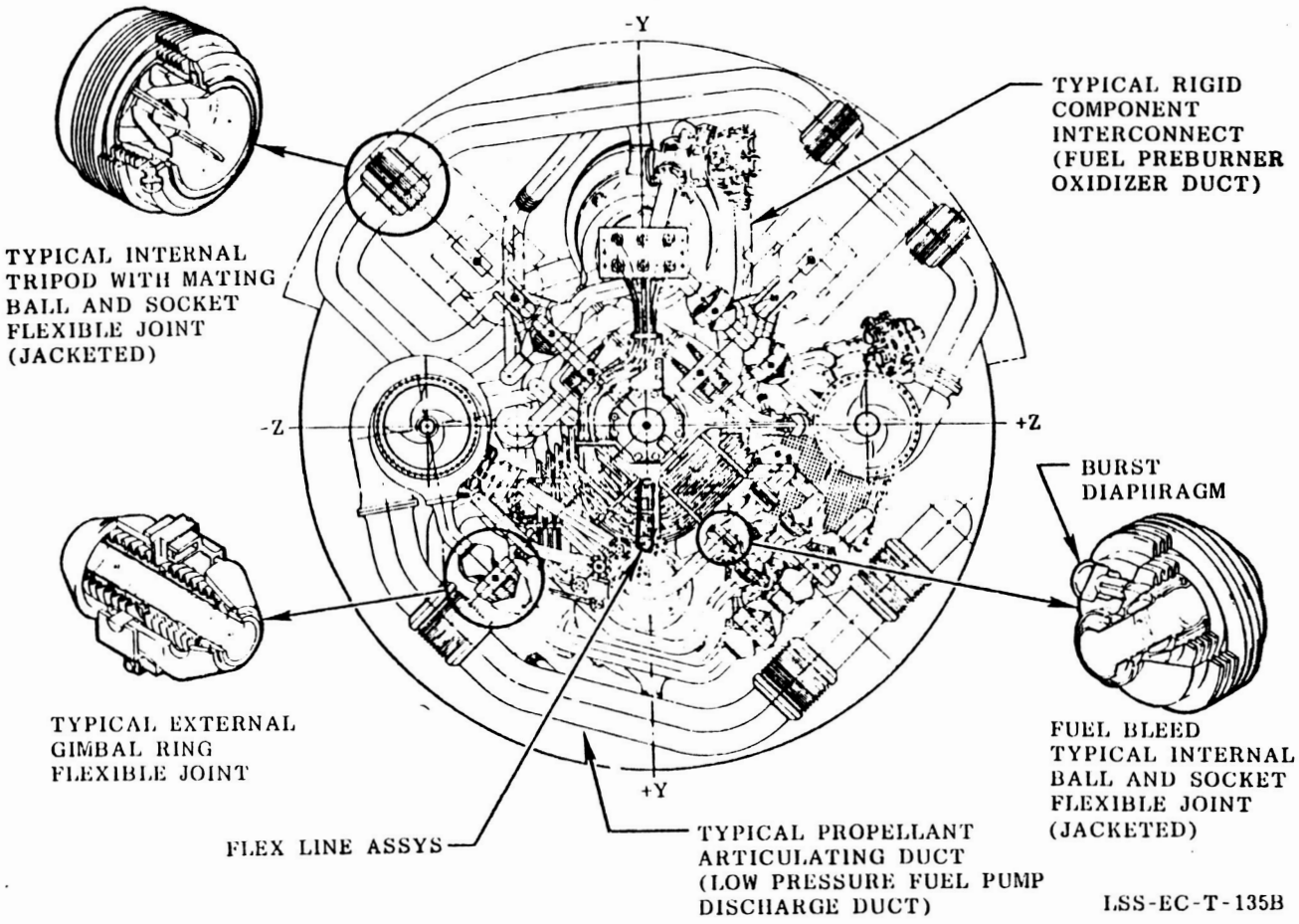

Figure 69 Typical Flex Bellows Application

Articulating metal-bellows flex joints are used in main propellent ducts that cross the gimbal plane and are capable of accommodating the engine gimbaling motions of up to 11°. These ducts service the vehicle-mounted low pressure turbopumps and are configured to wrap around the main gimbal bearing thrust axis.

The articulating lines used as fluid interface lines are similar to the main propellant ducts with wrap around configuration, but smaller in diameter. The term wrap around derives from the line centerline geometry that wraps around the engine gimbal assembly.

Flexible hoses are used for small diameter vehicle to engine lines such as for hydraulic supply.

Hard lines are defined as lines without flex joints. They are used for non-gimbaling applications which connect to the fluid interface panel and for all non-gimbaling engine component interconnections on the SSME.

Bolted flange joints with static seals are used throughout the engine for connecting ducts and components. Separable static seal joints are necessary for servicing and maintenance of the engine. The deflection loaded, pressure assisted Naflex-type static seal concept is used for static seal joints for component assemblies and at the interconnection of components.

Load Transmissibility. The different type of ducts have different high frequency load transmissibility from end to end. Rigid ducts walls have a greater capacity to transmit a high frequency energy than articulating ducts or hoses. The basic design configuration of a hose or bellows markedly limits the energy transmissibility across them. No such limitation is present in a rigid duct.

Engine to Engine Variations. The basic design requirements and packaging philosophy of an engine define the type of lines that are used on an engine.

Gimbaled engines require some type of articulating duct to accommodate large angular motion between the engine and stage. This can be accomplished either through bellowed joints or flex lines. Both are used on rocket engines. There are also variations in lines routed between engine mounted components. The J-2 engine applied the articulating bellowed joint to all primary duct lines. This effectively minimized the static misalignment loads as well as uncoupled the high frequency transmissability between primary structure from the ducting. Other engines like the XLR129 and SSME Use rigid hard line ducting primarily for non-gimbaled ducts and accept the potential for higher installation loads and dynamic load transmission. The RS-44 adds complexity to the ducts by using some of the ducts as primary support structures for the pumps.

Future engines will undoubtedly use variations of all the duct configurations discussed above.

General Design Considerations. In order to furnish an overall perspective of ducts and lines, the basic design requirements controlling the configuration of the ducts include: 1) System operational requirements, 2) Engine structural strength requirements, 3) Low cycle fatigue criterion as applied to engine gimbaling, 4) High cycle fatigue criterion as applied to engine vibration environment. Important design considerations include 1) Accommodation of thermal deflections, misalignments, installation adjustments and operational deflections, 2) Withstanding operational fluid pressures and temperatures initially estimated by engine balance, scaled values from other engine experience and then subsequently based on actual engine experience, 3) Accommodation of engine gimbaling deflections (articulating ducts), 4) Separation of bellows mechanical and flow induced excitation vibration frequencies where applicable, 5) Accommodation by bellows of each specific joint angle resulting from engine gimbaling deflections (articulating ducts), 6) Additional design requirements on bellows for buckling (squirming) for high pressure lines, and 7) Use of flow sleeves or liners on bellowed joints to prevent coupling of natural and flow vibration frequencies.

For the high pressure oxidizer duct, which is a hard line concept, design considerations involving gimbaling and flex joints do not apply. Figure 70 shows the HPOTPDD.

Individual Load Summary. Details of the individual loads are covered in the following sections. A loads summary is furnished in Table 16. The summary is categorized to address basic questions related to individual loads. For ducting, most of the critical loads are well defined. Some of the static loads such as misalignments, gimbaling and acceleration are treated from a maximum condition and are not usually "drivers" on the analysis. The dynamic pressure loads on components such as the HPOTP discharge duct have so much energy that they are a driver for high frequency vibration problems. This is a phenomena that had not been a major problem on earlier engines.

INDIVIDUAL LOADS	HOW MEASURED	FORM AVAILABLE	DEGREE OF CERTAINTY	HOW USED
. STRUCTURAL DYNAMICS . TRANSIENT . STEADY STATE	ACCELEROMETERS	TIME TRACES, PSD'S, ISOPLOTS	HIGH	INPUT TO DYNAMIC ANALYSIS
. STATIC PRESSURE	MEASURED, CALCULATED FROM MODEL	AMS, TIME TRACES	HIGH	STRUCTURAL ANALYSIS
. DYNAMIC PRESSURE	PRESSURE FROM MODEL	PSD, AMS, ISOPLOTS	HIGH TO MODERATE	INPUT TO DYNAMIC ANALYSIS
. TEMPERATURE LOADS	PREDICTED FROM MODEL	MAX, MIN, NOMINAL VALUES	HIGH	STRUCTURAL ANALYSIS
. MISALIGNMENT . GIMBALING . ACCELERATION . FLOW MOMENTUM	PREDICTED MAXIMUM VALUES	VALUE	LIMIT HIGH ACTUAL LOW	STRUCTURAL ANALYSIS

Table 16 Individual Load Summary HPOTP Discharge Duct

SSME POWER HEAD

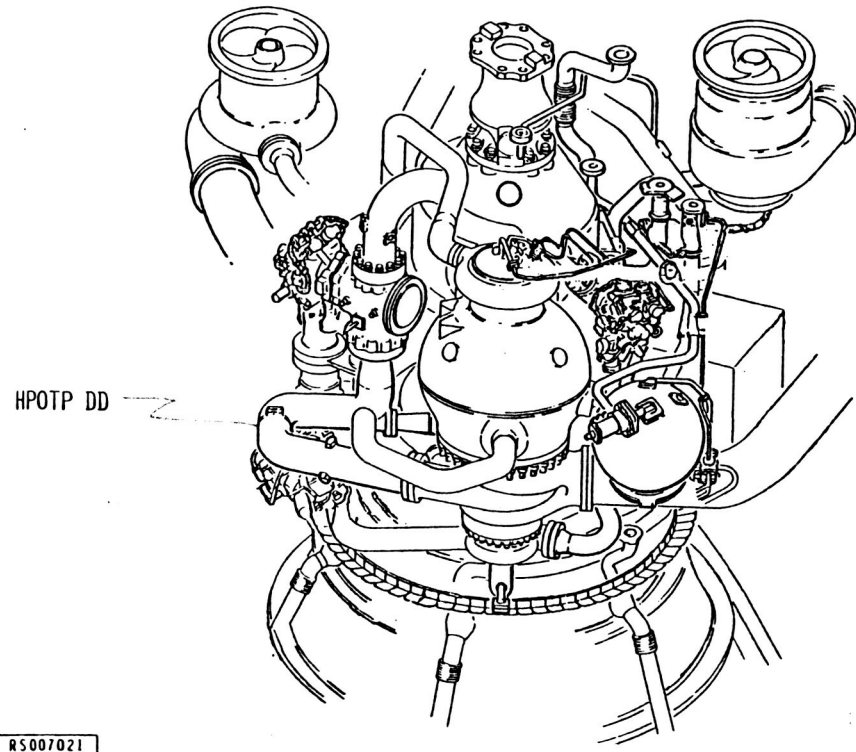

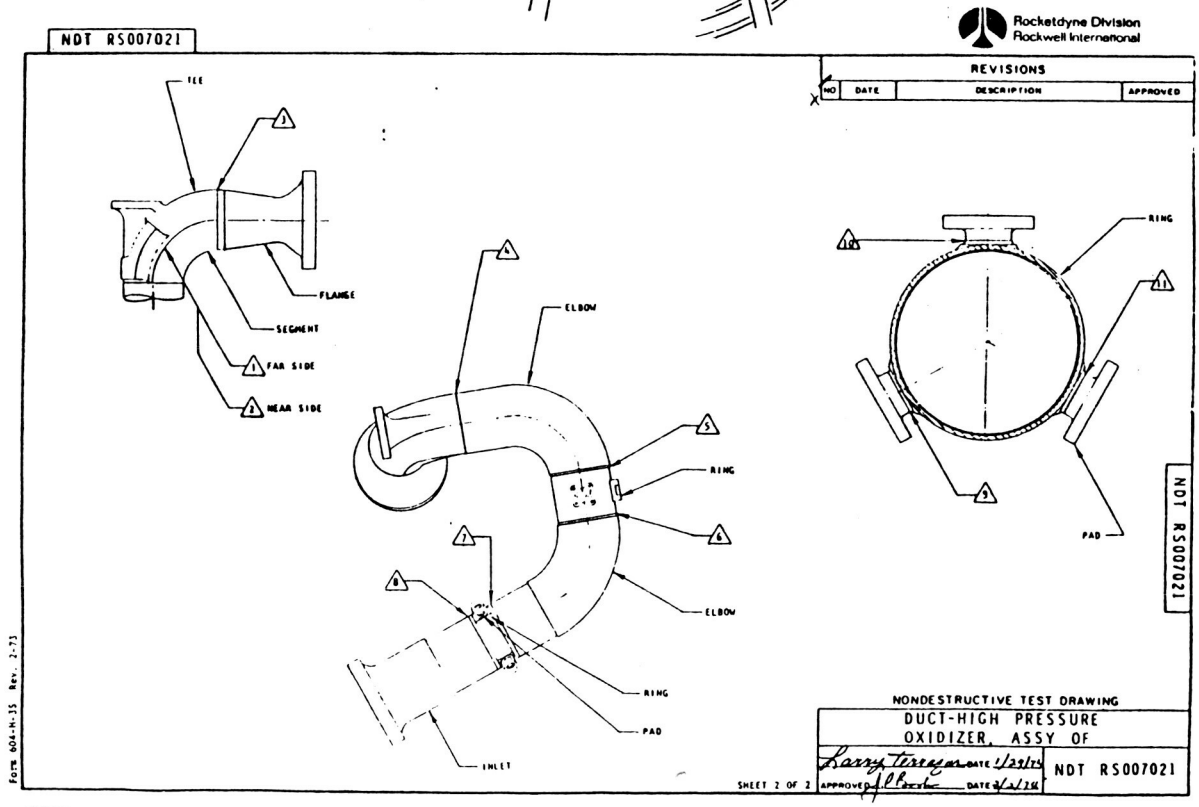

C4270

Figure 70 High Pressure Oxidizer Discharge Duct

Combined Loads Assessment. The loads are combined in the structural analysis to calculate component strength and life. A standard procedure is used to select maximum load cases from gimbaling , misalignment and thermal, gimbal adjustment, interface misalignments (where applicable) and shock and mechanical vibrations. Approximate maximum compatible loads from the above loads along local duct axes are found that maximizes the bending loads. The duct pressurization is included to determine maximum loads and stress factor of safety. The vibration loads are calculated and combined with the static stresses for fatigue life evaluation. The thrust dependent loads are normally considered to act for a full 7.5 hours of operation at maximum thrust condition. For some of the development hardware, a mission mix of power levels is used to define a more realistic assessment of the life of the part.

11.3 SSME Main Combustion Chamber Liner

Introduction. The combustion chamber line is one of the candidates for the 4th loads analysis component. It is a channel wall combustor which is quite different than the tubular construction of the J-2 or RL-10. Therefore, some background information and history of channel wall designs is furnished along with the discussion of the MCC liner. Rocketdyne has designed and tested several channel wall thrust chamber configurations over the last 15 to 20 years. Hot fire testing of this class of chambers shows that locally the hot gas wall material at the center of the channel progressively thins from the inside of the channel and the material moves and thickens the adjacent material (Fig. 71, 72 & 73). This phenomenon is attributed to a thermal ratchet condition termed "cyclic creep". In some cases the center of the channel thins sufficiently such that the wall fractures with an attendant local loss of coolant through the wall. Small cracks have occurred mid-land on the SSME as predicted by analysis, but they have not grown large enough to cause a problem. The cyclic creep mode of local channel cracking has usually been associated with local hot spots from injector effects.

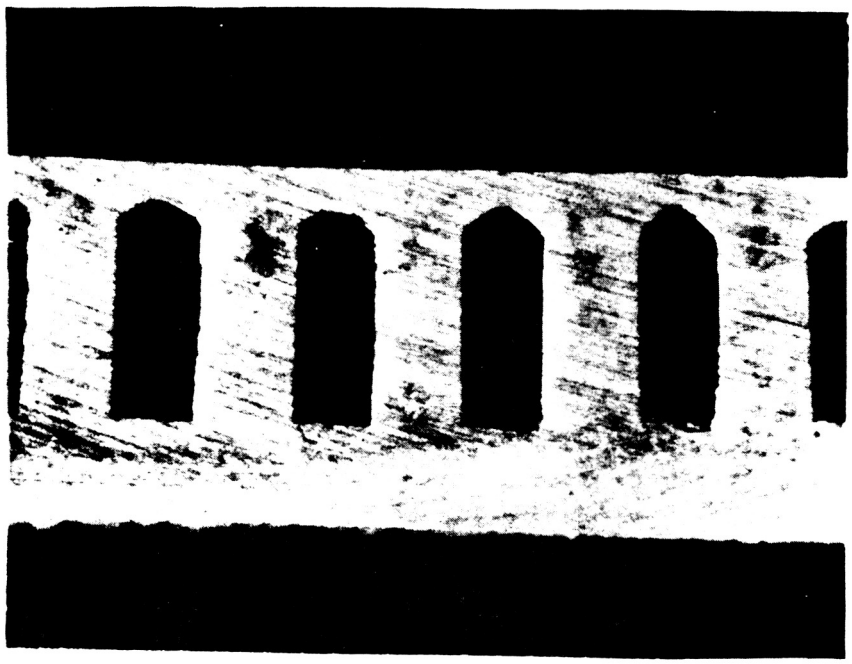

Figure 71 Throat Section of SSME-MCC Showing Thinned Hot-Gas Wall

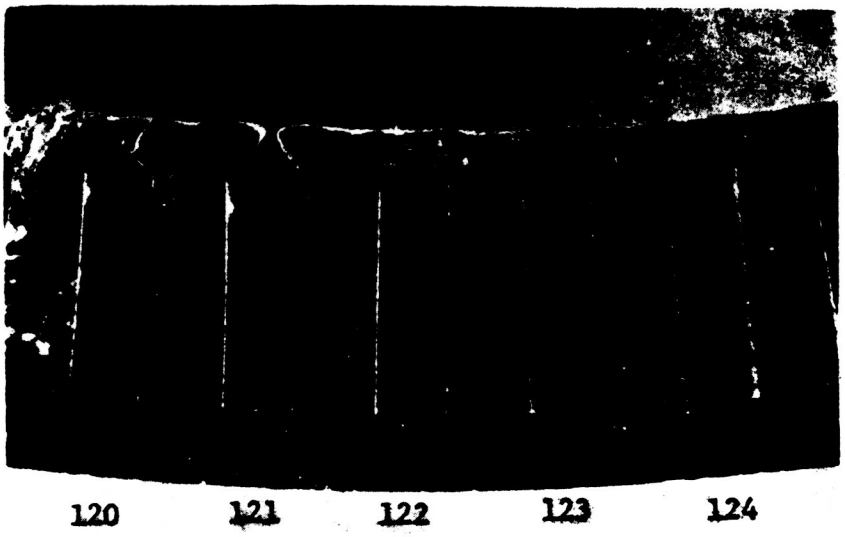

Figure 72 40K Chamber Section Through a Hot Spot Near the Throat

Figure 73 40K Chamber Section Showing Typical Channel Deformation Near the Throat

SSME History and Status. The main combustion chambers (MCC) for the SSME have been hot-fired over 1500 times in static ground tests. Durations of these tests have ranged from less than 1.0 second to over 830.0 seconds. The present operating range of the SSME is 65 to 109% of rated power level (RPL), and encompasses a combustion chamber pressure range of 1950 psia to 3270 psia P_c. For certain test objectives, SSME's have been tested up to 111% of RPL, and as low as 50% of RPL.

The current SSME MCC meets all design and operational requirements even though the local injector effects may cause small areas of channel wall cracking.

The initial main injector design had no provisions for film cooling of the MCC. After inception of hot-fire development testing, it was discovered that local circumferential areas of the combustion chamber had experienced overheating. The overheating resulted in conditions ranging from blanching to surface roughening or surface erosion. Surface erosion was generally resolved by the addition of film coolant holes and larger face nuts in the outer region of the main injector faceplate. These modifications increased the fuel flow along the walls of the combustion chamber, resulting in reduction of the hot gas wall temperature. In extreme cases, film coolant holes are locally enlarged to provide an extra measure of protection for the combustion chamber hot gas wall.

During the early stages of SSME testing, MCC hot gas wall roughening due to hot fire operation was not considered detrimental to engine operation. As testing progressed, it was discovered that roughening contributed to escalating heat loads and further roughening and degradation of the hot gas wall. Polishing of the MCC liner between tests with fine grit sandpaper was chosen as the method for reducing the deterioration of the hot gas wall. The smoother hot gas wall surface is credited with reducing local distress, especially on long duration tests. Certification testing of the MCC, up to and including full power level (FPL--109% RPL), has shown the component to have the capability of meeting a certification cycle without deterioration

of the hot gas wall. This is accomplished with minor maintenance between tests; by polishing the hot gas wall if necessary and selectively increasing the film coolant flow over local hot spots that indicate signs of duress. Even with these modifications, the MCC has encountered minor cracking. This damage occurs only in local spots and is attributed to injector effects (anomalies) rather than a general deficiency in the cooling capability or design of the chamber.

No performance degradation has been observed in the SSME engine with as many as 20 thermal cracks or thermal pin holes in the hot gas wall. These cracks tend to close during mainstage when the material is hot and result in little or no leakage. Extrapolation of observed degradation of the MCC liner and resulting performance effects indicates the MCC will meet minimum performance requirements for the required cycle life.

The degradation of the SSME combustion chambers with operating cycles and time is very consistent among components. Cyclic creep damage can be observed from initiation to development of a crack in the coolant channel.

SSME Configuration and Operation. The SSME MCC configuration and cross section shown in Fig. 74 and 75 depict the basic geometry and component details. The design requirements and how they were achieved are summarized in Table 17. The overall requirements include minimum weight, extended cyclic life and performance. These were achieved through the use of a channel walled high strength ductile material--NARloy Z. The high throat heat flux from the SSME led to the use of the channel wall construction. Figure 76 shows how the heat flux requirement has markedly increased from the Redstone era to the J-2 and then almost a three-fold increase for the SSME. The design considerations for the channel wall configuration are listed in Table 18. The design consists of an outer structural jacket following the shape of the combustion chamber liner and carrying the internal pressure and external loads from interfacing components. The liner is attached to the jacket at the ends of the structure. It ducts hydrogen

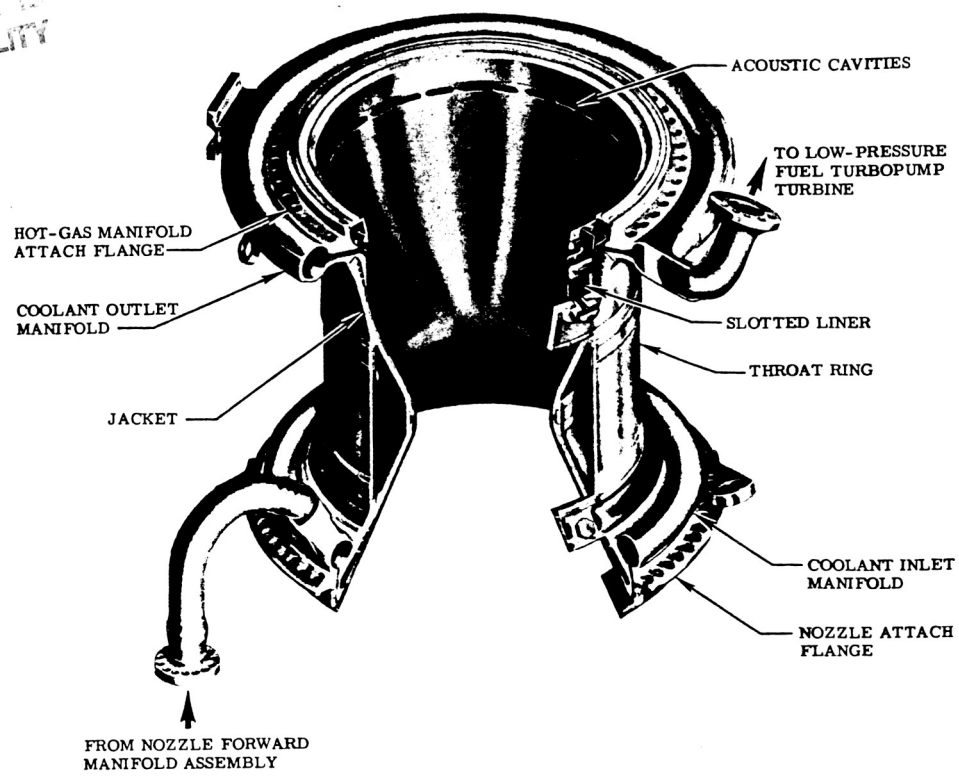

Figure 74 Main Combustion Chamber

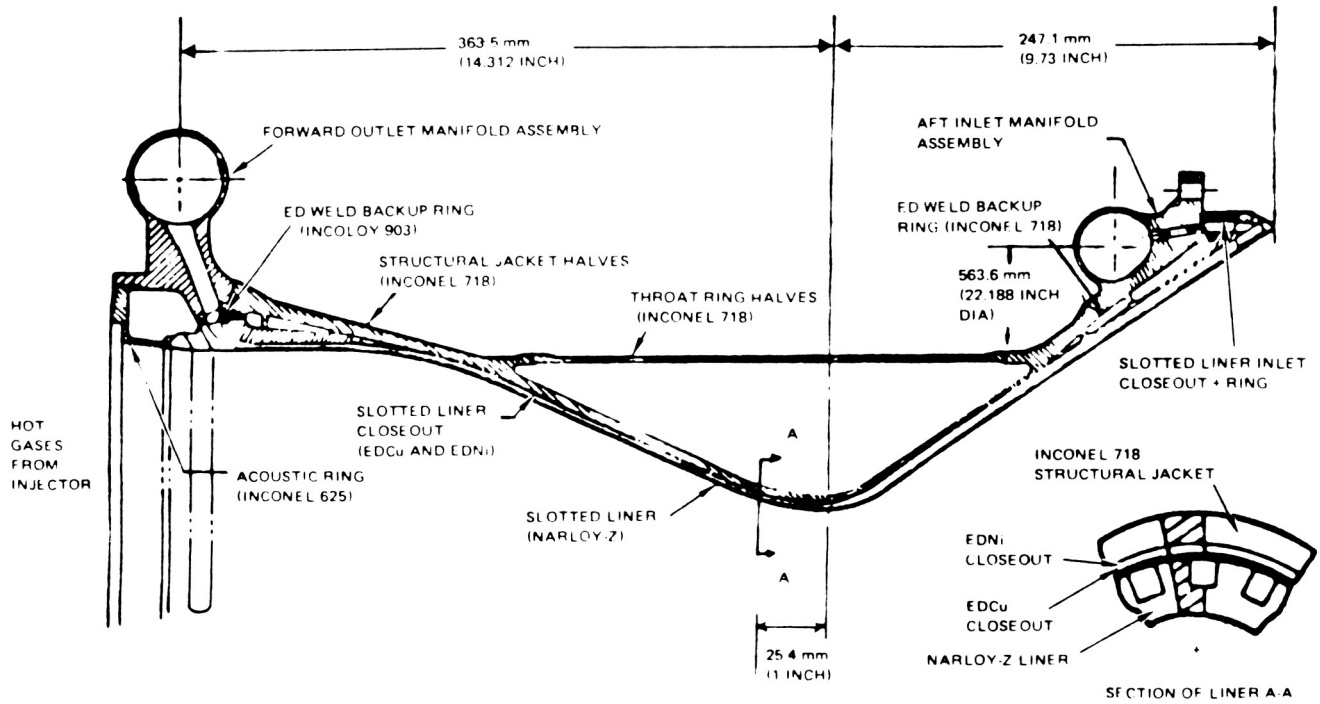

Figure 75 Main Combustion Chamber Liner Materials and Part Name

DESIGN REQUIREMENTS	NOW ACHIEVED
• MINIMUM ENGINE WEIGHT	• HIGH STRENGTH-HIGH DUCTILE MATERIAL
• 240 CYCLE LIFE CAPABILITY	• CHANNEL CONFIGURED COOLANT PASSAGES
	• COMBUSTOR CONTOURED FOR MINIMUM GAS WAS TEMPERATURE
	• HIGH THERMAL CONDUCTIVITY - HIGH DUCTILE MATERIAL
• MAXIMUM PERFORMANCE	• REGENERATIVELY H_2 COOLED COMBUSTOR
• DYNAMICALLY STABLE COMBUSTION SYSTEM	• ACOUSTIC ABSORBER

Table 17 Main Combustion Chamber

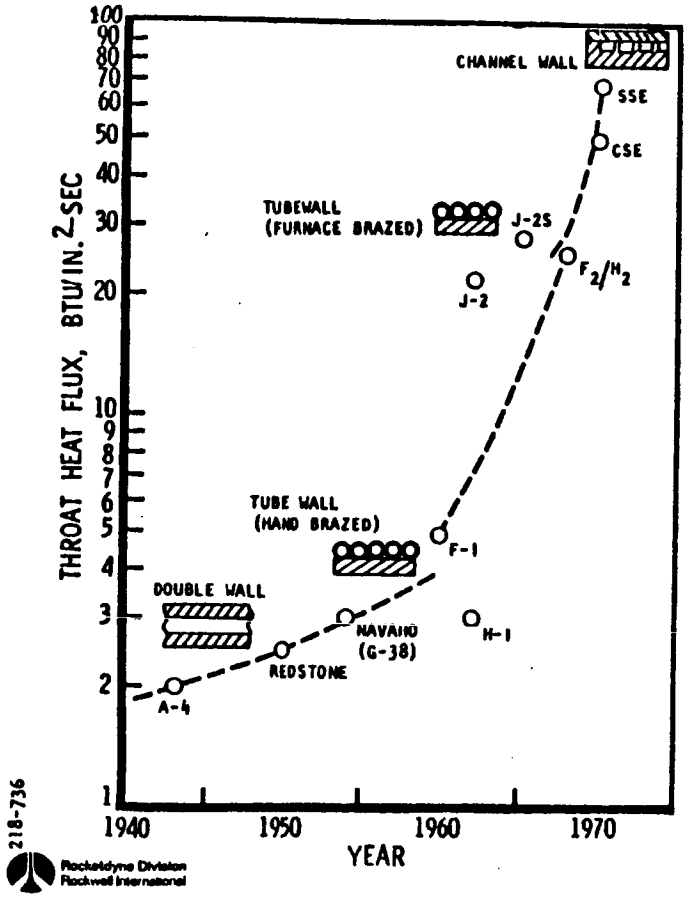

Figure 76 Throat Heat Flux Chronology

Table 18 Main Combustion Chamber

COMBUSTOR DESIGN CONSIDERATION

DESIGN PARAMETER	DESIGN CONSIDERATION
• COOLANT CHANNEL WALL THICKNESS	• MATERIAL COINING
• COOLANT CHANNEL WIDTH	• STRUCTURALLY COMPATIBLE WITH WALL THICKNESS
• COOLANT CHANNEL LAND WIDTH	• PLATING CAPABILITY
• COOLANT CHANNEL HEIGHT	• HEAT TRANSFER
	• PRESSURE DROP
• CHAMBER LENGTH	• PERFORMANCE
• CONTRACTION RATIO	• ENGINE WEIGHT
	• PRESSURE DROP
• THROAT RADIUS OF CURVATURE	• DISCHARGE LOSS
	• THROAT HEAT FLUX

coolant along axial channels and acts as a thermal barrier between the jacket and the combustion gases, and as a heat exchanger for the hydrogen used to drive the low pressure fuel pump. The regeneratively cooled liner forms the desired combustion chamber profile. The slotted liner is closed out with EDCu and EDNi to form channels for the hydrogen coolant. The liner is supported by a high strength structural jacket, and is attached only at the ends of the jacket. Structurally, the liner is required to strain and contact the structural jacket to react the differential pressure load between the coolant and the combustion gases, and to accommodate the cyclic and racheting strain ranges from the extreme thermal operating environment. The structural jacket is required to provide external support for the liner, react the internal combustion pressure loads and the resulting thrust and gimbaling loads generated during hot-fire operation. Even though the liner is not attached all along the MCC, the liner motion is restricted by the motion of the external jacket. During steady-state operation, the liner hot-gas surface temperature varies along its length (Fig. 77) with a maximum of 1100 F, and the back wall on the jacket side is typically at -150 F.

During start and cutoff, the complete liner bulk temperature reaches approximately -400 F. This total cycle is a severe thermal cycle to accommodate. At the critical analysis location near the throat, the internal pressure of the coolant hydrogen is 6300 psi, which is 4200 psi greater than the hot wall combustion zone chamber pressure of 2100 psi.

Hot-Spot Cracking. After a series of duty cycles, the geometry of the channel cross-section gradually distorts, thins along the channel hot wall, and cracks. Figure 71 shows typical cross-sections of the SSME MCC hardware-through hot spots like the ones shown in Fig. 78.

The geometric changes of the channels that result in cracks are a small portion of the total surface area of the MCC. The cracked channels are located typically in the center of the elliptical-shaped hot spots that occur just forward of the throat. The two cross-sections show that the deformation pattern occurs over a 5 to 10 channel width, and each channel has its own geometric change. The liner consistently shows a thinning of the center of the coolant channel's hot wall, plus a thickening and rounding of the corner forming the intersection of the channel and land. Detail measurement of channel geometries indicate that material volume has essentially been conserved; the thinned section is balanced by the thickened shape at the channel corner.

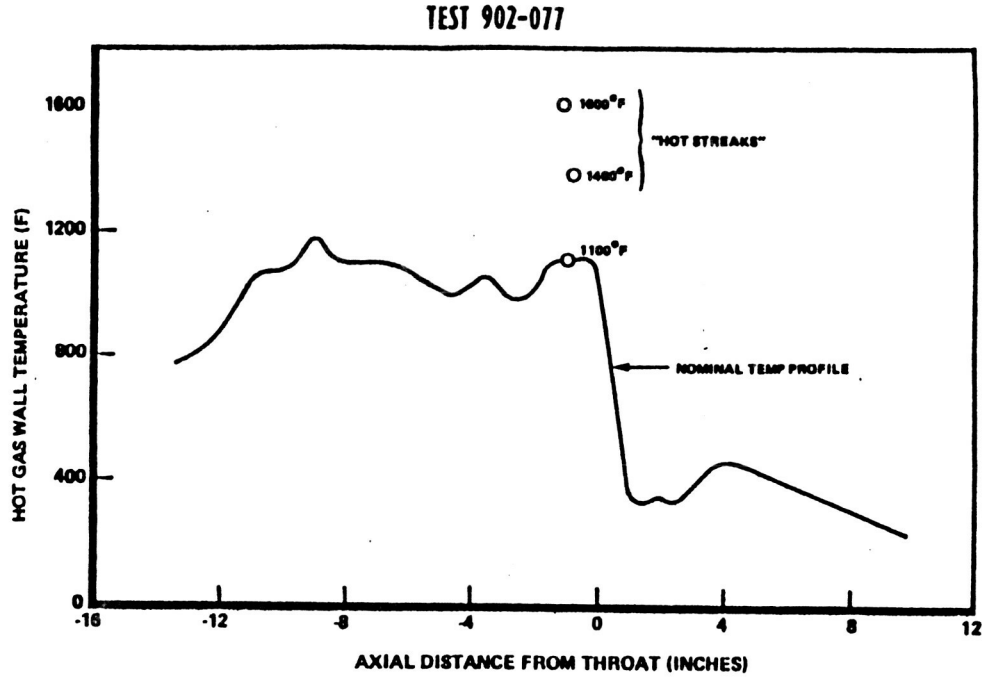

Figure 77 MCC Wall Temperature at RPL

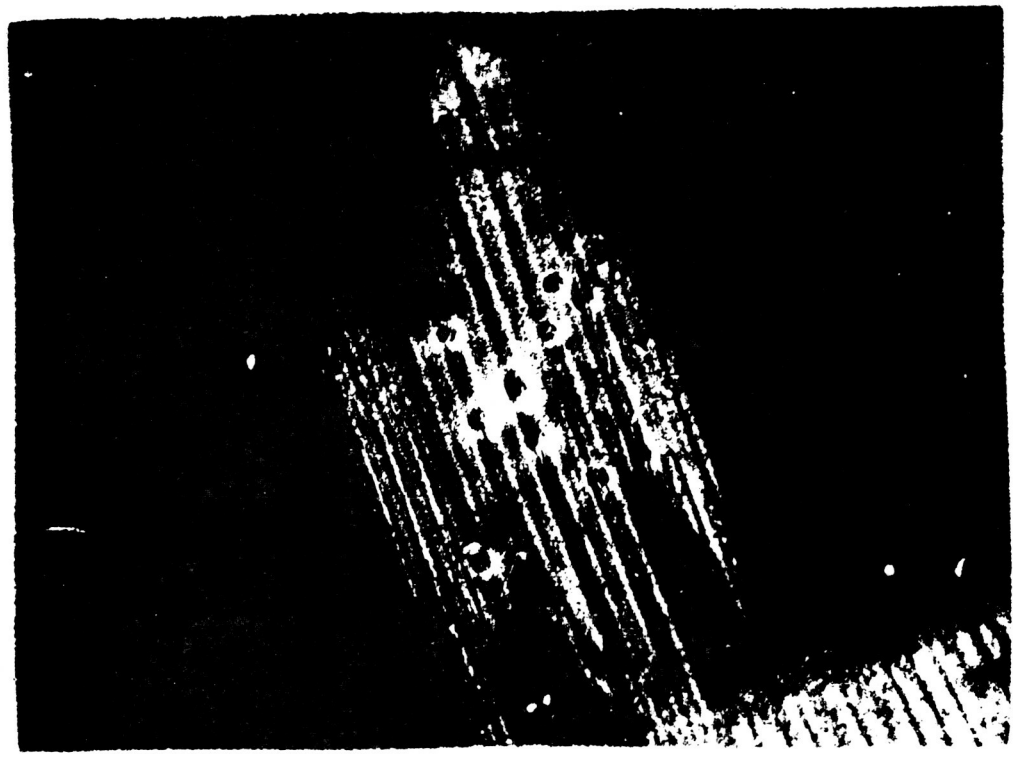

Figure 78 Typical SSME MCC Hardware-Through Hot Spots

Loading Environment. As previously stated, the maximum average liner channel wall temperature is approximately 1100 F. The maximum best estimated liner temperature of 1500 F in a local hot spot is well above the creep activation temperature for NARloy-Z. However, the temperature gradient through the hot wall is approximately 750 F, which results in half of the hot wall being at temperatures below the creep activation temperature. The primary load-differential coolant pressure in the MCC can be easily supported by this low temperature portion of the wall. This essentially changes the load condition from a potential load-dependent creep problem to a local relaxation phenomenon. The stress state on the hotter portion of the wall reduces to a displacement-limited, steady-state condition. The primary load is essentially shifted to the cooler half of the channel wall. Therefore, the creep/relaxation effects are a minor addition to the biased loading in this hardware, whereas it could be a more significant parameter if the total hot wall was above the creep activation temperature. This can occur in a plugged channel unlike a hot-spot condition. Plugged channels crack earlier than a typical hot-spot condition. Creep relaxation test results for NARloy-Z from standard materials test specimens show evidence that relaxation occurs rapidly, within less than one second of hold time, and achieves an approximate steady-state condition within 10 to 20 seconds. For the SSME engine duty cycle, this means that steady-state creep relaxation occurs during every typical test firing of 50 to 800 seconds. The creep effects are basically test-cycle dependent, not test-time dependent.

The liner loading is different than most other structures on the engine. It lays up against a structural jacket that is designed to take the primary loads from the engine. The liner only has to support itself, act as a thermal barrier, heat exchanger, and duct hydrogen flow internally. The jacket is structurally designed to take all the internal pressure loads even though the liner inherent structure supports some of it.

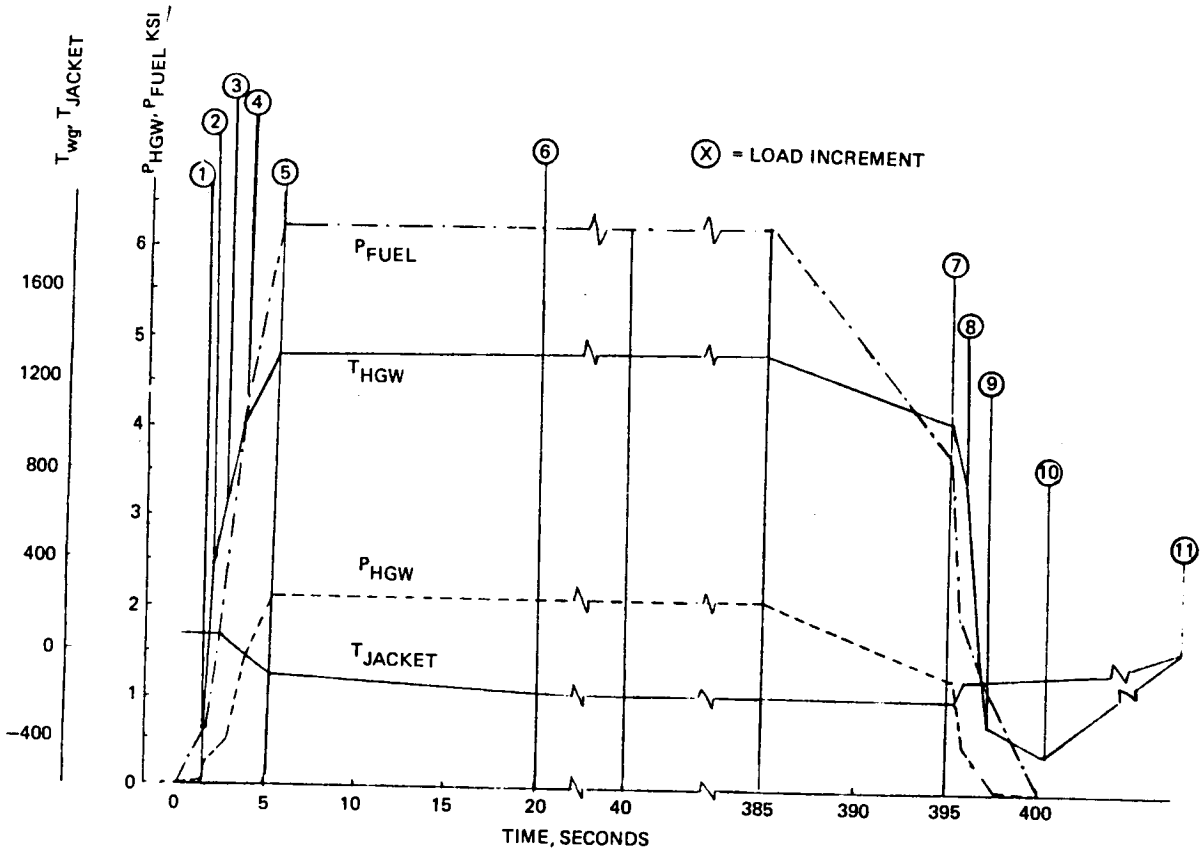

Figure 79 SSME MCC Life Analysis Duty Cycle & Pressure Display with Time Slices Noted

Individual and Combined Load Summary. The individual duty cycle loads applied to the liner are depicted in Fig. 79. The duty cycle was divided into 11 load increments where significant events occur in the cycle which have discrete changes in the load increment. The first load increment (1) is during the hydrogen lead preignition time period when the hydrogen gas chills the liner uniformily to below -350°F. Next, the chamber pressure and temperatures gradually rise to the operating conditions at increment (5). At increment (6) the jacket temperature has stabilized and operating conditions are constant until throttling down at the end of flight and engine cutoff. The liner continues to cool down with the post cutoff hydrogen flow until it again stabilizes at about -350°F. Post test the liner warms back to room temperature.

The primary probabilistic factor in the liner analysis is the randomness and variability of the hot spots. Hot spots are related to injector effects that are caused by slight manufacturing variations in the injector, contamination restricting flow in the injector or degradation of the injector with operation. The details of the individual loads are covered in Appendix F and are summarized in Table 19. The individual load components are restricted to pressure, thermal and jacket displacements.

11.4 SSME Nozzle Feedline

Introduction. The nozzle feedline was chosen as one of the candidates for the 4th component because of the large magnitude start and cutoff transient load on the nozzle. The sea level operation of the SSME results in a nozzle flowing in a highly overexpanded condition; that is, the wall exit pressure is much less than the ambient pressure. The SSME, like the J-2 engine, has a modified bell contour nozzle with a large expansion ratio that requires shallow exit angles. The load aspects of ignition flow separation are divided into sideloads, breathing mode loads and oscillating shock loads. The classical sideload is a gross imbalance of the pressure forces and results in large body-bending loads on the engine and large actuator loads. This phenomena has a relatively low frequency and has been extensively

measured and studied. The breathing mode is also due to asymmetric flow but is of a more local variation in separation and higher frequency that induces nozzle bell displacements, i.e., breathing modes. The oscillatory shock transients is more of an axisymmetric high frequency >100hz phenomena that caused the steerhorn failures and distress of the nozzle tubes in the nozzle exit zone.

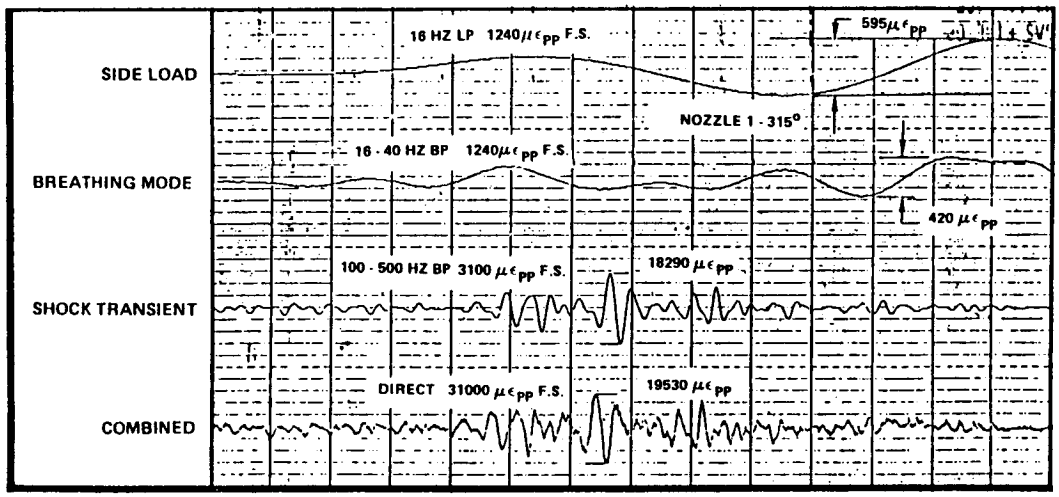

308-975

Rockwell International
Rocketdyne Division

Figure 80 Filtered Strain Gage Data from Engine Test 902-160

The high frequency shock transients resulted in dynamic motion of the aft manifold where the fuel lines (see figure) attach. These shocks excited a natural frequency of the steerhorn with a mode shape having high strains at the welds. To evaluate the loading dynamics, a series of subscale air flow tests were carried out. The results from these tests were used to develop a dynamic forcing function that is used to evaluate the high frequency shock.

The nozzle feed line is part of the nozzle cooling system, supplying coolant to the nozzle. Several cooling methods such as radiation, ablation, film cooling, dump cooling or regeneration cooling can be employed in the nozzle design. It is also possible that different cooling systems can be employed in different regions of the same nozzle. When the regenerative cooling type is used, the nozzle structure is usually made out of tube bundles reinforced by an external outer shell and circumferential hat bands. The coolant which flows in the tubes is normally fuel such as hydrogen in SSME. The integrity of the nozzle feed line is critical, as any failure in the feed line will result in a LOX-rich mixture with high temperatures that can cause extensive damage to a major portion of the engine. In the SSME, the nozzle feed line is made out of INCONEL 718 material and carries coolant at approximately 6000 psi and 93°R at steady state operating conditions.

Geometrical Considerations. The actual geometrical details of the nozzle feed line depend upon the cooling concept used in the regeneratively cooled nozzle. It can employ single pass, pass and a half, or double pass methods. In SSME, the concept used is the single pass method in which the coolant is introduced to the lower inlet manifold, using three feed lines with branching ducts which are spaced 120° apart (Figure 81). The attachment of the nozzle feed line to the nozzle is made at selected hat bands. The intermediate supports allow the feed line to move freely along the axial direction, and the end support brackets provide a rigid condition. The redesigned nozzle feed line contains a loop to provide flexibility in the axial direction to accommodate the thermal contraction.

Individual Load Summary. The nozzle feedlines are subjected to internal pressure, thermal transient, thermal shrinkage, inertial shock, and

mechanical vibration loads. The thermal transient occurs during low pressure conditions (start and cutoff) and is not a significant load. The internal pressure furnishes a high mean stress and is a main primary load on the feedline. The thermal shrinkage is accommodated through flexing the curved "steam loop" and is a relatively unimportant secondary load. The steady state random vibration loads are low. The other primary load is the start and cutoff transient load caused by flow separation that is highly variable test to test.

The individual loads are presented in Appendix F, and a summary is furnished, Table 19.

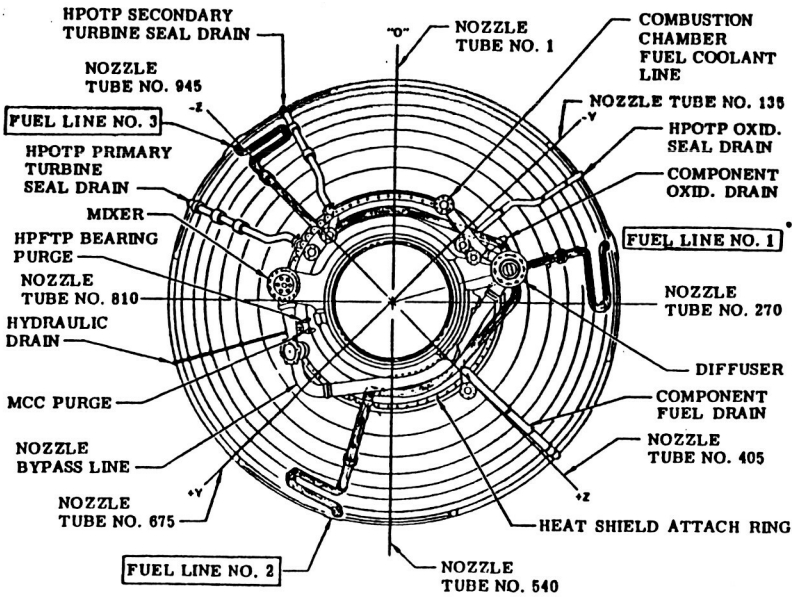

Figure 81 Flight Nozzle Features

INDIVIDUAL LOADS	HOW DETERMINED	FORM AVAILABLE	DEGREE OF CERTAINTY	HOW USED
.STATIC PRESSURE	MEASURED FROM ENGINE TEST	DUTY CYCLE	HIGH	STRUCTURAL ANALYSIS
.THERMAL .FEEDLINE TEMP.	CALCULATED	TABULATED POINTS	MODERATE	PRIMARY LOAD STRUCTURAL ANALYSIS
.RESTRAINT	CALCULATED BASED ON LINE & NOZZLE SHRINKAGE FINITE ELEMENT MODEL	LOAD CASE FROM STRUCTURAL ANALYSIS	MODERATE	STRUCTURAL ANALYSIS
.MECHANICAL VIBRATION (STEADY STATE)	MEASURED ACCESS ON HATBANDS & MANIFOLDS	PSD'S AMS, STATOS	HIGH	DYNAMIC ANALYSIS
.MECHANICAL VIBRATION (TRANSIENT)	ACCESS, STRAIN GAGES, MODEL FLOW TESTS	PRESSURE PULSES TO NOZZLE & TEST	MODERATE	DYNAMIC ANALYSIS
.INERTIAL FROM GIMBALING AND FLIGHT ACCELERATIONS	ANALYTICAL CALCULATION	G-LOAD EQUIVALENT	HIGH	STRUCTURAL ANALYSIS

Table 19 Individual Load Summary Nozzle Feedline

11.5 Fourth Component Selection.

The evaluation of the three components was addressed using the selection criteria previously discussed in addition to a comparison of each component's individual loads.

Table 20 summarizes the selection criteria comparison. The nozzle steerhorn received considerable attention during the development phase of the engine when there were feedline failures. These failures have been resolved through a design change. As part of the redesign effort, extensive test data was obtained characterizing the start and cutoff load transient. These loads are felt throughout the engine and are considered in several other components and are considered as part of the transfer duct and LOX post loading.

The steerhorns are in close proximity of the actual load application and take more of the brunt of the local energy.

The MCC liner hot spot degradation does not appreciably affect the functional operation of the engine. The minor adjustments made to the injector combined with polishing of the surface allows the liner to meet design life goals for the SSME. From a generic standpoint, the problem could be a more critical problem on reusable upper stage engines like the OTV where adjustments and refurbishments would be much more limited. The liner problem is interesting from a structural analysis standpoint in that this is a large deformation cyclic creep problem. The loading and failure mode is unique to chambers and nozzles.

The HPOTP discharge ducts is representative of ducting on the engine. There is considerable interest in a more precise definition of ducting life so that hardware can be safely used for more tests before retiring the duct. The additional loading aspect of this duct is that it is just downstream of the HPOTP pump discharge (see Figure 70). The high pressure, high energy, high density LOX flow in this line has caused flow induced failures of

	NOZZLE STEERHORN	MCC LINER	HPOTPDD (DUCTS IN GENERAL)
.LOTS OF ATTENTION	YES-4 YEARS AGO	NO	YES-NEED TO MORE PRECISELY CALCULATE USABLE LIFE
.AVAILABILITY OF DATA	YES	NO QUANTITATIVE DATA	YES
.TYPICAL OF LARGE NUMBER OF COMPONENTS	NO	NO	YES-1 OF 30 DUCTS
.UNIQUE LOADING	NO	YES	TYPICAL EXCEPT FOR HI FLOW LOADS
.IMPORTANT FOR PSAM	NO	YES-TO TEST CAPABILITY OF CODE	YES-GOOD MODEL FOR EVALUATING PROBABILISTIC ASPECTS
.EXTENDS PROBABILISTIC FORMULATION METHODS	NO	NO	HI ENERGY FLOW EFFECTS
.COMMENTS	SIDELOAD PROBLEM ADDRESSED TO A LESSER EXTENT ON OTHER COMPONENTS	PART FUNCTIONS WITH CRACKS; MORE IMPORTANT FOR OTV--NO REFURBISHMENT CASE	DO NOT HAVE GOOD HI ENERGY FLOW SCALING TECHNIQUES--CAN AT LEAST ADDRESS THE PROBLEM

Table 20 Selection Criteria

structures either in the flow or containing it. Any development of scaling methodologies or loading design guidelines for high energy flows that might develop from using this as the fourth component would be an important advancement in loads definition.

Table 21 is a comparison of the individual loads for the three components under study. The individual load list includes all of the loads that have been previously discussed. The primary loads on the components are circled to emphasize their importance.

The MCC liner is again atypical of the other components. It has only three loads of which temperature and pressure are significant. The steerhorn and the HPOTP discharge duct have similar individual loading. The HPOTP discharge duct is more critical for steady state operation vibration loads, whereas the feedline is primarily a shock transient mechanical loading.

Based on the survey effort and the above comparisons, Rocketdyne recommended that the HPOTP discharge duct be considered the baseline fourth component.

INDIVIDUAL LOAD	TURBINE BLADE	TRANSFER DUCT	LOX POST	HPOTPDD	LOAD FORM
.STATIC PRESSURE	X	X	X	X	DUTY CYCLE*
.DYNAMIC PRESSURE					
.CHUGGING(TRANSIENT)	-	X	-	-	AMS, STATOS
.TURBULENCE					
.SINUSOIDAL					
(REPEATED PULSE)	X	X			AMS, PSD, STATOS
.RANDOM	-	X	X	X	AMS, PSD
.CENTRIFUGAL	X	-	-	-	DUTY CYCLE*
.TEMPERATURE	X	X	X	X	DUTY CYCLE*
.STRUCTURAL VIBRATION					
.TRANSIENT					
.SIDELOAD	-	X	X	X	AMS, STATOS
.POPS	-	X	X	-	AMS, STATOS
.STEADY STATE					
.SINE	-	X	X	X	AMS, PSD, STATOS
.RANDOM	-	X	X	X	AMS, STATOS
.DEBRIS	X	X	X	-	HISTORY
.RUBBING	X		-	-	EXPERT OPINION
.INSTALLATION	-	-	X	X	EXPERT OPINION
.FAB	X	X	X	X	
.FRICTION	X	X	X	-	PSEUDO LOADS
.TOLERANCES	X	X	X	X	

*LOW FREQ. & TRANSIENT

Table 21 Summary Matrix of Individual Load vs Component

12.0 COMPOSITE LOAD SPECTRA CODE

12.1 Introduction

An executive driven modular software system is being developed that will incorporate the various individual and composite load spectra models. This code is configured as an "expert system".

These models will be probabilistic models with data dependent coefficients and/or functions and will be developed at increasing levels of sophistication with respect to prediction reliability and confidence level. Associated with these models will be guidelines to select the coefficients and functions in the generic models to achieve a specified prediction requirement. The potential complexity and the expertise inherent in effectively using the generic models to construct specific load spectra models justifies embedding these models in an integrated software system configured as an expert system that can advise users in the employment of the generic load models.

The code is being developed in four incremental versions. Each subsequent version will add a new engine component, additional load types and more sophistication to the probabilistic load definition and decision making process.

The technical core of the final integrated system will be an interactive expert system that will:

1. Construct specific load spectra models based on user supplied descriptions of the component and the load environment.

2. Incorporate the probabilistic models so as to enable a dialogue between the system and the user which will help the user select the best model parameters for his problem.

3. Be able to describe the process of constructing a specific load spectra model, including decisions made by the expert system and the rationale for those decisions.

The expert system is being configured so that specific simulated load spectra models are built by accessing a knowledge base of facts and rules. The knowledge base contains a module of decision-making data (facts) and a module of rules and decision criteria (rules) for constructing the load spectra model. All numerical results needed to construct the specific load spectra model will be computed or retrieved automatically by the expert system. The knowledge base and the inference mechanisms needed to search the knowledge base will be developed as part of this project. They will be strongly dependent upon the probabilistic generic load spectra models and engine component loading.

The expert system is being constructed to easily accommodate additions and deletions to the knowledge base. This allows the expert system to "get smarter" and to adapt to new information, both in the test and validation stage of each code version and in the expansion of the expert system to incorporate future models in the later versions of the code. The expert system is interactive to allow the system to query and guide the user as to the system operation (e.g., required user's input). The knowledge base and inference mechanism is being designed to minimize redundant data requests from the system to the user. The software system is modular in conformance with modern programming practice. The source program is written in the FORTRAN language.

The following portions of this section discuss individual parts of the code development. First the initial code objectives are discussed. The basis of the probabilistic load model in the initial code was previously presented and is part of the probabilistic load model survey under Probabilistic Analysis on Load Combination Models, Section 7.3. The validation and verification of the probabilistic load model is covered. The details of the expert system follow, and finally, a discussion of the turbine blade loads implementation.

12.2 Initial Code Objectives

The initial code that implemented turbine blade loads had the following limited objectives:

1. Vehicle to test methodologies
2. SSME simulation only
3. Validation and verification of probabilistic load model concepts
4. Representative database
5. Turbine blade loads for slowly varying duty cycle loads

These objectives required the development of the essential elements or skeleton of the expert system. The implementation of a probabilistic load model and the capability to input test data and requirements into the database.

12.3 LDEXPT, The Load Expert System

Implementation Philosophy. The composite load spectra project is a complex task that requires analyses of a large volume of engine flight data and test data. The probabilistic approach for the load spectra generation requires complex statistical analyses. This demands a good database management system and a user friendly interface to guide users to execute the correct procedures and to retrieve the right data for calculations. The approach for this task is to build an expert system to manage and control the probabilistic load generation and to select the correct data and procedures based on the built-in expertise.

EX-TRAN, an expert system development tool by Intelligent Terminals Limited, suitable for building diagnosis/classification expert systems,
was evaluated to see if it could help speed up the expert system development process for this project. EX-TRAN is currently being used for other SSME data analysis work. EX-TRAN is a user friendly system, and produces efficient IF-THEN production rules from user's input examples. Therefore, EX-TRAN was selected to help us develop the expert system. A simple expert

system driver was developed and modeled after EX-TRAN (a minimal subset) such that it could run rules developed by EX-TRAN. This driver is the control program for the LDEXPT system.

This prototype expert system has a simple control scheme that is similar to the expert system built by EX-TRAN and EXPERT-EASE. It follows a decision tree built with the IF-THEN rules and prompts users at each node to select the decision path. This simple control mechanism is adequate for our purpose. The main task of this project is analytical in nature. The expert's knowledge on data analyses and load generations is being built into LDEXPT's load database and probabilistic models.

With these data and models correctly built in the system, we have a powerful expert system. Other interference techniques will be examined in the future and implemented if found to be suitable and useful for this application.

Algorithm, Probabilistic Methods and Component Load Generation

Influence Coefficient Method. Deterministic methods have been developed and employed at Rocketdyne to perform engine performance analysis (steady state) and have been used for the past 25 years. Many tests are statistically evaluated and the mean hardware characteristics are used to baseline the algorithms. The test results can be standardized or normalized using these same algorithms. This data reduction program exceeds 2 MB of CPU and is expensive to operate. An approximate method is used to provide for flight predictions, mission control anomaly evaluation, malfunction confirmation, etc. This method uses linearized values as percentage changes (influence coefficients) of independent engine variables. These sets of coefficients can describe the engine over the expected range of operation within prescribed tolerances. A similar set of coefficients-nominals are determined that relate the nominal engine operating conditions as a function of the power level. The influence coefficient method allows the calculation

coefficient method allows the calculation of the expected changes in an engine variable from a nominal value due to changes in the set of independent variables. The set of influence coefficients was derived from regression analyses of a large volume of SSME engine performance data.

The influence coefficient (C) is defined as follows:

$$\frac{\Delta Y_i(X_j)}{Y_{io}} \equiv (C)_{ij} \frac{\Delta X_j}{X_{jo}} \qquad (1)$$

where

X_{jo}	is the j_{th} independent variable, nominal value
ΔX_j	is the change in X_j, i.e. $X_j = X_j - X_{jo}$
Y_{io}	is the i_{th} dependent variable, nominal value
$\Delta Y_i(X_j)$	is the change in Y_i due to change in X_j, $\Delta Y_i = Y_i - Y_{io}$
$(C)_{ij}$	is the influence coefficient for evaluating change in Y_j due to change in X_j

The total change in Y_i for a given test is therefore equal to the sum of all the changes in independent variable multiplying the corresponding influence coefficients, i.e.

$$\frac{\Delta Y_i}{Y_{io}} = \sum_j (C)_{ij} \frac{\Delta X_j}{X_{jo}} \qquad (2)$$

Influence coefficients and a set of nominal values were extracted from a non-linear algorithm model (Prediction Balance Model) of the SSME and mathematically fitted using a polynominal regression method. The influence coefficients and the nominal values of the dependent variables are strongly correlated with power level. These are then mapped into the engine power level with other independent non variant. The polynominal functions employed are shown below:

$$Y_{io} = a_i^0 + a_i^1 T + a_i^2 T^2 + a_i^3 T^3$$

$$C_{ij} = C_{ij}^0 + C_{ij}^1 T + C_{ij}^2 T^2 + C_{ij}^3 T^3$$

Y_{io} is the nominal value of the i^{th} dependent load at the power level of interest. It is evaluated as a function of power level with a set of constant coefficients a_i^0, a_i^1, a_i^2 and a_i^3, different i for different dependent loads

C_{ij} is the influence coefficient, correlates, the dependency of the i^{th} dependent load to the i^{th} independent load. It is evaluated as a function of power level with a set of constant coefficients C_{ij}^0, C_{ij}^1, C_{ij}^2 and C_{ij}^3.

Probabilistic Methods (Discrete Probability Distribution Model). Three probabilistic methods: Discrete Probability Distribution (DPD), Monte Carlo and Barrier Crossing Model have been evaluated by Battelle. The Monte Carlo and the DPD are operational in the current implemented version of Battelle's ANLOAD (An load generation program). Only the Discrete Probability Distribution Model has been tested and included in LDEXPT. The implementation of the DPD model will be herein discussed.

The probability method assumes that the loads are random variables which have stationary distributions (for the model considered at the present time). The dependant variable loads are combined statistically from input loads according to the influence coefficient formulas. All input loads are independent random variables. The formulism employed in the DPD model is presented below:

$$Y_i = Y_{io} + Y_{io} \sum_j C_{ij} \frac{X_j - X_{jo}}{X_{jo}}$$

$$P_r(Y_i) = \prod_j P_r(X_j)$$

Where, X_j and Y_i are random variables

$Pr(X_j)$ and $Pr(Y_i)$ are probabilities of variables X_j and Y_i, respectively

X_i is the value of the i^{th} independent load

X_{io} is the nominal value of the i^{th} independent load at a fixed power level, power level at 1.04 was chosen.

Y_j is the value of the j^{th} dependent load

Y_{jo} is the nominal value of the j^{th} dependent load at the power level of interest.

C_{ij} is the influence coefficient, correlates the dependency of the j^{th} dependent load to the i^{th} independent load.

X_j and Y_i are random variables. The distribution functions of X_i's can be a uniform distribution, a normal distribution, a lognormal distribution or a Rayleigh distribution. The RASCAL algorithm, a version of the DPD method developed by Battelle was implemented in LDEXPT. This algorithm differs from the conventional DPD method in that not all, but a preset number of random combinations of input random variables X_j's are combined to generate a distribution for Y_i.

Component Turbine Blade Loads. The component turbine blade loads of interest in the initial code are the centrifugal load, the airfoil pressures, the dynamic and temperature loads. A scaling model is implemented to generate these loads. The model assumes that any of the turbine blade loads depend on a single dependent load or two dependent loads or a combination of them . For example, the centrifugal load depends only on the turbine speed. It can be rescaled by a constant coefficient:

$$F_c = C_{fc} W^2$$

The axial airfoil pressure depends on the difference of the turbine inlet pressure and the turbine outlet pressure:

$$F_a = C_{fa} \Delta p = C_{fa}(P_{in} - P_{out})$$

The turbine inlet pressure and the turbine outlet pressure are strongly correlated variables.

The scaling models for a single dependent load and two dependent loads were implemented using DPD method. The model for the two dependent loads provides two options that the two dependent loads are not correlated or they are strongly correlated.

LDEXPT Design. The goal of this project for the first year was to produce a prototype expert system to test out the expert system model and the probability methodology employed to generate the rocket engine component load spectra. Structure design method was implemented from the beginning of this project. The modular approach was employed throughout the LDEXPT system. Individual modules were designed separately to perform specific sets of tasks. The composite load spectra project requires analysis of a large volume of rocket engine flight and test data. The probabilistic approach for load spectra generation requires complex statistical analyses. These requirements dictate an efficient database management system and an expert system to control and manage the load generation task.

The load expert system LDEXPT has two main systems: (1) RBMS, the Rules-Base Management System, and (2) KBMS, the Knowledge-Base Management System. Each system has two modules and its associated files. Figure 82 shows the top level structure of the load expert system. Two objectives for the 1st year were achieved: (1) the prototype expert system must be simple and user friendly, and (2) the load database must have uniform format. The first objective was achieved by modeling the expert system driver after the EX-TRAN model. To simplify the task, the rules that governed the information retrieval were coded into the computer program along with the probability load generation processes. In the next phase of this project, more user interaction with the load generation process will be built into the system, and we may also test an inference engine approach.

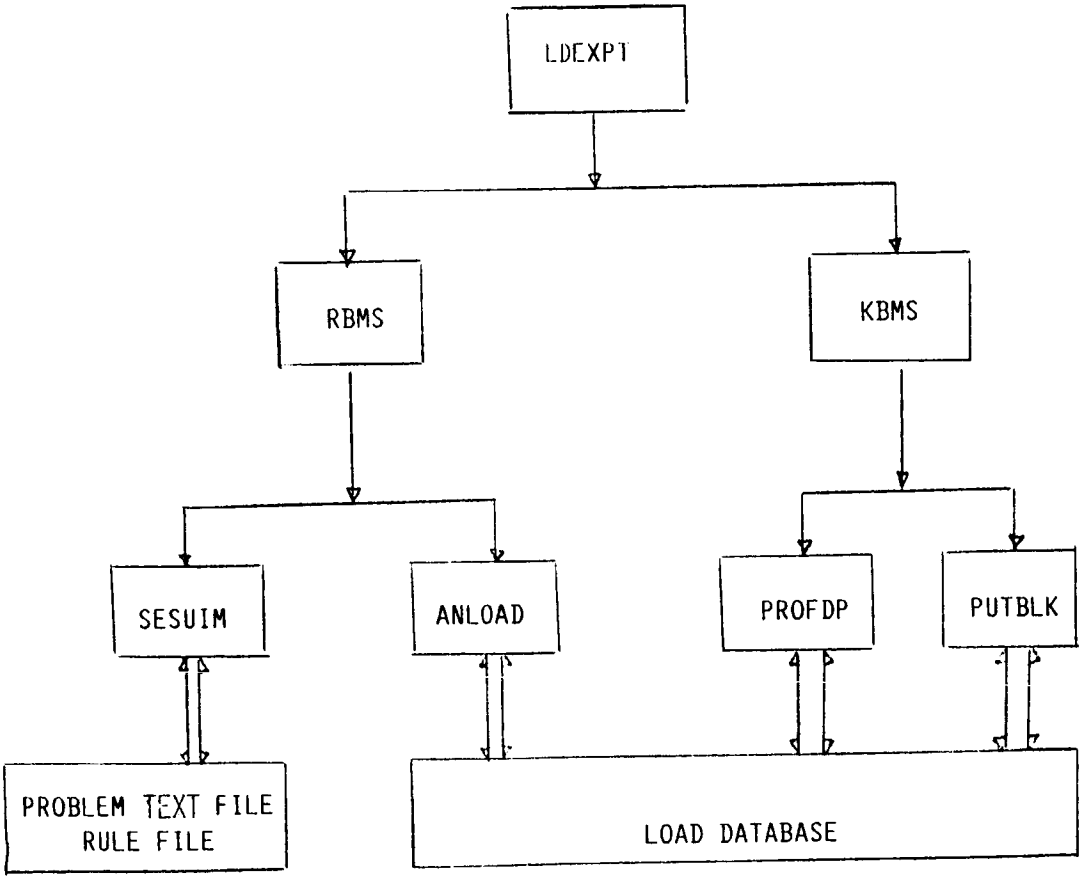

Figure 82 LDEXPT: Load Expert System

The second objective was achieved by utilizing a generic set of read/write routines for database management. Existing in-house routines were modified and incorporated into the load expert system. These routines create data files in a unique format and have been successfully used in a group of in-house analysis programs.

RBMS. The rules-base management system has two modules: (a) SESUIM (Expert System Driver) and (2) ANLOAD (Load Generator). The main functions of the RBMS are to manage information retrieval and to control the load generation processes. The SESUIM module contains a built-in set of rules for load data retrieval from the load database. It interfaces with users by generating queries, answering "why were the questions asked?" and showing how the decisions were made. It also prepares an input file for ANLOAD by prompting the user for information about the desired load generations. This input file will then be used by ANLOAD to control the load generation process.

The ANLOAD module from Battelle includes all the statistical analyses routines. As mentioned earlier, the load generation process was hardwired into the program and no user interface on the generation process was built. The only user interface to this module is through the ANLOAD input file.

SESUIM communicates with users with the help of a problem text file and a rule file. The problem text file is used to generate queries. It contains questions for a set of predefined attributes relevant to the expert system on hand. It also contains possible values for each attribute. The IF-THEN rules constructed in SESUIM follow the taxonomy of attributes (an attribute tree). The expert system driver searches through the tree of attributes from root forward, and obtains a value on the way for each attribute from user's response to the queries. The rule file contains the IF-THEN rules written in plain English. It is used to show users the logics built in the expert system. It prints out the relevant section of rules in plain English when a user asks why the query was made.

KBMS. The Knowledge-Base Management System has two modules: (a) PROFDF (data processing) and (b) PUTBLK (utilities). The main functions of the KBMS are to create and maintain a load database and to allow users to scan and change load data. The PROFDP module takes care of opening a new database, adding new group of profile data to an existing database, and listing available data groups in a database. The PUTBLK module is a utility package. It allows users to scan through a database and to correct erroneous data, and to put blocks of data of any form into a database. More features such as delete a data group, garbage collection, copying a group of data from one database to another, etc. will be implemented in future versions.

As mentioned earlier, a set of generic read/write routines implementing a unique format was incorporated in the KBMS system. A database begins with a file header block and ends with a file trailer block. In between, it contains groups of data, each has a unique group name limited to 4 characters long. Each group of data begins with a group header record and ends with a group trailer record. In between, it contains data for the group. Database with this format can be constructed by the PUTBLK module.

In the load database, profile data have been identified as the most often used data form. Examples of this form are the time dependent power level profiles for engine tests. A set of routines in PROFDP was designed to read/write these data groups. The format for the profile data group was fixed. It consists of a group header record, a title (not more than 28 characters) block of a single record, a X-title block of one record for the x-axis annotation, a Y-title block of one record for the y-axis annotation, a block of x values, a block of Y values, a block of standard deviations for the corresponding Y values and a group trailer record. As the load database grows, more data groups will be included. Different data may be written in different forms which will be defined accordingly. When a particular form of data come into use frequently, new routines will be implemented in PROFDP to facilitate the READ/WRITE process.

12.4 LDEXPT User's Guide

1) LDEXPT is a command driven expert system for probabilistic load generation. A menu will appear on screen when LDEXPT is executed. On this top level, the following commands are available:

?RBMS: Go to Rules-Base Management System

?KBMS: Go to Knowledge-Base Management System

?HELP: List available commands on LDEXPT level

?QUIT: Exit LDEXPT, i.e., stop the program

2) RBMS is the Rules-Base Management System. It's main functions are to manage load data retrieval and to control the probabilistic load generation process. The available commands are:

?EXDR: Expert system driver carrying out the expert system consultation session.

Available subcommands are:

?WHY: Asking the expert system why the question was asked.

?HOW: Asking the expert system how the decision was reached.

?PEEK: Peek at data files of interest as selected during the consultation session.

?PLOT: Plot the last peeked profile data file.

?INPP: Prepare input file for ANLOAD using data file selected in the last consultation session.

?ANLD: Run ANLOAD, the probabilistic load generator, interactively. Note: ANLOAD can also be run as a batch job using the same input file prepared by ?INPP.

?HELP: List available commands in RBMS.

?RETN: Return to LDEXPT.

?QUIT: Exit LDEXPT.

There are several files associated with the RBMS system. The expert system consultation session as carried out by executing ?EXDR requires a problem text file and a rule file. The consultation session generates a log file which records the progress of the session and could be saved as a data file for later examination. ?INPP needs access to the load database to retrieve the required data for load generation. ?ANLD requires the influence coefficient data file 'INFLUENC.DAT'.

3) KBMS is the Knowledge-Base Management System. It's main functions are to create and maintain the load database. The available commands are:

?OPNF: Open an existing database and retrieve the desired profile data

?ADDF: Add a new profile file

?DLST: List the last accessed profile data

C-3

?GETY: Retrieve data points from a profile

?PLOT: Plot the last accessed profile data

?NLST: List available group names on the
opened database

?WAMI: Where am I?

?PUTR: Utility module

Available subcommands are:

?OPNF: Open an existing file or open a new file
and write a file header record and a title block

?PUTG: Write group header record

?PUTA: Write vector data records

?PUTS: Write scalar data records

?ENDG: Write group trailer records

?ENDF: Write file trailer record

?SCAN: Scan file and correct erroneous data

?RETN: Return to PROFDP

?RETN: Return to LDEXPT

?QUIT: Exit LDEXPT

KBMS communicates with a load database file. AT this time, group data other than the profile data, e.g., the component turbine load coefficient data, shall be entered into the load database using the ?PUTR module.

12.5 Turbine Blade Loads

The initial code has individual loads defined for the 1st stage HPFT rotor blades. The loads are the airfoil pressure and dynamic Δp and the centrifugal loading. The thermal loads were defined too late to implement in the initial code, but will be discussed from a technical standpoint.

A discussion of the methodology used by Rocketdyne for the SSME turbine blade analysis to obtain pressure and dynamic loads are furnished in Appendix B. Essentially it is a series of steady state point designs using analysis codes to define overall turbine parameters. The parameters of interest to structural analysis include speed, torque and blade pressure loading. The pressure loading is furnished in one of three forms that are available from the hydrodynamic analysis--blade mid-point axial and tangential forces, distributed axial and tangential forces on the blade, and pressure distributions on the airfoil. All of these forms are used in structural analysis and are included in the methodology. For the CLS program, the loading over the total duty cycle is required, but only limited point design data are available, and not necessarily in the form desired. Also, accuracy in scaling over reasonable power levels--65 to 109% power level is required. The approach for obtaining technical data for the CLS program is to use available information except for limited correlation or scaling studies. A series of point design turbine analysis were run for the HPF turbine to develop scaling information over the spectrum of power levels. The 1st stage turbine blade concentrated force and distributed load correlations were obtained.

The design features and operating conditions of the SSME HPF turbine are shown in Figure B.12 in Appendix B. This turbine has a secondary flow circuit for cooling the rotating hardware and includes cooling of the shank portion of the turbine blades. This cooling circuit affects the pressure and temperature description of the blades. The flow interruptions upstream of the blades create the dynamic pressure loads.

.SCALABLE VARIABLES

.AIRFOIL

.TURBINE ΔP PRESSURE .TURBINE TORQUE

SHANK ZONE

.COOLANT PRESSURE

.3 METHODS FOR REPRESENTING AIRFOIL PRESSURES

A. F_A & F_T @ BLADE MID-POINT
ΔP = (INLET-OUTLET) TURBINE PRESSURE

$$F_{T1} = \frac{109}{9378} T_1, \quad F_{T2} = \frac{180}{9378} T_2$$

$$F_{A1} = \frac{140}{1423} \Delta PI \quad F_{A2} = \frac{112}{1423} \Delta P$$

B. DISTRIBUTED FORCE DISTRIBUTION ON BLADE SCALED SIMILARILY TO "A" WHERE F_{T1}, F_{T2}, F_{A1} & F_{A2} REPLACED BY DISTRIBUTED FORCE INCREMENTS

C. PRESSURE DISTRIBUTION ON BLADE CROSS-SECTIONS

P_I = OPERATIONAL PRESSURE AT POINT I ON BLADE.

P_I = PAVE + ΔP_I

I = 1 TO NUMBER OF POINTS IN AIR FOIL X-SEC.

. PRESSURE DISTRIBUTIONS AVAILABLE FOR 2 OR 3 CROSS-SECTIONS FOR EACH TURBINE BLADE-TIP, MID, HUB

. ALL AIR FOIL PRESSURE DISTRIBUTIONS CORRELATED VARIABLES

.SHANK PRESSURES

.EQUAL TO LOCAL COOLANT FLOW TEMPERATURE .NOMINALLY CONSTANT

Figure 83 Pressure ΔP Loads

Figure 83 summarizes the scaling techniques used for the pressures and Δp. For the blade load analysis, the distributed airfoil loads are considered correlated. This means that only one probabilistic variable is required to define the airfoil loads for each load component (as discussed in the previous section). An example of how the static pressure distribution is scaled is shown in Figure 84. The pressures are divided into an average pressure scaled to the inlet pressure and a variable pressure that is scaled with torque. The pressure distribution shown is for the pressures at the hub of the first stage blade.

HPFTP 1-R HUB EXAMPLE

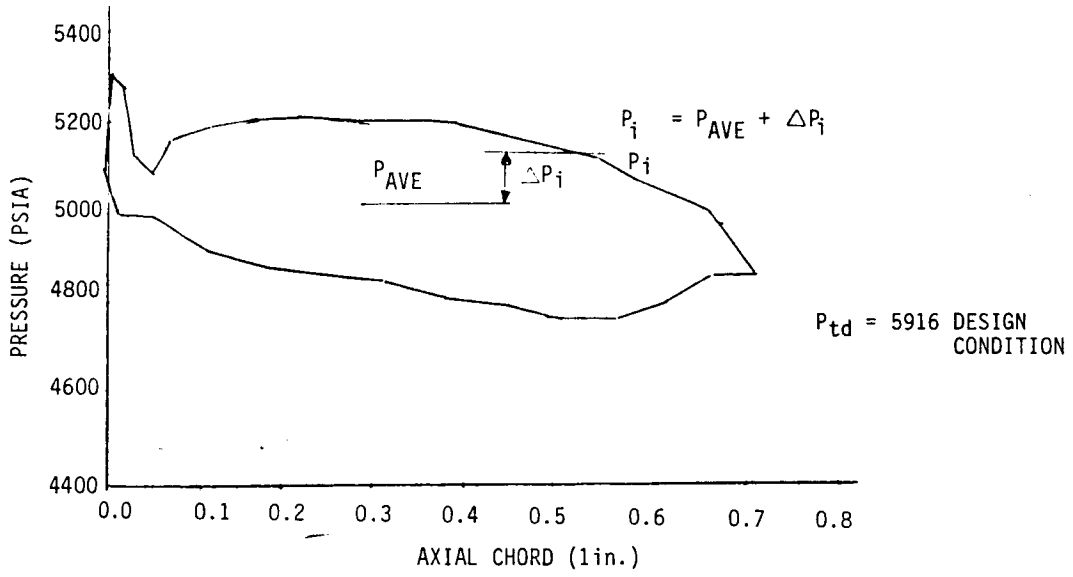

P_T - TOTAL INLET PRESSURE TO TURBINE (INSTANTANEOUS)

STATIC AVERAGE PRESSURE VS PRESSURE FLUCTUATION

$$P_{AVE} = \frac{5000}{5916} P_T$$

Figure 84 Pressure Change from Design Condition from Static Pressure

The baseline temperature loading for the HPFTP first stage turbine blade are defined for a typical duty cycle. These profiles were obtained for cross sections in the airfoil, platform, and two locations in the shank (See Fig. 85a). Between seven and eleven points are defined at each cross section. Figure 85b is the airfoil cross-section. The temperatures of all other locations on the blade are obtained by interpolating among the defined inputs. These represent nominal temperatures for a level of operation at rated power level (100%).

A variety of analytical models and experimental observations were used to obtain these temperatures. Some of the data used were from models of the second stage HPFTP blade and from the first stage blade airfoil. The second stage blade information is applicable because the boundary conditions on that blade are roughly a mirror image of those on the first stage blade. Most of the analyses are steady state, but there have been a large enough number of one dimensional transient models done to establish the general transient trends. As more detailed analyses are performed on the first stage blade, the results can be used to update these temperatures.

Most of the airfoil temperatures were based on a model of the HPFTP first stage nozzle. The biggest difference between the nozzle and the blade is that the nozzle has a hollow core. This causes the nozzle transient temperature gradient to be somewhat less than that in the blade. Since the entire airfoil is essentially at the hot gas temperature during steady state operation, only the transient variations are really of interest. Figures 85c and 85d are examples of start transient temperatures at selected points in the cross-section.

The portion of the second stage blade in the vicinity of the platform has been modeled in some detail due to cracks in that area. The platform itself is nearly isothermal during steady state operation, but there are transient variations. The temperatures presented for the platform were obtained by reversing the leading and trailing edge temperatures from the second stage model. The airfoil temperatures were taken into account as well.

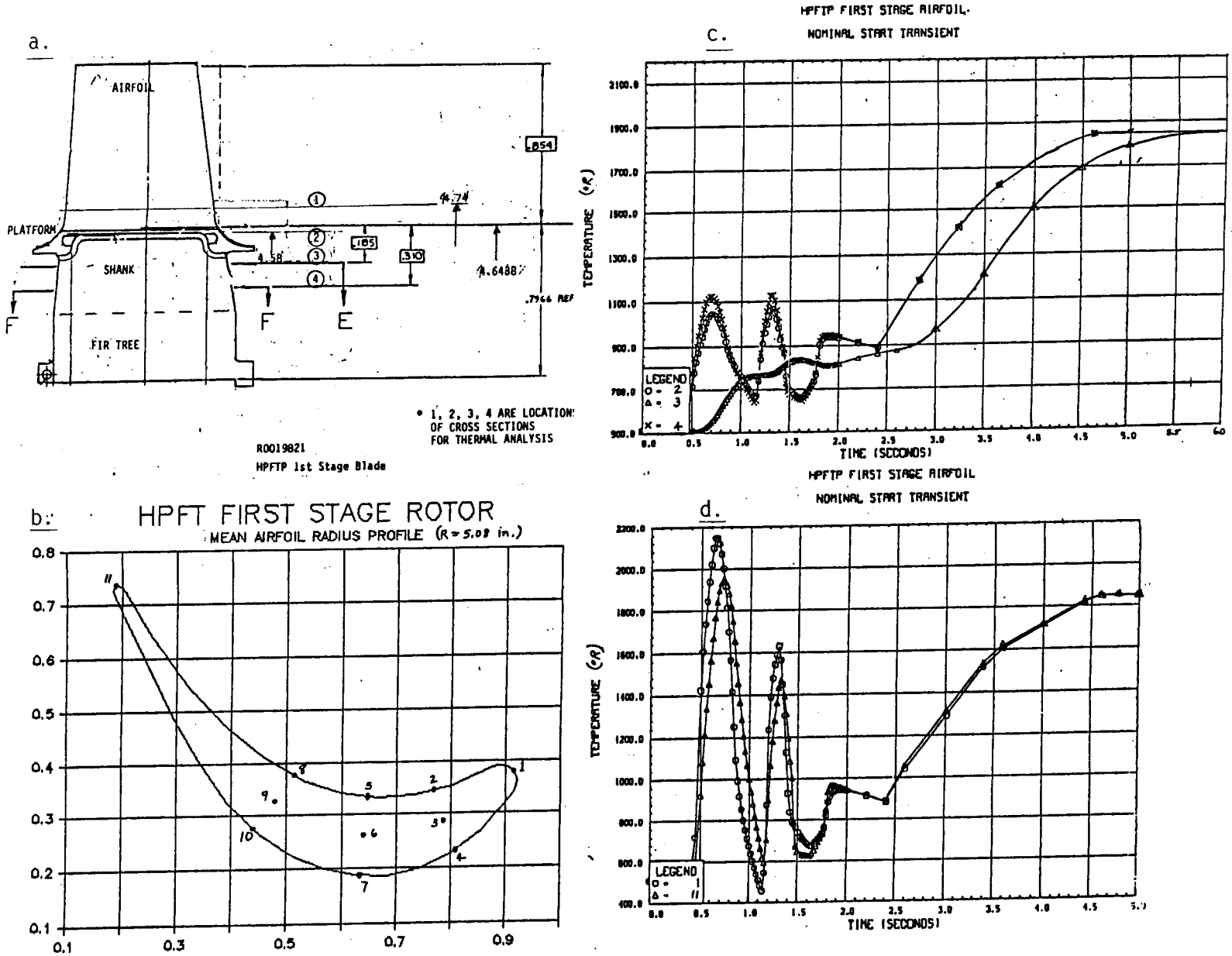

FIGURE 85 TEMPERATURE LOADING

The shank temperatures were also largely obtained from the second stage blade models. In actuality, the coolant and hot gas flows around the shank are very complicated. The hardware shows large variations in oxidation discoloration (which is a rough indication of temperature) from pump to pump, indicating that as the various seals wear the flow circuit resistances change. A fairly large tolerance band will have to be imposed on these temperatures to account for these flow variations.

A method of developing the total blade temperatures from the discrete points at four cross-sections is conceptually planned as shown in Figure 86. A coarse finite element model can be defined encompassing the blade, cross-section and points. With this information as input, the TRANCITS code could be used to develop the overall blade temperatures.

- TEMPS AT 4 X-SEC & SELECTED POSITIONS
- DEFINE COARSE SOLID MESS
- USE TRANCITS (TITAN) CODE TO MAP ON DETAIL STRUCTURES MODEL

TEMP VS TIME

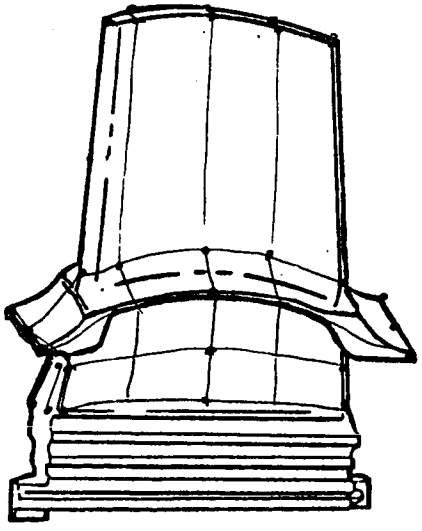

- NOTE: SIMILAR TECHNIQUE FOR PPESSURES

Rockwell International
Rocketdyne Division

Figure 86 Overall Blade Temperatures

12.6 Probabilistic Load Model Validation and Verification

Introduction. The previous discussions in the loads survey section led to the recommendation of three probabilistic methods for the space propulsion load simulation: (1) Monte Carlo; (2) Discrete Probability Distribution; (3) Barrier Crossing. In order to determine the adequacy of these methods two steps must be taken. First, the methods must be verified, to the extent possible, against standard probabilistic problems. Secondly, the codes must be validated by comparing the predicted results with actual measured data. Because the validation phase will depend critically upon the method of data analysis, it is important to identify the salient features of the selected techniques. The verification of the probabilistic methods will examine how well each of the methods reproduces a normal distribution and the combination of two normal distributions. The reason for selecting this case for the verification is that the mean of the sum of two normals is equal to the sum of the individual means while the variance is given by:

$$V(x + y) = V(x) + V(y) + 2\rho(V(x)*V(y))^{1/2}$$

Therefore, a theoretical distribution for the sum of two normals can be calculated and compared to the probabilistic load model results. The validation of the probabilistic load model will be performed for steady state loads on the turbine blades. Three variables will be used for this analysis: HPFT turbine speed, HPFTP discharge temperature, and HPFT discharge temperature. These variables have been selected primarily because they have been measured for both SSME tests and in flight. The following subsection describes the data analysis used for the initial load calculations. The results of the verification runs are presented, and finally, sample calculations for the validation of the code are discussed.

Data Analysis. The standard data analysis performed for SSME test stand and in-flight data consists of four steps: (1) moment calculations, (2) probability distribution function determination, (3) stationarity testing, and (4) joint density function calculations. The basic methods of analysis

were described previously. The purpose of this discussion is to update this description in the context of data analysis for the SSME data. Not all of the SSME load data important to the turbine blade load analysis is directly measured. For these loads, influence functions have been developed to predict the value of the load from measured or known, engine parameters. The influence coefficient calculation proceeds as follows. For a given power level, denoted PL, the influence coefficient for dependent load J given the value of the independent load K is

$$G_{J,K} = \sum_{I=1}^{4} C_{I,J,K}(PL)^{I-1}$$

The nominal value of the independent variable is given as M_K. The nominal value of the dependent variable is denoted M_J. The actual value of the dependent variable, denoted V_J, due to the change in the independent variable from its value for the nominal engine operating conditions is given by

$$V_J = M_J\,(1.0 + G_{J,K}\,(V_K - M_K)/M_K)$$

where V_K is the value of the independent variable. As an example, assume that the mixture ratio is changed from its nominal value of 6.0 to 6.01 and it is desired to assess the effect of this change on the HPFTP turbine speed at 100% power level. From the table of influence coefficients:

$$M_K = 6.0$$
$$G_{J,K} = -0.707499 + 1.14417 - 0.777 = -0.34033$$
$$M_J = 34625$$

Therefore,

$$V_J = 34625\,(1 + (-0.34033)((6.01 - 6.0)/6.0)$$
$$V_J = 34605$$

If there are more than one independent variables being changed from the nominal conditions then

$$V_J = M_J \left(1.0 + \sum_{k \epsilon K} G_{J,k} \left(V_k - M_k\right)/M_k\right)$$

where $k \epsilon K$ means that independent variable k has been changed from its nominal condition. This is done strictly to save computational time since if the variable has not been changed from its nominal value the second term will be zero. The question now becomes how is the distribution for the dependent parameters and loads, V_J, calculated when the independent parameters and loads are random variables? For this case, the subset in which all of the independent variables are normally distributed is first examined. In such an example

$$V_J = M_J \left(1.0 + \sum_{k \epsilon K} G_{J,k} \left(N(\mu_k, \sigma_k) - M_k\right)/M_k\right)$$

From the algebra of normal distributions the expected value of V_J is:

$$E[V_J] = M_J \quad \text{provided that } E[N(\mu_k, \sigma_k)] = M_k$$

and the variance is

$$\text{Var } (V_J) = \sum_{k \epsilon K} \frac{(M_J G_{J,k})^2}{M_k} \text{Var } (V_k)$$

This will be an important test case in the validation of the probabilistic load model for the following reason. The influence coefficients, $C_{I,J,K,}$ are fit to the output of a sophisticated computer code which performs an engine balance for the fluid and thermodynamic conditions in the SSME. However, since these coefficients are based on computer simulation, they do not include the effects of "measurement" error for unaccounted variables. This implies that the range of the load variables predicted by the probabilistic model will be smaller than the range given by the data. Therefore, by inputting normal distributions for the independent load parameters an estimate of the "measurement" error can be made.

Data Analysis Results for Selected Independent Parameters. The verification and validation of the probabilistic load model does not require that all twenty-three independent load parameters be included in the analysis. Rather, it is sufficient to demonstrate that the model works well with several variables since adding additional values only increases the computational time but does not change the program logic. Additionally, it becomes increasingly difficult to interpret the code output if many variables are included since the amount of data to be examined becomes overwhelming. With this in mind, five independent variables have been selected for the initial studies of the load model. These five parameters were selected based on data availability and variety in the results of the probabilistic characterization of the variable during data analysis. These five variables are listed in Table 22 together with the best fit distribution parameters listed first and the normal distribution listed second.

Table 22 Data Analysis Results for Five Independent Parameters

Variable	Distribution: Parameters	Normal Distribution Parameters
Mixture Ratio	Uniform: 5.974 6.051	Mean: 6.0127 Std. Dev.: 1.2774x10-2
Fuel Inlet Pressure	EV Type I: 25.2314 0.1737	Mean: 28.5546 Std. Dev.: 7.3842
Lox Inlet Pressure	Normal: 64.334 21.037	Same
Fuel Inlet Temperature	Lognormal: 3.613 0.01626	Mean: 37.0886 Std. Dev.: 0.5996
Lox Inlet Temperature	Lognormal: 5.1017 0.01072	Mean: 164.317 1.7614

There are other data analysis efforts which are ongoing. These include additional independent variable analysis between engine variation characterization and test stand versus flight data variation. These and other data analysis efforts have provided preliminary results but are not yet complete. As new results are obtained, they will be documented.

Probabilistic Load Model Verification Studies. The verification of the probabilistic load methods requires that a theoretically tractable problem be examined in order to demonstrate that the underlying mathematical formulation is correct. To demonstrate this for the probabilistic load model two verification studies have been undertaken. In the first case, a normal distribution with a mean value of 10.0 and a standard deviation of 4.0 is examined. The second study combines two normal distributions each of which has a mean of 10.0 and a standard deviation of 4.0.

Verification Study One. The results of the first verification study are shown in Table 23. Because the mean and standard deviation of the normal distribution are known, it is possible to calculate the theoretical values corresponding to the desired percentile values. The worst set of Monte Carlo runs is included to illustrate the probabilistic nature of the analysis. In this set of runs, the 95% confidence intervals missed the theoretical value six times. Using a different sequence of random numbers and a 2000 run simulation found the 95% confidence intervals covering all twenty of the percentile values - a situation which, on the average should only occur 1/3 of the time. The RASCAL results provide an extremely accurate representation of the normal distribution. However, this should be the case since the discretization by RASCAL is based on an integration of the normal and not a random sampling. This is most clearly illustrated in Figure 87 where the accuracy of the two methods is plotted. The solid line is the theoretical cumulative distribution function (CDF) of the normal distribution.

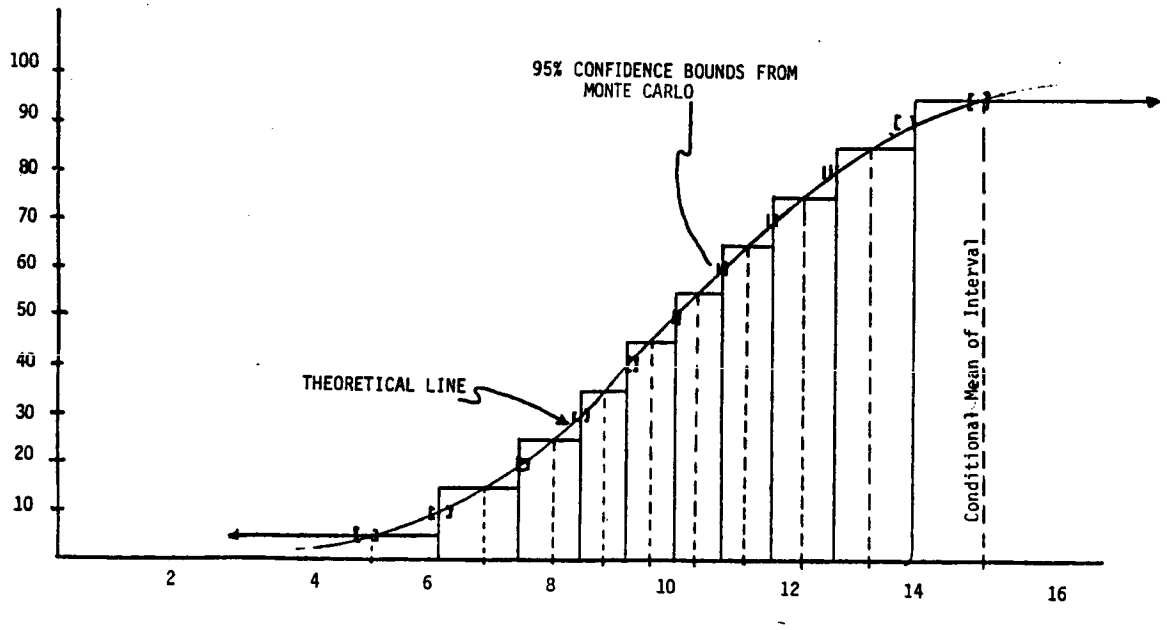

Figure 87 Verification Study One Results

Table 23 Results of Verification Case 1

	MONTE CARLO		RASCAL	
PERCENTILE*	THEORETICAL	CALCULATED	THEORETICAL	CALCULATED
5 (.0625)	5.065	5.194	4.660	4.505
10 (.1125)	6.155	6.285	5.931	5.914
15 (.1625)	6.890	7.016	6.725	6.723
20 (.2125)	7.475	7.591	7.339	7.338
30 (.3125)	8.427	8.519	8.318	8.318
40 (.4125)	9.240	9.326	8.874	8.867
50 (.4875)	10.000	10.053	9.906	9.876
60 (.6125)	10.760	10.768	10.857	10.957
70 (.7125)	11.573	11.582	11.682	11.862
80 (.8125)	12.525	12.530	12.661	12.732
85 (.8625)	13.110	13.161	13.275	13.257
90 (.9125)	13.845	13.827	14.069	14.056
95 (.9625)	14.935	14.857	15.340	15.303

*Due to the nature of the RASCAL method, 1/(2*NBIN) must be added to percentile value to obtain the desired result (or subtracted if percentile <50)

The square brackets indicate the 95% confidence limits calculated by a 2000 run Monte Carlo simulation. If these brackets enclose the theoretical line then the simulation is doing well. The histogram plot represents the RASCAL method for discretizing the continuous distribution. In the actual calculation forty discrete points were used, however, only a 10 discrete point case is shown. The solid lines represent the discrete break points which are calculated by RASCAL and correspond to those points which enclose 1/NBIN (in this case 1/10) of the probability mass. However, for calculational purposes RASCAL places

this probability mass at the conditional mean of each interval. The conditional mean is calculated as

$$C_m = \int_{d_{i-1}}^{d_i} x\, f(x)dx \Big/ \int_{d_{i-1}}^{d_i} f(x)dx$$

where the d_i are the break points and f(x) is the PDF of the random variable x. The conditional mean points are shown in the Figure as dashed lines. This Figure also helps to illustrate why the conditional means must be used. If the interval endpoints are used and the CDF is drawn through these points then it is obvious that an artificial shift, i.e. bias, has been introduced. As the Figure clearly shows, the conditional mean points are the only ones which will not introduce such a shift and, therefore, during calculations will produce the only set of unbiased results. While these results are very good, the methods are not severely tested in simply reproducing input distributions. A better test of the results is provided in the second verification study when two random variables are combined.

Verification Study Two - Sum of Two Normals. For the calculation of the sum of two normals, only the RASCAL and Monte Carlo methods are viable. To compare the theoretical and load model results it is noted that from the algebra of normal distributions the following is true:

$$E[x+y] = E[x] + E[y]$$
$$V[x+y] = V[x] + V[y] + 2\,\rho\,(V[x] * V[y])^{1/2}$$

When X and Y are independent and uncorrelated then ρ is equal to 0.0. For a mean of 10 and a standard deviation of 4, the random variable Z given by

$$Z = X + Y$$

has a mean of 20 and a standard deviation of $\sqrt{32}$. Since the theoretical value of the CDF for X can be calculated comparisons similar to those made for the single normal distribution can be made. The results of the RASCAL and Monte Carlo calculation both agree well with the theoretical results.

From these analyses, it is concluded that the basic underlying mathematics and computer programming of the probabilistic load model is correct. The next step is to compare these results with actual data.

Probabilistic Load Model Validation. For the five input variables which were analyzed in the previous subsections, three engine parameters were studies:

(1) HPFTP Turbine Speed (HPFTP-TS)
(2) HPFTP Discharge Temperature (HPFTP-DT)
(3) HPFT Discharge Temperature (HPFT-DT)

Because the results of the discharge temperature analysis are similar only the HPFT-DT case will be discussed of these two in order to clarify the discussion. In addition, only the RASCAL results are presented since the same information was obtained with the Monte Carlo analysis. The mean and standard deviation as calculated by the probabilistic load model and from the data is given in Table 24. While the mean values are extremely close, there is a large discrepancy in the calculation of the standard deviation. As referred to previously, it is believed this error is due to the "measurement error" in the data. Recalling the expression developed for the variance due to the random nature of the input variables we can write

Table 24 Probabilistic Load Model Results and Comparison to Load Data

OUTPUT	MEAN		STANDARD DEVIATION	
VARIABLE	LOAD MODEL*	DATA	LOAD MODEL*	DATA
HPFTP-TS	34621	35202	131.0	566.4
HPFT-DT	1703	1698	8.7	56.8

* At 100% power

$$V_{Data} = \sum_{k \epsilon K} \left(\frac{M_J G_{Jk}}{M_k} \right)^2 Var\,(V_k) + V_{ME}$$
$$= V_I + V_{ME}$$

where

V_{Data} : Variance observed in the data
V_{ME} : Variance due to measurement error and/or unaccounted for variables
V_I : Variance due to the combination of random input variables.

Using the Table of influence coefficients for 100% power level for the five input variables, the value of V_I for the HPFT-DT is found to be

$$VI = 72.7$$

From Table 25, V_{Data} is approximately 3226. Therefore,

$V_{ME} = 3226 - 72.7 = 3153.3$
$\sigma_{ME} = 56.1$

The result is that the ratio of the standard deviation due to measurement error to the mean value is approximately 3.3%. This is on the order of the percent error one would expect from measurements of temperature. The result of the probabilistic load model calculation is shown in Figure 88. Also shown in Figure 88, are the $\pm$ 2σ bounds. Figure 89 shows these same results when the data is superimposed on top of the data in Figure 88. Figure 89 illustrates that the mean trend of the data is being well predicted but, if measurement error is not accounted for on the analysis, the spread in the data is underpredicted. While Figures 88 and 89 plot the results of 135 sets of data in which the power level varies Figure 90 plots

only the 100% power level. In addition, the two different measurements of temperature are given as Channels A and B. As this Figure shows the larger variation in the data is not due to changes in the power level and thus must be due to "measurement" error. It is also important to note that the measurements from the two different channels have introduced systematic differences in the "measurement" error. That is the channel A measurement produces a lower mean value than the conglomerate set while channel B gives a higher mean. It is believed that this difference is due solely to the instrumentation location and that it is valid to accept the average of the measurements as equivalent to the true value of the discharge temperature (plus, of course, some error).

The results of the HPFTP-TS calculations were similar in many aspects to the HPFT-DT analysis. The calculated value for V_I is 25333.

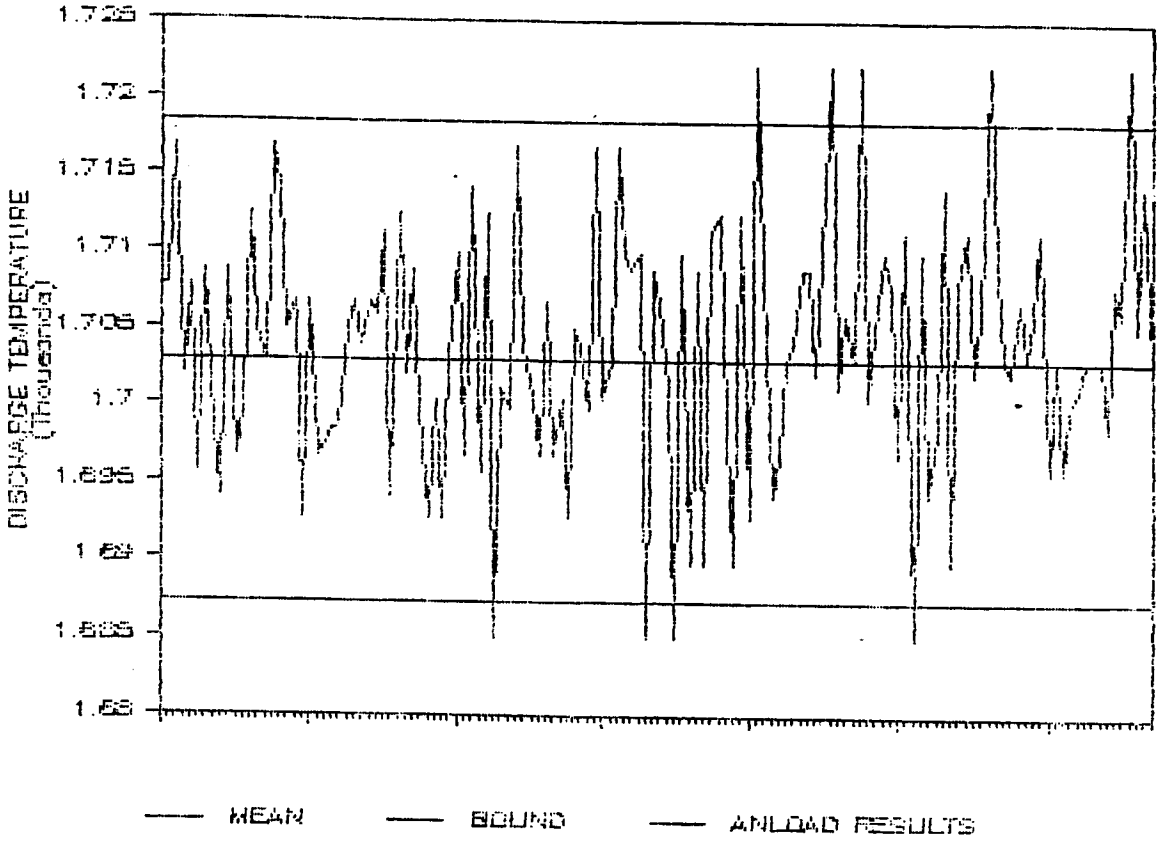

Figure 88 HPFTP Discharge Temperature

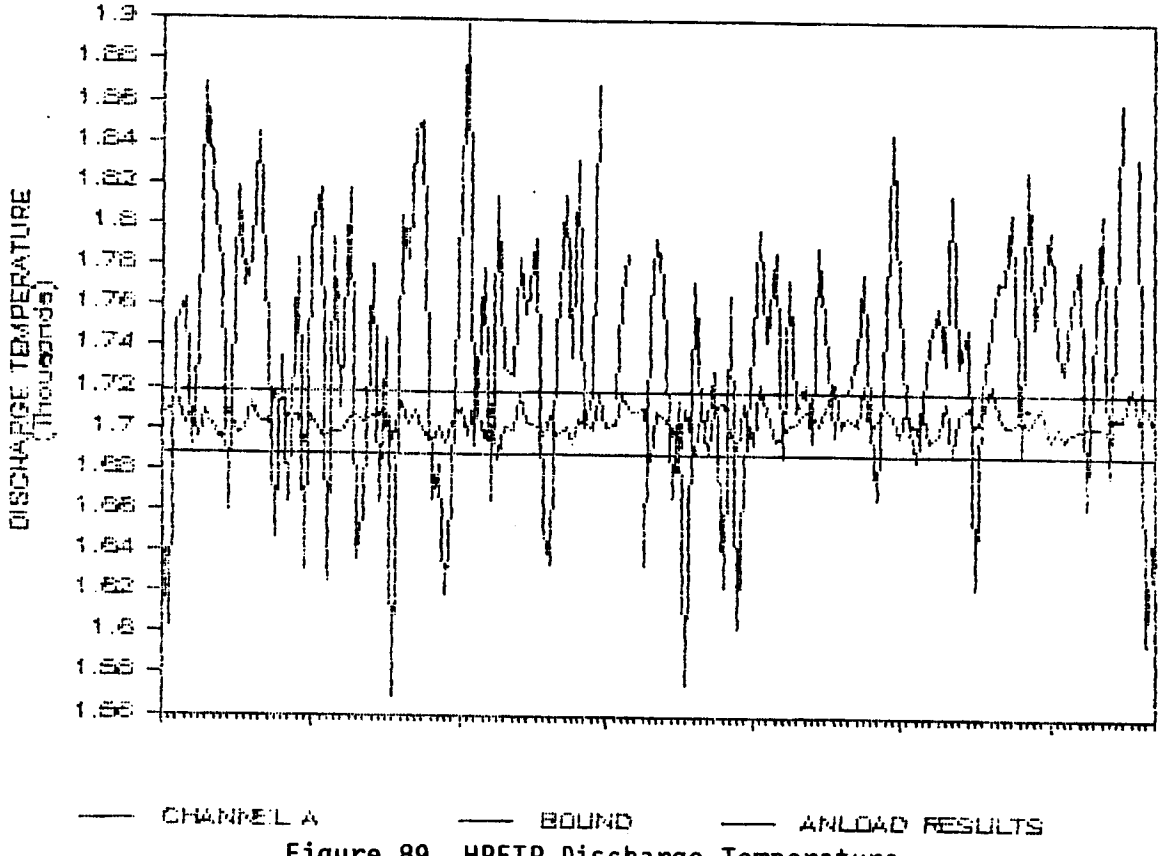

Figure 89 HPFTP Discharge Temperature

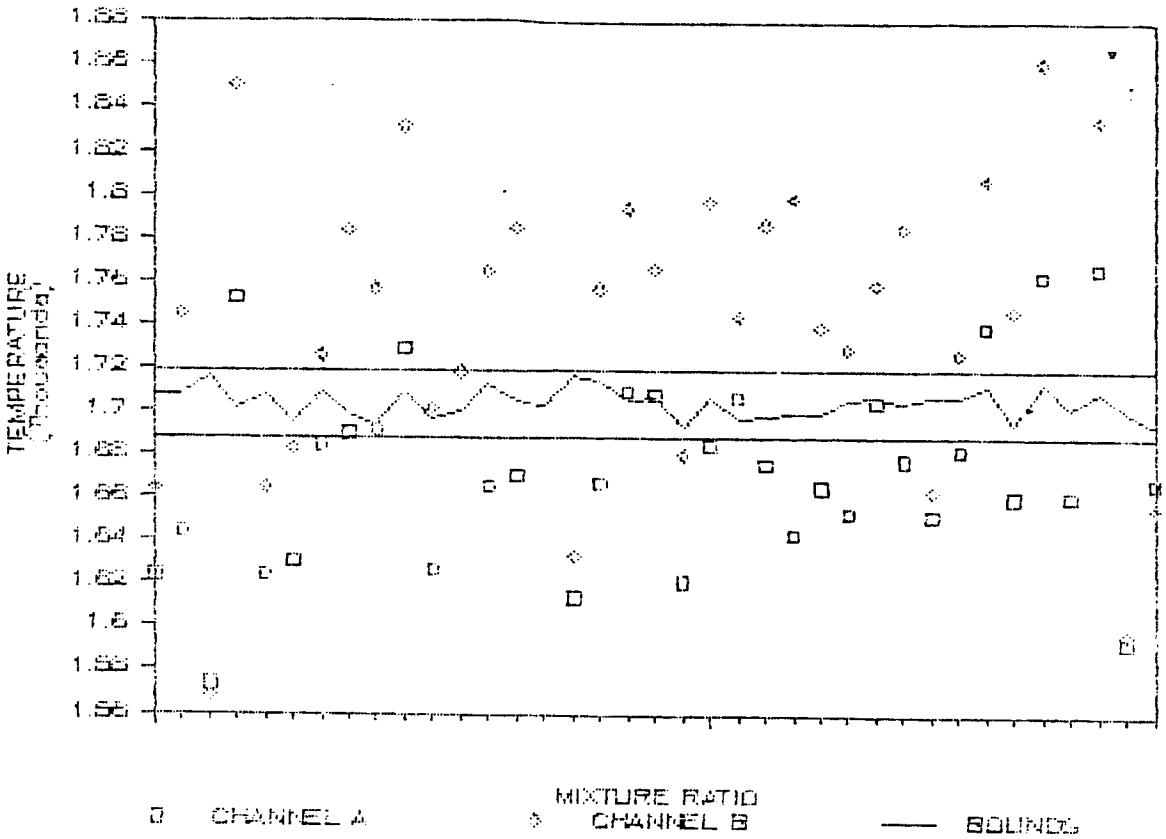

Figure 90 HPFTP Discharge Temperature

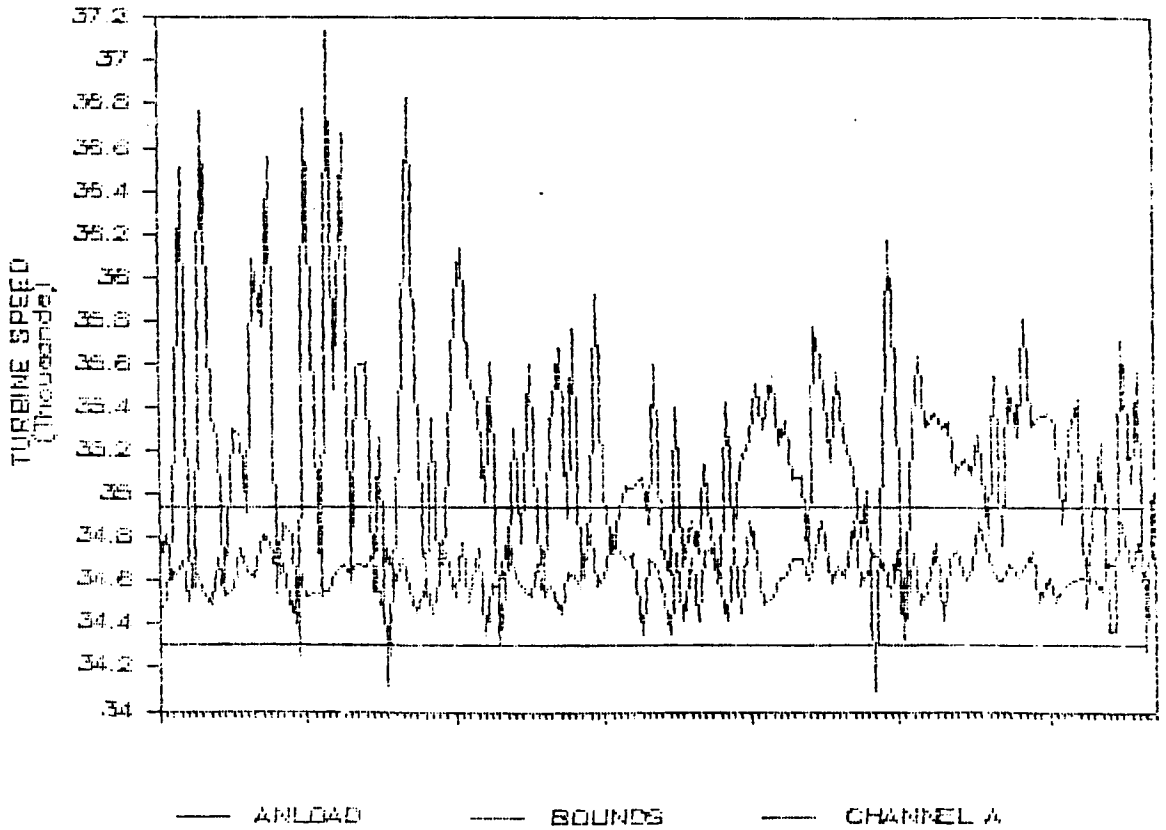

Figure 91 HPFTP Turbine Speed

Therefore,

V_{ME} = 321000 - 25333 = 295667

σ_{ME} = 544

Therefore, the ratio of σ_{ME} to the mean is approximately 1.6%. Again, this is not unexpected and is believed to be typical of measurements of this type. The one difference between the two analyses can be seen in Figure 91. In this Figure, the data seems to be systematically one to two percent higher than what is expected if the effects of "measurement" error are removed by assuming it to be gaussian distributed about the mean. In order to insure that this effect was not caused by the 104% power level data, Figure 92 plots only the 100% power level data. Since the same upward trend is noted alternative explanations must be sought. Two are believed to be the most likely currently. Either the method for taking the measurement always errs to higher values than a gaussian assumption would predict or one of the input variables is slightly higher (or lower for negative influence coefficients) than was input to the model. While the difference is slight (less than 1.5%) the cause is being investigated.

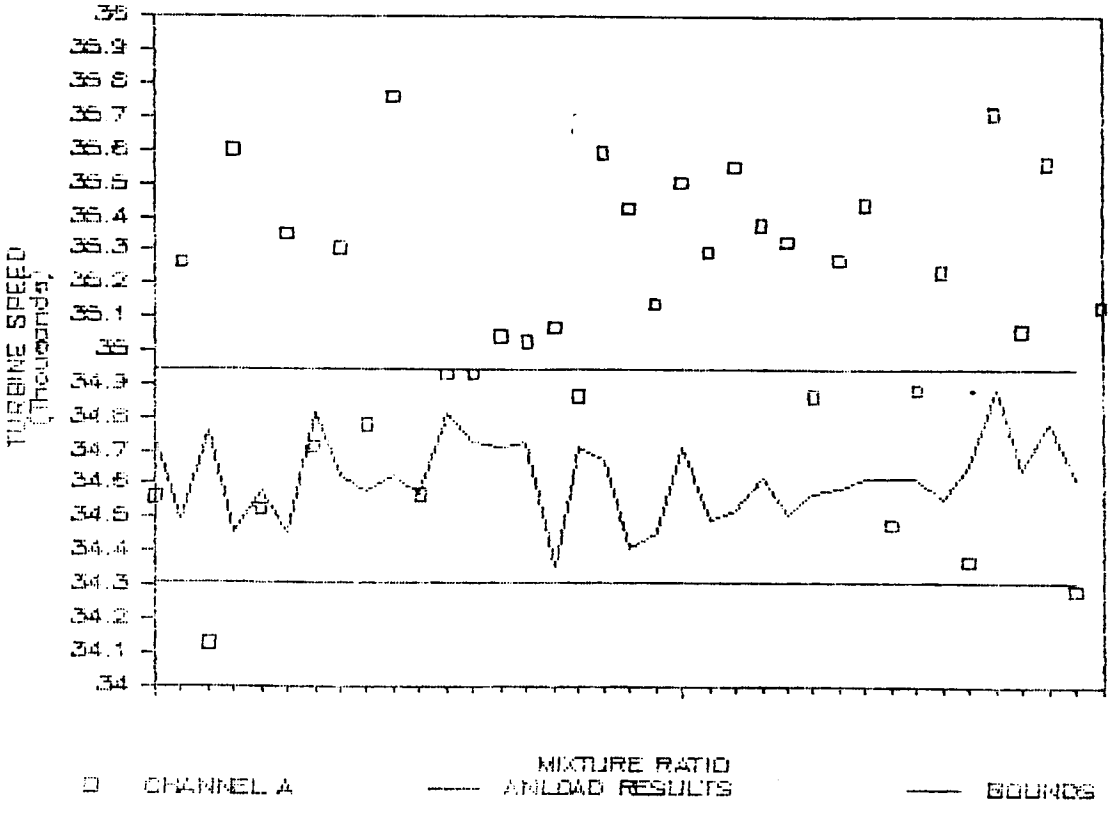

Figure 92 HPFTP Turbine Speed

References

1. AD881744, Air Force Reusable Rocket Engine Program XRL129-P-1 Final Report, January 1971.

2. NASA SP-8110 Liquid Rocket Engine Turbines, January 1974.

3. RI/RD80-218-2, Orbit Transfer Vehicle Advanced Expander Cycle Engine Point Design Study, Volume II: Study Results, 12 December 1980, Rocketdyne.

4. RSS-8559-1-1-1, Space Shuttle Main Engine, September 1983

5. AEDC-TR-16-74, Space Tug Engine Performance Verification, August 1976.

6. The EX-TRAN manual, version 7, Intelligent Terminals Limited

APPENDIX A - STOCHASTIC COMBINATION OF COMPOSITE LOAD SPECTRA: COMPILATION OF LITERATURE SURVEY

APPENDIX A

STOCHASTIC COMBINATION OF COMPOSITE LOAD SPECTRA: COMPILATION OF LITERATURE SURVEY

The following is a compilation of references relevant to stochastic composition of composite load spectra. This literature survey was performed in order to find those mathematical models and techniques currently available to account for random combinations of various loads to form a composite load at a particular point of interest. As a result of these findings, a probabilistic model will be developed which will produce probability functions for loads and load combinations for components in the space shuttle main engine.

A.1 Survey Criterion

Viable probabilistic models for use in load combinations in the shuttle main engine were evaluated according to the following criteria:

1. Consider the random or unknown component of the load at a point in the main engine due to varying values of the individual loads.

2. Incorporate the random timing of the occurrences of these loads and their possible combination at selected critical components of the engine.

3. Individual loads under consideration may occur due to pressure, thermal gradients, acoustics, vibrations, etc. The model must be capable of fitting a probability distribution function to a load spectrum based on physical interpretation of the causal relationship between state parameters such as pressure, vibrations and the loads they induce.

4. The flexibility of applying the same general probability model to various components in the shuttle main engine.

A.2 Classification of Cited References

The references cited are classified according to three categories.

Classification	Description
I	Specifically Relevant References. These references discuss probabilistic models most applicable to composite load spectra.
II	General Background References. The references in this category discuss stochastic load combination, but are not directly applicable to composite load spectra for space propulsion components.

A.3 Survey Methodology

The literature search was conducted in two ways:

1. Abstracts from engineering and mathematical indexes were screened for key phrases such as "probabilistic loads", "stochastic load combination", etc. A list of abstracts bearing these key phrases were provided through a thorough computerized search. Following this, each entry in the list was judged for applicability based upon the description provided in the abstract.

2. Authors were identified who had previously done significant work in stochastic load combination. Work performed by such individuals was then studied for potential use in this project.

A.4 Survey Results

Classification I

Allan, R. N.; Leite da Silva, A. M.
University of Manchester Institute of Science and Technology, England
IEEE Proceedings Part C vol. 128 n. 5
September 1981 p. 280-287
" **Probabilistic Load Flow Using Multilinearizations** "
Probabilistic load flow is a technique which recognizes the probabilistic nature of the input parameters and takes account of the uncertainties and random variations of generation and load within one computer run. Many formulations have been presented to implement this technique. The majority have assumed either a linear model to represent the load flow equation, or the output random variables to be normally distributed, or a combination of both of these concepts. This paper first uses Monte Carlo simulation to show the effects of nonlinearity in the network equations and that the assumption of a normal distribution for the output random variables is completely unreliable. A completely new algorithm for the probabilistic load flow is then proposed which accounts for the nonlinear effects. This new technique is shown to five new impetus to probabilistic load flow analysis.

Breitung, K.; Rackwitz, R.
Institut fur Massivbau, Technical University of Munich,
Munich, West Germany
Journal of Structural Mechanics, vol. 10, n. 2, p. 145-166.
" **Nonlinear Combination of Load Processes** "
An important problem in structural reliability is the combination of time-variant stochastic loadings. The failure probability in the case of nonlinear combinations of stochastic processes can be approximated by the mean crossing rates of time-variant loadings out of the safe domain of structural states. Except for linearly bounded safe domains, these rates are difficultto compute; therefore, the quality of various linearization points is investigated. Comparisons are made of some examples showing that for time-variant problems

the Hasofer-Lind point is often suboptimal. A linearization at the point of maximum local outcrossing density might generally produce non-degenerate, sufficiently accurate results.

Cederkvist, Jan
Technical University of Denmark, Lyngby
Journal of Structural Mechanics, vol. 10 n. 1, 1982 p. 49-65
" **Design of Beams Subjected to Random Loads** "
Nonuniform Timoshenko beams subjected to a given stationary random excitation are considered. The general equations relating the spectral density function of the response to the cross spectral density of the load are derived. The optimal shape of the beam is defined as the shape which, for given constant volume of the beam, minimizes the maximum root-mean-square value of the bending stress in the beam. The shape of the beam is described by a limited number of orthogonal design functions, and their optimal combination is found by sequential linear programming with move limits. From numerical results, it is seen that slight modifications of the beam shape give a considerable reduction of maximum r.m.s. stress for most loading cases.

Contreras, H.; Scholl R. E.
URS/John A. Blume and Associates, Engineers.
130 Jessie Street, San Francisco, CA 94105 USA
Transactions of the International Conference on Structural Mechanics of Reactor Technology 5th v M. Methods for Structural Analysis, Berlin, Germany, August 13-17, 1979.
Published by North-Holland Publishing Co., Amsterdam.
Netherlands for Comm. of the European Communities,
Brussels, Belgium, 1979. Paper M 10/6, 8 pages.
" Stochastic Finite Element Structural Models "
In a new approach to accounting for the main sources of uncertainty in the analysis and design of structures, stochastic differentialand difference equations are combined with the finite-element method. Loads for multidimensional structures are idealized as stochastic processes and

incorporated into finite-element models with uncertainty in their parameters. The theoretical basis of the stochastic differential and difference equations and of the finite-element method are presented. Stochastic finite elements are introduced as a means to identify or consider uncertainty in parameters. Seismic disturbances are used as an illustration of simulating loads with stochastic processes. Numerical examples show the capabilities and feasibility of the proposed methodology.

Cornell, C. Allin (Chairman); Esteva, Luis (Vice-Chairman); Meli, Roberto (Editor)
Tall Building Criteria and Loading. Chapter CL-7, published by Asce (Monograph on the Planning and Design of Tall Buildings, vol. CL). New York, NY 1980 p. 535-643.
" **Structural Safety and Probabilistic Methods** "
The chapter provides an introduction to the probabilstic methodology which is a fast growing part of structural engineering, including the use of probability and statistics in generalized approaches to structural safety. Sections of the chapter introduce some of the elementary terminology and mathematics applied in the discipline, code specifications of structural safety, economics of engineering safety decisions, load and load combination analysis, system reliability theory as applied to frame buildings, and design recommendations for and implications of a thorough probabilistic safety analysis.

Corotis, Ross B.; Tsay, Wen Yang
John Hopkins University, Baltimore, Md. USA
Journal of Structural Engineering vol. 109 n. 4
April 1983 p. 859-874
" **Probabilistic Load Duration Model for Live Loads** "
A stochastic model of the live load process in buildings provides a basis for the study of load duration. The combined load modelis comprised of a sustained load process and multiple extraordinary load processes. Complete probability distributions of total time above a fixed reference load, duration of a single excursion upcrossing the reference load, and number of excursions

for a fixed designed lifetime are derived. These quantities are necessary for computing long-term deflection and settlement of structures and critical load combinations for creep-rupture materials, such as wood. The derived distributions are applied to several building occupancy types. Results indicate the sensitivity of some duration characteristics to the extraordinary load and the need for even further refinement of the stochastic load model.

Datta, P. K.
Indian Instit. of Technology, Aeronautical Engineering Dept., Kharagpur
Transactions of Canadian Society of Mechanical Engineering
vol. 6 n. 4, 1980-1981 p. 234-239
" Nonlinear Behavior, Under Acoustic Excitation, of a Fuselage Panel with a Central Opening"
The results of an experimental study, depicting the nonlinear behavior of an aluminum alloy panel with a central opening, subjected to combined in-plane static tensile loading and acoustic excitation, are presented. The specimens represented typical aircraft fuselage panels and were tested in an acoustic tunnel to a maximum sound pressure level of 135 dB with in-plane uniaxial and biaxial tensile loading. The nonlinear behavior of the panel has been examined under sinusoidal and broad-band random excitation. It was observed that for a narrow opening, the response behavior was governed by a combination of hardening-softening spring-type nonlinear characteristics near the buckling stress. The response characteristics become completely those of the hardening spring-type for wider openings. The statistical properties of the strain signal for random excitation showed a significantly-skewed probability density curve with high kurtosis values indicating strong nonlinearity near the buckling stress,and for high sound-pressure level.

Der Kiureghian, Armen
University of California, Berkley
ASCE Journal of Structural Division, vol. 106 n. 2
February 1980 p. 411-429
" Reliability Analysis Under Stochastic Loads "
The random nature of loads affecting structures as well as uncertainties associated with their resistances, necessitate a probabalistic approach to the

analysis of structural safety. The second-moment structural reliability approach, which uses means and variances of loads and resistances, is well recognized as a practical method for safety analysis and as a basis for development of rational for design codes. simplicity and the fact that in many structural problems information beyond second moments is not available to justify a more exact approach.

The main objective of this paper is to develop a method for analysis of structural reliability and design under combination of time-varying loads that is consistent with and is a logical extension of the second-moment reliability approach. The load combination procedure is the basis for this development. It is assumed throughout the paper that:

1. The principle of the superposition of load effects holds
2. Loads are independent and stationary stochastic processes,
3. Structural resistances are independent of loads and remain constant in time.

Gaver, D. P.; Jacobs, P. A.

US Navy Postgraduate School, Monterey, CA USA

SIAM Journal of Applied Mathematics vol. 40 n. 3

June 1981 p. 454-466.

" **On Combinations of Random Loads** "

Structures are subject to changing loads from various sources. In many instances, these loads fluctuate in time in an apparently random fashion. Certain loads vary rather slowly (called constantloads); other loads occur more nearly as impulses (shock loads). Suppose that the stress put on the structure by various loads acting simultaneously can be expressed as a linear combination of the load magnitudes. In this paper, certain simple but somewhat realistic probabilistic load models are given and the resulting probabilistic model of the total stress on the structure caused by the loads is considered. The distribution of the first time until the stress on the structure exceeds a given level x, and the distribution of the maximum stress put on the structure during the time interval (0, t) are studied. Asymptotic properties are also given. It is shown that the asymptotic properties of the maximum stress are related to those of the maxima of a sequence of dependent

random variables. Classified extreme value type results are derived under proper normalization.

Ghannoum, Elias
Hydro-Quebec, Que, Canada
IEEE Trans. Power Appar. Syst. vol. PAS-102 n. 9
September 1983 p. 3057-3064
" **Probabilistic Design of Transmission Lines Part I: Probability Calculations and Structure Reliability** "
This is the first in a series of two papers dealing with design criteria for transmission lines based on probabilistic concepts. This part covers calculations of the probability of failure of a line when both load and resistance are random variables for the first time the influence of two important parameters have been studied: the use factor of towers and the effect of a load event that acts simultaneously on N towers.
The results outlined in this paper allow one to calculate equivalent ice or wind loads in a line, that correspond to a target reliability. These results are used in part II to establish design criteria for transmission lines based on probabilistic methods.

Giorsetto, Paul; Utsurogi, Kent F.
Hawaii Electric Co., Honolulu USA
IEEE Transactions on Power Apparatus Systems vol. PAS-102 n. 1
January 1983 p. 134-144
" **Development of a new Procedure for Reliability Modeling of Wind Turbine Generators** "
A method for determining the impact of wind generation on system reliability is developed. This method combines the effects of wind turbine forced outage rates and varying power output due to wind speed variations. Since individual wind turbines on a windfarm all have an output related to wind speed, each turbine's output cannot be assumed to be independent random variables. Because of this situation, special steps must be taken in order to arrive at the cummulative distribution function for the windfarm. This distribution

function using simple convolution and so the windfarm can be easily incorporated into a Loss of Load Expectation computer program. The method can then be used to determine the effective load carrying capability of a windfarm and also to supply better estimates of the benefits of wind generation to the overall system.

Kao, Samuel C.; Shooman, Martin L.
Brookhaven National Laboratory, Upton, NY, USA
Proceedings of the Annual Reliability and Maintainability Symposium 1981, Philadelphia, PA, USA
January 27-29, 1981. Published by IEEE, New York, NY, USA, 1981
Available from IEEE Service Center (Cat n. 81ch1618-8).
Picscataway, NJ, USA p. 28-32
In the design of building structures, mechanical and civil engineers no longer deal with the stochastic nature of the load and material strengths by merely introducing large safety factors. Modern techniques of design utilize sets of load factors to combine simultaneous loads. The load factors are chosen on a probability basis. Thus, the authors are actually designing for the reliability of the struture. The theoretical formulation of problems of this type have been referred to in reliability literature asstress, strengths, and time-problems in the past. Rather than use the term stress, which is a force per unit area, the term load is used in this paper. The term responses describes in general the motion of selected positions of the structure when the excitation(s) is applied.

Pearce, H. T.; Wen, Y. K.
University of Illinois, Department of Civil Engineering, Urbana, Illinois, U.S.A.
Civil Engineering Studies on Structural Response Series:
University of Illinois, Urbana-Champaign Department of Civil Engineering n. 507 June 1983

" **Method for the Combination of Stochastic Time Varying Load Effects** "
The problem of evaluating the probability that a structure becomes unsafe under a combination of loads, over a given time period is addressed. The loads and load effects are modeled as either a pulse (static problem) processes with random occurrence time, intensity and a specified shape or intermittent continuous (dynamic problem) processes which are zero mean Gaussian processes superimposed on a pulse process. The load coincidence method is extended to problems with both nonlinear limit states and dynamic responses, including the case of correlated dynamic responses. The technique of linearization of a nonlinear limit state commonly used in a time-invariant problem is investigated for time-varying combination problems, with emphasis on selecting the linearization point. Results are compared with other methods, namely the method based on upcrossing rate, simpler combination rules such as Square Root of the Sum of Squares and Turkstra's rule. Correlated effects among dynamic loads are examined to see how results differ from correlated static loads and to demonstrate which types of load dependencies are most important, i.e., affect the exceedance probabilities the most.

Pook, L. P.; Smith, R. A.
National Engineering Laboratory, Glasgow, Scotland
Fracture Mechanics: Current Status, Future Prospects, Proceedings of a Conference, Cambridge University, England
March 16, 1979 Published by Pergamon Press (Int. Ser. on the Strength and Fract. of Matter and Structure), Toronto, Ontario and New York, NY, 1979
p. 29-67
" **Theoretical Background to Elastic Fracture Mechanics** "
Over the last decade or so great advances have been made in the engineer's ability to assess quantitatively the fracture and fatigue properties of materials containing cracks. Similitude of small scale laboratory tests and real components have been achieved through the stress intensity factor parameter.
This paper reviews the characterization of crack tip stress fields by the stress intensity factor and the limitations which define the applicability of

linear elastic fracture mechanics (L.E.F.M.). The plane strain fracture toughness, a measure of a material's resistance to catastrophic crack advance, is discussed. The use of the stress intensity factor range to quantify fatigue crack growth is described, together with threshold

Raab, A.
SIKOB, Sweden
Paper Presented at the International Symposium on Wind Energy Systems, 3rd, Lyngby, Copenhagen, Denmark
August 26-29 1980 Published by BHRA Fluid Engineering, Cranfield, Dedford, England 1980 Paper D1 p. 169-182

" **Combined Effects of Deterministic and Random Loads in Wind Turbine Design** "
Loads on wind turbine blades are periodic because of the rotation of the blade. Well defined (deterministic) loads are those due to the mean wind shear, tower shadow (interaction of the tower with the mean wind), gravitation and centrifugal forces, on condition that the mean wind is specified. They cause the major part of fatigue damage. Random forces take rise from turbulence and its interaction with the deterministic loads precipitate fatigue. Thus, a global treatment of all kinds of loads is necessary. Two methods will be considered: numericalsimulation and probabilistic interaction. For simulation, a digital filter technique and a method using triangular decomposition of the correlation matrix are known. Work on the latter is in progress. Principles of the probabilistic methods will be shown.

Rackwitz, Rudiger; Fiessler, Bernd
Institut fur Massivbau, Technical University of Munich,
Munich, West Germany
Computers and Structures, vol. 9 p. 489-494.
" **Structural Reliability Under Combined Random Load Sequences**"
An algorithm for calculation of structural reliability under combined loading is formulated. Loads or any other actions upon structures are modeled as independent random sequences. The relevant limit state criterion is pointwise approximated by a tangent hyperplane. The combination of time-variant actions

then reduces to the calculation of the maximum of a sum of random variable which is facilitated through proper, discrete approximation of extreme value and other non-normal distribution functions by normal distributions. The iteration algorithm searches for an approximation point on the limit state criterion where the probability content of the failure domain limited by the tangent hyperplane reaches its maximum. Any type of continuous limit state criterion and any distribution for a section of a wall without tensile strength loaded by a bending and a normal force.

Veneziano, Daniele
Massachusetts Institute of Technology
The Annals of Probability, vol. 7, n. 1, 62-74.
"**Envelopes of Vector Random Processes and Their Crossing Rates**"
Vector-valued random processes can be "enveloped" by set- valued random processes to which they belong with probability 1 during any finite length of time. When applied to scalar processes, the set-definition of envelope includes and is richer than the familiar point-definitions. Several random set-envelope processesin n-dimensional space are defined and the mean rates at which they "cross" given regions of n-dimensional space are calculated. Comparison is made with the mean crossing rates of associated envelope Gaussian processes.

Woodward, Wayne A.; Parr, William C.; Schucany, William R.;
Lindsey, Hildegard
Journal of the American Statistical Association
September 1984 vol. 79, n. 387, p. 590-598.
" **A Comparison of Miminum Distance and Maximum Likelihood Estimation of a Mixed Proportion** "
The estimation of mixing proportions in the mixture model is discussed, with emphasis on the mixture of two normal components with all five parameters unknown. Simulations are presented that compare minimum distance (MD) and maximum likelihood (ML) estimation of the parameters of this mixture-of-normals model. Some practical issues of implementation of these results are also discussed. Asymptotic variances and relative efficiences are obtained for further comparison of the MD and ML estimators.

Classification II

Anon
Univ. Hamburg, Ger.
Ocean Eng. vol. 7 n. 5
1980 88 p.
" Ship Structure Loads and Stresses "
This paper deals with methods of determining loads on ships and their application in dimensioning ship structure. Main topics are: description of measurements on board ships, comparison of measured and computed transfer functions, hydrodynamic and statistical investigations concerning wave loads, still-water load statistics, combination of loads and optimization of structural safety.

Aoki, S.; Sakata, M
Tokyo Inst. of Technol. Jpn.
Int. J. Fract. vol. 16 n. 5
Oct. 1980 p. 459-469
" Statistical Approach to Delayed Failure of Brittle Materials"
Delayed failure tests or static fatigue tests were performed on soda-lime glass in water environment. Testing consisted of four-point bend and three-point bend with constant load. The time-to-failure and fraction location of specimens were measured. The theory of stochastic process is combined with the extreme value distribution in stress and the time predict the time-to-failure of specimens as well as the location of fracture. It is shown that the theoretical prediction is in good agreement with the experimental data.

Bodo, Byron; Unny, T. E.
Univ. of Waterloo, Dep. of Civil Engineering, Waterloo, Ont., Can.
J. Environ Eng. vol. 109 n. 4
August 1983 p. 812-829
" Sampling Strategies for Mass-Discharge Estimation "
Methodology derived from sampling theory is presented for theestimation of in-stream contaminant mass-discharge or load. The historical record is

stratified into relatively homogeneous units in order to approach normality in the subpopulations thereby reducing the inaccuracies introduced by the highly skewed populations. Within strata a ratio estimator is employed to estimate the load and variance of the forms of inaccuracy. Estimates for individual strata are combined to produce pooled estimates for the desired period of interest. With a prior data base, sampling theory is employed to devise sampling strategies designed to produce load estimates of a specified target precision in future studies. Case studies demonstrate the significance of flow events as the primary transport mechanism for suspended sediment and the need to sample such events intensively in order to achieve reliable load estimates.

Brekalov, V. G.; Vafin, R. K.; Ivanov, V. A.
Izv Vyssh Uchebn Zaved Mashinostr n. 6
1982 p. 61-63
" Teoreticheskoe Issledovanie Zagruski Gvigatelya Gusenichnykh Mashin. [Theoretical Investigation of Tracked Vehicle Engine Loading]"
A theoretical sollution is proposed to the problem of engine loading of a tracked vehicle. It is based on a probabilistic evaluation of combinations of external factors affecting the vehicle motion.

Casciati, F.; Faravelli, L.
Univ. of Pavia, Italy
Eng. Struct. vol. 2 n. 2
Apr. 1980 p. 113-122
" Calibration of the Load Enhancement Factors "
This paper presents a calibration procedure capable of deriving load enhancement factors from fully probabilistic calculations, to apply to the design of a wide range of types of structure. For this purpose the selection of a target relability level and the load combination treatment are discussed first. Thenthe policy for estimating the load partial safety factors is illustrated. Under suitable assumptions, required to perform numerical computations, the calibration problem is formulated as a linear programming problem. Finally the numerical values of the enhancement factors are

determined with reference to the more meaningful combinations of structural self weight. Imposed dead load, wind action and snow load.

Cornell, C. Allin
MIT, Cambridge, Mass, USA
Eng. for Prot. from Nat. Disasters, Proc. of the Int. Conf., Bangkok, Thailand, Jan 7-9, 1980, Publ. by John Wiley & Sons, Ltd. Chichester, Engl. and New York, NY, 1980 p. 809-818
" Stochastic Modeling of Natural Hazards "
Experience modeling a broad variety of hazards to structures leads to some general observations about stochastic modeling. In particular starting from the needs (in this case structural safety analysis) may reduce the general scope of the hazard model to simply an extreme-value model. Event- based hazards models appear to be the most effective in providing observational data is always scarce. Load combination needs demand additional information from the natural hazard model, but that information can be very limited in practical applications.

Galambos, Theodore V.; Ellingwood, Bruce; MacGregor, James C.; Cornell, C. Allin
University of Minnisota, Minneapolis, USA
ASCE J. Struct. Div. vol. 108 n. ST5, May 1982 p. 959-977
" Probability Based Load Criteria: Assessment of Current Design Practice "
The paper describes a study conducted to develop probability-based load factors and load combinations suitable for use with the loads specified in American National Standard A58 on design loads with all common construction materials and technologies. The study involved the selection of a probabilistic methodology for performing the necessary reliability analyses and the collectionand examination of statistical data on structural resistance and loads.

Gaylord, Edwin H. (Ed.); Mainstrone, Rowland J. (Ed.)
Univ. of Ill. Urbana
Tall Build Criteria and Loading Publ. by ASCE (Monogr. on Plann. and Des. of Tall Build. v. CL), New York, NY
1980 888 p.
" Tall Building Criteria and Loading "
This is one volume of a five-volume Monograph entitled Planning and Design of Tall Buildings, which brings together current knowledge about tall buildings themselves and about their interactions with the urban environment. This volume deals with the loads to which tall buildings are subjected, and with the precise definition of the related structural requirements that are necessary before a client's basic needs can be translated into a safe design. It contains seven chapters, all of which are indexed separately. The first five chapters deal with different classes of load $EM DASH$ gravity loads and temperature effects, earthquake loads, wind, fire, and accidental loads. The two concluding chapters discuss quality control $EM DASH$ control of the variations of material strenghts and workmanship $EM DASH$ and overall safety considerations. Also included are a discussion of current questions, problems and research needs, a glossary, a general reference/bibliography for the entire volume, and a list of contributors. The previously published volumes (SB and CB) were indexed in the March 1980 Engineering Index Monthly.

Krogh, B.; de Llinas, E. S.; Lesser, D.
Westinghouse Electric Corp., Pittsburgh, PA, USA
IEEE Trans. Power Appar. Syst. vol. PAS-101 n. 9
Sept. 1982 p. 3284-3289
" Design and Implementation of an On-Line Load Forecasting Algorithm "
This paper presents a short-term load forecasting algorithm for Energy Control Center applications. Regression techniquesare combined with Auto Regresive Integrated Moving Average (ARIMA) models to produce hourly MW load values for the upcoming seven days. Results of several studies are discussed along with a description of the on-line implementation. The assumption in all the approaches considered for forecasting the peak load values is that the weather is the primary factor causing the day-to-day variations in the peak load.

Leipholz, Horst H. E.; Piche, Robert
Univ. of Waterloo, Dep. of Civid Engineering, Waterloo, Ont., Can.
J. Eng. Mech. vol. 110 n. 3
March 1984 p. 367-379
" Stability of Follower-Force Rods with Weight "
The effect of follower forces and weight on the stability of elastic rods is studied, using the 2-mode Galerkin method. Stability boundaries are presented to show how various combinations of the loads lead to divergence or flutter instability. Results are presented for pinned-pinned rods, clamped-free rods and free-free rods. The free-free rod corresponds to a flexible missil with distributed follower forces due to drag, and weight-like forces due to thrust. It is shown that a good choice of mass distribution can eliminate flutter instability for all practical loading situations.

Lubinski, Mieczyslaw; Gizejowski, Marian
Tech. Univ. Warsaw, Pol.
Arch. Inz. Ladowej vol. 26 n. 1
1980 p. 41-62
" Lateral Buckling Analysis of Continuous Beams Subjected to the Combined Loading "
The problem of buckling in establishing designs for continuous beams by the limit state method is considered. Allowance is made for the random nature of the main factors affecting the safety of the structure in conformity with a semiprobabilistic solution of the limit state method. To determine the bucklingcoefficient, a formula resulting from the probabilistic solution is applied. The buckling parameters are determined with allowance for the interaction between the dead and live loads acting on the spasms of a continuous beam. The theoretical considerations are illustrated by the results of calculations for continuous beam with dead and live loads uniformly distributed over the spans.

Manusov, V. Z.; Kucherov, Yu. N.
Power Eng. (New York) vol. 18 n. 2
1980 p. 18-26
" Analysis of Steady State of Electric Power Network with Random Network Parameters "
A numerical method is proposed for calculating probabilistic characteristics of service parameters of an electric network. The combined effect of the randomness of the parameters of the equivalent circuit and of node loads on the probabilistic characteristic of node voltages is investigated.

Nottingham, Dennis; Drage, Brent T.; Christopherson, Alan B.
Peratrovich & Nottingham, Inc., Alaska, USA
North Eng. vol. 14 n. 1
Spring, 1982 p. 11-18
" Ice-Resistant Structure Design: State of the Art in Alaska"
In Alaska, ice loads are usually so large that one loading combination will dominate, that being dead load plus ice load. It is important to assess ice and dead loads accurately with the understanding that they are real and not probabilistic. After establishing a realistic design condition, conventional design allowable stresses are applied, which contain safety factors, as found in most codes without increases. The extreme event should also be assessed, and the structure reanalyzed to assure that collapse cannot occur; for example for steel this usually means keeping below yield stress levels.

Rojiani, Kamal B.; Woeste, Frank E.
Va. Polytech Inst. & State Univ. Blacksburg, USA
Eng. Struct vol. 4 n. 4
Oct. 1982 p. 233-241
" Probabilistic Analysis of Steel Beam-Columns "
A probabilistic analysis of steel beam-columns in a typical medium rise office building designed in accordance with current AISC specifications was conducted. Risks were evaluated in terms of failure of probability for several failure modes and for various combinations of dead, live and wind loads. Effects of uncertainties in the resistance and the loads as well as

modeling and prediction errors were included in the reliability analysis which is based on a first order second moment approach. Upper and lower bounds on the probability of failure of beam-columns were evaluated. Results obtained indicate the risk levels for the building considered.

Suvilova, A. V.
Hydrotech Constr. vol. 16 n. 6
June 1982 p. 302-308
" Methods of Modeling Design Seismic Loads for Large Power Installations "
The paper examines the main questions of the practical solution of the problem of providing seismic stability of large power installation. Optimization of the solution of the problem is achieved by optimizing the method of determining the initial data and modeling itself. The important aspects of the optimal (at the given stage) approach to modeling of seismic loads for the needs of hydrotechnical and power construction and to determining the design parameters based on a combination of genetic and probabilistic approaches are given.

Zavalich, I. G.; Shefer, L. A.
Chelyabinsk Polytech Inst., USSR
Probl. Prochn. n. 10 (160)
Oct. 1982 p. 25-30
" Prognozirovanie Ustalostnoi Dolgovechnosti Na Osnove Kharakteristicheskikh Parametrov Protsessov Nagruzheniya. Predictionof Fatigue Life from Characteristic Parameters of Loading Processes "

The relationship between characteristics of fatigue life under harmonic and random processes of loading has been considered for light-weight MA15, AMg-6, IMV2, 01420, AMg-61, 2024T3 alloys, heat-resistant EI678 steel and organic plastic. Identification of the damaging part of the process and its statistical description permitted fatigue life characteristics to be calculated from one loading to another without making process flow charts and hypothesis of fatigue damage accumulation. Serviceability of the suggested procedure is

also confirmed by results of tests under two-frequency loading and under a combined effect of harmonic and random processes.

APPENDIX B - SSME TURBINE BLADE LOADS

B.1 INTRODUCTION

This appendix furnishes an assessment of the individual loads on the SSME turbine blades and where potential information can be found for the validation of the probabilistic load models. The information in this appendix is summarized in sections 8.3 and 8.4.

B.2 Centrifugal Loads

Centrifugal effects are a primary consideration in sizing both turbine blades and disks. The turbine speed which determines centrifugal loading essentially mirrors the thrust profile of the engine in shape with minimal oscillations over a nominal value. A typical generic profile test is shown in Figure B.1 for the HPFP speed from two tests. On the SSME, three of the four pump speeds are measured quantities and the fourth, the HPOTP, is obtained from accelerometer responses of synchronous speed frequency or one of its higher harmonics. Figure B.1(a) shows a typical speed trace for a typical thrust profile. Figure B.1(b) is an expanded plot of the 32000 to 36000 pump speed range on a pump signature test where the thrust is gradually reduced at 1% power level per three seconds of test. The expanded trace shows minor random appearing oscillations on the speed that are interpreted as real data. Figure B.1(c) is a high frequency response AMS trace of the HPFP speed from the same signature test. Both low frequency digital and high frequency analog measurements are taken for this parameter. The shape of the start transient speed profile is shown in Figure B.2. Detail study of test to test variations will furnish a good statistical database for this load.

B.3 Pressure Loads

The pressure loads on a turbine blade are a function of the flow conditions at the inlet and outlet of the turbine and result in a torque to drive the pump.

(a)

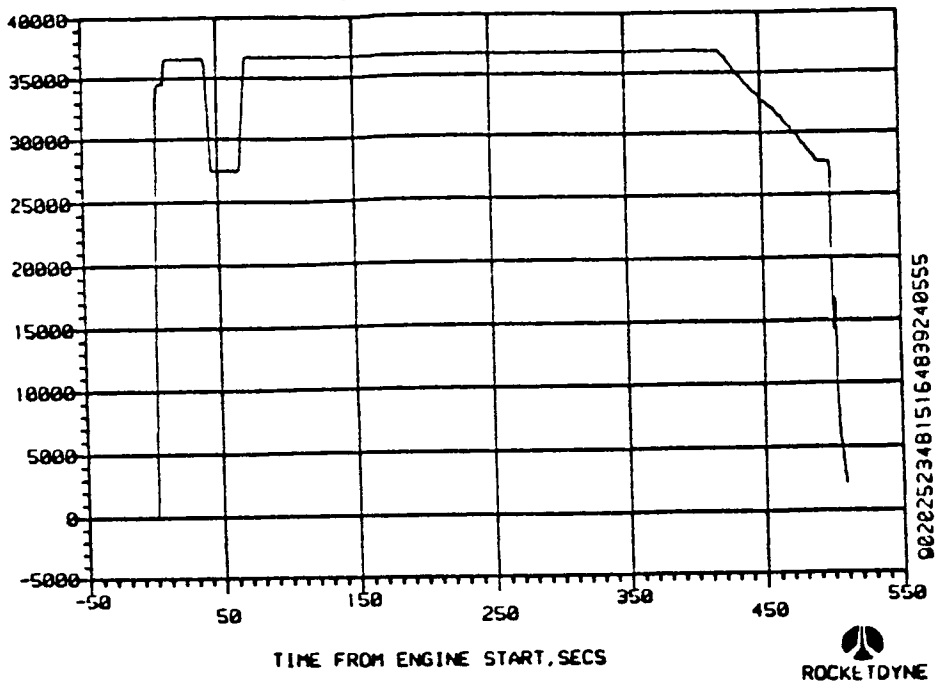

(b)

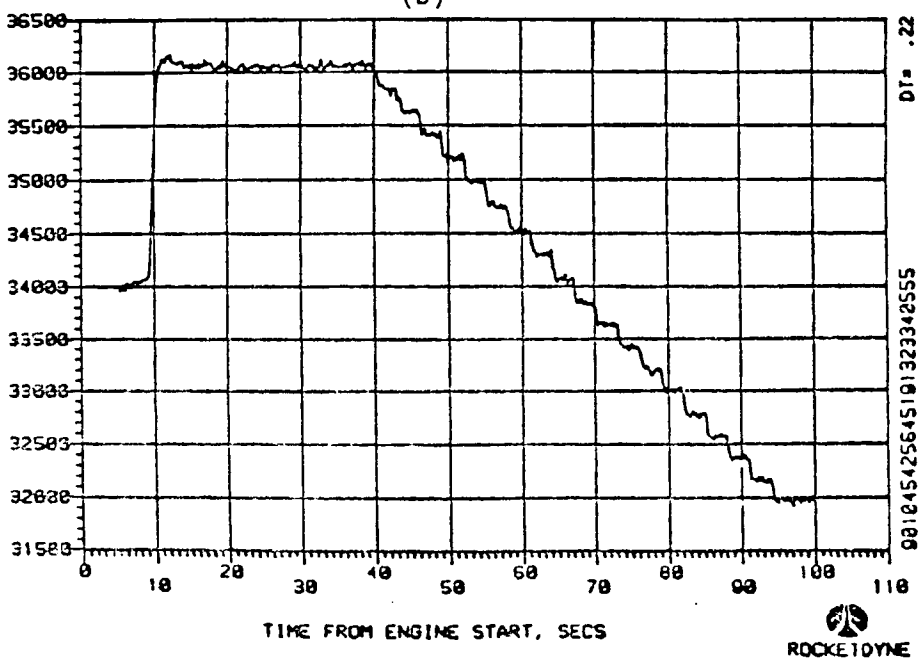

PUMP SPEED (RPM VS. TIME)

(c)

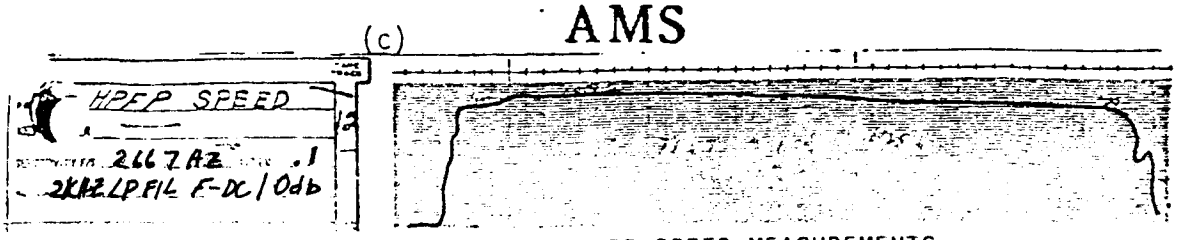

FIGURE B.1 TYPICAL HPFTP SPEED MEASUREMENTS

Pressure loads at Rocketdyne are calculated based on a steady state design point condition using a turbine design gas path calculation code. The gas path model includes representative blade row loss correlations as well as tip clearance and configuration losses, leakage losses, and other parasitic losses. The model determines the turbine performance and geometry for the

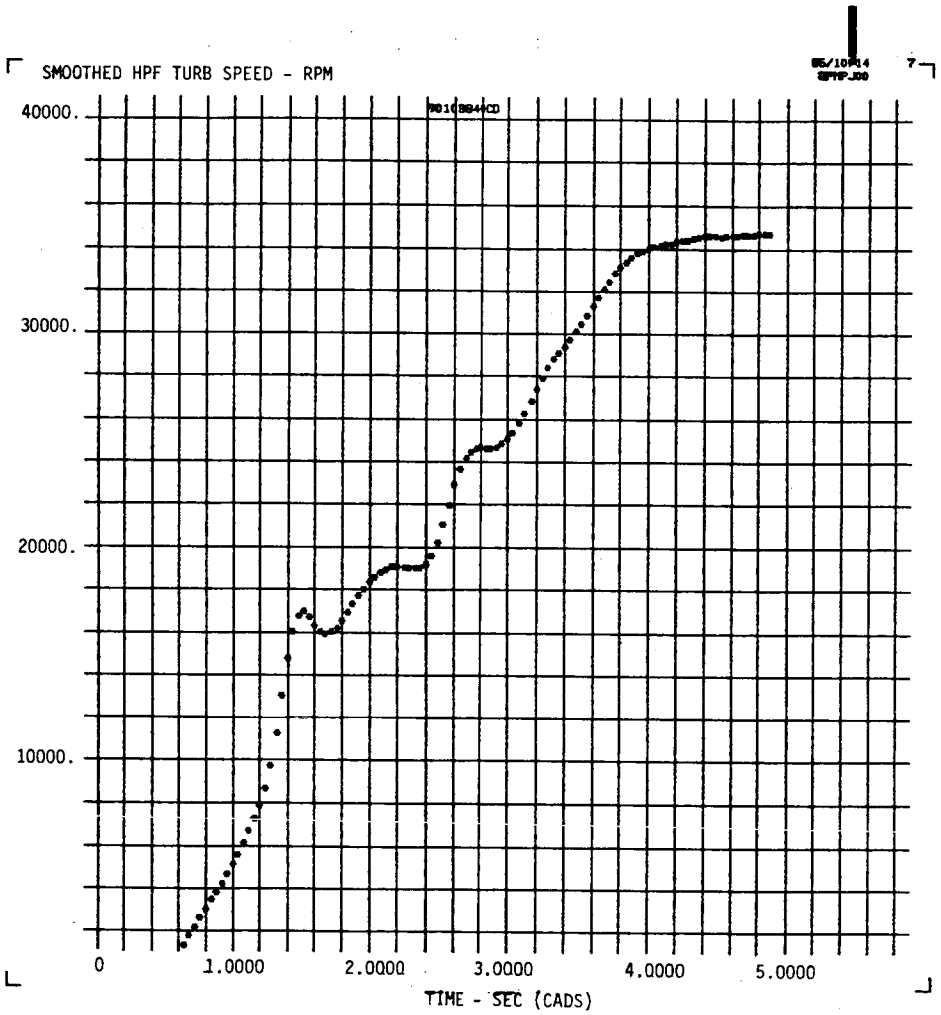

FIGURE B.2 HPFTP TURBINE SPEED

overall and interstage design conditions to produce the highest efficiency within the structural and envelope limits. The design energy distribution between stages and blade rows and radially from hub to tip sets the overall blade row loads. These loads are distributed on the turbine blade as the pressures, temperatures, and torques on the upstream and downstream surfaces of the blade. The velocity vector diagrams indicate the resultant inlet and outlet velocities and flow angles from which the overall loading at a specific radius is calculated. Each profile section is meant to satisfy the gas path performance. The profile suction and pressure surface distributions of velocity, pressure and temperature are determined using an exact, incompressible blade to blade computer calculation. Figure B.3 shows a blade model indicating the blade streamline locations, one example of which is illustrated in Figure B.4. Figures B.5 and B.6 show an example of the corresponding surface velocity and static pressure distributions. The detailed loading of the design profile at the streamtube radius is shown by the surface distribution curves.

As previously stated, these calculation methods are for steady state design point operation and are available for several operating conditions. The engine turbine torque is the sum effect of all the blades on the wheel(s) in the turbine, so torque is proportional to blade pressure. The mission-history-profile is similar in shape to that of the speed and power level shapes (see Figure B.7).

The engine test measured plus calculated quantities of turbine torque and inlet and outlet flow conditions will be used to calculate and scale steady state turbine blade pressure distributions. The transient pressure loads will be based on the flows and torques from the engine dynamic model.

The typical torque (pressure) load will have test to test variation during transient and steady state operation about a nominal shape that essentially mirrors the power level mission duty cycle.

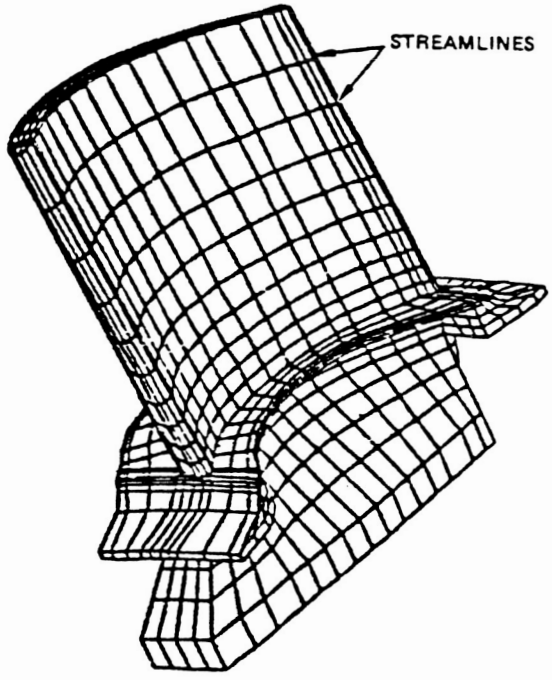

FIGURE B.3 TURBINE BLADE FINITE-ELEMENT MODEL SHOWING BLADE STREAMLINES

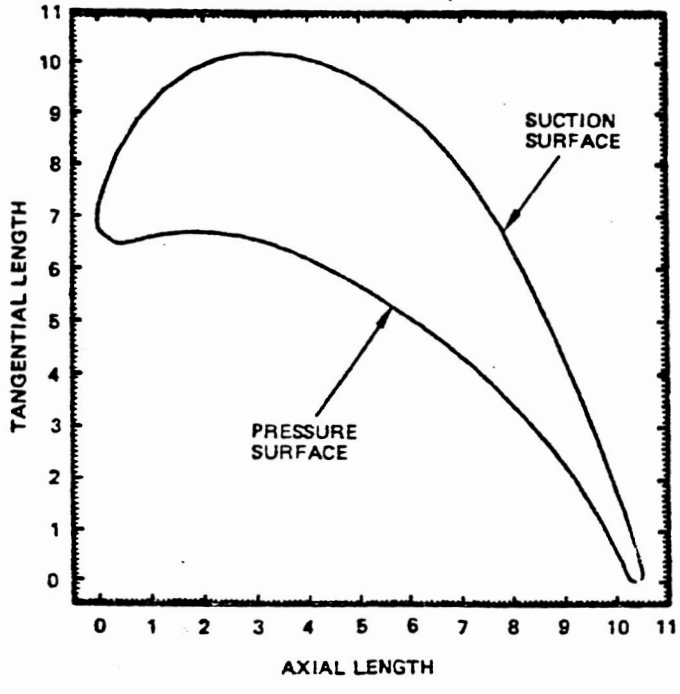

FIGURE B.4 TYPICAL TURBINE BLADE STREAMLINE PROFILE

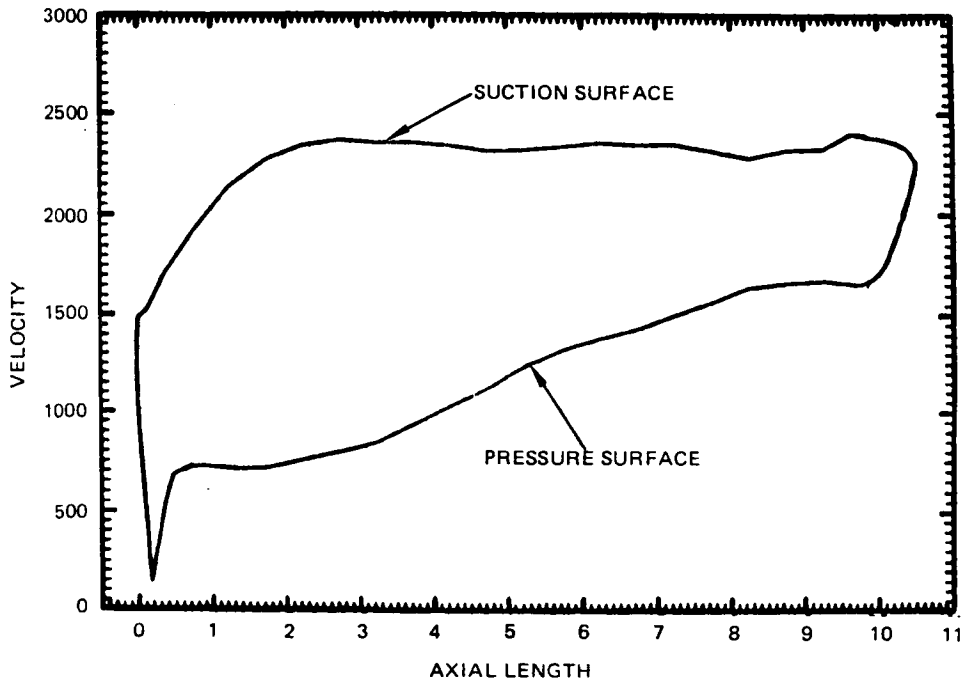

FIGURE B.5 TYPICAL TURBINE BLADE STREAMLINE VELOCITY PROFILE

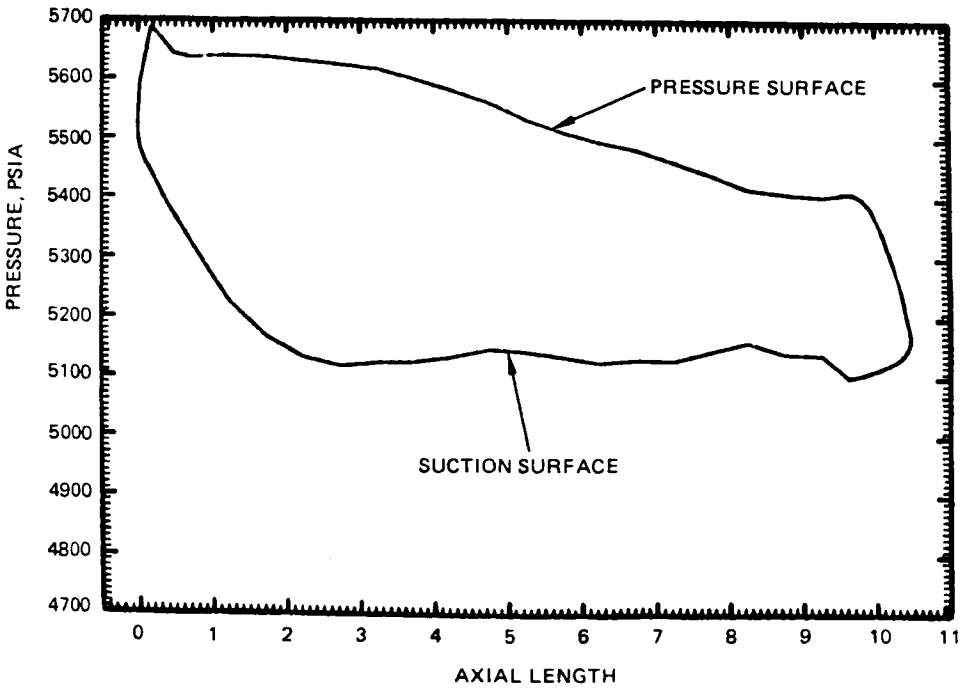

FIGURE B.6 TYPICAL TURBINE BLADE STREAMLINE PRESSURE PROFILE

B.4 Dynamic Pressure Loads

The static pressure loads assume that the turbine blade gas path calculations have no obstructions in the flow, which is not the physical condition when upstream nozzles are closely spaced to the rotor.

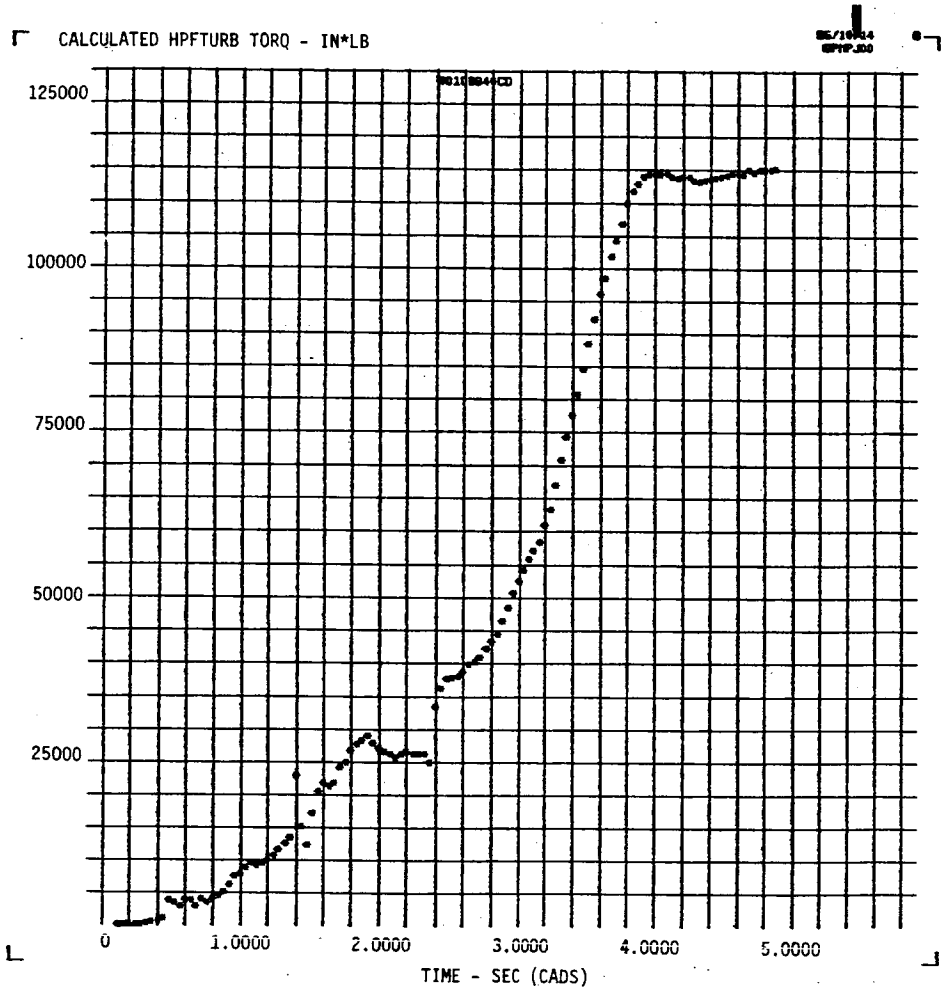

FIGURE B.7 HIGH PRESSURE FUEL TURBINE TORQUE

In general, a turbine blade will be excited by passing through disturbances caused by both upstream and downstream obstructions in the flow. The wakes from these upstream obstructions will propagate downstream, with diminishing amplitude. Similarly, wakes from downstream obstructions will propagate upstream. It is generally thought that the wake propagating upstream decays more rapidly.

Figure B.8 shows a schematic presentation of the wake development downstream of a nozzle.

This velocity description has been measured for the SSME high pressure fuel turbine first-stage nozzle and upstream strut combination. The relationship of the nozzle and strut to the rest of the turbine is shown in Figure B.9.

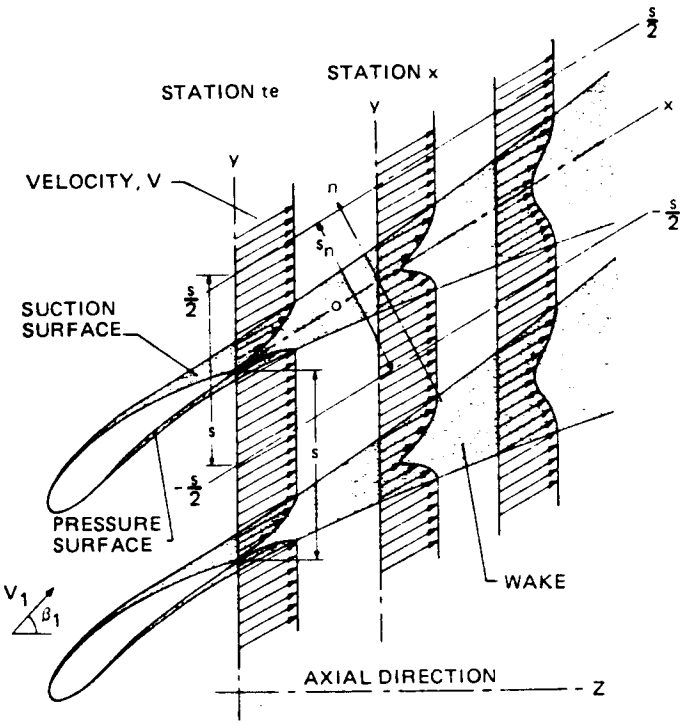

FIGURE B.8 SCHEMATIC REPRESENTATION OF WAKE DEVELOPMENT IN FLOW ABOUT CASCADE BLADE SECTIONS

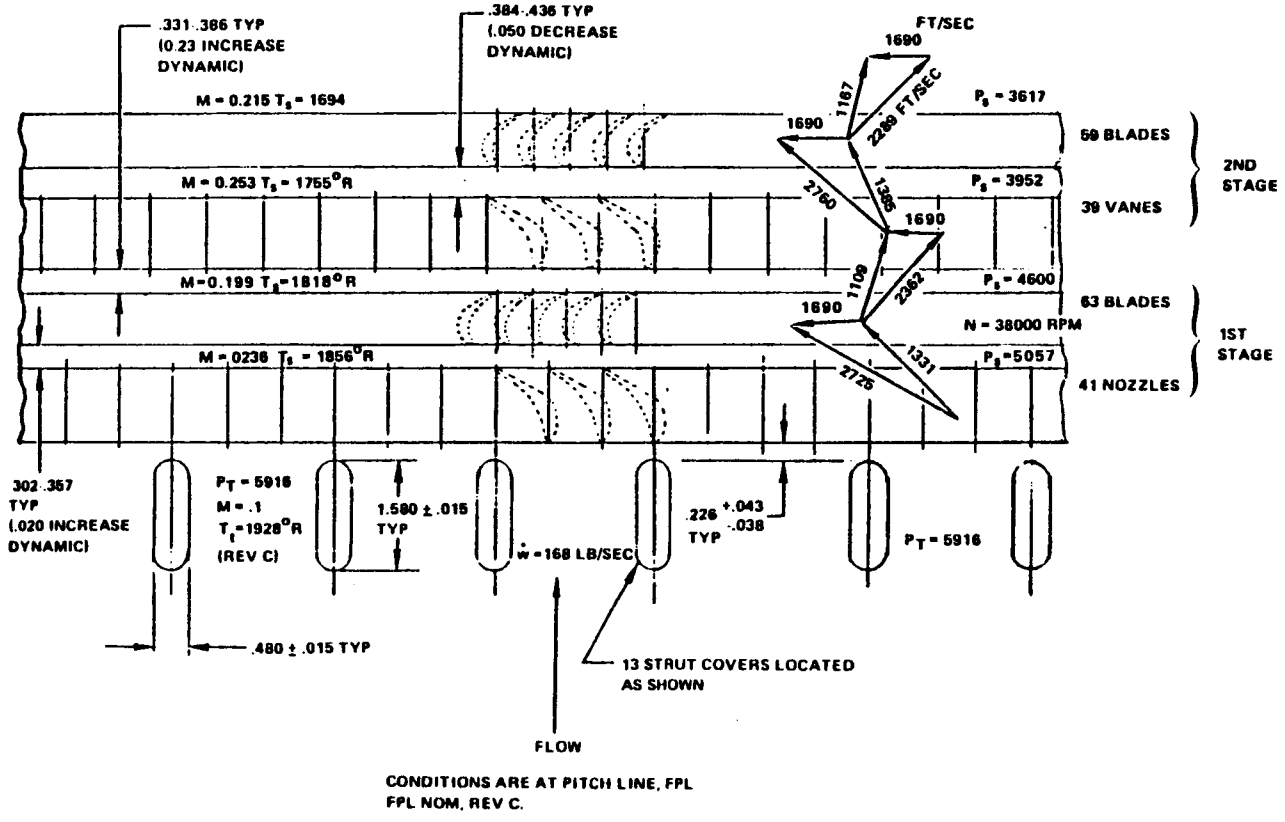

FIGURE B.9 FLOW ELEMENTS FOR SSME HPFTP TURBINE

The test was conducted by flowing air through a nozzle and measuring the circumferential variation of velocity at a station .3 inches downstream of the nozzle. Figure B.10 is a plot of this velocity variation over a portion of the circumference.

An empirical approach to assessing the wake velocity is to simulate the blade nozzle geometry on a rotating water table. Here the flow field is simulated and the integrated blade forces are measured. Therefore, the critical assumption of wake size can be avoided. This type of test has been conducted for the SSME high pressure fuel turbine first-stage nozzle with limited success.

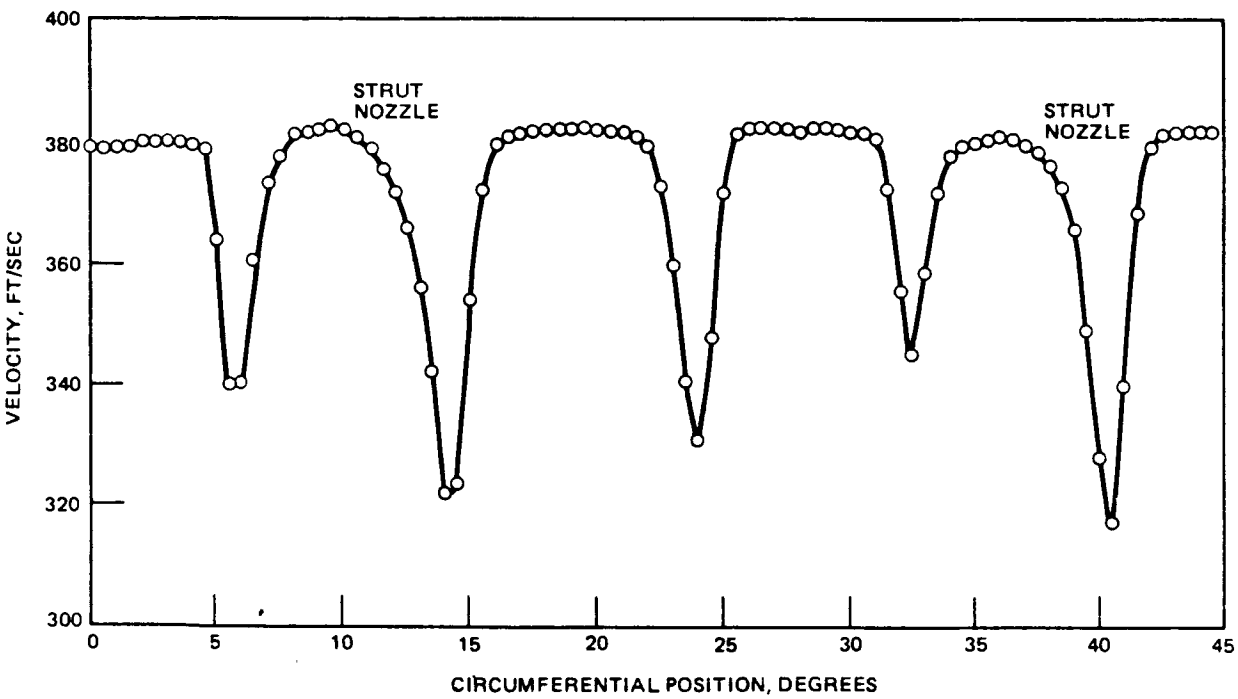

FIGURE B.10 SSME VELOCITY PROFILE BEHIND INLET NOZZLES

An analytical approach to quantifying the forcing function amplitude is to utilize the wake velocity description from Figure B.10. This consists of calculating blade loading for the minimum velocity in the wake and for the free stream velocity. The velocity description across the wake can be used to describe the forcing function shape while the peak-to-peak amplitude is the

blade loading for the two velocities. This approach is conservative in that the width of the wake is presumed to be at least as wide as the blade to blade flow path. An example of the blade loading variation for the SSME high pressure fuel pump turbine first-stage blade is shown in Figure B.11. When no more accurate method is available, the analytical approach is utilized and sealed by expert opinion. The magnitude of the forcing function and spacing of impulses vary with power level and have determinate test-to-test variations similar to power level.

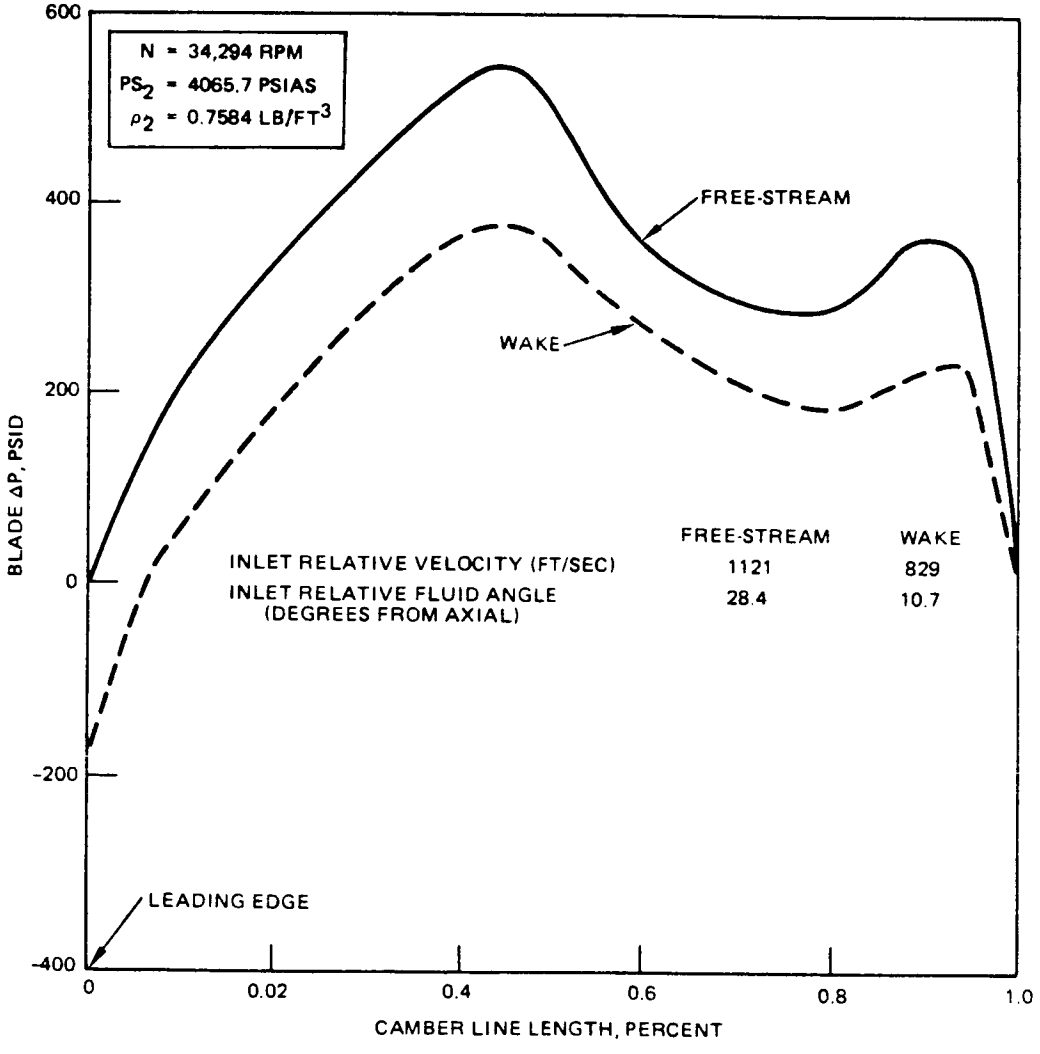

FIGURE B.11 SSME HPFTP TURBINE FIRST STAGE BLADE LOADING VARIATION

B.5 Temperature Loads

Turbine blade temperatures depend on the hot gas flow characteristics of the turbine, coolant flow and geometry. The start and cutoff characteristics of the engine cause transient thermals that results in significant thermal stresses. At steady state operation, the air foil portion of the blade is operating at gas temperatures. The J-2, RL10 and RS44 did not operate at temperatures such that turbine disk or blade coolant flow was required. For the XRL129, an SSME active coolant flow was used to cool the turbine disks. For the SSME HPFTP, see Figure B.12, coolant flow is also used to cool the shanks and fir tree area of the blade. In the XLR129, the blade is not cooled, the coolant flow is dumped between the blade and stator and mixes with the hot gases. Figure B.26 shows a typical SSME turbine inlet temperature transient duty cycle. These hot gas temperatures and the high

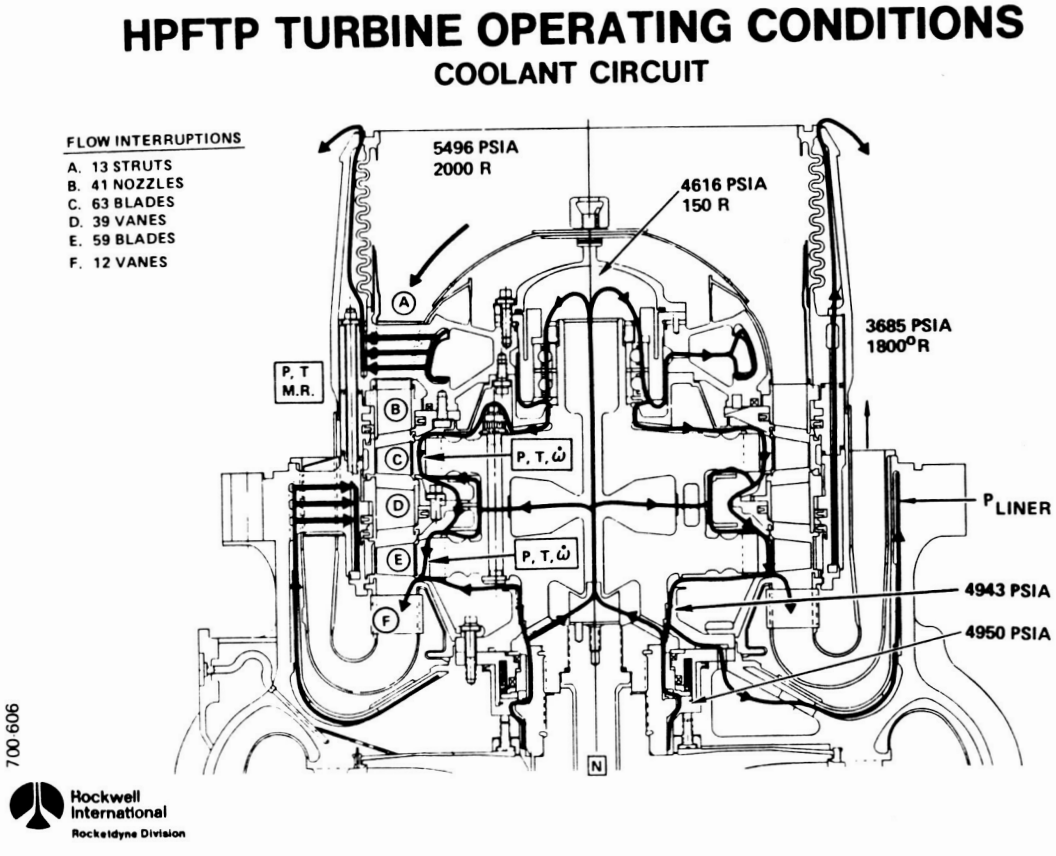

FIGURE B.12

convective heat transfer coefficients resulting from the high velocity flows, produce very high heat fluxes during transient conditions. This duty cycle has two temperature spikes in the start. The first spike is related to ASI ignition and the second one to a fuel side oscillation. The rapid transient gas temperatures and spikes from specific start or cutoff events are typical of rocket engines. The magnitudes of the spikes and events causing these may change from engine to engine. Figure B.13, is a SSME oxidizer turbine discharge temperature trace. This is a low frequency digital measurement that does not accurately pick up the start and cutoff spikes. This trace does show the turbine temperature mirrors the power level profile and has small random oscillations in steady state operation. One approach to obtaining inlet temperature data is to scale the discharge temperatures based on relationships obtained during the instrumented turbine testing.

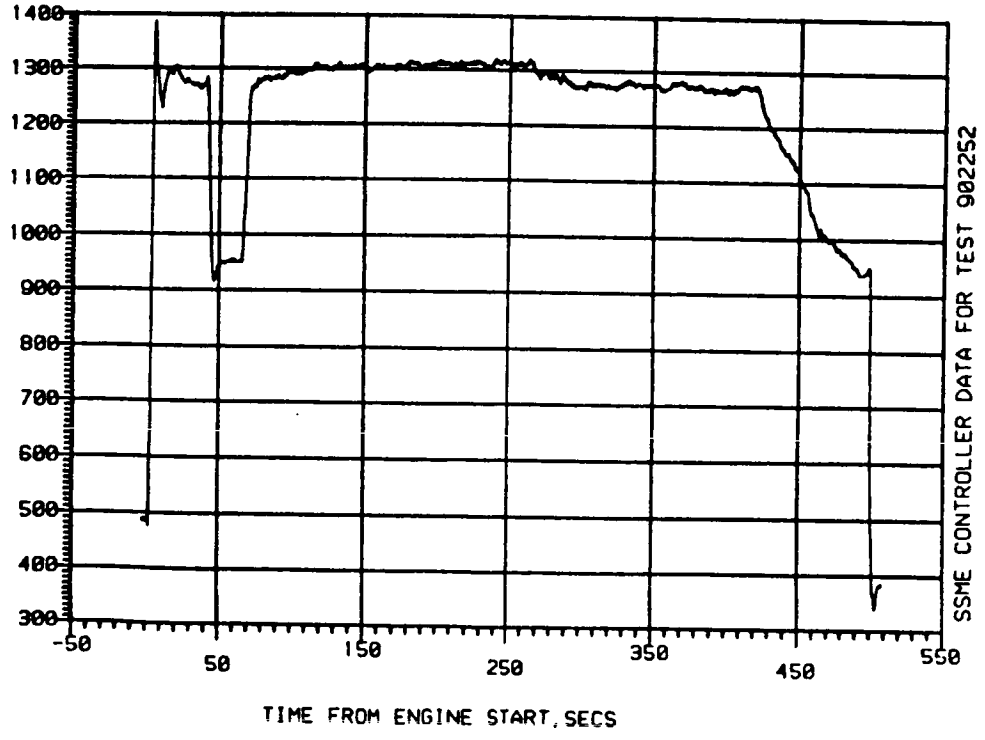

FIGURE B.13 HPOT TURBINE DISCHARGE TEMPERATURE

The transient temperatures of the airfoils are affected by the blade geometry. Hollow blades are sometimes used to reduce wall thicknesses and reduce transient thermal strains. Therefore, this aspect of geometric configuration is also important in airfoil temperatures.

For this project, the blade metal temperatures are required as the loads. These mission history profiles will be based on SSME turbine flow conditions, and calculated blade temperatures.

As previously discussed, a small amount of engine test data exists, and this has been used to correlate the analytical results. (See the Mission-History-Profiles validation/verification section for more details). Although it is virtually impossible to measure the actual blade temperature in an operating engine, stators or nozzles have been instrumented on a very small number of turbopumps. These nozzle temperature measurements have given added insight to the boundary conditions used in the blade thermal analyses. Since a fairly large number of SSME engines have been tested, many turbine blades have been available for post-test inspection. Examination of the color variations of a blade give an indication of the temperature gradients the blade has seen in operation. This information has been used to refine and verify model boundary conditions.

Another factor which must be considered is the effect of coolant. In the SSME high pressure fuel turbine, for example, coolant and hot gas are mixed between the first and second stage blades, and this mixed gas impinges on the blades in the shank and fir tree regions. The actual flowrate and temperature of the gas is affected by changes in the integrity of the various seals that control leakage flows throughout the turbine. Examination of a large number of turbopumps that have been tested revealed that there were a range of coolant conditions on different turbopumps. Expert opinion was used to bracket such hardware effects so that reasonable gas temperatures and flowrates could be included in the blade analyses.

The start transient flow conditions for the hot gases and coolant flows around the blade shank are significantly affected by the temperature spikes flows.

Back flows of hot gases past the blade platform and into the shank zone during the start transient can cause local combustion and high temperatures. During steady state this zone has coolant flow.

Cyclic temperature loads occur on the blade surfaces as a result of the blade rotating at high speed through variable temperature gas media. The gas temperature oscillates sinusoidally between the extreme temperatures and transfers heat to and from the blade by convection.

Surface coatings on the blade provide protection against severe gas convective environments, such as oscillating gas temperature mentioned above, engine start or cutoff gas temperature spikes, and other steady-state temperature variations. Surface coatings can either be a layer of ceramic (e.g., ZrO_2) or a layer of metallic (e.g., nicrally), or both where the metallic coating is the sublayer. Ceramic coatings are more effective in reducing steady-state temperature gradients within the blade. Both metallic and ceramic coatings can be effective in reducing or eliminating transient blade surface temperature gradients. One and two-dimensional finite-difference thermal models are used in evaluating the effectiveness of coatings.

The approach to obtaining blade temperatures for use in the mission-duty cycle definition is summarized below.

Flow analyses of the SSME turbine blades are performed by the Hydrodynamics unit. The results of their analyses are plots of free stream Mach number versus chord length for both the suction and pressure sides of the airfoil at mid-span. This information is used as input for a boundary layer analysis that calculates the convection heat transfer coefficients on the blade. Since both the flow and boundary layer analyses are steady state, the resulting convection coefficients are scaled according to flowrate to obtain startup and cutoff values.

The temperature of the hot gas must also be determined in order to obtain blade temperature profiles. Gas temperature is measured in the SSME just downstream of the turbine, but the transducer time response is too slow to

accurately record the startup transient temperatures. This measured engine data, however, can be combined with transient simulation analysis results to project the actual gas temperature as a function of time.

Once the hot gas convection coefficient and temperature time histories have been determined, they can be used as inputs to various thermal models. A number of different models has been constructed to analyze various parts of the SSME turbine blades. The models generally represent some relatively small but critical part of a blade. A few models have been made of an entire blade, but the detail required to obtain satisfactory results has made this type of model unsatisfactory for most general purpose analysis. Constructing profiles of the blade temperature distribution is often best accomplished by combining results of a number of these different models. These profiles will be scaled to engine test measurements to develop a test by test variation in mission-duty-cycle loading.

The results shown in Figures B.14 and B.15 reflect the start and cutoff transients of the first stage high pressure fuel turbine nozzle and airfoil. These time histories are what would be expected for the same locations on the fuel turbine blades (nose and trailing edge). The hot gas temperature is also shown in these figures. These gradients show the effects of the start and cutoff transients and spikes shown in the turbine inlet temperature. Figures B.17 through B.19 show typical contour plots of the airfoil cross-section during start and cut-off. The small steady-state perturbations of inlet or discharge temperature are not significant to airfoil or blade temperatures.

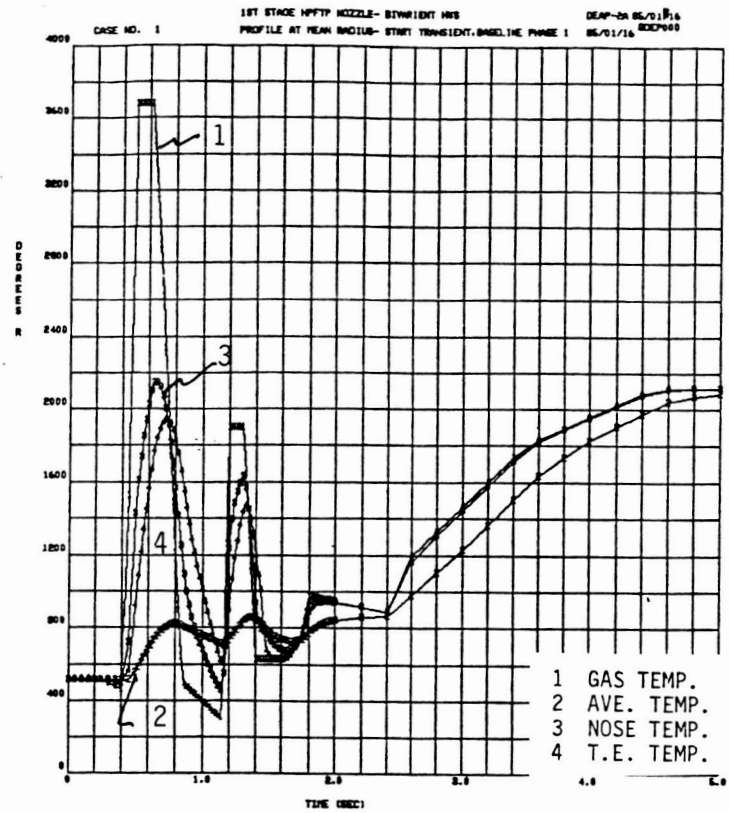

FIGURE B.14 START TRANSIENT HPFTP NOZZLE TEMPERATURE

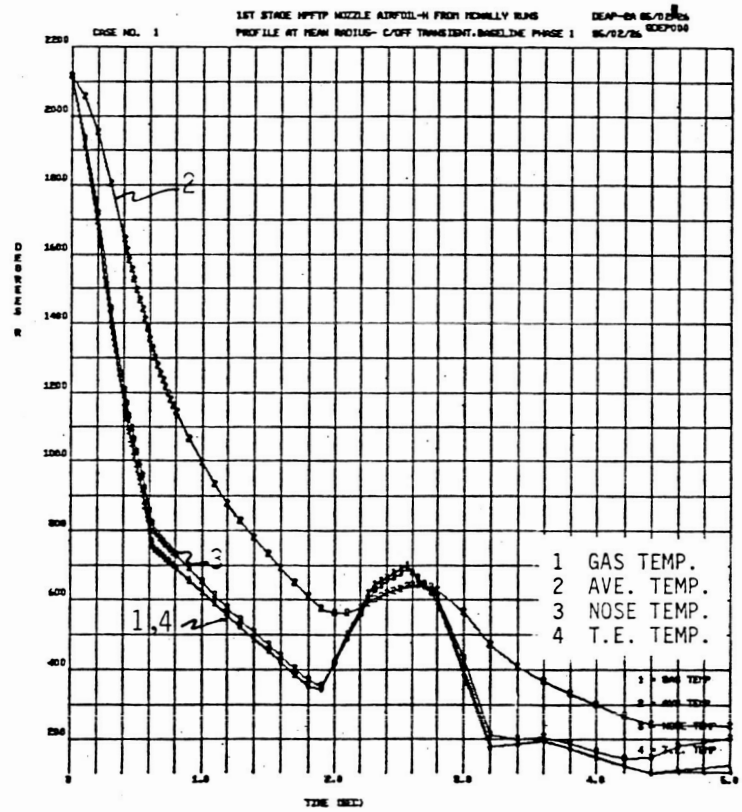

FIGURE B.15 CUTOFF TRANSIENT HPFTP NOZZLE TEMPERATURES

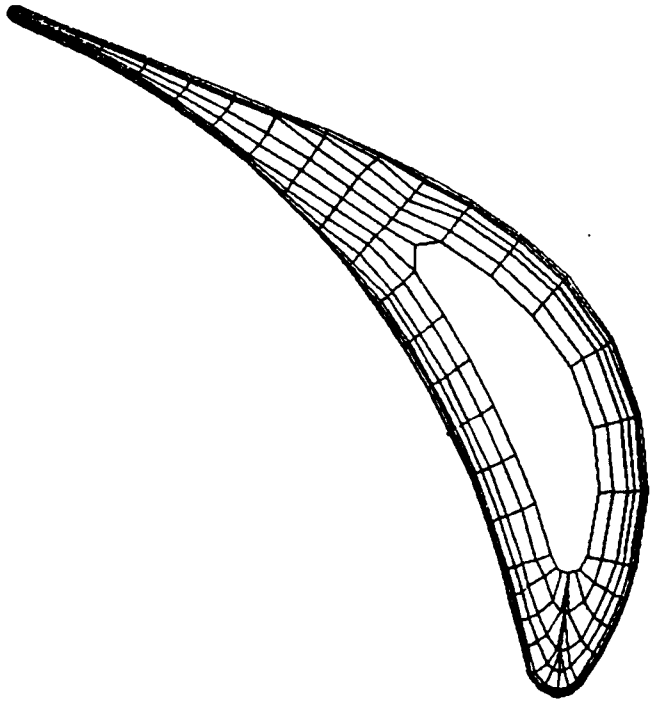

FIGURE B.16 TWO-DIMENSIONAL GRID DEVELOPED FOR LIFE EXTENSION STUDY OF HIGH PRESSURE FUEL TURBINE FIRST STAGE NOZZLE BLADE

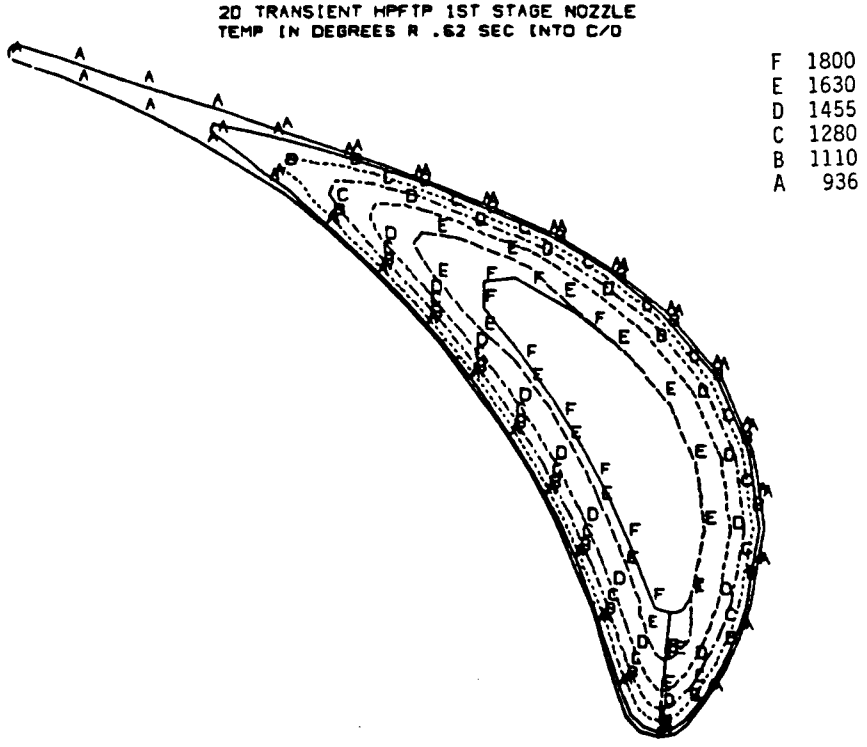

FIGURE B.17 HPFTP FIRST STAGE NOZZLE TEMPERATURE CONTOUR AT 0.62 SEC TEMPERATURE SPIKE

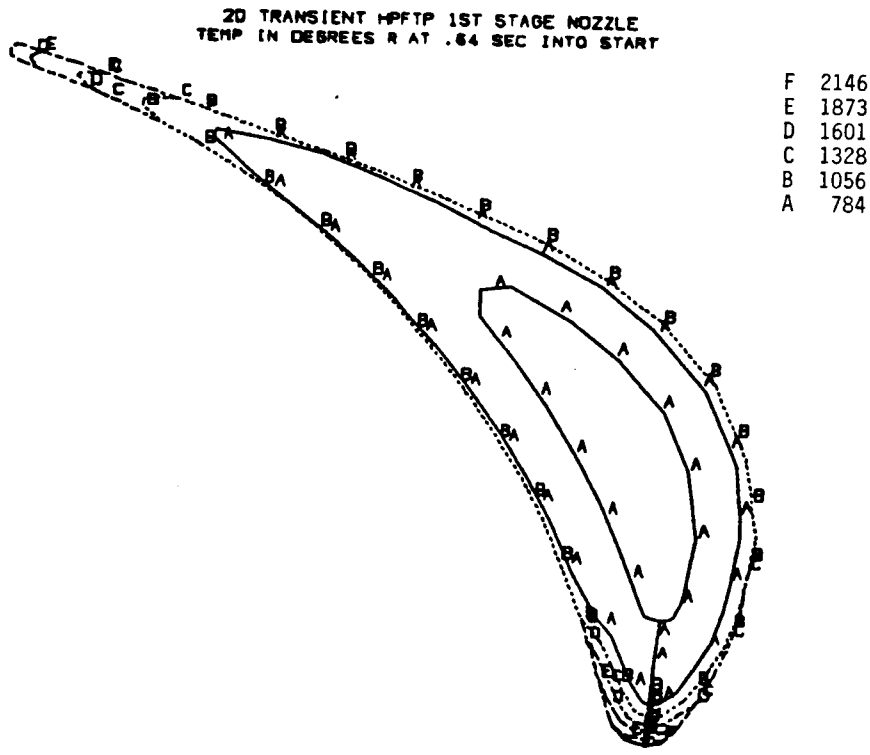

FIGURE B.18 HPFTP FIRST STAGE NOZZLE TEMPERATURE CONTOUR AT 0.64 SEC TEMPERATURE SPIKE AT START

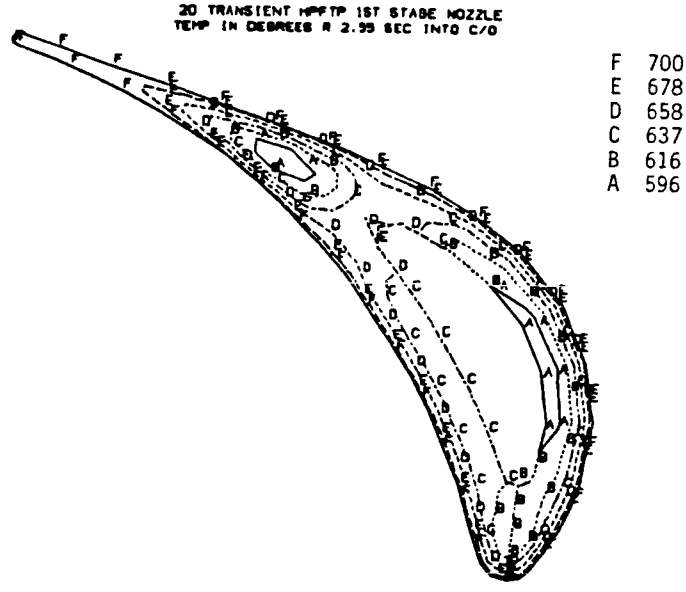

FIGURE B.19 HPFTP FIRST STAGE NOZZLE TEMPERATURE CONTOUR AT 2.55 SEC TEMPERATURE SPIKE AT CUTOFF

B.6 Debris Loads

Shock loads on turbine blades from the injection of debris is statistically a low probability, but one that practically occurs during engine development or flight. The debris comes from somewhere upstream of the turbine blades and the debris characteristics are somewhat a function of the engine configuration, turbine system and local construction of the combustion zone.

For example:

1. Solid propellant spin start systems like the J-2S can have propellant particulate in the flow during start.

2. Expander cycle engines debris would have to come primarily from the basic flow system, e.g., contamination, since they have no preburners and relatively low flow energy or thin sheet metal in the system to generate local structural pieces.

3. Instrumentation probes positioned ahead of the turbine are of a high potential for losing a tip.

4. On the SSME fuel preburner, small cylindrical spacers are held by compression and friction around the inner cylinder of the lox post. These are susceptible for discharge into the hot gases.

5. Thin sheet metal used in cooling liners can crack and tear out small pieces that are injested through the turbine.

The characteristics of the mission-history-duty cycle for debris loading then are:

1. Engine and system dependent
2. Variable size
3. Variable injestion direction and speed
4. Low frequency random occurrence
5. Shock loading
6. Potential to locally block flow

The size of the debris and the manner in which the debris approaches the turbine blades are part of the probabilistic characteristics of the loads.

Debris loading is primarily for failure analysis considerations in that the turbine blades should, by design, have low potential for failure from typical debris injestion. A typical example of this type of injection damage is shown in Figure B.20. Teardown inspection of the fuel turbopump turbine showed no significant discrepancy except for thermal distortion of the first stage turbine rotor tip shroud and minor dents on the first stage turbine blade leading edges resulting from ingestion of small fragments of instrumentation (Reference B.1).

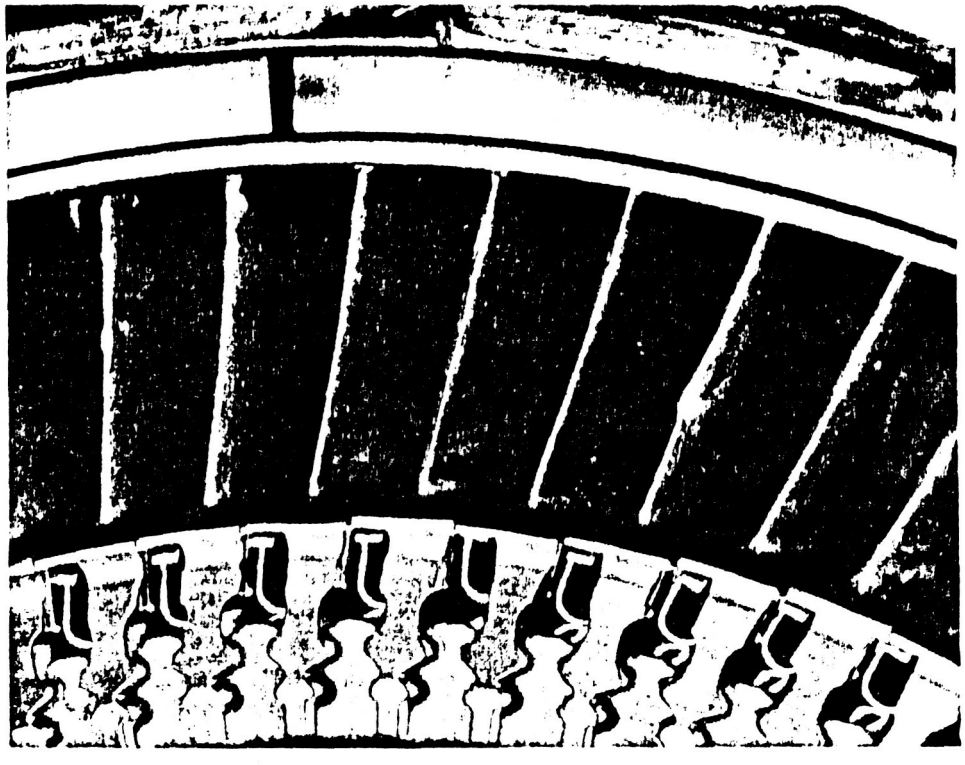

FIGURE B.20 TYPICAL TURBINE BLADE DAMAGE FROM DEBRIS LOADING

B.7 Seal Rubbing

Most rocket engine turbines have some sort of seal to minimize the leakage across the tips of the turbine blades. The desire to hold small gaps between the seal and blades means that some rubbing occurs. This rubbing typically occurs early in the life of a turbine since wear quickly eliminates the rubbing. Usually, an abradible material like honeycomb is used as a seal medium to minimize the load into the turbine blade. The SSME HPFTP started with such a seal, but has evolved to a solid RENE41 seal that is also eccentric to the rotor to account for a lateral rotor displacement from circumferential Δp loads. The use of the more rigid seal furnishes higher initial rubbing loads until the seal and blade tips erode and no longer touch. The load magnitude and excitation function are not quantified. Rocketdyne has never attributed a blade failure from this load, but has considered it during incident investigations.

B.8 Pseudo-Loads-Fabrication, Dampers, Friction, Tolerances

There are fabrication and design conditions that can be considered as pseudo loads. Pseudo loads are inputs needed for structural analysis that may or may not be a load depending on how the analysis is performed. For instance, the damper load is often statically accounted for using a point or distributed pressure load that is equivalent to the centrifugal loads on the damper.

These loads are considered secondary to this project, but may be included for completeness. The database is a convenient place to collect probabilistic data for these pseudo loads.

Certain fabrication residual stress conditions are more appropriately approximated from an analysis approach, e.g., braze stresses. Others, like shot peening, could be quantified and expressed as a probabilistic residual stress for use in a fatigue analysis consideration.

The weight of the damper and a lot distribution of its variations in weight can be used for defining their probabilistic loads.

Because of the small size of rocket engine turbine blades, geometrical variation of blade axes and cross section are critical in the blade analysis. Manufacture of turbine blades is characterized by strict geometric tolerances that are enforced. These tolerance limits are imposed by stress considerations and aerodynamic considerations in that order. It is not unusual for the scrap rates of turbine blades to be very high. Variations in geometry affect centrifugal stresses. A discussion of geometric variations and their effect on stresses is presented for the second stage blades of the high pressure oxidizer turbopump (HPOTP).

The HPOTP turbine blades geometry is defined by an upper platform, airfoil, lower platform, shank, damper slot, and fir tree. The blade also has a hollow core section. The blade contours are usually inspected by contour tracing machines or more recently by a laser inspection machine. The laser inspection machine has the advantage of storing x and y coordinates automatically in a file that can be machine processed for blade acceptability. Typically the points are those that are specified in master dimension chart. An example of contour and laser output is shown in Figure B.21 for four sections. Based on contour measurements the blades are evaluated for profile area, blade twist and lean and tilt. The designed lean and tilt are critical dimensions as any variation in the location of center of mass affect the designed centrifugal stresses. This becomes an important criterion as blades are designed such that centrifugal stress are to counteract power bending stresses. Variations in centrifugal stresses result in variations in mean and alternating stresses that affect the fatigue life of the blade.

An analysis of the variations in geometry and their effect on equivalent alternating stress is presented in Figure B.22 for a critical point. A similar study is done for all the critical stress points in the blade. The figure compares the results of the analysis of blades manufactured after a tooling change and of those blades that have been actually used in engines,

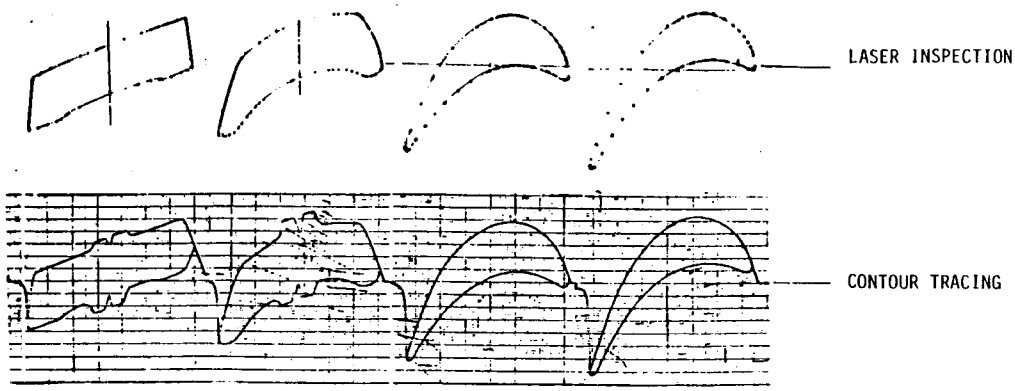

FIGURE B.21 A TYPICAL OUTPUT FROM LASER MACHINE AND TRACING MACHINE OF HPOTP SECOND STAGE BLADE

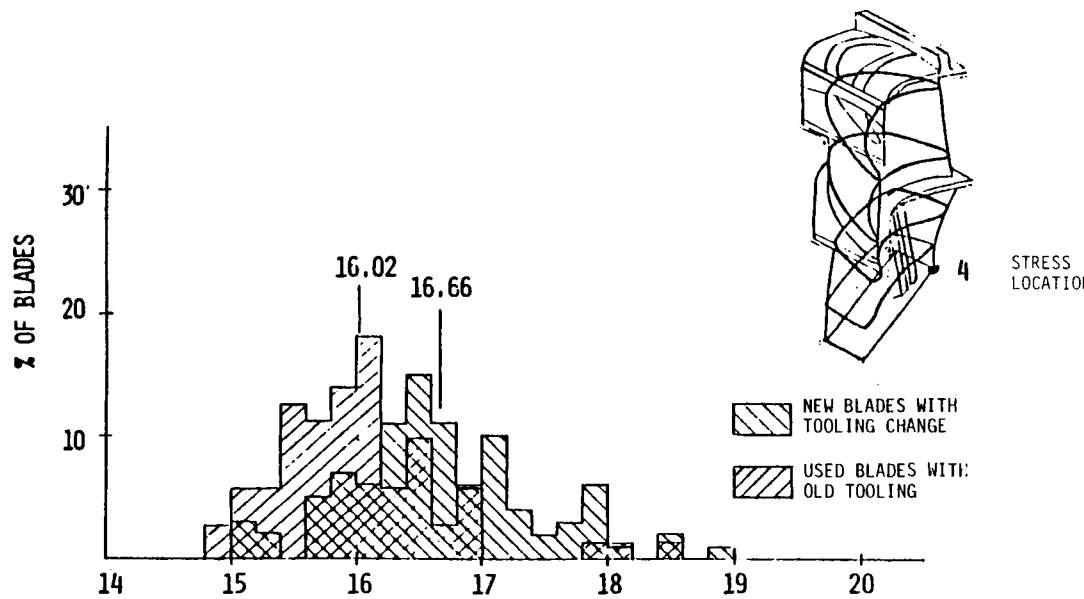

FIGURE B.22 IMPACT OF GEOMETRICAL VARIATIONS IN ALTERNATING STRESSES ON HPOTP SECOND STAGE BLADE

to investigate the range of operating experience. Other critical dimensions that are routinely inspected include root and valley discrepancies in fir tree, core offset, damper slot depth and upper and lower platform discrepancies. The blade measured data is available for developing a probabilistic distribution of geometric data that could be included in the database.

B.9 Available Mission-History-Profiles for Theory Verification/Validation

B.9.1 Introduction. The amount of available mission-history-profiles for use in either developing the loads or validation/verification varies with the load component. For load components that are measured each test or calculated each test - pump speed and torque (blade Δp force) at steady-state operation - there are any of the profiles or tests that are used in engine test or flight. The other load components validation/verification must be addressed by a combination of limited data on instrumented turbopump and analysis. Table B.1 summarizes the currently available data, planned measurements in 1985-1986 as part of the SSME Development Program and test bed engine instrumentation plan for 1987 or later testing.

- ENGINE DATA FOR MEASURED PROFILES
  - SPEED
  - TORQUE (CALCULATED)
- MEASURED DATA
  - INSTRUMENTED HPFTP
    - LIMITED TURBINE BLADE AIRFOIL STRAIN GAGES TESTS 750-151 AND 750-152
    - NOZZLE THERMOCOUPLES TESTS (902-278 TO 902-285 AND TESTS 750-169 TO 750-175
- PLANNED MEASURED DATA - 1985 AND 1986
  - INSTRUMENTED HPFTP
    - THERMOCOUPLES
    - SIMILAR TO PREVIOUS TESTS
    - 3 DUCT AND 2 DUCT HOT GAS MANIFOLD CONFIGURATIONS
    - MODIFIED START AND CUTOFF TRANSIENTS
- LIFE EXTENSION STUDIES FOR HPFTP
  - ANALYTICAL STUDY OF START AND CUTOFF TRANSIENT OPTIMIZATION
- TEST BED ENGINE - 1987 AND LATER

TABLE B.1 AVAILABLE MISSION HISTORY PROFILES FOR THEORY VALIDATION/VERIFICATION

To date there have been instrumented HPFTP's that had: 1) limited strain gage and thermocouple measurements on turbine blades and 2) thermocouple measurements at the turbine discharge, first stage stator and in the preburner zone. These tests can be used to relate the test-to-test measured turbine discharge temperatures to the stator temperatures and blade temperatures. This will furnish more precisely calculated thermal conditions in the overall turbine.

Planned tests as part of the current SSME development contract include additional HPFTP instrumented turbine tests. Also, the on-going development life extension study effort has looked at the HPFTP first stage turbine nozzle temperatures in detail as a function of start and cutoff parameters. This is the best available transient analysis work that is closely related to turbine blade temperatures. As previously mentioned, there is an ongoing HPFTP first stage turbine blade analysis that will cover the total duty cycle and will be available for this programs effort.

The test bed engine design effort has started and the current asked for instrumentation includes a good survey of turbine component temperatures and limited turbine blade strain gages.

Instrumented HPFTP Temperature Measurements. Engine firing data and failure history of HPFTP turbine blades have indicated that SSME HPFTP first stage blades see much higher temperatures than the nominal design values. Post test inspection of blades have further given an indication of temperature gradients present in the blade by surface condition and discoloration. The detection of incipient melting conditions show that some blades have seen temperatures greater than 2715°R. The standard flight instrumentation measures temperatures at the turbine exhaust at only two locations. The measurement devices used in these flight transducers have a slow response to rapid temperature spikes or thermal transients. In order to obtain a better understanding of the temperature environment in the turbine, three turbopumps were extensively instrumented with thermocouples and tested on two engines.

The instrumentation was designed to measure rapid thermal transients, gas temperatures at turbine outlet and inlet at several positions around the circumference. Other objectives of the test included modification to fuel preburner and fuel preburner oxidizer valve start sequence.

A typical start temperature transient for the HPFTP is examined first. The start temperature transient is plotted to an expanded scale in Figure B.23 for the first 10 seconds at the Kaiser hat location (just ahead of the turbine inlet). The transient is characterized by two temperature spikes, the first one being termed as the ignition spike at 0.75 seconds and the second one as the fuel oscillation spike at approximately 1.3 seconds.

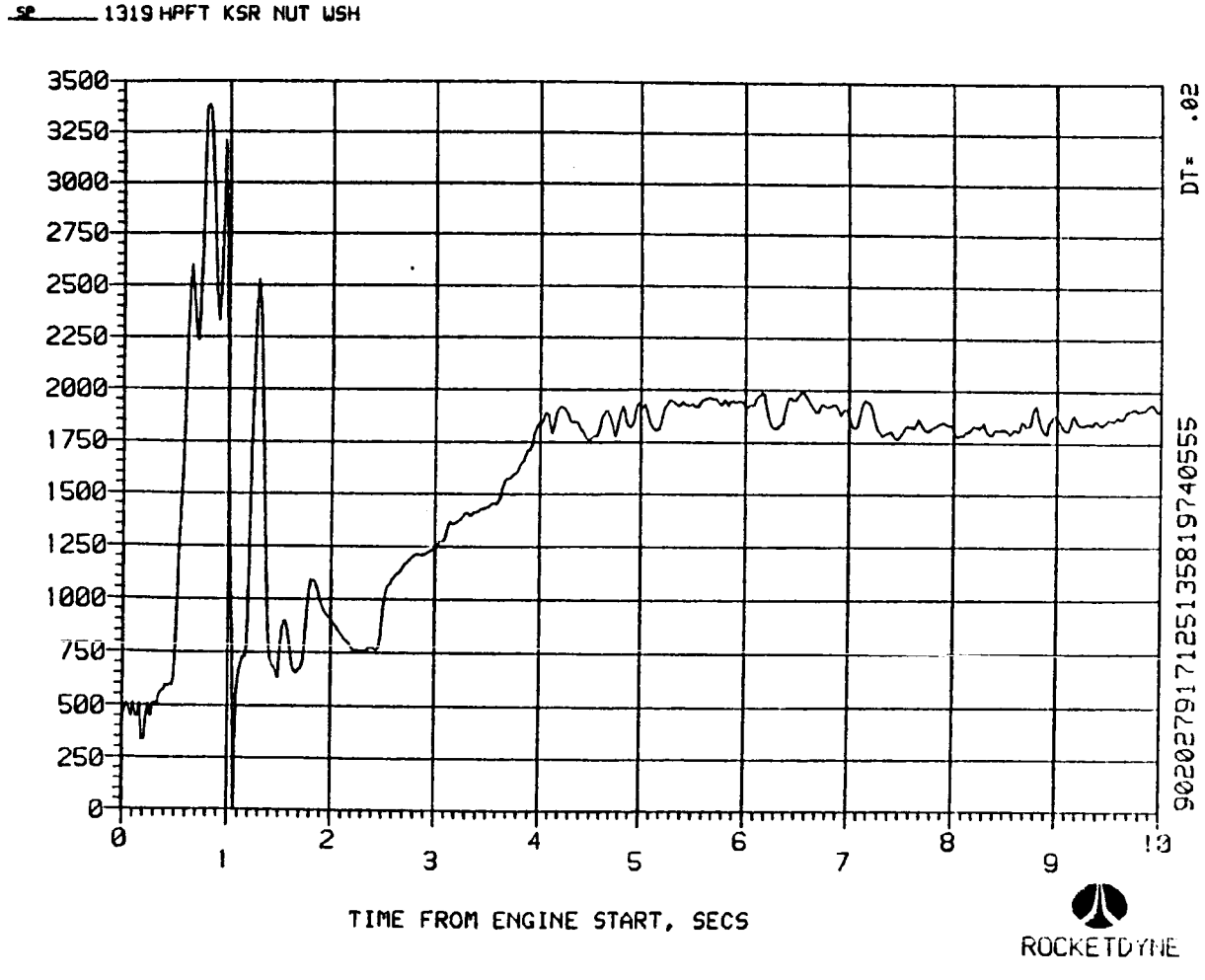

FIGURE B.23 TEMPERATURE SPIKE AT START TRANSIENT AT KAISER HAT LOCATION

The first spike is caused by the lox rich mixture as a result of reduced fuel flow due to the sudden increase in fuel preburner chamber pressure at ignition. The second spike is due to fuel oscillation which is a cyclic phenomenon observed in SSME. The net effect of this phenomenon is the reduction in fuel flow to the fuel preburner at about 1.3 seconds. As the engine pressure increases, the oscillation vanishes and the engine reaches the main stage operation. Figure B.24 through Figure B.25 illustrate several aspects of this start transient phenomenon.

There are variations in data between firing to firing, engine to engine and from turbopump to turbopump. The inlet temperature can vary between firings appreciably for the same spatial location. This is illustrated by comparing the PID 1319 measurement between 750-171 and 902-279 test measurements. Both the firings used the same start sequence but the engines and turbopumps were different. Figure B.25 illustrates the variation in turbine inlet temperatures at transient due to modifications in start sequence. Turbine blades may experience large cyclic temperature changes at start transient and to a lesser extent at mainstage operation. This is illustrated in Figure B.26 where T_1 through T_7 are temperature measurements at different clock positions. The temperature spikes as measured in the turbine exhaust are much less than that observed in turbine inlet. This is illustrated by comparison of Figure B.26 and Figure B.27 which were measurements from test 750-171.

There is also a variation in gas temperature based on clock positions. The regular flight transducers instrumentation (Figure B.28) sensor is so large a mass that it shows a reduced temperature spike during the start transient. Figures B.29 shows some of the similar effects that occur during the cutoff transient.

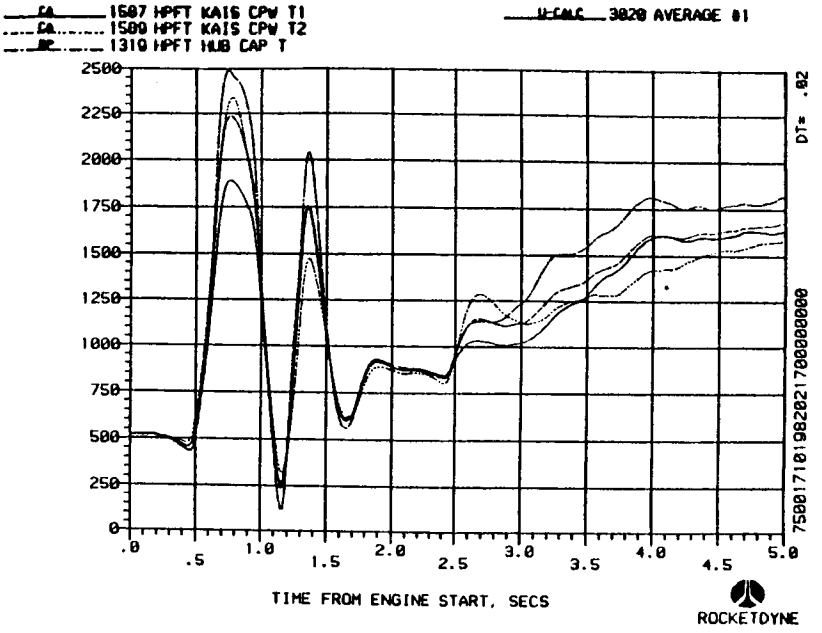

FIGURE B.24 START TRANSIENT TEMPERATURE MEASUREMENTS AT KAISER HAT FOR TEST 750-151

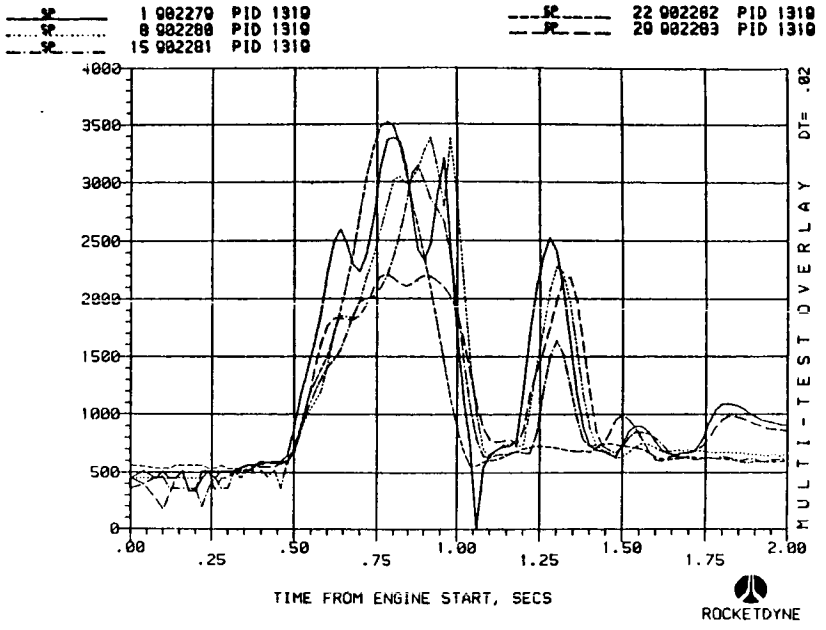

FIGURE B.25 COMPARISON OF KAISER HAT TEMPERATURE MEASUREMENTS WITH VARIATIONS IN START SEQUENCE

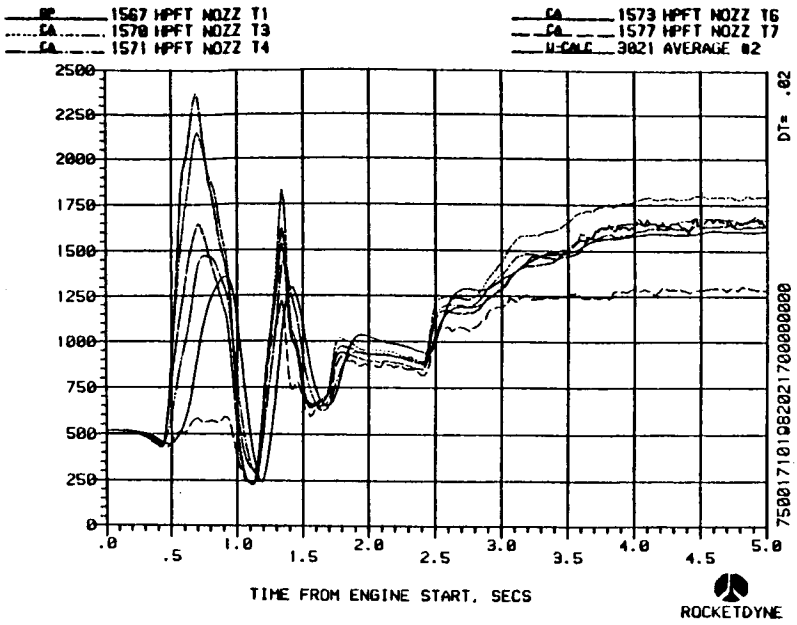

FIGURE B.26 VARIATION IN TURBINE INLET TEMPERATURES AT NOZZLE AT VARIOUS CLOCK POSITIONS

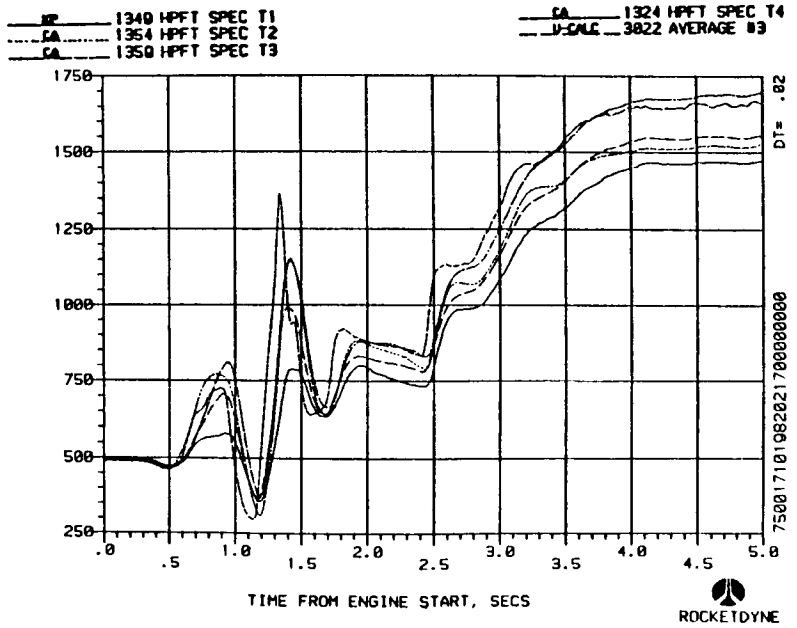

FIGURE B.27 TURBINE EXHAUST TEMPERATURE MEASUREMENTS AT START TRANSIENT

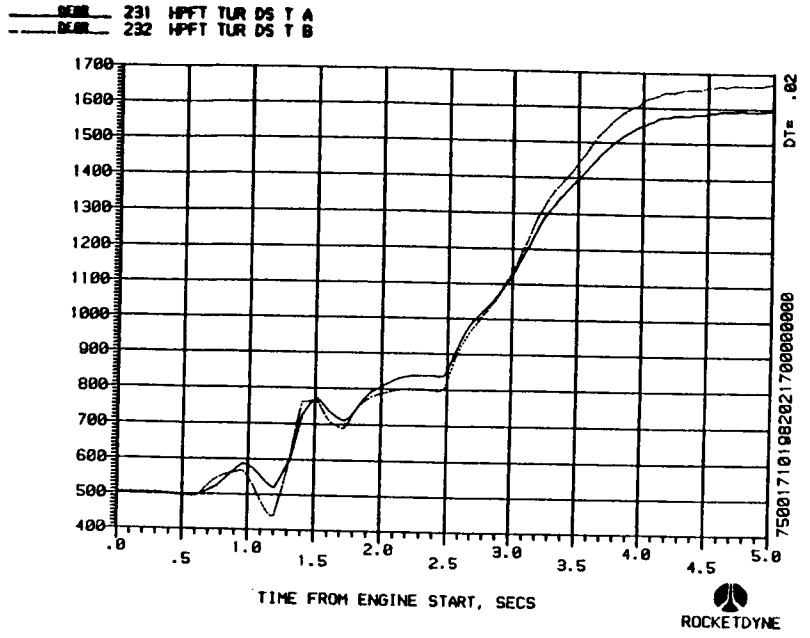

FIGURE B.28 TEMPERATURE MEASUREMENTS AT TURBINE EXHAUST USING A AND B TRANSDUCERS

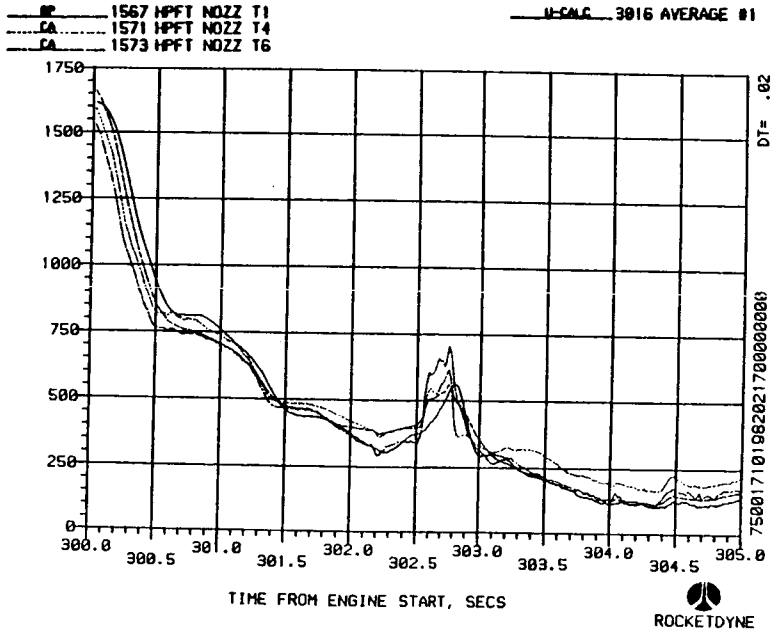

FIGURE B.29 TURBINE NOZZLE TEMPERATURES AT CUTOFF TRANSIENT

B.9.3 Planned Instrumented Turbine Tests in SSME Development Program and Test Bed Engine

The current SSME Development plan has tests to characterize the fuel turbine environment. Tests are planned with an instrumented turbine, see Figure B.30. The instrumentation will consist of extensive measurements of the hot-gas pressures and temperatures at the turbine inlet, in the first-stage nozzles, in the second-stage platform area, and at the turbine exit flange.

The instrumented turbine design will be similar to units tested in Phase I with special instrumentation. Data will be obtained with both the two-tube and three-tube hot-gas manifolds to provide a characterization of both transient and main-stage operation with each configuration.

The basic objective is to measure the radial and circumferential temperature distribution at the inlet, the circumferential pressure and temperature distributions at the second rotor exit, and at the turbine exit flange (G-6 flange).

The first instrumented unit will be tested with the three-tube hot-gas manifold. These data will provide (1) confirmation of fuel preburner design decisions to minimize transient and steady-state thermal effects on the hardware, (2) verification of the turnaround duct analysis and flow tests that form the basis for the turnaround duct redesign, and (3) definition of the bellows shield dynamic environment. The instrumentation design will be reviewed for potential changes to the types and locations.

Following test completion, the instrumented turbine will be returned to Canoga Park, refurbished, and prepared for further testing. The data acquired from the instrumented turbine will be essential in assessing the improvements derived from the two-duct hot-gas manifold and the preburner injector modifications.

The MSFC SSME test bed engine has plans for extensive instrumentation of the entire engine. The design and fabrication will be completed in 1987. Instrumentation currently planned that is of interest to the turbine blades are primarily in the HPFTP. Measurements of turbine temperatures, blade strains and temperatures are planned.

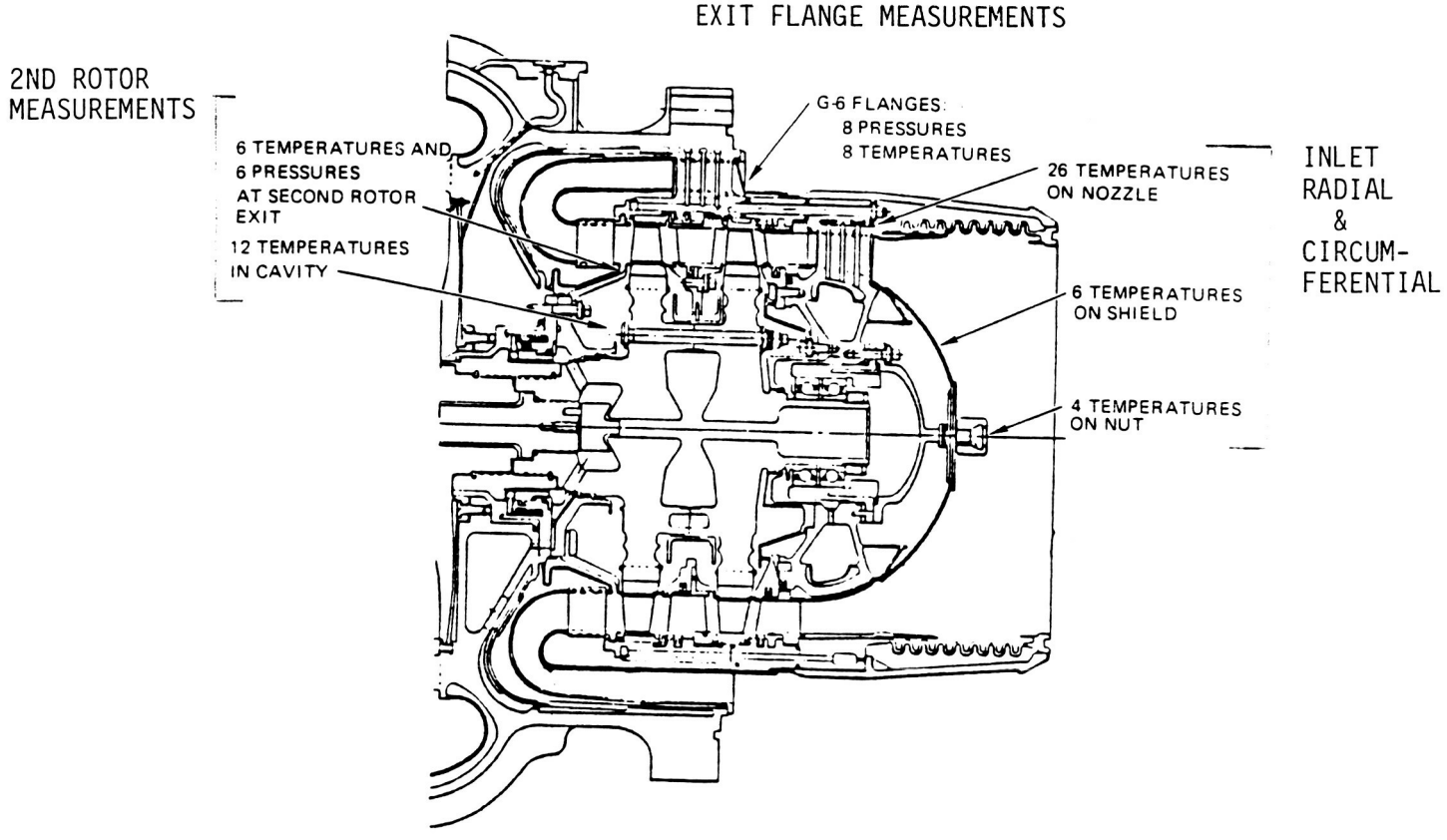

FIGURE B.30 PLANNED HPFTP TURBINE SPECIAL INSTRUMENTATION

APPENDIX C SSME LOX POST LOADS

C.1 INTRODUCTION

This appendix furnishes an assessment of the individual loads on the SSME LOX posts in the preburners and main injector. The available test data for potential use in validation of the load model is also included. The information in this appendix is summarized in sections 9.4 and 9.5.

C.2 Structural Dynamic Excitations

The structural dynamic excitations for LOX posts and injectors are measured responses. Accelerometers are located on external structure of the injector such as the location(s) shown on the SSME main injector (the LOX dome interpropellant plate or the gimbal bearing flange connection, Figure C.1). The accelerometers are standard measurements on test firings and engine flights. The measured responses are used as dynamic base input accelerations for either individual LOX posts, or as input accelerations to an injector assembly model with the entire set of LOX posts, interpropellant plate and LOX dome, etc. The current state of the art is to use the response as an input rather than transform the responses back to the actual load functions - the transform is not sufficiently accurate. Accelerometer data is limited to one or two measured directions and furnish local magnitude and frequency. The data is insufficient to discriminate mode shape so simplifying assumptions are made. These include independent assessment of vibrations by load direction and mode shape descriptions that are judged reasonable for the analysis in question.

The generic mission-history-profile is complex since it can be made up of several different load components whose significance is variable and dependent on engine and component parameters (J-2, SSME, OTV, etc.). Pictorially, the mission-history profile is shown in Figure C.2. The loads can be categorized as:

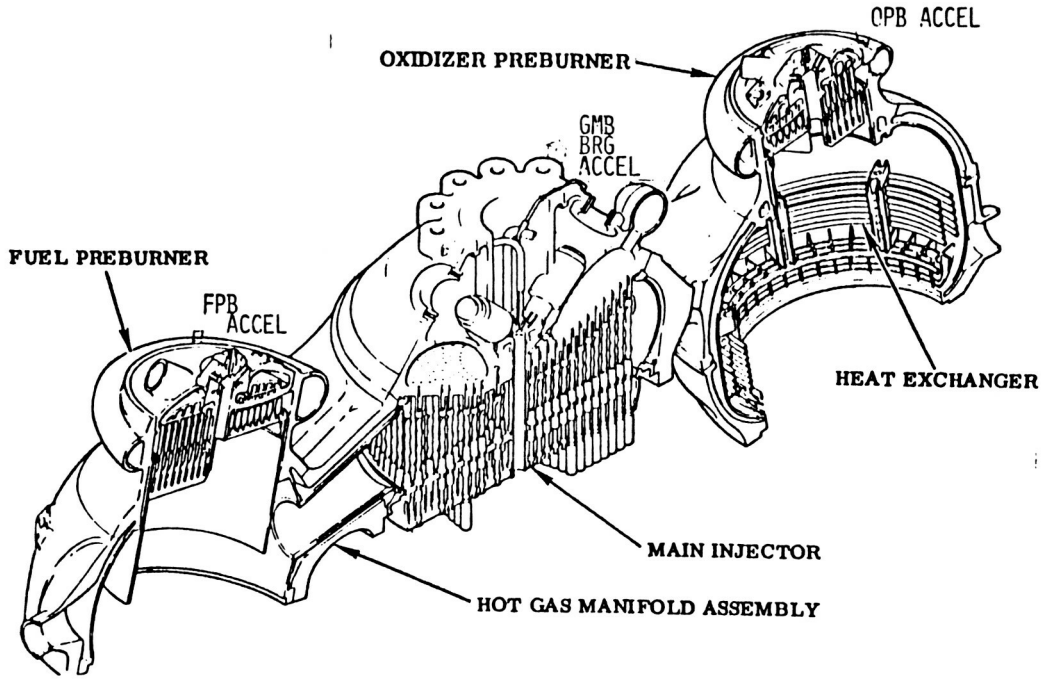

FIGURE C.1 CUTAWAY VIEW OF HOT GAS AND LOX MANIFOLDS

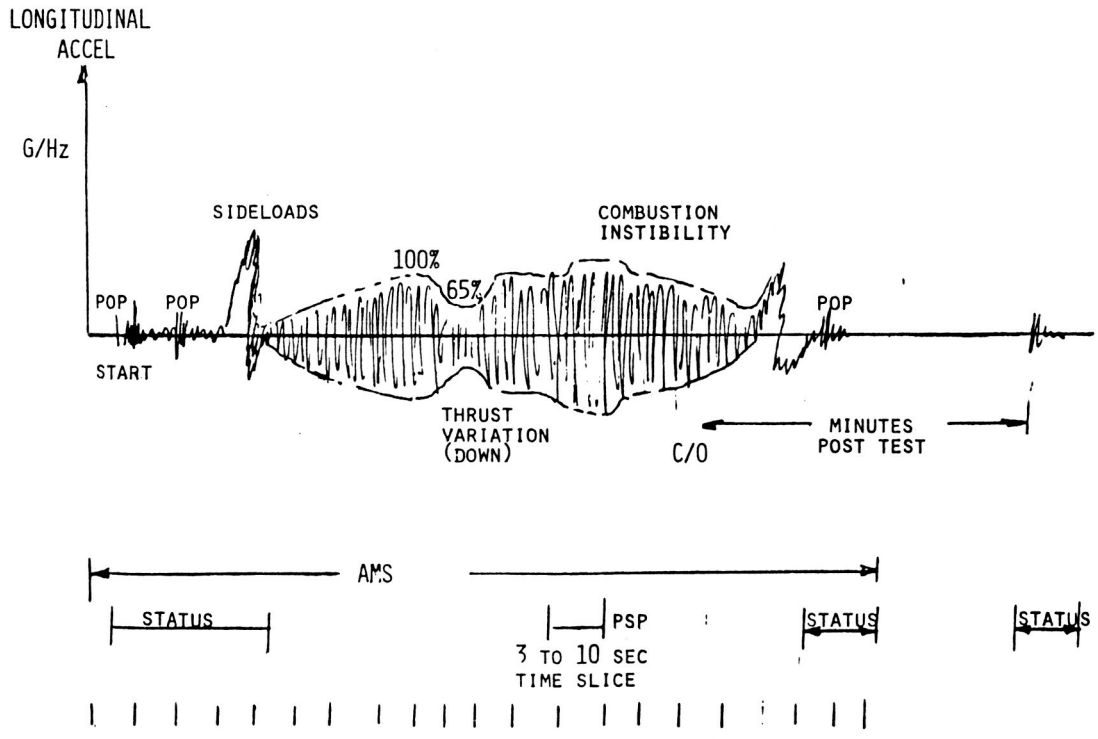

FIGURE C.2 PICTORIAL REPRESENTATION OF GENERIC INJECTOR RESPONSE AND DATA PROCESSING

1) Transient Loads

a. Random pops (high frequency shock) - local combustion detonations during start and cutoff and up to minutes after cutoff.

b. Engine side load reactions (low frequency oscillations) - overall structural loading from the nozzle separation that is reacted by the primary load path through the main injector gimbal bearing and gimbal actuators.

c. Nominal random vibration - energy that builds up with the magnitude of the combustion related engine power level. This varies as the engine power level is transiently changed throughout the test.

2) Steady State Operation Loads

a. Nominal random vibration - combustion related mainly from the local combustor but potentially from other combustors on the engine.

b. Random periodic shape - high frequency combustion instability that is looked for on every combustor (SSME has shown virtually no measurable combustion instability, but it has been a significant parameter on other engines and is tested for during engine development).

c. Steady state sinusoidal vibration - significant discrete sinusoidal vibrations are measured at multiples of pump speeds on turbopump, preburner and main injector accelerometers. The high level of transmissibility from the pumps on the SSME is due to the rigid structural power head package encompassing the high pressure pumps, preburners, main injector and power head. These sinusoids track with pump speed and are in the 5 to 20KC frequency band. The main injector-LOX post and other component primary structural responses are below this bandwidth, but the preburner LOX post structural responses overlap the mid-range of this frequency band.

Extensive engine test measurements have been taken with these accelerometers, virtually every engine test. The signals are processed with AMS, ISOPLOTS and STATOS records. Figures C.3 through C.8 show typical data from test 901-454 including preburner accelerometer processing. Vibration levels and pops are tracked on a test-by-test basis.

Zonal shock and vibration criteria are defined for all three SSME combustors, the fuel preburner criteria is shown in Figure C.8. The methodology used for defining the loads envelopes the maximum responses from at least three tests each on two engines at the power level within a specified range (e.g., 65 to 109% PL). This is considered a 2σ response. The shock and vibration loads are used by dynamist as input to structural models of individual LOX posts or entire injector assemblies including LOX posts.

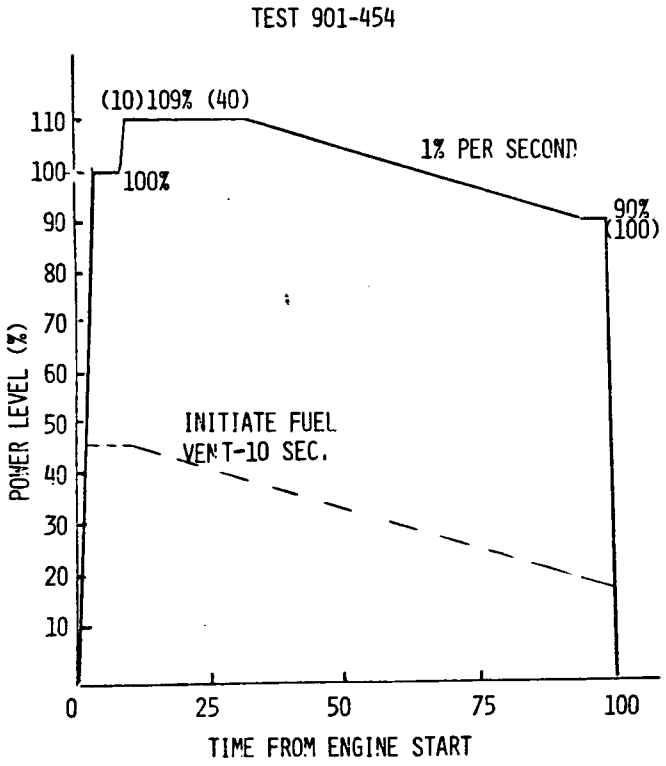

FIGURE C.3 PUMP SIGNATURE TEST 100 SEC. DURATION

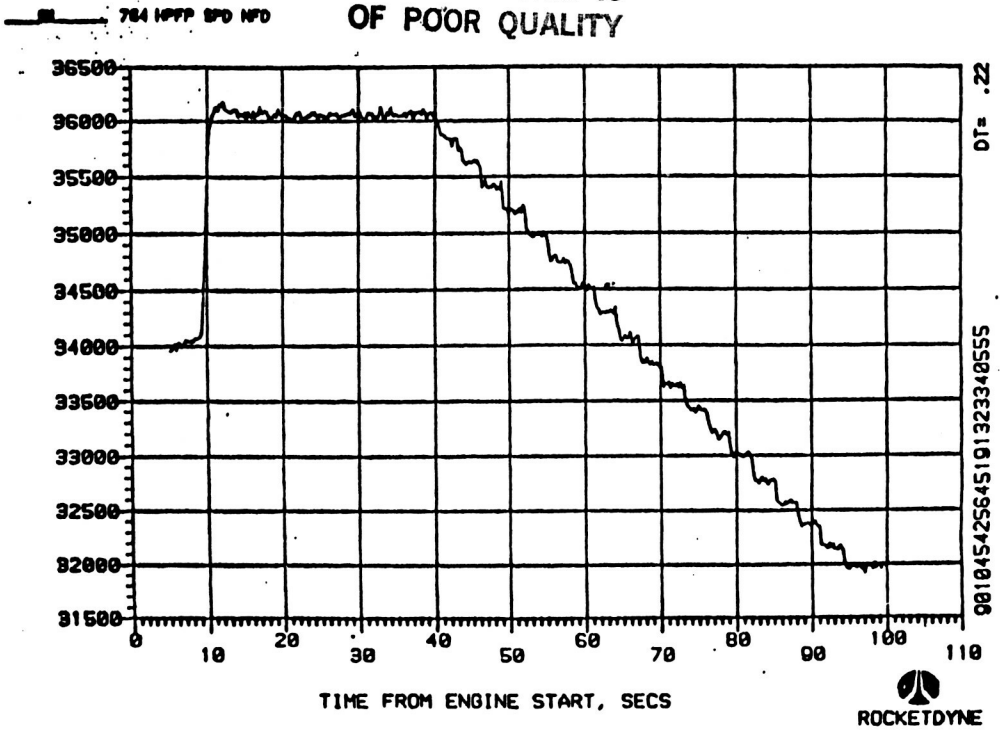

PUMP SPEED (RPM VS. TIME)

FIGURE C.4 PUMP SPEED (RPM VS TIME)

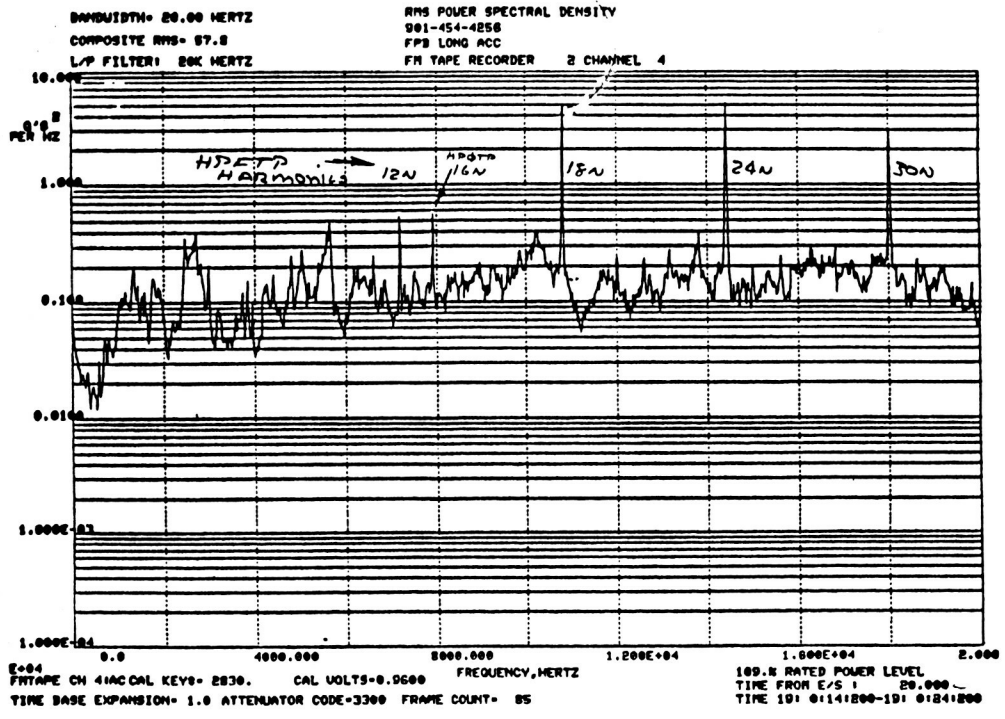

PSD

FIGURE C.5 FUEL PREBURNER LONGITUDINAL ACCELEROMETER PSD

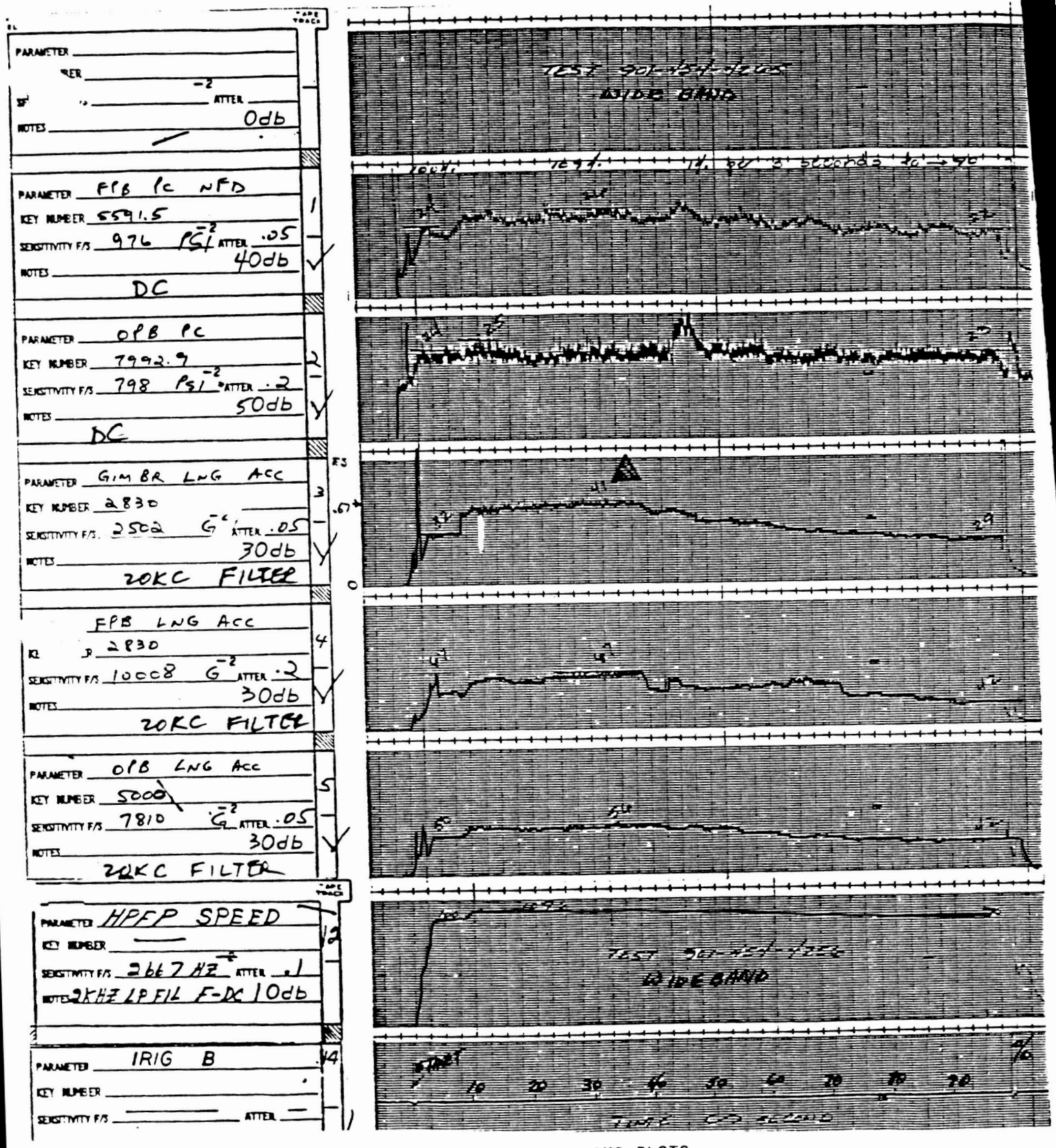

FIGURE C.6 AMS PLOTS

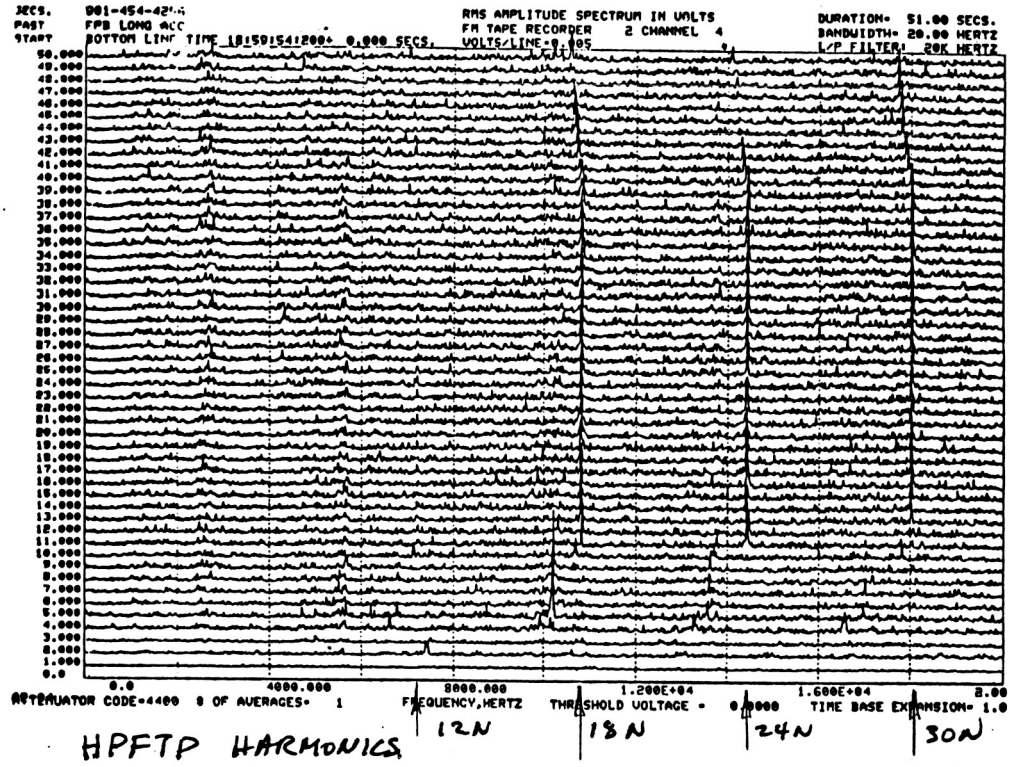

ISOPLOT

FIGURE C.7 FUEL PREBURNER LONGITUDINAL ACCELEROMETER ISOPLOT

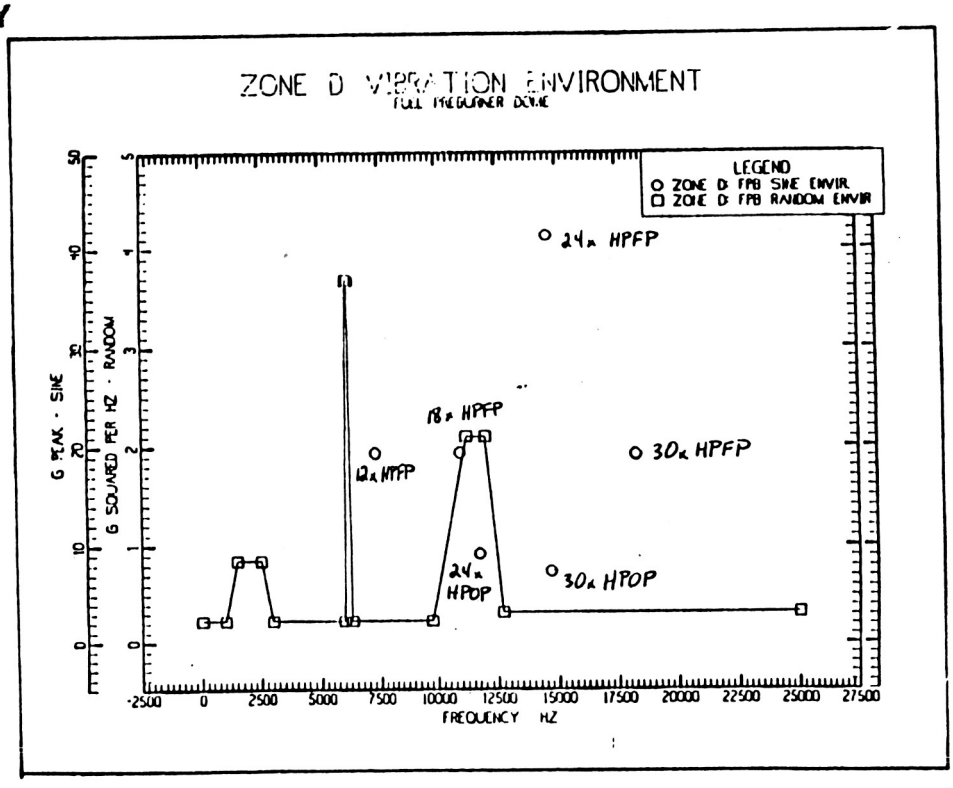

FIGURE C.8 FUEL PREBURNER ENVIRONMENT ENVELOPE - PSD

The three accelerometers show transient side load effects at start and cutoff as well as variations in power level effects. The pops are not discriminated from these traces. The main injector - gimbal accelerometer shows more effect from the sideload since it is in the primary thrust load path whereas the preburners are not. Figures C.5, C.7, are PSD and ISOPLOT for the FPB accelerometer. The isoplot shows the strong HPFTP sinusoidal harmonics at multiples of pump speed that are measured at this point as peaks over the random signal. The effects of thrust variation are easily noted as the sinusoidal responses vary with pump speed. The PSD shows similar response data for a shorter time slice. There are also HPOTP related sinusoidals and one is also noted on the PSD.

Figure C.3 is the thrust profile of the test. This test does not simulate a flight test, but is used to develop the operational characteristics of the pump between 90% and 109% power level. Figure C.4 shows the HPFP speed variations in the test. The trace shows that the actual test thrust change as in 1% power level measurements per 3 sec rather than a constant. Figure C.6 are AMS Plots of the complete test of accelerometer and chamber pressures on the preburner and main injector, a repeat of the HPFP speed and the IRIG B time trace. The Pc measurements show transient spikes (pops) and relatively smooth steady state operation that varies with thrust. There are some minor transient conditions that occur during the thrust ramping from 109% to 90% power level.

Figure C.8 shows the vibration, zonal vibration used for the FPB. Both the enveloped random environment and the sine environment are shown. Some of the key injector and LOX post modal responses are between 5 and 15 KHZ which requires using environments on this component up to a 20Hz level. The main injector by comparison has such lower modal responses that the environment is not utilized above a 5KC level. These PSD and ISOPLOT traces show that there is significant coupling between the pumps, preburners and main injector because of the stiff lead path in the powerhead assembly.

The individual engine test data is available as processed, or can be reprocessed on a limited basis for special needs for developing the

probabilistic loads and for later theory validation and verification. Key engine variables are time phased and recorded for correlation with these responses.

C.3 Flow Loads - LOX Posts

The dynamic flow induced loads on a rocket engine injector are a consequence of the fuel or fuel-rich hot gas, entering the injector and impinging on the posts. These streams are high velocity, highly turbulent fluids. The characteristics of the flowfield that enters the injector are strongly dependent on the geometry of the ducts upstream, as well as on the configuration of the interface between the ducts and the injector. As this size approaches a characteristic dimension of an immersed body, its effect on the body increases. The effect of geometry is its influence on the turbulent eddy size. Another factor is the presence of separated regions in the flow upstream of an injector. The flowfield downstream of a separation is much different than one which is merely turbulent but not separated.

For rocket engine systems, the geometry through which the flow streams pass is typically quite complex. Analytical determination of the location and size of separated regions, or the nature of the turbulent fluctuations throughout an engine mission history duty cycle is not yet possible. The four main mechanisms that may cause flow-induced vibrations of LOX posts are:

1) Fluidelastic excitation (self-excited vibrations)
2) Turbulence
3) Vortex shedding
4) Jet impingement through orifices on the post.

Fluidelastic Excitation. A main cause of large-amplitude tube vibration that has resulted in rapid deterioration of tubes in heat exchangers has been determined to be fluidelastic excitation, a self-excited vibration mechanism, first identified by Westinghouse. The similarity of the SSME main injector LOX post array to the tube arrays found in heat exchangers

that have been effected by fluidelastic excitation, makes it a reasonable belief that the potential may exist for fluidelastic excitation to be present in the SSME. The mechanism is characterized by a critical flow velocity below which vibration amplitudes are small and above which the amplitudes increase very rapidly. It is this fact, coupled with the previous observations, that makes the fluidelastic excitation mechanism by far the most critical of the three flow-induced vibration mechanisms listed.

Turbulent Excitation. Turbulence causes narrow-band random vibration of tubes at about the natural frequencies of the tubes in the fluid. The vibration amplitudes vary randomly in time and in direction. Turbulence is thought to be the main cause of tube vibration in heat exchangers when the possibility of fluidelastic excitation has been eliminated. Turbulence is the primary load for the main injector row 13 LOX posts that have flow shields. The flow shields have a large frontal area that is buffeted by the turbulent flow.

Vortex Shedding. When fluid flows across a circular cylinder, the wake behind the cylinder contains vortices. The vortices are shed from the cylinder in a regular manner. They give rise to an alternating force in the direction transverse to the flow. An alternating force is associated with the vortex shedding frequency. For a single cylinder, large amplitudes can develop when the vortex shedding frequency coincides with a tube natural frequency. Methods are available for predicting tube vibration caused by vortex shedding. However, the practical importance of vortex shedding excitation in closely packed arrays is questionable. Vortex shedding excitation has been observed in laboratory tests on tube arrays in uniform cross flow at relatively low Reynolds numbers. However, a number of factors tend to greatly reduce the significance of vortex shedding in SSME.

Jet Impingement Flow. A more local flow effect that has caused LOX post failure on a preburner post is the flow included vibration of the post when vertical (swirl) flow exists in the annulus. The swirl can result when feed holes are symmetrically offset from their intended radial direction, see Figure C.9.

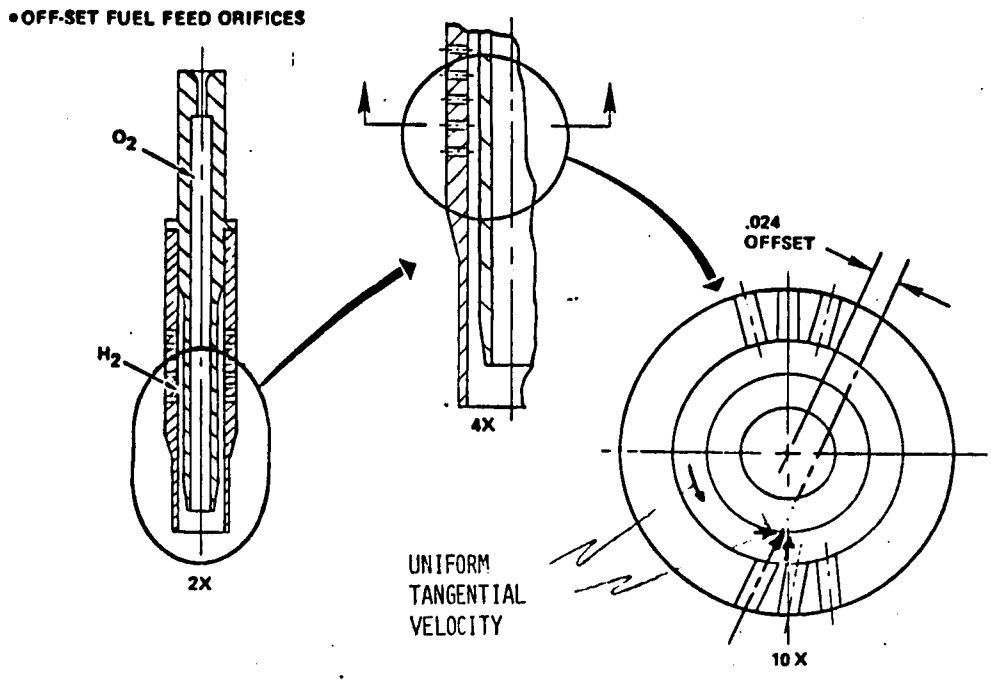

FIGURE C.9 LOX POST CROSS SECTION DEPICTING OFFSET FLOW IN A COAXIAL LOX POST

The net resultant force is in a purely normal direction to the original perturbation. Despite the small magnitude of the force, it is not balanced by the restoring bending moment of the LOX post. Thus, the LOX post experiences unchecked tangential acceleration. This increases the eccentricity of the LOX post which in turn results in an even greater transverse force. The process continues until the speed and amplitude of the rotational vibration of the LOX post have reached such magnitude that invalidates the stationary post assumption of the calculations, at which point a new equilibrium state, if it exists at all will be established. The speed of the post center then is likely to be large, of the same order of magnitude as the uniform tangential velocity itself.

Therefore, as long as vertical flow exists in the annulus, an infinitesimal amount of perturbation to the LOX post will immediately set it into vibration.

The recent use of computational fluid dynamics has allowed these flow fields to be much better defined for steady state operation, but still do not address transient flow or local effects on model components like LOX Posts. In the absence of this type of complex, detailed analysis, it is necessary to rely on measured data either hot fire or simulation, and judgment . Engine measurements are difficult to obtain and there is only a small database. Cold flow simulations are usually relied on for this type of measurement.

The limited direct measurement of the combined effect of the flow loads on the SSME LOX posts are obtained from engine test data. Static and dynamic Pressures are obtained for the hot gas manifold at ports CGIP and/or CGIC. These measurements are rough indications of the static and dynamic pressure loads on the LOX posts in the vicinity of the measurements. They have been correlated with LOX Post strain gage measurements made during hot fire tests of engine 0110F, as well as the extensive cold flow tests on a hot gas manifold-injector simulator. Figure C.10 shows the instrumentation used on engine 0110F. The strain gages survived only a few tests and are the only available LOX post engine measurements at this time. There are plans and hardware assigned for additional LOX post strain gage measurements.

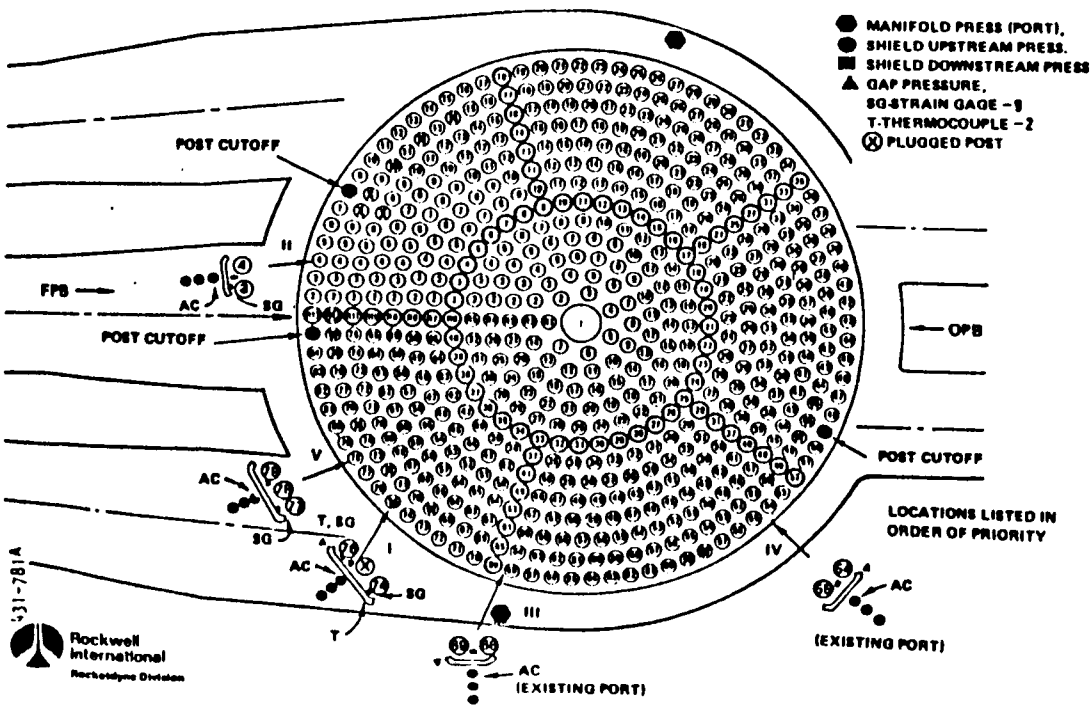

FIGURE C.10 SSME MAIN INJECTOR INSTRUMENTATION ENGINE 0110F

Figure C.11 shows the correlation between the strain gage data and power level. Similar correlations were made vs CGIP dynamic pressures. Figure C.12 shows the correlation of the strain gage data vs frequency and calculated strain. This was used to develop a measure of damping for the row 13 shielded LOX posts and accounts for the total damping effect from threaded connections, thermal shields, etc. A lower value of damping is assigned the row 1-12 LOX posts that do not have flow shields.

Figures C.13 and C.14 relate the dynamic CGIP measurements on a selected test by test basis to high pressure turbopump measurements and the distribution of pressure level within a test. This data along with the strain gage correlations and flow measurements has been used to cast a statistical distribution of pressure for individual LOX posts in the main injector.

The other complementary method of assessing the flow loads on the main injector LOX posts in the SSME consisted of simulation tests in which ambient temperature air was used as the fluid with full scale hardware. By using a flowrate that produced Reynolds numbers equivalent to engine conditions at 65% Power level, it was possible to get data that could easily be scaled to full power level conditions. Extensive instrumentation allowed for fairly complete characterization of the flowfield entering the main injector. These tests were correlated to the limited hot fire instrumented injector data which was available. The correlations also aided in the development of scaling techniques.

It should be pointed out that, as in any injector system, each post in the SSME Main injector is in the midst of a slightly different array geometry. Since the flow exits the injector in the axial direction while entering radially, the magnitude and direction of the velocity approaching each post is different. Post loading must therefore be characterized based on a posts position in the injector and the approach flow conditions. A typical mission history profile of high frequency pressure in the main injector for the SSME is show in Figure C.15.

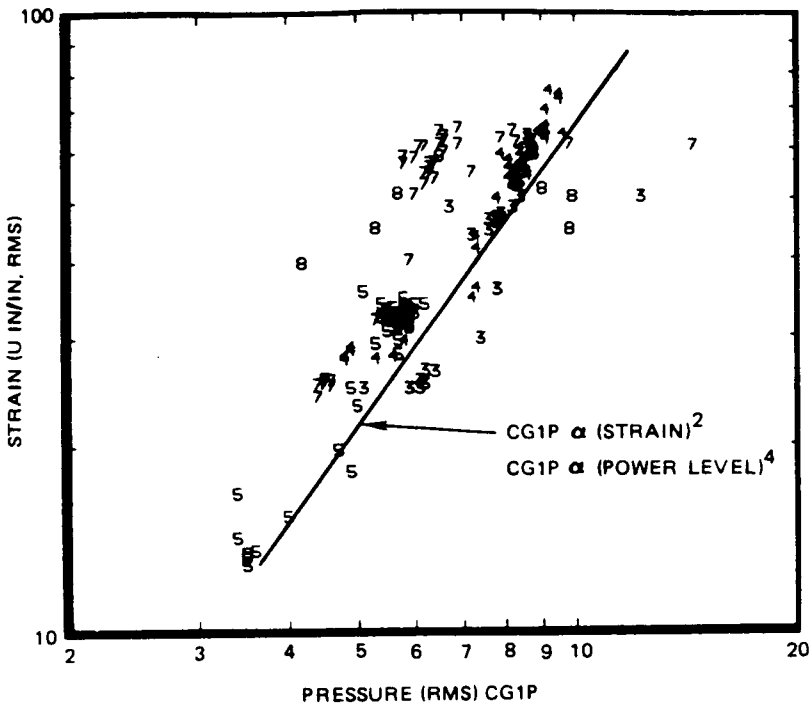

FIGURE C.11 LOX POST RMS PRESSURE VS STRAIN CORRELATION

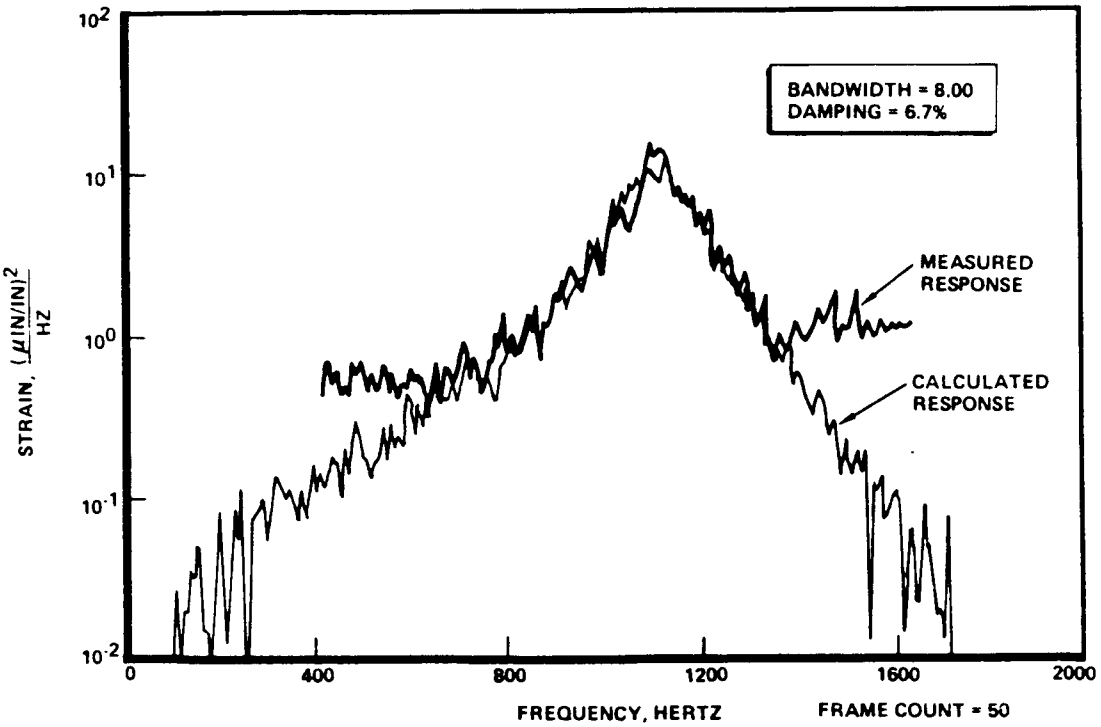

FIGURE C.12 LOX POST STRAIN GAGE RESPONSE - ANALYSIS VS TEST AT DAMPING = 6.7%

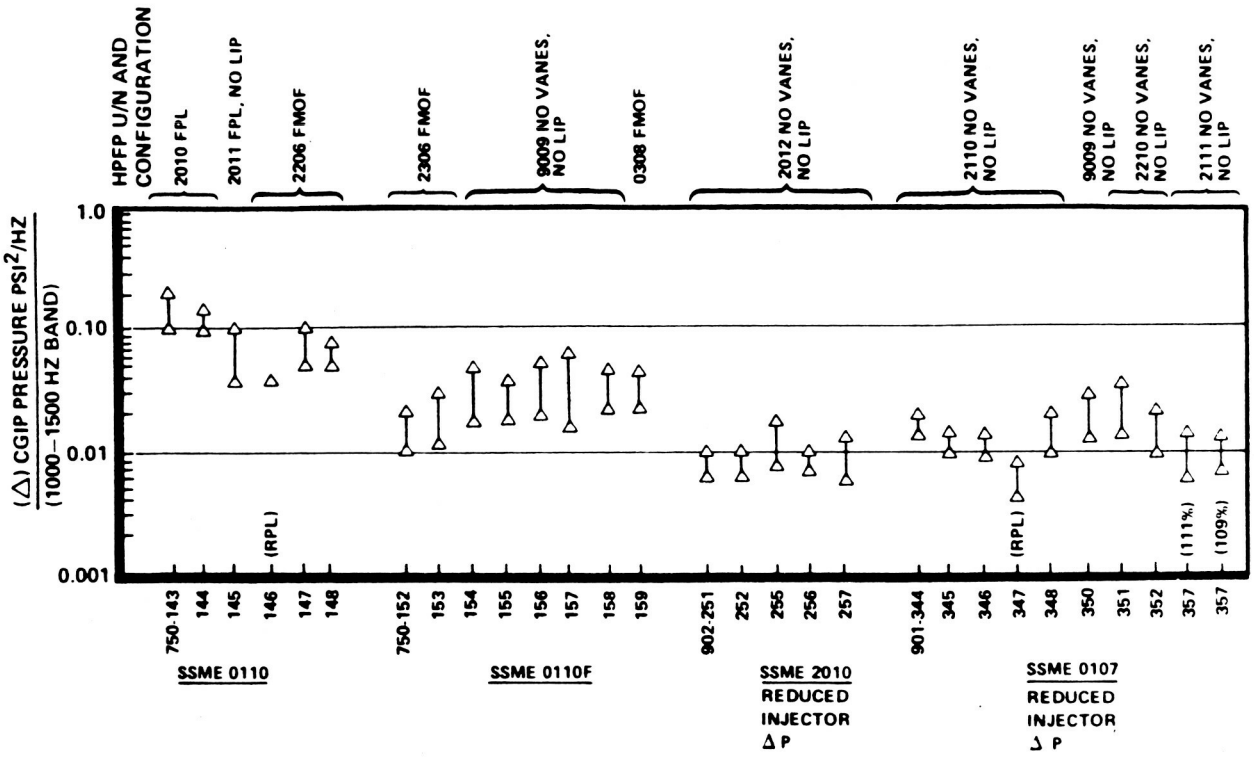

FIGURE C.13 SSME HGM PRESSURE FLUCTUATIONS AT FPL

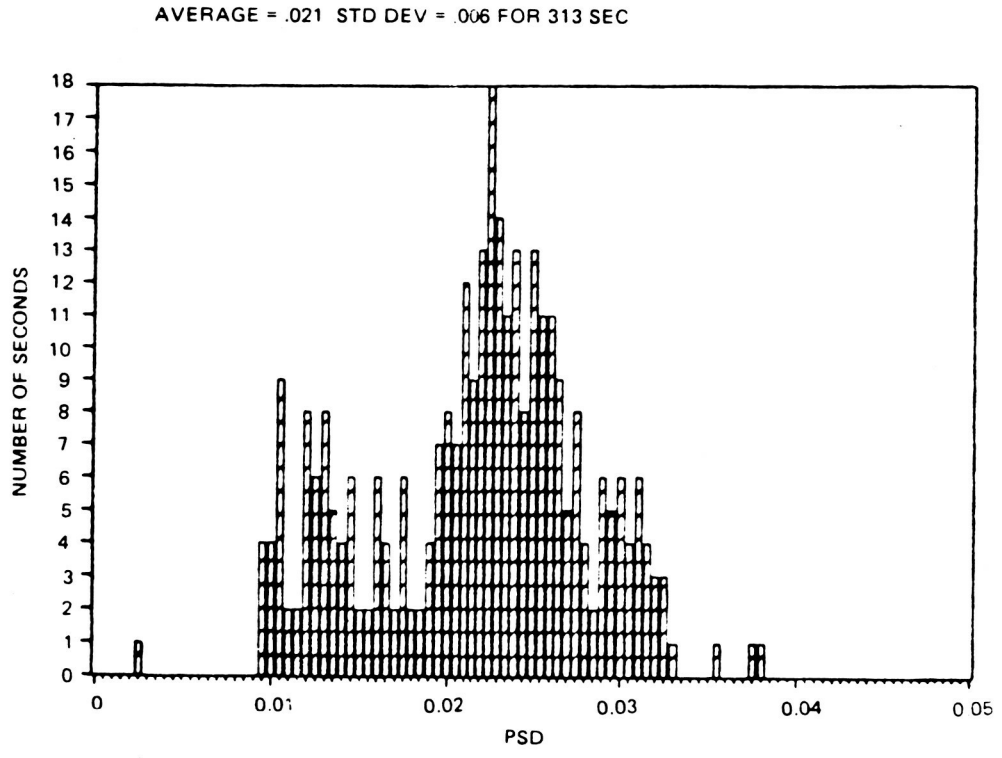

FIGURE C.14 CGIP PSD DATA FOR 9X09 HPFTP ON A-3 TEST STAND FOR 313 SECONDS OF TESTING

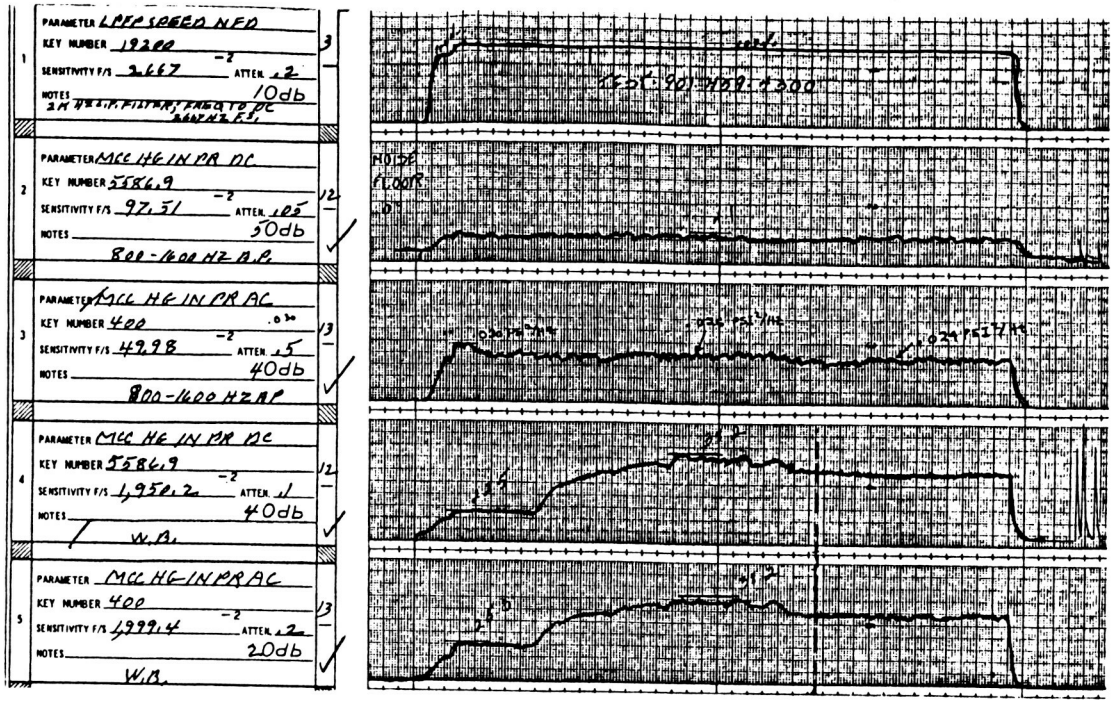

FIGURE C.15 TYPICAL VARIATION OF HIGH FREQUENCY PRESSURE IN MAIN INJECTOR

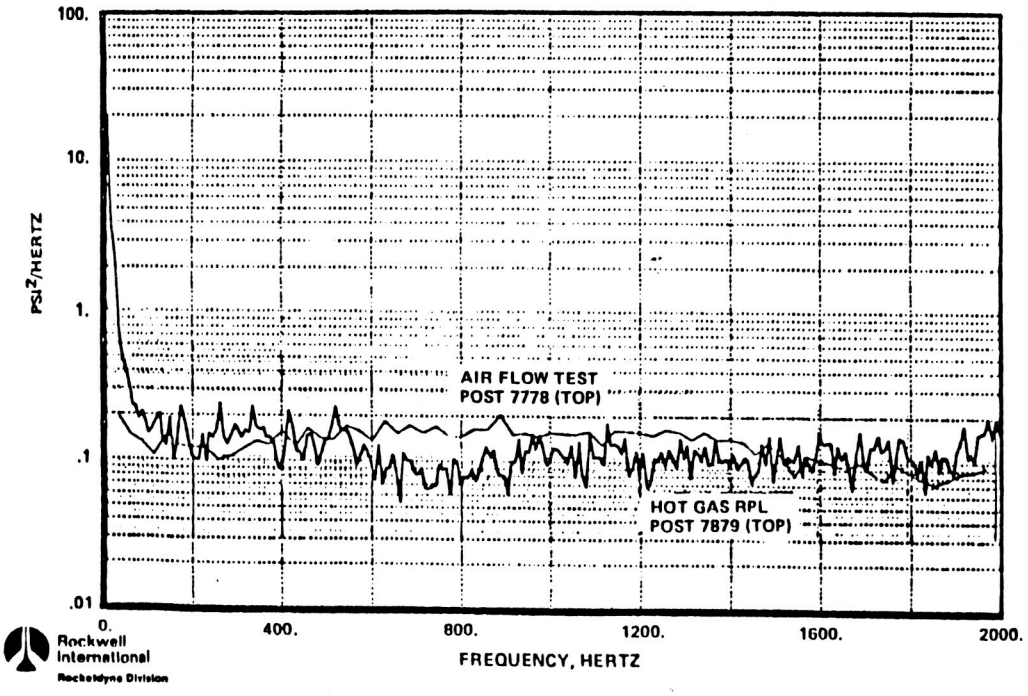

FIGURE C.16 COMPARISON OF EOTIOF & AIR FLOW TEST DATA -- LOX POST SHIELD PRESSURES

Figure C.16 shows the flow field survey from the simulation tests of the engine O11OF configuration. The characteristic shape is a mean random level with some variation in excitation superimposed. For the SSME, the fluctuating pressure in the main injector is random. Figure C.16 also shows the steady state operation comparing engine data with scaled simulation test data. The randomness in both sets of test data can easily be seen. Since this type of data is available for SSME, scaling techniques can be developed which will allow this data to be extended to the other similar injector configurations.

C.4 Temperature Loads

General. The thermal load on a LOX Post is the result of the temperature difference between the LOX flowing inside the post, the geometry of the post. and the fuel flowing across or along the outside of the post. These thermal loadings, combined with the heat transfer coefficients and conduction capabilities, result in the metal temperatures that herein are considered as temperature loads. The temperatures and gradients on LOX posts vary considerably from engine to engine or injector type to injector type. The primary difference is the heating effect of the fuel rather than the effect of the LOX. For coaxial injector elements, considerable care is taken so that all LOX Posts in an injector have the same inlet and outlet pressures as well as the same flow from performance considerations.

The allowable temperature range of the LOX Is also quite narrow. i.e., less than 50° for the engines considered. The flowrates vary considerably, by a factor of 10, for these same engines (see Table C.1). The fuel temperatures are a strong function of the engine cycle. For the staged combustion cycle, like the SSME, the preburners have cool hydrogen fuel (280R) and the main injector has hot hydrogen enriched steam (1600R) as a fuel. This difference in gas temperature makes the thermal loads on the main injector an important variable in structural analysis, and an insignificant one on the preburners. The thermal loads will always be a consideration in the main injector of a staged combustion cycle engine, and usually for an expander cycle engine, since these two types of engines end up with significant ΔT's across an individual post.

TABLE C.1 DESIGN GEOMETRY OF COAXIAL ELEMENTS (GH_2/LO_2) FOR VARIOUS ROCKET ENGINES

ENGINE	#COAX ELEMENTS	(IN) FUEL SLEEVE DIA. (O.D.)	(IN) OX. POST DIA. (I.D.)/O.D.	(IN^2) AREA OX/FUEL	LB/S FLOWRATE PER ELEMENT OX/FUEL	LBS. THRUST/EL	CUP RECESS	ΔP_{OX}	ΔP_{FUEL}	P_C	INJECTOR DIA. (IN)	INJECTOR FACE TO THROAT LENGTH	CONTR. RATIO	AT THERMAL LOX TEMP	AT THERMAL FUEL TEMP
J2	614	.332	.182/.244	15.97/25.26	.741/.118	325.0	.200	207	102	787	18.50	17.926	2.30	180°R	195°R
H1	3248	.334	.210/.290	139.5/70.15	.831/.153	300.0	.231	335	175.0	1000.0	42.17	30.0	1.74	180°R	140°R
SSME M.C.C. (FPL)	600	.389	.188/.220	16.66/46.38	1.42/.4298	783.0	.255	641.7	251.2	3000.0	17.74	14.0	2.96	191	1444
J2S	614	.323	.119/.254	19.10/19.20	.849/.132	431.0	.200	210	130.0	1245	18.50	17.926	1.51	180	257
RL-10	216	.186	.014/.120	.9289/3.426	.130/.024	10.3		52.4	77.6	395.0	10.30	15.0	4.0	167	451
ADV. EXP. CYCLE	108	.190	.094/.126	--	.247/.0357	--	.093	--	--	1540	5.0	20.0	3.85	183	660

For most injectors, the fuel flow relative to the post is a cross flow from a distribution manifold at the outer diameter of the injector with flow radially inward. The flowrate reduces from a maximum at the manifold to something less at the center of the injector as a portion of the fuel flow is metered to each LOX post.

As previously discussed, the spray bar injector is different in configuration, but there is still hot gas transverse flow across the tapered manifold portion of the bar and axial flow along each individual LOX tube.

For a specific injector design, each LOX post will have a somewhat different temperature. For radial flow injectors, the fuel flowrate in the radial direction is reduced as the radius decreases. This causes the inner cylindrical rows of posts to be cooler than the outer rows. LOX post temperatures within a given row are affected by the non-uniform circumferential distribution of the radial flow. Manifold design for a given injector is the primary contributor to this inlet flow non-uniformity.

Another key variable in a LOX post temperature profile is the geometry of the post and its associated hardware. In cases where the thermal loads are a minor load, the LOX post is a simple tubular structure, such as the SSME preburners, J-2, etc. For the SSME main injector, where the temperature loads on the LOX posts are a primary load, considerable thought and special protection is utilized to keep the LOX posts cool in critical areas. The heat shield retainer shown in Figure C.17 is an example of a thermal protection barrier that is used to keep the injector to LOX post weld joint cool. The flow shields in this same figure, which are not for thermal protection, also cause perturbations on the ROW 13 (outer row) LOX posts.

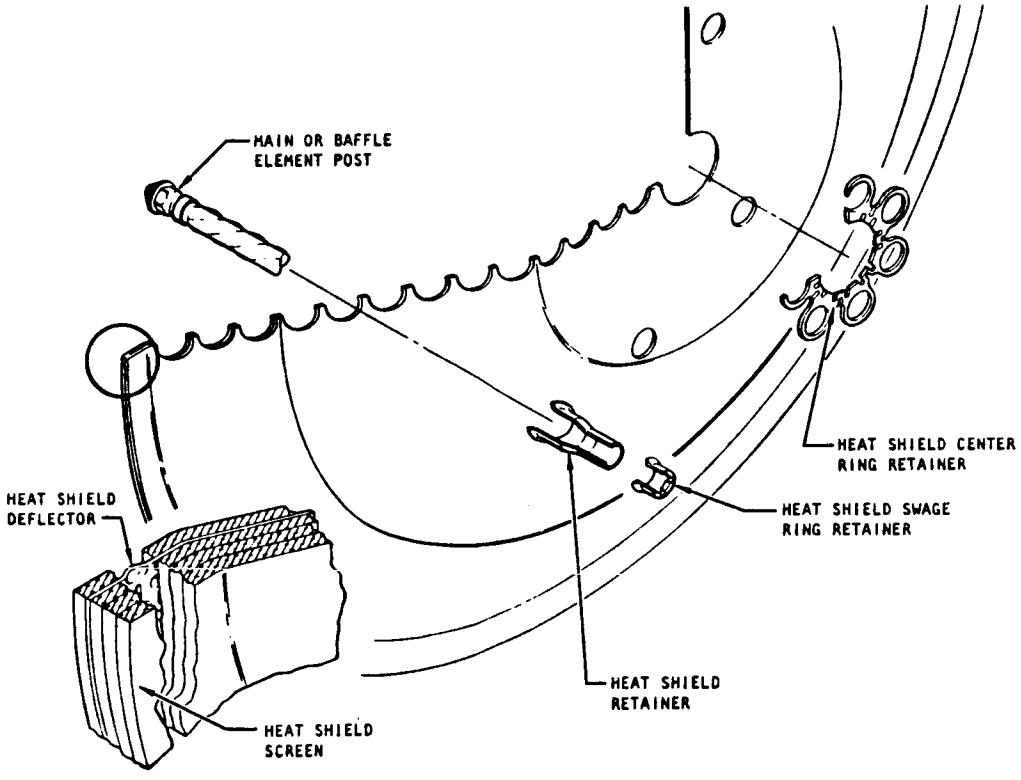

FIGURE C.17 EXPLODED VIEW OF HEAT SHIELD ASSEMBLY (RS009142)

A combination of engine measurements and calculated parameters will be used in the definition of the actual injector thermal load distribution. Measured data, such as MCC fuel injector pressure, MCC oxidizer injector pressure, and turbine discharge temperature are recorded for each SSME engine test. A large data base of these measurements is available. Typical pressure data is shown in Figures C.18. Actual LOX post temperature has not been measured during SSME engine tests.

For the SSME, simulation tests have been performed using full scale hardware to define the flowfield entering the injector. Further discussion of the flow effects are covered in the flow loads discussion. These simulation test results will be used with calculated variables to furnish flow conditions on the LOX posts. This data will then be combined with the measured engine data and used to obtain LOX post temperatures. Analysis results are available that describe post temperature for the baseline SSME configuration. These baseline results can be scaled on an engine test by test basis to cover a wide range of operating profiles based on the combination of measured and calculated pressures, temperatures and flow conditions described above. Actual LOX post thermal loads will, therefore, be based on calculations anchored to measured flow data, but not actual LOX post temperature measurements. The procedure used in calculating the baseline SSME main injector LOX post temperatures is summarized at the end of this section.

Main injector LOX Post Thermal Loads. Main injector LOX posts require accurate thermal analysis because of their long and slender profile in an environment which exposes them to high velocity hot gas (hydrogen-rich steam) across the outside and high velocity LOX flowing axially through the interior of the post. Due to profile contour changes on the exterior of the post for attachment at either end and the main body swirl section, the posts have stress concentration areas in the region of high loading. An accurate assessment of temperatures helps to given an accurate prediction of structural safety factors and is essential to determination of thermal cyclical fatigue.

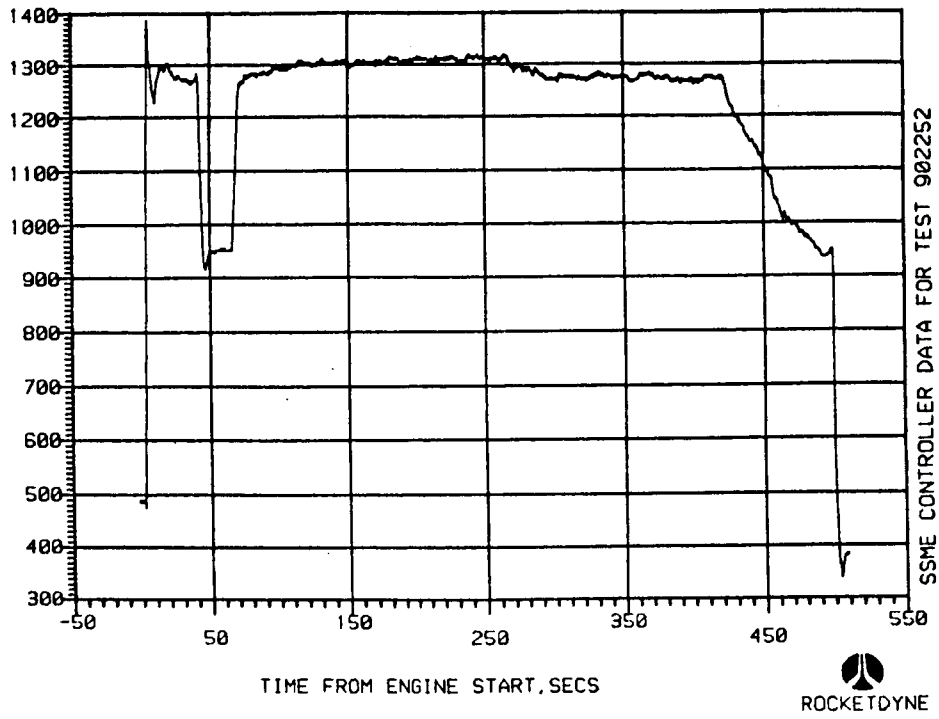

FIG. C.18 HPOT TURBINE DISCHARGE TEMPERATURE

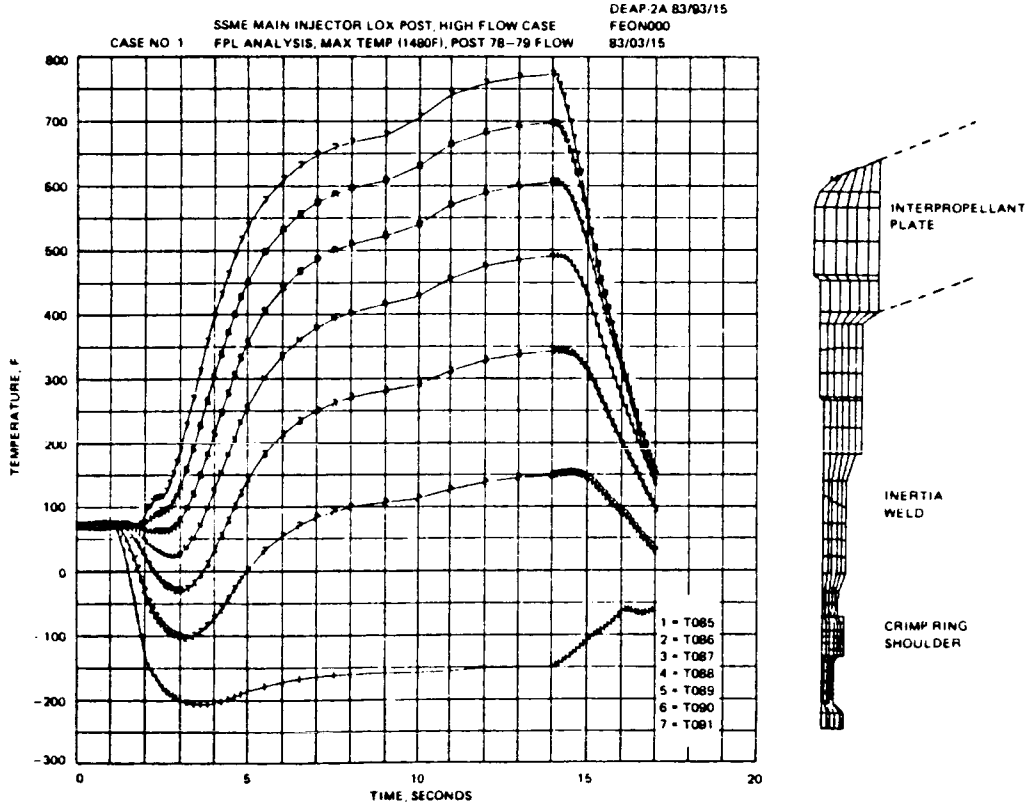

FIG. C.19 LOX POST UPPER END FULL TRANSIENT CYCLE

Thermal Load Analysis Methodology. The heat transfer through the post, from hot gas to LOX, is affected by six factors: (1) exterior hot-gas temperature; (2) exterior hot-gas film coefficient; (3) thermal conductivity of the post walls; (4) peripheral ports on the post surface (heat shield retainer, stage ring, secondary faceplate retainer); (5) interior LOX temperature; and (6) interior LOX film coefficient.

Hot-gas temperature is measured at the turbine exit, upstream of the injector post field. The hot gas is cooled slightly as it travels to the main injector. The hot-gas temperature changes slightly from test to test, with more significant variations between engines, engine configurations and power levels. These variations can be up to hundreds of degrees apart due to all the influencing factors.

The hot-gas heat transfer coefficient is based on characteristics of cross flow over tube banks (as encountered in many heat exchanger arrangements). where results of various investigations have been correlated into a formula. This correlation is for smooth, regularly spaced tubes in cross-flow. The main injector LOX posts are not smooth, the hot-gas flow has a significant axial component, and although tube spacings are generally regular they are not in a uniform pattern. A test program in the year 1982 verified that in the main body section of the posts, this cross-flow over tube banks correlation was applicable to the LOX posts in the outer four rows. Therefore, the hot-gas heat transfer coefficient in the outer rows, where failures have predominantly taken place, can be closely modeled by established and verified analytical methods.

At the ends of the post (near the interpropellant plate and the secondary faceplate), the film coefficient is modified following classical trends. This modification of the "main body" film coefficient then allows the ends of the post to be analyzed with high confidence.

Thermal conductivity through the post wall is a well-defined phenomenon. The thermophysical properties of the post have been documented and with the geometry of the post known, the thermal resistance through the post is established.

Additional parts added onto the post affect the heat transfer into the post. Added material acts either to increase the path length of heat transfer through the metal, or as a convection shield to the post, protecting it from the impingement of high velocity hot gas. Knowing the size, shape, and orientation of these parts, their effects can be added into the computational basis for heat transfer through the post.

The temperature of the LOX (the heat sink for the LOX post) is well defined by engine instrumentation, LOX pressure, and flow considerations. The LOX temperature does not vary much, as it is within an approximately 20 degree operational envelope for all engine configurations and power levels of operation.

The interior of the post has a heat transfer coefficient that is calculated with a classical "flow through a tube" method. This is very representative of the actual flow of LOX through the interior of the cylindrical post. This heat transfer coefficient is calculated differently for the entrance end of the post because of both diameter changes and entrance effects as the LOX begins axial flow through the post. Both of these effects have theoretical correlations. The most suitable were selected for application to this specific case.

Detailed thermal models of the LOX post have been made all along the post-upstream end, swirler, post-retainer, tip end. A typical model is the upstream end of the post that includes the interpropellant plate attachment, inertia weld, and the post to the crimp ring, Figure C.19.

A thermal test program in the year 1982 verified to a large extent both the heat transfer coefficients used in analytical simulation of SSME operation and the overall energy balance of the main injector operation. Confidence on an overall basis is very high. For a local area, the strength of the analysis is directly related to the accuracy of the assumptions. The smaller the local area, the more important the assumptions (part to part contact, effectiveness of a seal, boundary conditions) become. When the assumptions are not well known, a range of realistic conditions are selected which will bound the extremes of actual operating conditions.

Temperature Mission-History-Profile. The typical mission history profile for a LOX post is shown in Figure C.19. This is a duty cycle thermal analysis of the upper end of the LOX post. The temperatures are for thermal nodes through the inertia weld cross-section. The basic mission-history-profile will be a nominal value with statistical variations about this profile. The start and cutoff flow transients do not have sufficient shock effects to reflect a measurable post temperature oscillation. Transients are small gradients, and steady-state temperatures have no thermal shocks or high frequency variations.

C.5 Static Pressure Loads. The pressures on LOX Posts for the SSME engine are based on measured data in manifolds and pressure cavities on the injectors. The final LOX post pressure is the combustion chamber pressure that is the lowest pressure in the injector. System pressures to feed the injector are based on this required exhaust pressure. The pressures are measured on each engine ground test so there is a large available data base. Most of the measurements are low frequency digital data parameters, such that high frequency content of the signal is lost. Only the preburners have high frequency pressure instrumentation. By using a combination of the main injector and preburner data, a realistic generic mission-history-profile can be developed that has both low frequency and high frequency content. The significant features of injectors relative to LOX/LH_2 engine LOX post pressures are shown in Figure C.20 and Figure C.21. The primary LOX posts have both oxidizer and fuel related affects.

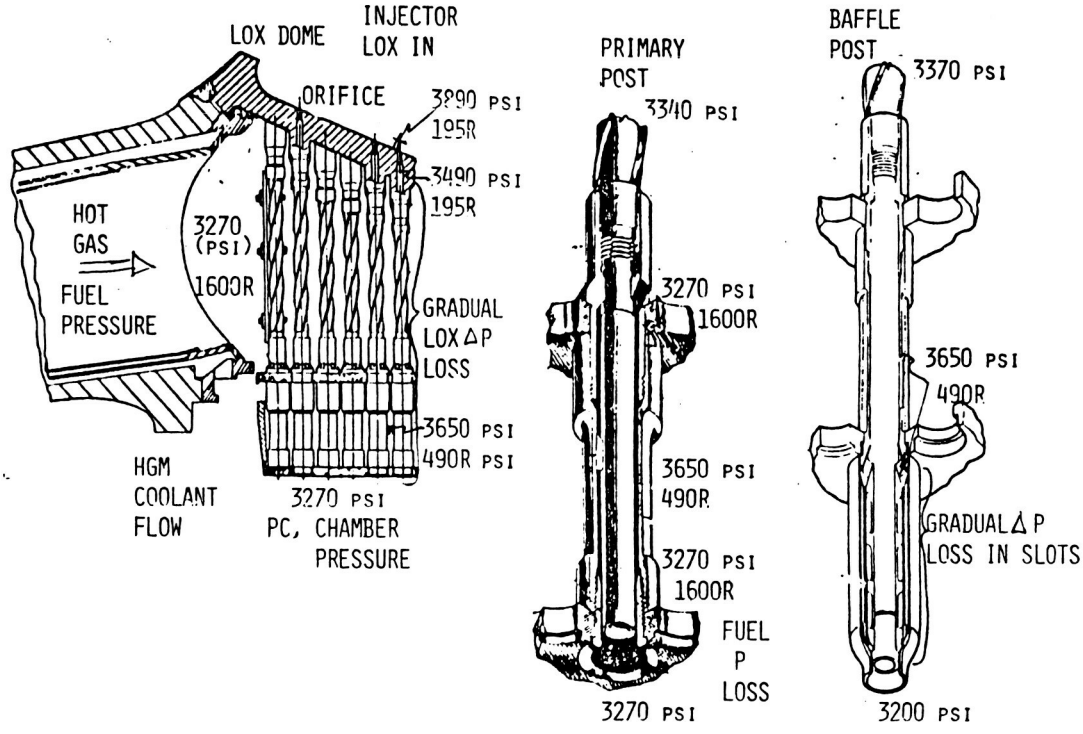

FIGURE C.20 MAIN INJECTOR LOX POST PRESSURES

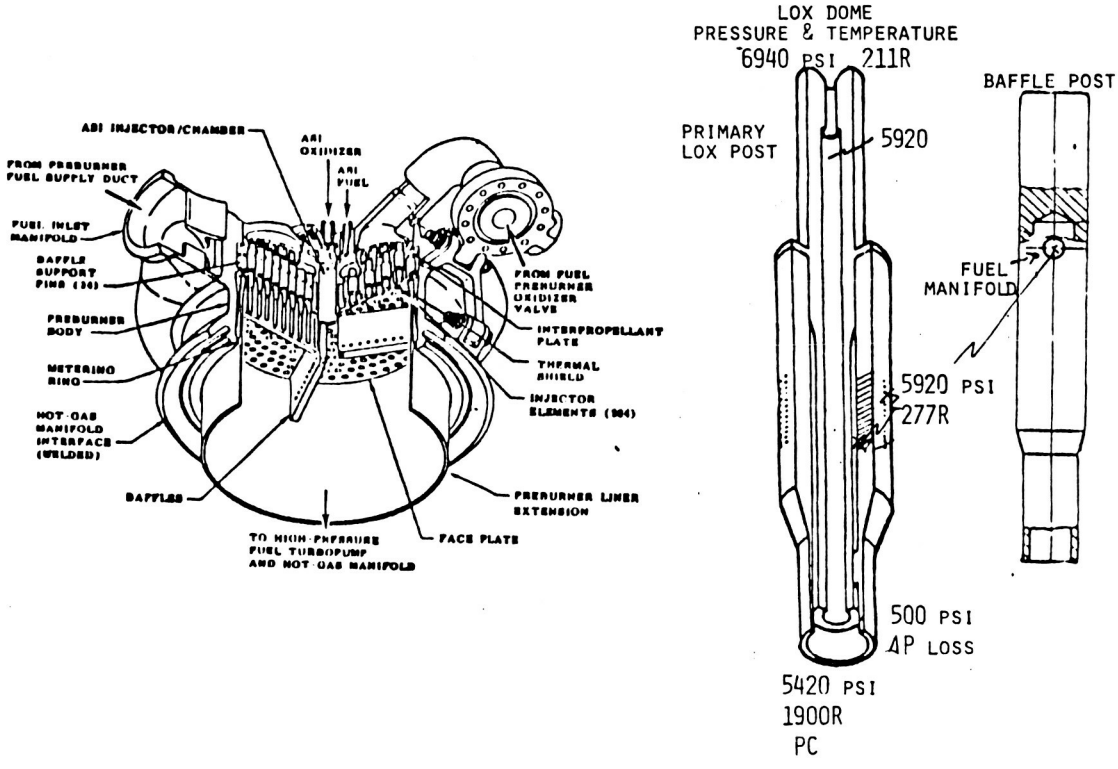

FIGURE C.21 FUEL PREBURNER LOX POSTS

Oxidizer related. A LOX dome and manifold that are designed to evenly distribute oxidizer to each injector post so that uniform combustion is obtained at the injector face. This is a primary consideration for engine performance so significant effort is placed in the design phase of all injectors to insure this "uniform" distribution. It includes inlet design of the ducting and manifold-LOX dome design, lab testing and engine evaluation through maldistribution indicators. The indicators are typically low performance and combustor wear such as hot spots and distress - that are attributed to "injector effects". The LOX systems are typically designed with a metering orifice at the inlet to the LOX post to aid in equalizing the flow to each post. The pressure loss along the inside of the post from fictional effects is small and a small ΔP loss occurs at the injection point into the chamber. The measured pressure is the LOX dome pressure.

Fuel Related. Typically, there is one fuel manifold and cavity for an injector that distributes the flow to the outer portion of the coaxial LOX post element that carries the fuel. This manifold is designed in a manner similar to the oxidizer distribution system to minimize pressure differences and flow for each LOX Post in the injector.

Baffle post elements may be different for each design or may be incorporated into a plate struture. The SSME has two basic configurations.

Main Injector. This element is an active combustion LOX post, but uses cold hydrogen gas for the fuel rather than the partially burned hot gases used for the primary LOX post. The cooler gas is required to keep the baffle extension in the main combustion zone at an acceptable temperature. In this element, the hydrogen is passed to the outer coaxial cavity through small holes in a cylinder. The major portion of the ΔP losses in the fuel are taken in the cooling slots in the baffle extension.

Preburner. The baffle posts are not true LOX posts in that they are closed to LOX and have a single hole that ducts fuel to the baffle plates. These ports are served by the same fuel flow system as the primary LOX Posts since the fuel is cool enough to keep the baffles at a reasonable temperature.

The injector inlet pressure has a low level pressure oscillation (CHUG) during injector prime followed by an increase in pressure to steady state. Pressures change in steady-state to meet power level requirements of the engine. At cutoff, pressures decrease with another minor chug as the system empties of fluid. The fuel pressures are similar except there is no chugging - the fluids are gaseous. The chamber Pc shows effects of chugging and ignition "pops" during both start and cutoff. There are also "pops" post test as all the residual GOX and GH_2 flash and burn up excess propellants. The Pc in steady state for the SSME engine shows no combustion instability effects, but from a generic description a random occurring pressure oscillation over the steady state pressure is included. This oscillation could feed back into the other pressures in the injector through back pressure changes in the system. The pops and chugging have not been shown to have a deleterious effect on the SSME LOX Posts. The chugging is very low pressure compared to the operational conditions. The pops have caused problems in other areas of the injector such as the preburner ASI.

Typical pressure magnitudes and distributions on an injector are shown in Figure C.18 and C.19. The SSME injectors primary structural sizing is not significantly affected by the static pressure loads. Off design pressure conditions that can occur during development and operation of the engine include:

1) Plugged ports where the LOX flow is eliminated.
2) Local starving of the main injector HGM coolant flow. This reduces cooling and increases the mixture ratio. Baffle tip erosion on two engines has been attributed to this problem.
3) Debris constricting the flow through the main injector LOX posts may result in LOX post tip erosion and off nominal combustion.
4) Face plate cracking and added film coolant holes can effect flow and pressures to a minor effect in the cavity between the faceplates on the main injector.

The AMS high frequency traces of the preburner Pc's show the start and cutoff ignition and dome prime effects - pops and chug effects, see Figure C.6.

C.6 Debris Loads

The hot gas flow area of the main injector lies at the end of the hot gas flow path of the engine and is effectively a strainer for contamination or missiles that occur in this system. These items can impact on the LOX posts or LOX post shields depending on their size and location in the flow. Judgment (expert opinion), the actual engine configuration, and some traceable history of these items can be used to define the debris occurrence and loading. The randomness and uniqueness of each occurrence makes the degree of certainty low for this load.

The information is used as a qualitative criteria or concern during design - e.g., it is a current consideration for keeping flow shields over the SSME injector and screens are used on other injectors. The effects of pieces removed from injector hardware are evaluated from an anomaly analysis. No SSME injector has failed from this type of loading.

C.7 Static Loads

Static loads on the injector and influencing LOX posts can include the following effects.

Engine gimbal bearing reactions when the injector is attached to the gimbal such as the SSME Main injector. The preburners do not use this load except for inertial effects from engine oscillations. These distribution loads are resolvable from engine or flight test data.

Fabrication loads can be divided into welding or brazing effects, assembly loads and overall static loads. Brazed in LOX posts have by the nature of fabrication, some residual stresses. These loads are of an indeterminate magnitude, but are a consideration from the brazing processing requirements and braze selection. The loads are usually not considered in a structural analysis except in very special applications.

The assembly of an injector like the SSME main injector with 600 posts where a flat faceplate must be butted against the injector retainers inherently builds in random loads in the posts even with close process control, e.g., there have been injector MRD's during fab with buckled or stretched posts during faceplate assembly. The loads are essentially indeterminate, but are one of the reasons the dynamic analysis considers the LOX post thread conditions to be variable from a fixed to pin condition - a needed probabilistic structural variable.

The other "static" loads on LOX posts are overall injector ΔP loads that are reacted across the faceplate and the differential thermal expansions throughout the injector and overall structural deflections such as loads in engine gimbaling.

Static loads that are analytically quantifiable are typically developed as part of an overall injector model where discrete load conditions in the duty cycle are analyzed and resulting LOX post loads or misalignments-end deflections determined. These loads are added as additional perturbations to individual LOX post analysis where temperature and pressures are considered. The overall injector is essentially elastic, so these loads are nominally accurate if the LOX posts act elastically - which is usually the case. The outer three or four rows of the SSME main injector LOX posts do not meet the elastic response requirement when combined with the total loads on the posts, but this is not considered a key parameter in the overall injector model.

C.8 Configuration and Material Effects

A $\pm$ 10% variation is allowed for in all sinusoidal forced vibration analysis This allows for any one of a number of small effects that would shift the forced response of the model. This can be thought of as either a load or a modeling variation. The shift can occur from tolerances, material property variation, component to component differences that vary performance and pump speeds and fabrication variations that can influence fixity of joints. This "load variation" should be included in part through the probabilistic distribution of the load components and probabilistic distribution for geometric variations in the PSAM contract work.

C.9 Damping

Vibration damping effects in the injectors are varied as a function of geometry. Damping usually is related to the amount of sliding surfaces available for developing Coulomb friction that is equated to equivalent viscous modal damping. The preburner posts are brazed assemblies with no rubbing structure and have low damping. The main injector Row 13 shielded post damping was determined from strain gage response related model results (Figure C.12) and the Row 1-12 damping was inferred from equivalent cracking assessment of engine hardware. The damping coefficients are utilized in the structural dynamics models and are a key parameter for determining post responses to loads. Test data and measurements are limited.

C.10 Available Mission-History-Profiles for Theory Verification/Validation

Introduction

The amount of data available for verification or validation varies with the individual load component. For load components where measurements are taken each engine test there is an extensive database - vibration accels, chamber pressure, manifold pressure. Other loads such as LOX post temperature have no engine verification.

To date, there has been one instrumented injector - Engine 0110F - that had LOX post strain gages and added pressure measurements to assess LOX post loads, see Figure C.10. Air flow simulation tests, though, maybe partial validation for this effort. There are planned tests for an instrumented injector in the current development contract and the test bed engine has instrumentation schedule for the main injector.

Air Flow Tests

Air flow testing of full-scale SSME hardware has been an important method for understanding the powerhead flowfield and testing new design concepts.

The tests are conducted at Rockwell's North American Aircraft Operations (NAAO) Division in El Segundo. Full-scale test models that have been used include a "solid-wall," three-duct hot-gas manifold (SWHGM) contour machined out of CRES, an actual three duct SSME hot-gas manifold modified to a two-duct design (Technology Model), and a more refined two-duct HGM Model machined from CRES, Figure C.22. All of the HGM test models contain hardware for the simulation of the fuel and oxidizer turbine exit flows and pressure drops. The main injectors used in the models are actual SSME Injectors modified as desired for the air flow test programs. All of the models contain extensive digital and high-frequency instrumentation.

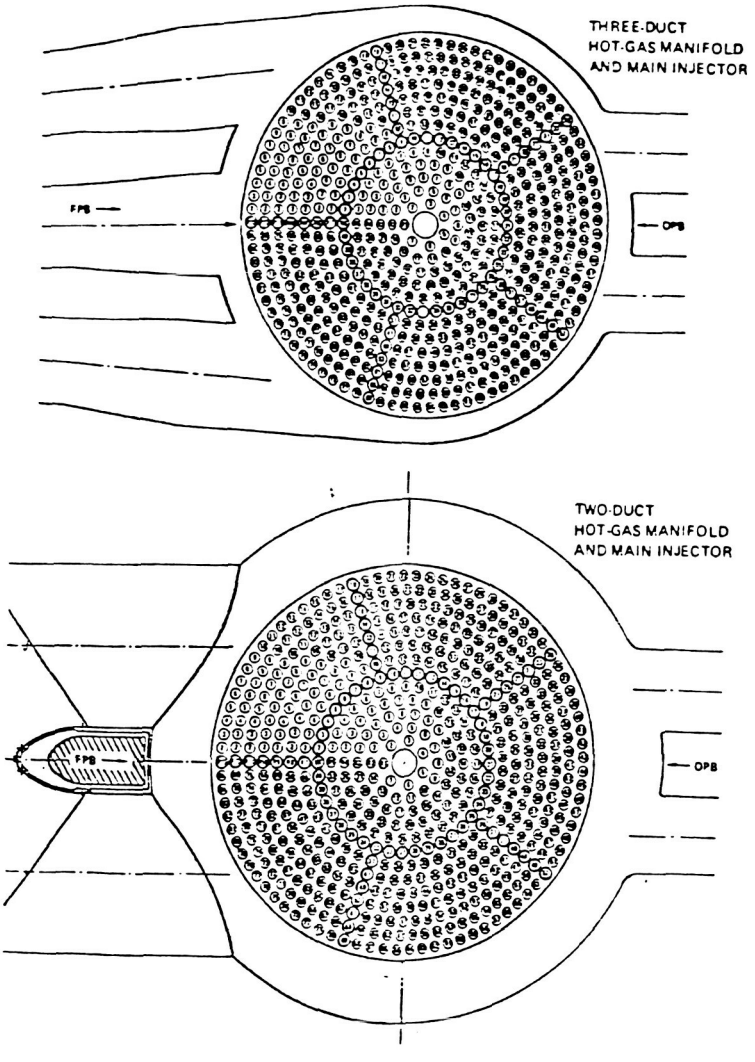

FIGURE C.22 THREE AND TWO DUCT HOT-GAS MANIFOLD DESIGNS

The air flow tests typically consists of a 30-second duration blowdown of ambient temperature, 2.27 MPa (330 psia) air. Mass flowrates during testing are nominally 45 kg/sec (100 lb/sec). This represents approximately 70% of the engine operating condition Reynolds number and since it is in the highly turbulent regime is sufficient for accurate modeling. The Mach number is far less than one, as it is in the engine, indicating incompressible flow. Methods for scaling fluctuating pressure measurements in the air flow tests to hot-fire conditions have been developed, and Figure C.23 shows the similarity in fluctuating pressure levels for hot-fire engine 0110F and scaled three-duct SWHGM air flow tests. These similarities add further confidence to the accuracy of the SSME flow modeling.

This air flow test technique has been used to provide valuable input for the evaluation of the two-duct HGM design. The Technology Model test results have indicated drastic improvement over the three-duct configuration in system and component pressure drops and main injector fluctuating pressure (Figure C.24). Testinq of the two-duct model has resulted in even further refinement in the two-duct design.

Interest in the flow field in and approaching the main injector has resulted in measurements of the transfer duct exit flow velocity. A Mach number profile of the fuel-side transfer duct obtained from two-dimensional probe data is shown in Figure C.25. High-frequency instrumentation has been used to measure LOX post fluctuating strains as well as transfer duct and LOX post fluctuating pressures. Further investigation of the main injector flowfield will be obtained in future tests that will use three-dimensional probes in the transfer ducts, two-dimensional probes in the main injector and extensive total pressure measurements in the main combustion chamber. These later data will be used to anchor the computational fluid dynamics model. Apart from understanding the SSME flowfield and testing new designs, a particular emphasis for certain air flow tests has been the investigation of LOX post stability.

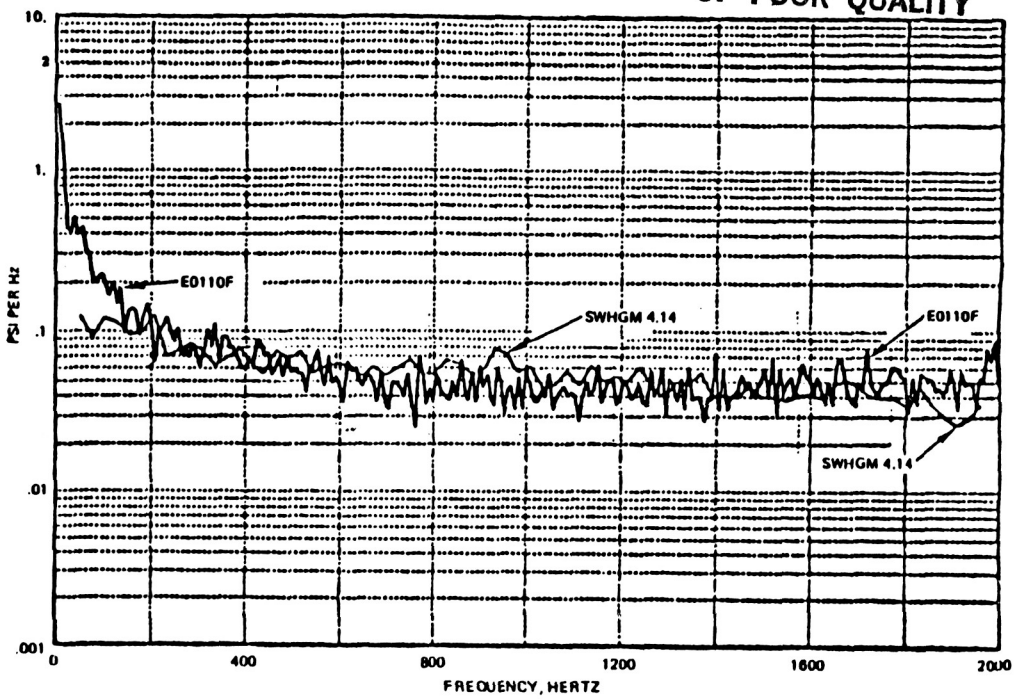

FIGURE C.23 FLUCTUATING PRESSURE RESULTS AT SHIELD 5455 FOR THREE-DUCT SWHGM TESTS (SCALED) AND HOT-FIRE ENGINE 01105

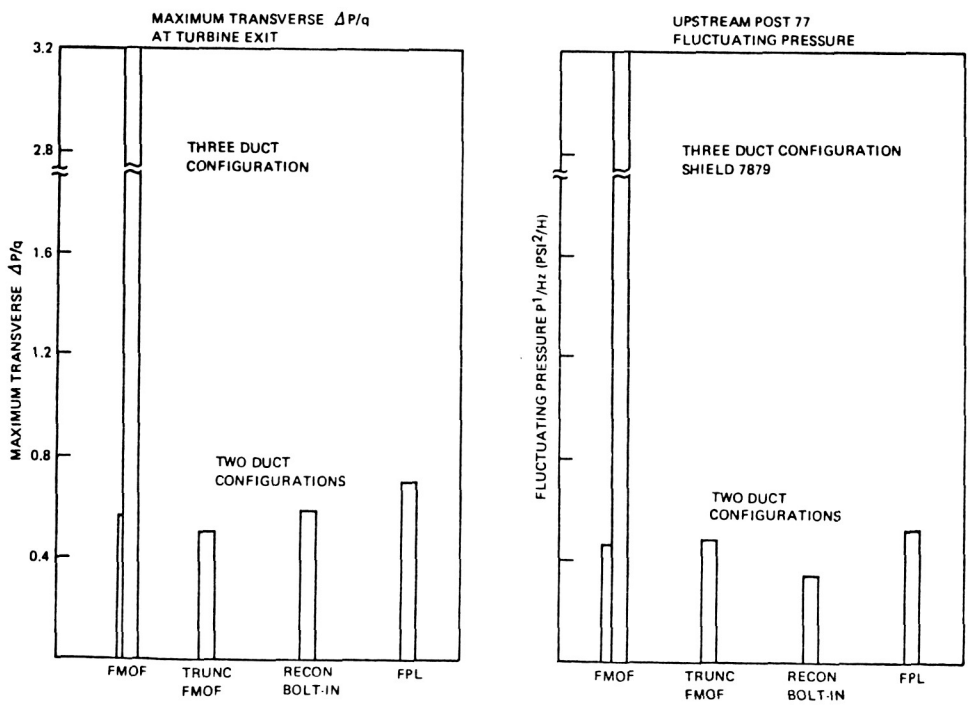

FIGURE C.24 TYPICAL PERFORMANCE OF TWO-DUCT HGM TURNAROUND DUCTS COMPARED TO THREE-DUCT HGM

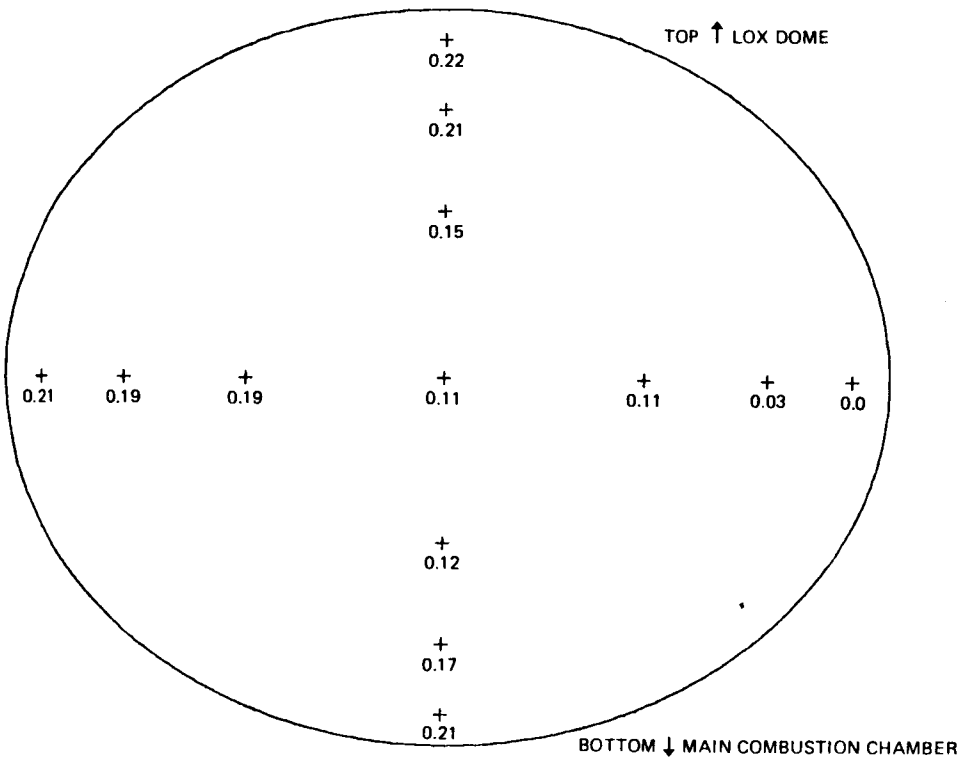

FIGURE C.25 TRANSFER DUCT EXIT MACH NUMBER MAGNITUDE AND DIRECTION FROM TWO-DUCT CONFIGURATIONS

Planned Instrumented Turbine Tests in SSME Development Program

The current development plan has planned injector measurements for the two-duct hot gas manifold. The main injector of Engine 0209 will have selected oxidizer posts fitted with strain gages which record metal strain at or near critical points of stress. while the two-duct hot gas manifold, with its larger flow areas and well-contoured transition zones, is expected to cause a more benign environment, comparisons with the three-duct HGM are desired. Considerable gage redundancy has been built into the measurements, since a high attrition rate of gages is expected throughout the manufacturing, processing, and testing process.

The injector will be fitted with 48 gages with 16 of the gages located at the oxidizer turbine discharge transfer ducts. The conditions on the oxidizer side are expected to be no worse than that of earlier engines, although no previous measurements have been made there.

APPENDIX D SSME HOT GAS MANIFOLD TRANSFER DUCTS LOADS

D.1 INTRODUCTION

An assessment of the individual loads on the SSME hot gas manifold transfer ducts are furnished in this appendix. The information potentially available for load model evaluation is also included. The information in this appendix is summarized in sections 10.4 and 10.5.

D.2 Structural Dynamics Excitations

The vibration and shock excitations into the transfer ducts are based on measured responses from the high pressure turbopump where the ducts are attached. For example, the input environment for the fuel side transfer ducts are located in Zone 1 of the engine, see Figure D.1, and are based on HPFTP accelerometer measurements. Figures D.2 thru D.4 are processed vibration data of representative accelerometer measurements in this zone. The AMS (amplitude squared) plots, Figure D.2, shows the vibration level characteristic for the entire test and furnishes a duty cycle characteristic shape for the random level. The start and cutoff transients furnish additional loading and are partially represented on the AMS Plot.

The ISOPLOT processing, Figures D.3, also represents the entire test as .05 seconds PSD (power spectral density) plots taken every second of the test. These plots show the sinusoidal harmonics of the high pressure pump speed and the variation in frequency vs. power level. Figure D.4 is a PSD of a 10 second snapshot furnishing detail level of the random and sinusoidal frequencies from 0 to 20KC frequency band.

The measured responses are used as dynamic base input accelerations for the individual transfer duct liner models. The actual zonal input used is enveloped data from several tests over a restricted frequency range. A generic load definition requires less restrictive definition of the loading and should cover a wider frequency band, i.e., to 10 or 20KC maximum frequency.

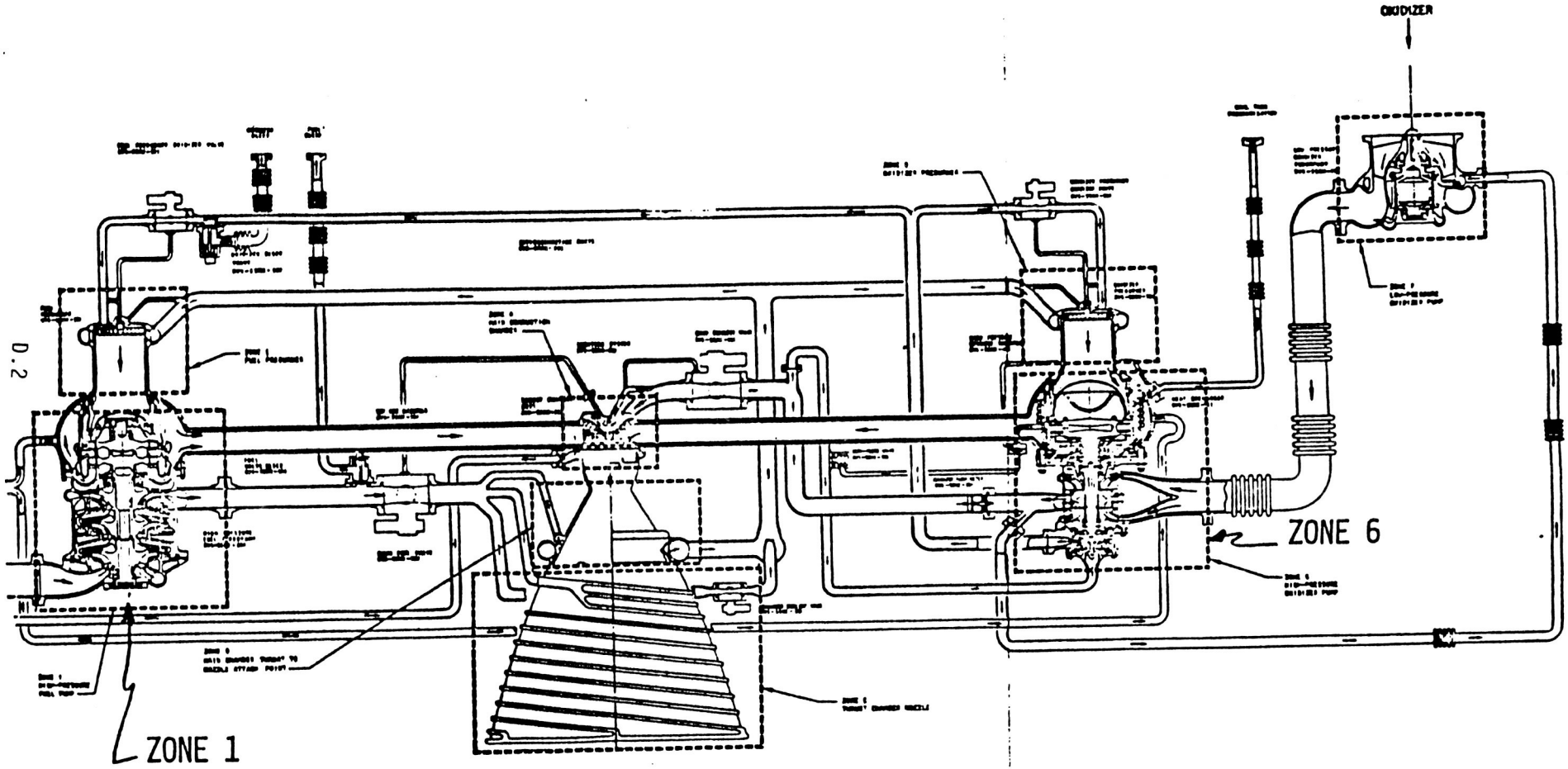

FIGURE D.1 MAJOR SOURCES OF VIBRATION (CRITERIA) ZONE LOCATIONS

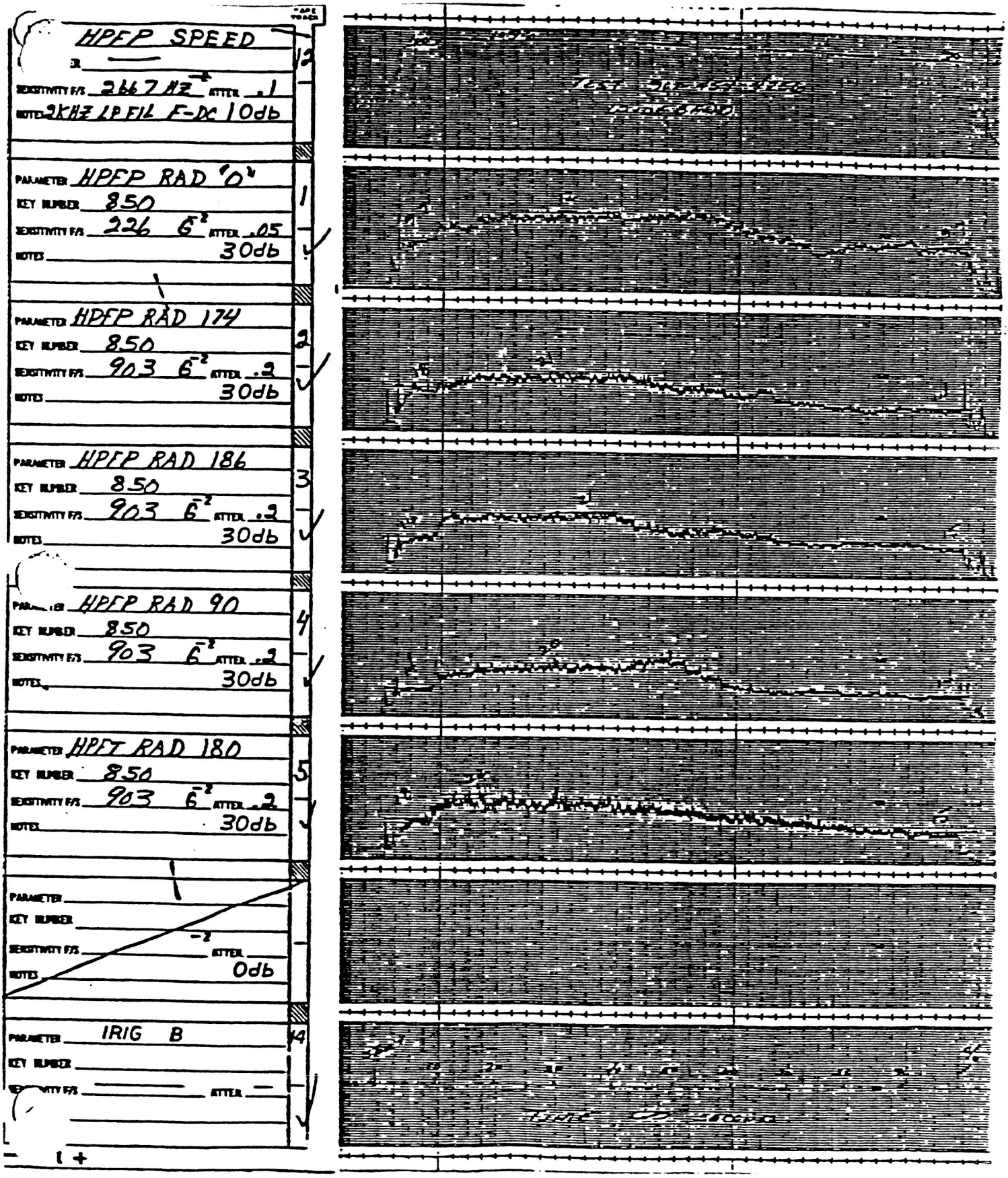

FIGURE D.2 AMS RESPONSES OF TRANSFER DUCT VIBRATION ZONE

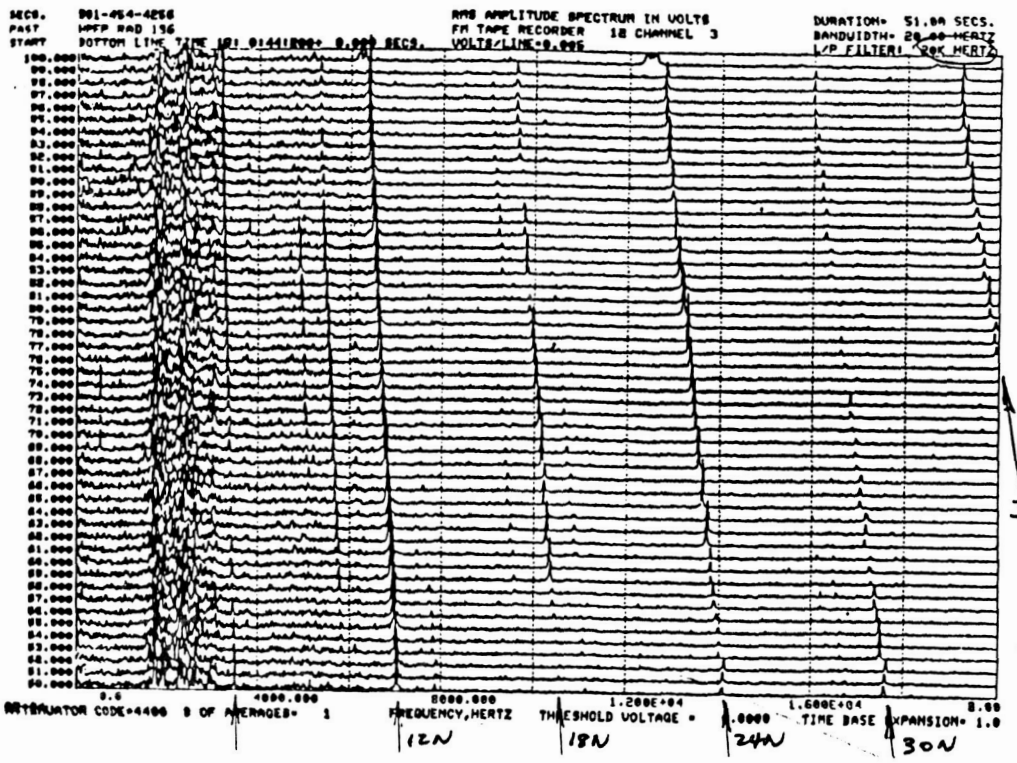

FIGURE D.3a ISOPLOTS OF TRANSFER DUCT VIBRATION ZONE

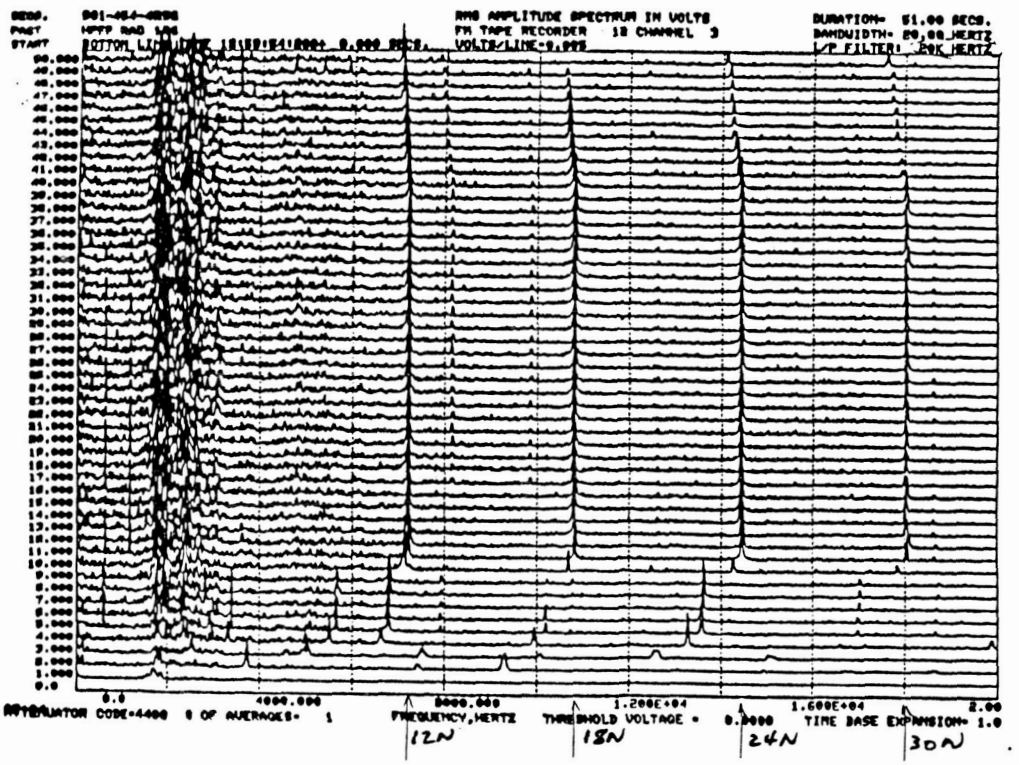

FIGURE D.3b ISOPLOTS OF TRANSFER DUCT VIBRATION ZONE

PSD

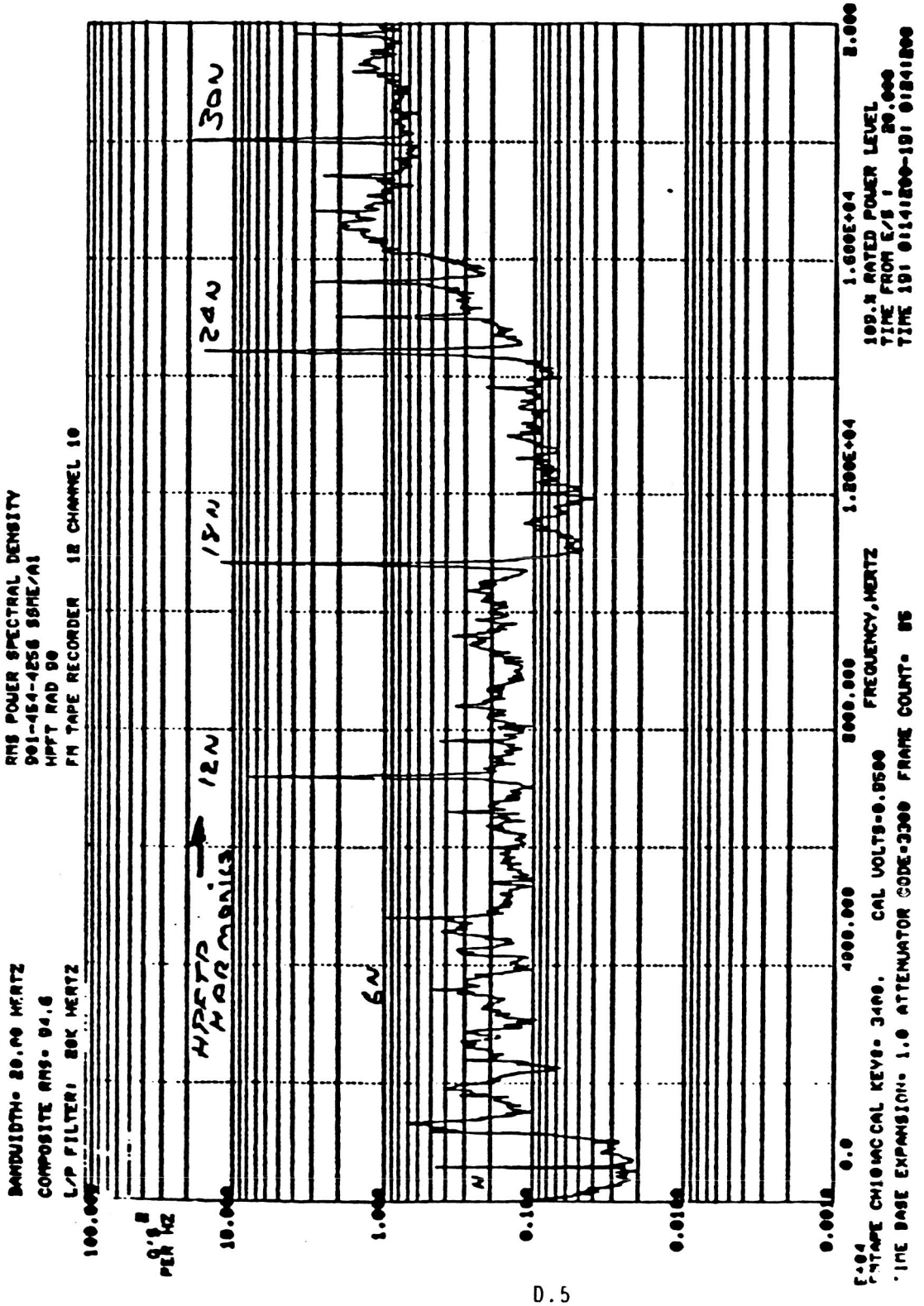

FIGURE D.4 PSD OF TRANSFER DUCT VIBRATION ZONE

The structural vibration mission history profile then is schematically shown on the AMS plot. It has a nominal level with multiple sinusoidal harmonics. The sinusoid level and frequency are dependent on power level and pump speed. Additional inputs to the mission history profiles are start and cutoff impulse loads from side load transients that add to the variable power level random vibration.

D.3 Static Pressure Loads

The pressure loads on the transfer ducts are based on measured pressures at location (CG1P) in the hot gas manifold (HGM) and scaled to conditions upstream of this measurement in the transfer duct. The engine transient and steady state models are used for obtaining the adjusted pressure values used for analysis. The HGM CG1P measurement is used only for the internal pressures on the duct. The external pressure of the coolant flow or the ΔP across the liner is based on the measured LPFP discharge pressure and the main injector chamber pressure. These values are also obtained from the engine model results. These "average" pressure loads assume uniform flow conditions through a cross section of the duct. Actual flow pressure distribution around the circumference of the ducts is based on airflow model measurements.

Figure D.5a,b thru D.6a,b are CG1P measurements from a specific test. On each figure the top trace shows DC pressure and furnishes the nominal average pressure. The shape of the curve is similar to the engine thrust curve. The bottom two traces on the figures are filtered AC traces scaled to pick up the low frequency, low amplitude chugging in the system. Included are expanded time traces of the start and cutoff time period of the engine which show the chugging pressure oscillations (Figures D.5a and D.6b). The start oscillation is from 6 to 8 psi p-p and a frequency of 210 to 240 hertz. The cutoff oscillation is from four to 37 psi p-p and at a frequency of 110 Hz. These oscillations initially started in the preburners as higher magnitude pressures that are dissipated to the lower values at the transfer duct location. The start oscillations are attributed to priming the injector, and the cutoff chugging is attributed to the helium purge flow.

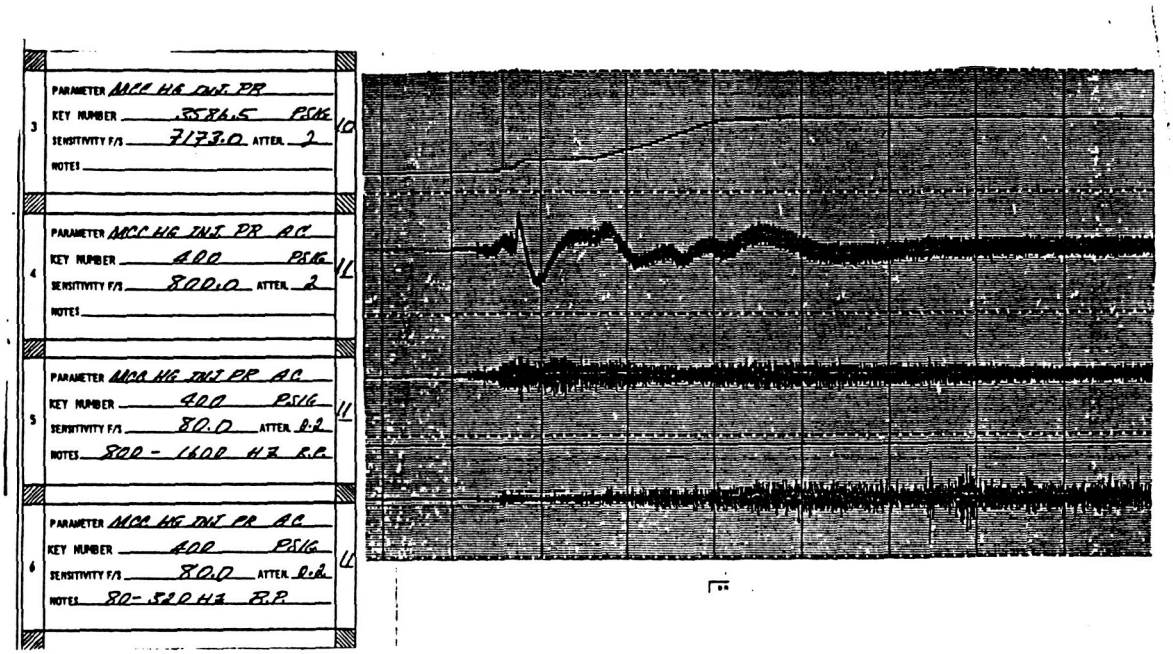

FIGURE D.5a CGIP START TRANSIENT PLOT

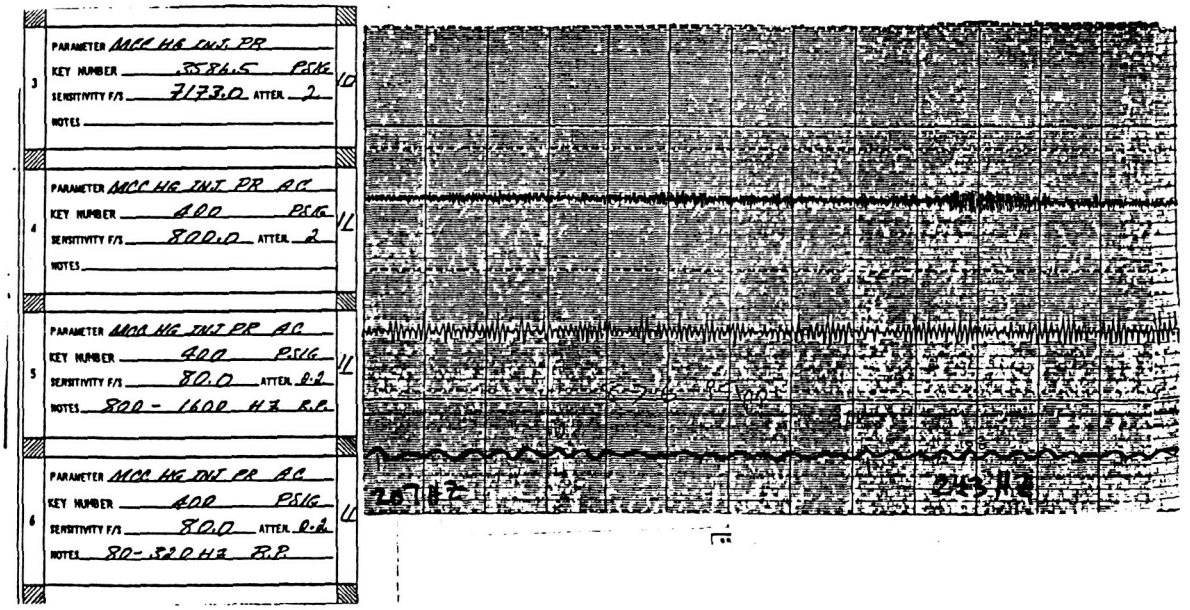

FIGURE D.5b CGIP START TRANSIENT PLOT

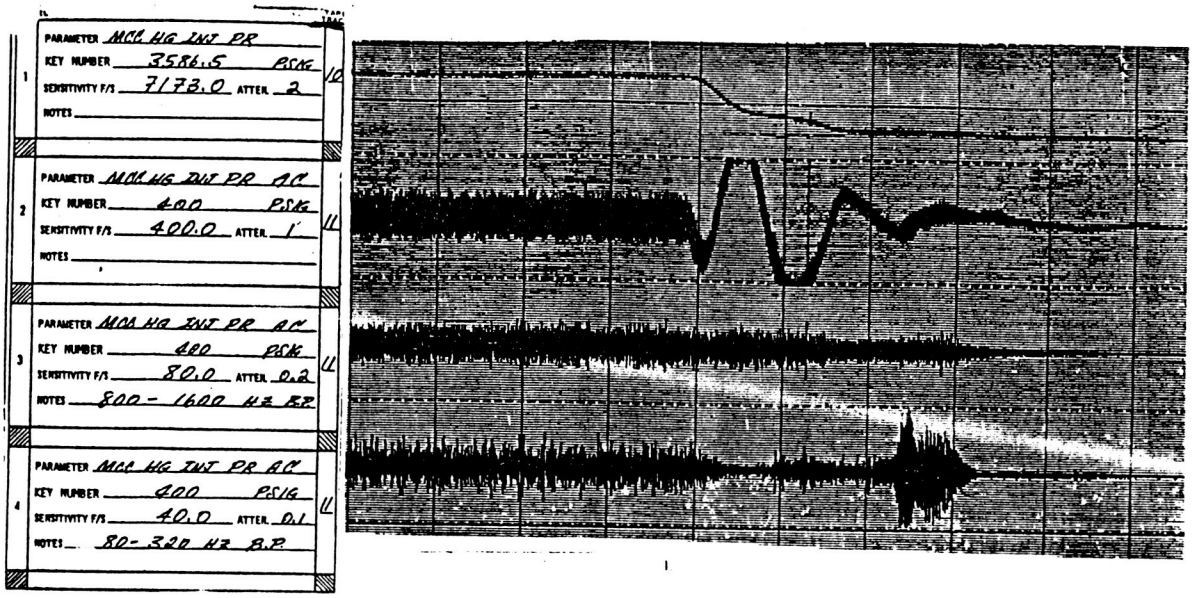

FIGURE D.6a CG1P CUTOFF TRANSIENT

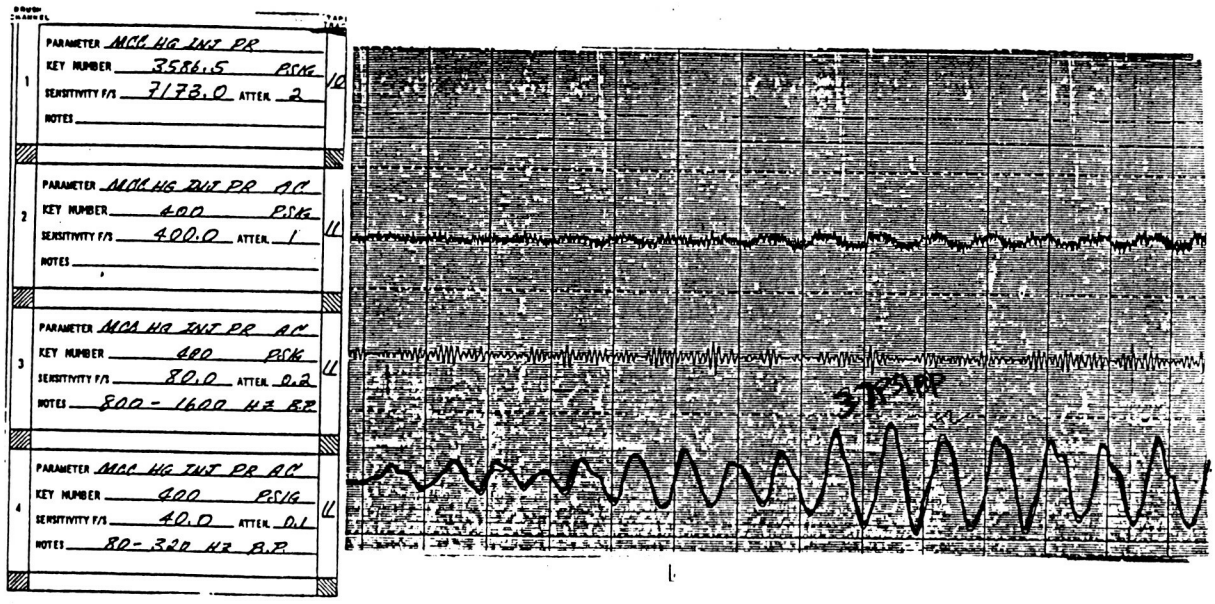

FIGURE D.6b CG1P CUTOFF TRANSIENT PLOT

The circumferential variation in liner pressure is based on airflow measurements that are scalable through the duty cycle. Flow separations occur in the duct that lead to these variations. Figure D.7 shows a typical pressure variation during airflow tests on the two duct configuration. The specific variation is measured at the transfer duct exit, but is actually quite close to the middle. These pressure variations can be scaled to obtain the average pressures in the duty cycle.

The coolant flow pressure duty cycle is usually determined as both a pressure and a liner ΔP using the average duct internal pressure. Figure D.8 is a plot of a typical coolant flow liner ΔP. This average ΔP applies along the length of the ducts and as previously stated is perturbed by the circumferential variation of the hot gas pressure. The coolant pressure is constant circumferentially around the duct.

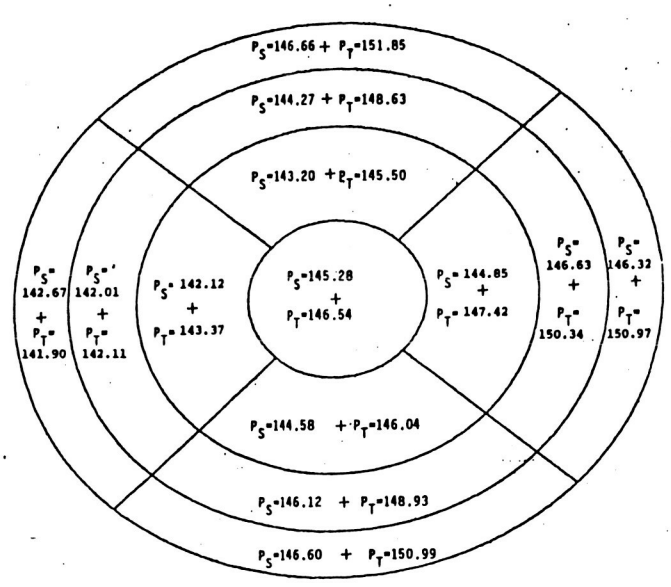

FIGURE D.7 MEASURED STATIC AND TOTAL PRESSURES FROM AIRFLOW MODELS

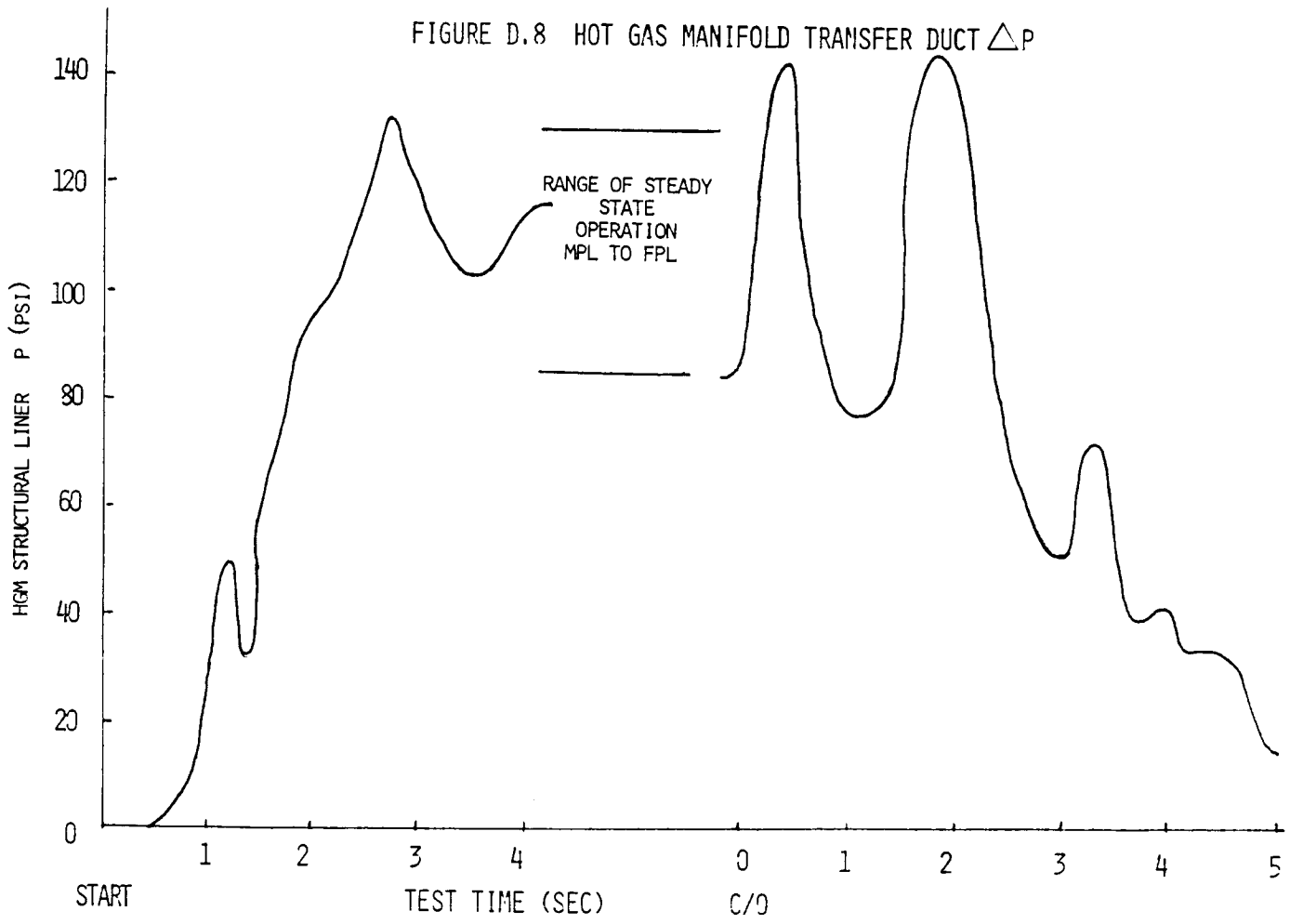

FIGURE D.8 HOT GAS MANIFOLD TRANSFER DUCT Δp

D.4 Pressure Oscillations

The major dynamic loads on transfer tube liners are the aerodynamic loads . Similar to many components in the hot gas path, the high cycle fatigue life of the liners are dependent on the flow pressure oscillations. There are no high frequency measurements of pressure fluctuations at the transfer tube during hot fire engine tests. Hence the analysis is based on scaled values from air flow tests for the duty cycle. The results are also correlated to the hot fire engine measurements at CG1P location and can be judged based on both airflow and engine measurements in closely related hot gas zones in the turnaround duct and turbine.

The pressure oscillation in transfer tube liners is closely linked to the hot gas flow circuit. Improved flow and pressure distribution throughout the circuit, decreased turbulence, reduced velocity and less system pressure losses all help in a more favorable environment for transfer tube liners. The two sources of pressure oscillation on the transfer tube liners that have been identified are the boundary layer noise and the flow separation effects. It is known that in the current SSME design there are large regions of separated flow (Figure D.9) in the center and outboard transfer tubes. In an analysis study of center transfer tube scrub liner cracking at FPL operation, the pressure fluctuations due to separated flow were identified as the source for liner high cycle fatigue failure. It was postulated that the separated bubble was excited by acoustics emanating from the turbine which in turn coincided with a sympathetic vibration mode of the scrub liner. The area of the separated flow was visualized by water flow tests. Tufts, bubble injection and dyes aid in establishing stream lines and separation patterns.

The air flow high frequency pressure measurements are made at the top and bottom of transfer tube inlet (Figure D.10). The measurements are done on the oxidizer and fuel transfer tubes. The air flow test results are scaled to 109% FPL and a typical set of pressure PSD diagrams from the two duct design on the oxidizer and fuel side transfer tubes are shown in Figure D.11 and Figure D.12. Analysis of data has indicated the top and bottom

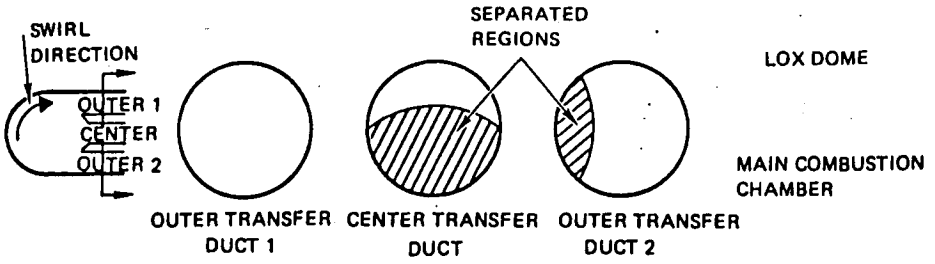

FIGURE D.9 SEPARATED FLOW REGIONS IN THE THREE-DUCT HGM DESIGN

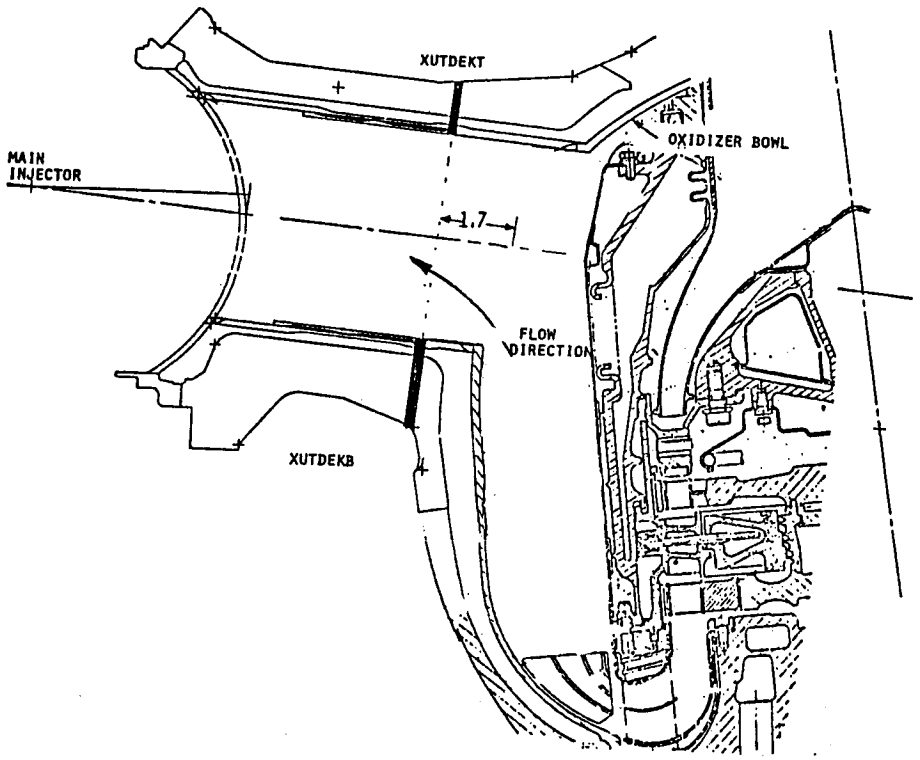

FIGURE D.10 HIGH FREQUENCY PRESSURE MEASUREMENT ON THE OXIDIZER TRANSFER DUCT FOR AIR FLOW TEST

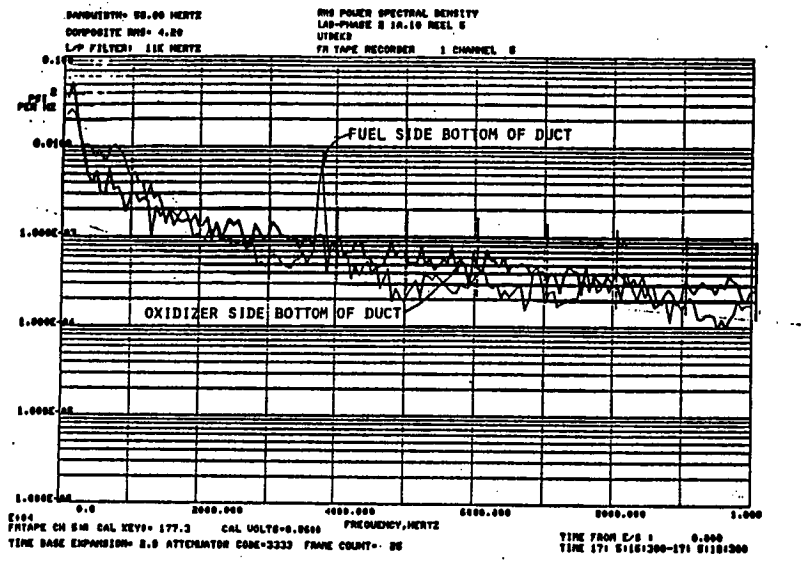

FIGURE D.11 OXIDIZER SIDE BOTTOM ENVIRONMENT SIMILAR TO FUEL SIDE (SCALED TO 109%)

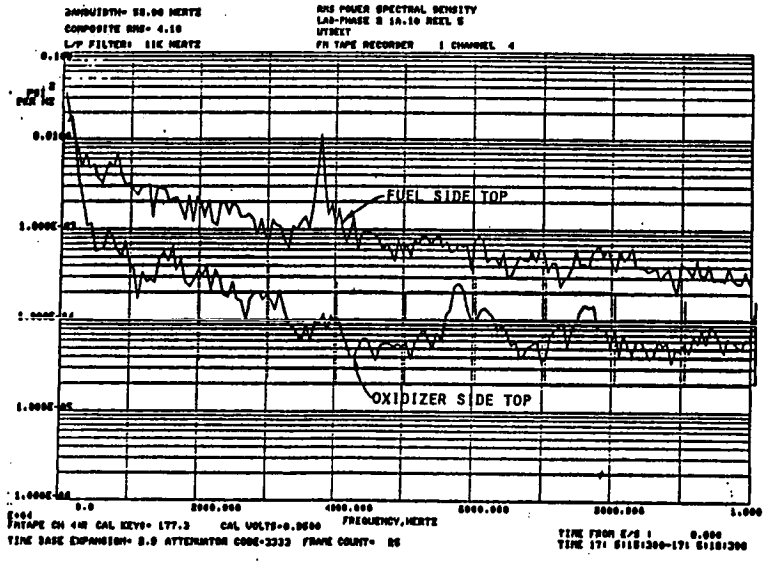

FIGURE D.12 OXIDIZER SIDE TOP ENVIRONMENT REDUCED COMPARED TO FUEL SIDE

measurements are uncorrelated. Due to limited measurements, the correlation distance circumferentially and along the length is unknown for the pressure fluctuations and have to be based on engineering judgment .

The current load definition for the pressure oscillation duty cycle consists of a varying random pressure oscillation whose magnitude is scaled by power level. The pressures along the duct are uncorrelated and have estimated correlation distances.

D.5 Thermal Loads

The thermal loads on a transfer duct liner are dependent on the design philosophy and geometry as well as the coolant and hot gas flow. For the SSME coolant liners, the structural liner has coolant flow on the outside and hot gas flow on the inside. The scrub liner has hot gas on both surfaces and has limited heat transfer path to the structural liner. This minimizes the heat load on the structural liner behind the scrub liner. The thermal loads on the liner are considered for the engine duty cycle and the structural liners average temperature away from the scrub liner. The typical hot gas and coolant temperatures at start transient, mainstage and shut down are shown in Figure D.13 and Figure D.14. The typical heat transfer model is shown in Figure D.15. Detail information from this type of model can furnish both average temperatures and temperature gradients throughout the duty cycle.

The temperatures are calculated based on flow, material and geometry. Thermocouple measurements are not currently available to verify the analysis although they are planned for the SSME test bed engine. Effects of test to test variation can be based on calculated flow conditions from the engine data reduction program.

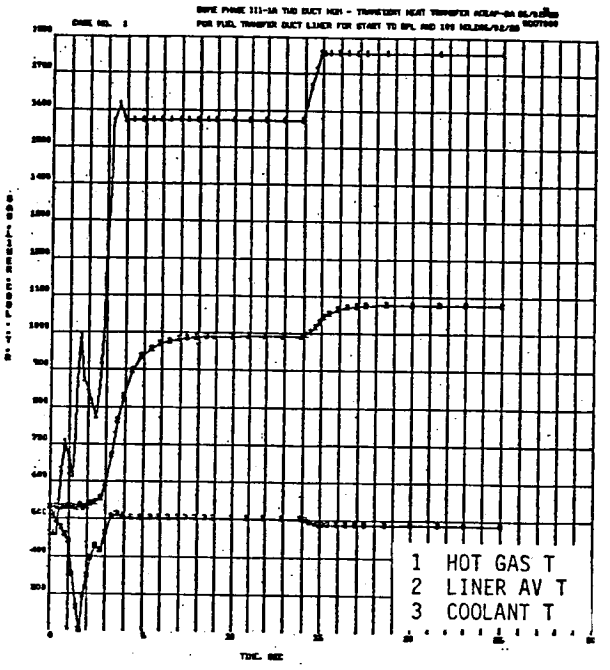

FIGURE D.13 FUEL TRANSFER TUBE LINER TEMPERATURE HISTORY AT START AND AT RPL

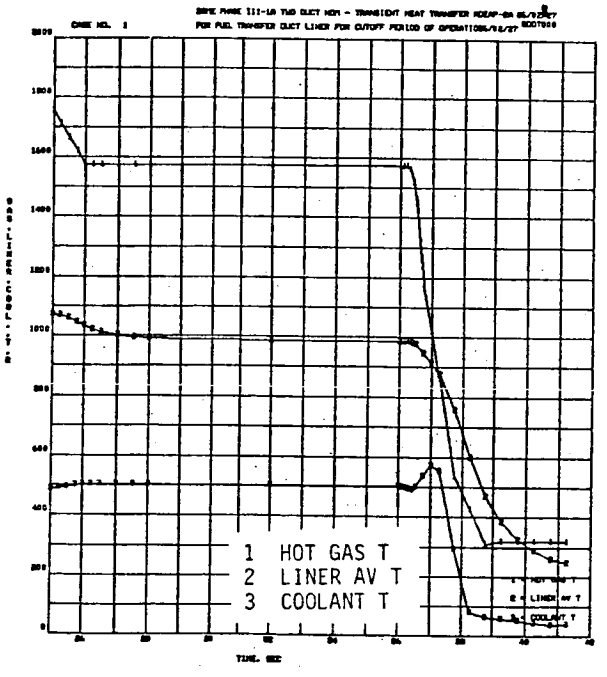

FIGURE D.14 FUEL TRANSFER TUBE TEMPERATURE HISTORY AT CUTOFF

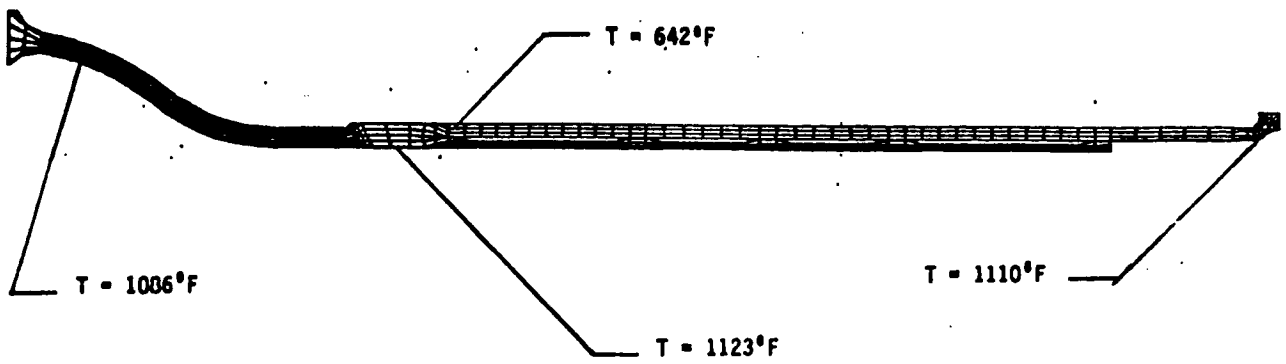

FIGURE D.15 FUEL TRANSFER TUBE LINER MODEL

D.6 Debris Loading

The transfer duct is out at the end of the hot flow system just ahead of the injector. So the ducts have the potential for impact from debris that is generated from the preburner faceplate, the turbine sheet metal and blading and the hot gas manifold preburner liner bowls. Since flow is essentially parallel to the transfer ducts on designs like the SSME, impact damage from debris should be minimal. Engine configuration and the history of missing pieces or known debris in the hot gas system are available. This can be used as a basis for developing the debris loading. Some of the occurrences of small pieces of debris in the hot gas system are summarized in Table D.1.

TABLE D.1 TYPICAL DEBRIS OCCURRING IN HOT GAS SYSTEM

ENGINE	PIECE SOURCE	PIECE SIZE	REMARKS
2012	HPOTP 1ST STAGE BLADE LEADING EDGE	0.008" X 0.005"	
2018	HPFTP BELLOWS SHIELD	.4" X .375" X .040"	RETRIEVED 4 PIECES FROM MAIN INJECTOR AFTER TEST 901-413. 2 PIECES NOT FOUND: .4" X .375" AND .35" X .375" ONE .4" x .3" PIECE FOUND POST FLIGHT 51-D
2019	LIFT OFF SEAL CARBON NOSE	0.03" X 0.005"	DISCOVERED DURING DISASSEMBLY (1-10-85). ANY IMPACT ON ENGINE OPERATION HIGHLY UNLIKELY DUE TO PARTICLE SIZE AND MATERIAL

D.7 Fabrication Loads

Portions of the structural liners have to be welded into the HGM assembly after heat treatment of the basic assembly. The ends of the coolant liners are included in this later phase of assembly and they have welded joints to the MCC liner shell and their respective preburner liner shell. This leaves the ends of the liners in an indeterminate residual secondary stress state.

D.8 Available Mission-History-Profiles for Theory Verification/Validation

The amount of data available for verification or validation varies with the individual load component. For load components where measurements are taken each engine test there is an extensive database - vibration accels and manifold pressure. Other loads such as random pressure oscillations have no engine verification.

To date, there has been no instrumented transfer ducts during hot fire test. Air flow simulation tests, though, may be partial validation for this effort. There are planned tests for an instrumented transfer duct in the test bed engine.

A generic discussion of the airflow testing work was presented in the lox post survey and will not be herein repeated.

The current test bed engine plans for instrumentation of the transfer ducts. Typical modifications required and placement of instrumentation are shown in Figure D.16. The measurements include transfer duct pressures and temperatures.

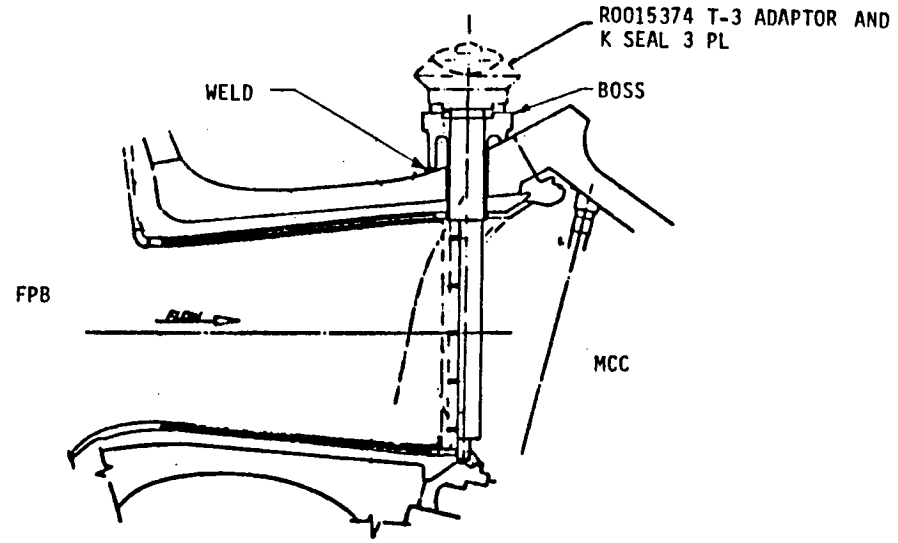

FIGURE D.16 HGM RS007051-1041 FUEL TRANSFER DUCT HOT GAS H.F. PRESSURE

APPENDIX E SSME HIGH PRESSURE OXIDIZER TURBOPUMP DISCHARGE DUCT LOADS

E.1 INTRODUCTION

An assessment of the individual loads on the SSME HPOTP discharge duct is furnished in this appendix. The information in this appendix is summarized in sections 11.2.5 and 11.2.6.

E.2 Static Pressures

The steady state pressures in the ducts are initially obtained from engine balance and subsequently refined from hot fire engine tests. Table E.1 illustrates the typical design configuration, pressures, temperatures and material for major propellant ducts in SSME.

TABLE E.1 SUMMARY OF MAJOR PROPELLANT DUCTS

DESCRIPTION	HARD OR FLEX	FPL (MAX) PSI PRESSURE	FPL (MAX) °R TEMPERATURE	I.D.	THICKNESS RANGE	MATERIAL	ELBOW RADIUS	ELBOW MAX. ANGLE	ELBOW THICKNESS
OXIDIZER									
1) LOW PRESSURE OXIDIZER PUMP DISCHARGE	FLEX	554 (695)	178	6.30	.032→.160	INCO 718	12.00	90°	.032→.160
2) LOW PRESSURE OXIDIZER PUMP TURBINE DRIVE	FLEX	4902	205	2.30	.090→.287	INCO 718 TI 6-6-2	3.50	90°	.086→.180
3) HIGH PRESSURE OXIDIZER PUMP DISCHARGE	RIGID	4902	205	-4.000.	104→.270	INCO 718	4.50	90°	.104→.127
4) PREBURNER PUMP OXIDIZER	RIGID	4801	205	2.3	.084→.120	INCO 718	2.75	90°	.084→.134
5) HEAT OXIDIZER SUPPLY	RIGID	4770	205	.555	.026→.075	INCO 718 INCO 628	2.00	90°	.026→.035
6) OXIDIZER BLEED	RIGID	230	554	.68	.030→.063	CRES 321 INCO 718	2.25	MOCK-UP	.026→.030
7) OXIDIZER TANK PRESSURANT	FLEX & RIGID DUCTS	4460	990	1.00	.138→.285	INCO 718	3.50	90°	.142→.172
8) PREBURNER OXIDIZER SUPPLY	RIGID	8309	221	1.982 1.097	.096→.205	INCO 718 INCO 675	4.50	90°	.101→.209

During start, shutdown or both conditions, the ducts experience a surge in pressure. This effect is more pronounced on the oxidizer side of the engine system where the fluid density is high. The surge pressures do not impact the high pressure ducts as much as the low pressure ducts since the surges occur well below the maximum operating pressures in the duct. A typical cutoff transient of the LPOTP shaft speed is illustrated in Figure E.1, where the power up of the pump at cutoff sequence must be noted. Corresponding typical pressure transients at cutoff are shown in Figure E.2 for the low pressure oxidizer discharge duct. Normally two pressure surge peaks are seen after the cutoff command. The first peak occurs at approximately cutoff plus 0.3 seconds. The magnitude of this surge is controlled by the system power down and is proportional to cutoff power level. The second peak occurs at approximately cutoff plus 2.0 seconds. This is driven by the main oxidizer valve schedule. The magnitude of this pressure surge is inversely proportional to the cutoff power level. The magnitude of the pressure surge, is related to minimum pressure prior to power up, the lower the dip, the higher the surge. This surge which is a significant percentage to LPOTP the discharge duct pressure is accounted for in the analysis. The surge phenomenon is also observed in high pressure ducts such as the HPOTPDD. However, the surge pressure occurs at a reduced power level and hence total pressure is less than the maximum pressures the ducts experience at steady state (Figure E.3). Typical duty cycle pressures are shown in Figure E.4.

E.3 Thermal Loads

The ducts primarily experience two types of temperature loading 1) Steady state temperature and 2) engine prechill condition temperature. There is typically no rapid thermal changes to cause large thermally induced loads. The steady state temperatures are listed in Table E.1 and are essentially uniform across the wall thickness. The engine prechill condition occurs when the prevalves located in the orbiter above the low pressure turbopump are opened approximately one hour prior to firing. On opening of the prevalves, the propellants flow through the low pressure turbopumps, and

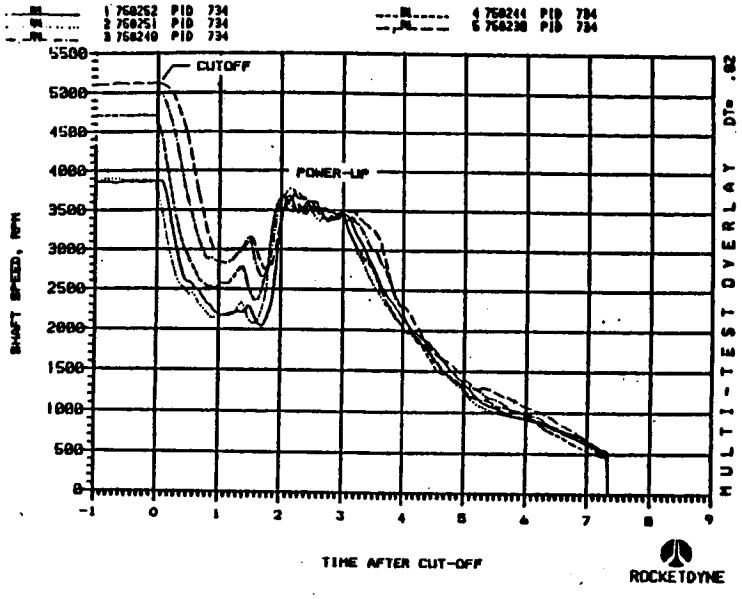

FIGURE E.1 LPOTP SHAFT SPEED FOR VARIOUS CUTOFF POWER LEVELS

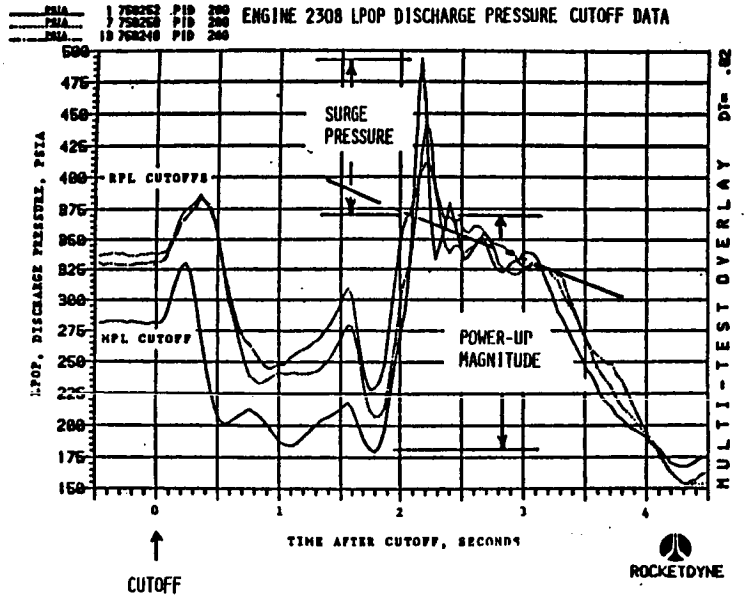

FIGURE E.2 LPOTP DISCHARGE PRESSURE CUTOFF DATA

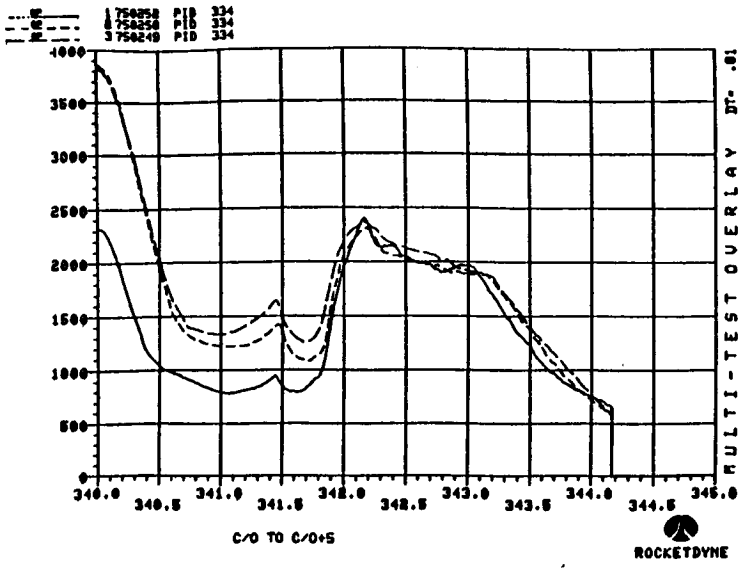

FIGURE E.3a HPOTP DISCHARGE PRESSURE AT CUTOFF DATA

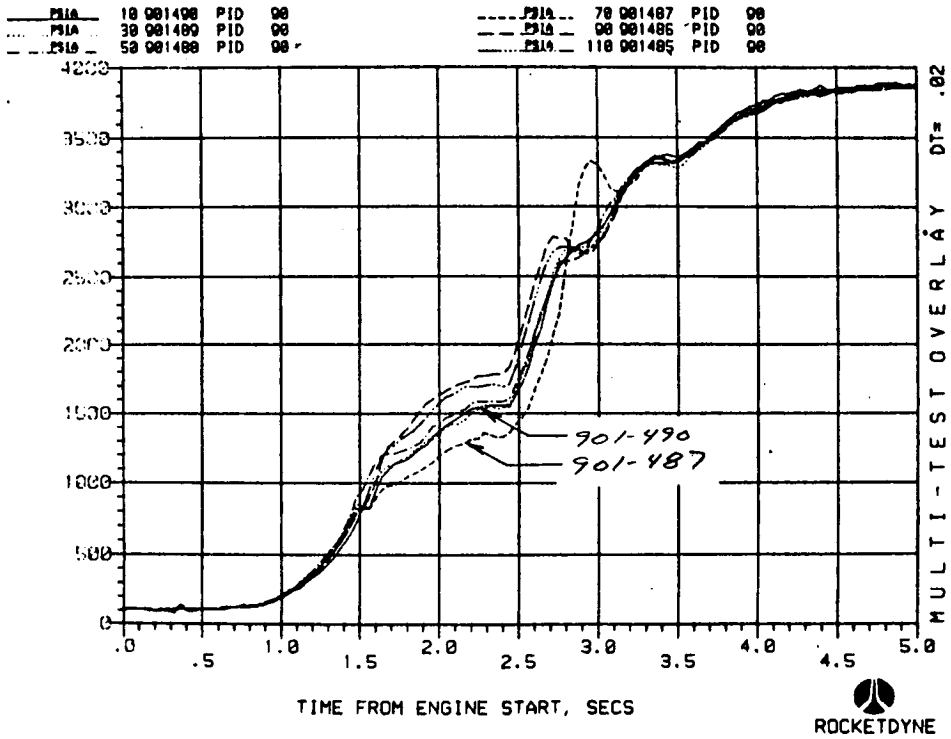

FIGURE E.3b HPOTP DISCHARGE PRESSURE AT START

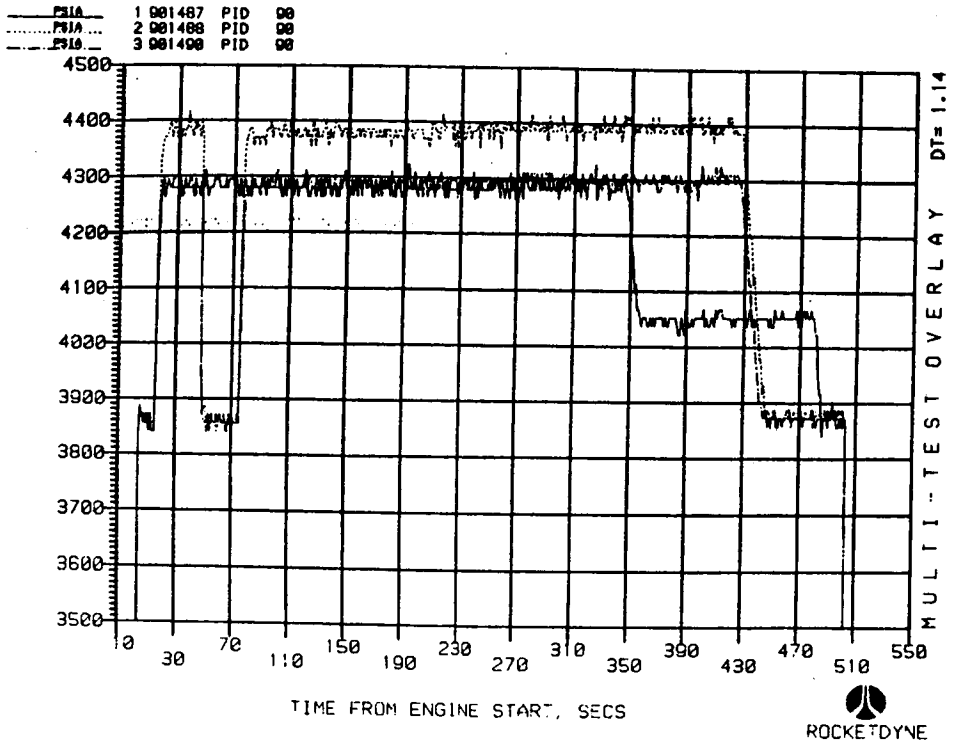

FIGURE E.4 TYPICAL HPOTP DISCHARGE DUTY CYCLE PRESSURES FOR THREE ENGINE TESTS

through the high pressure turbopumps and then to the main propellant valves. On the liquid oxygen side, the system also fills the preburner valves. The cryogenic propellants are held in the ducts for sufficient time to chill the engine and attain liquid conditions in the respective propellant systems. The chill process is aided by bleedlines which remove the gas as it is formed. The chilling to cryogenic temperatures (37°R for hydrogen and 164°R for oxygen) occurs during vented or low pressure and the gradual temperature changes do not control the design. The thermal conditioning of the system is an important part of the prestart sequence to get the engine ready for the proper start conditions. Similar start sequencing are used on other rocket engines.

E.4 Dynamic Loads

The dynamic loads that are considered in the duct analysis are: 1) Mechanical loading - Random base vibration loads and periodic pump generated base excitation loads, shock transients, and 2) Dynamic flow - random pressure loading or equivalent sinusoidal pressure loading at pump wake frequencies.

E.5 Mechanical Loading

Initial random and shock base excitation data was predicted using scaled values from J2-S engine data. Subsequently, the data is revised as more actual engine measurements become available. The loads are defined based on vibration zone classification. As an example for the case of the HPOTPDD the appropriate zones are A and G respectively. Typically SSME loads criteria (e.g., R4 environment) defines the spectra up to 2000HZ. When appropriate, the spectra is extended to a higher frequency range for specific components (Figure E.5). The extended spectra is used when the potential for high frequency modes of vibration can occur such as the HPOTPDD. The sinusoidal narrow band peak responses are related to speed harmonics from impeller blade wake effects.

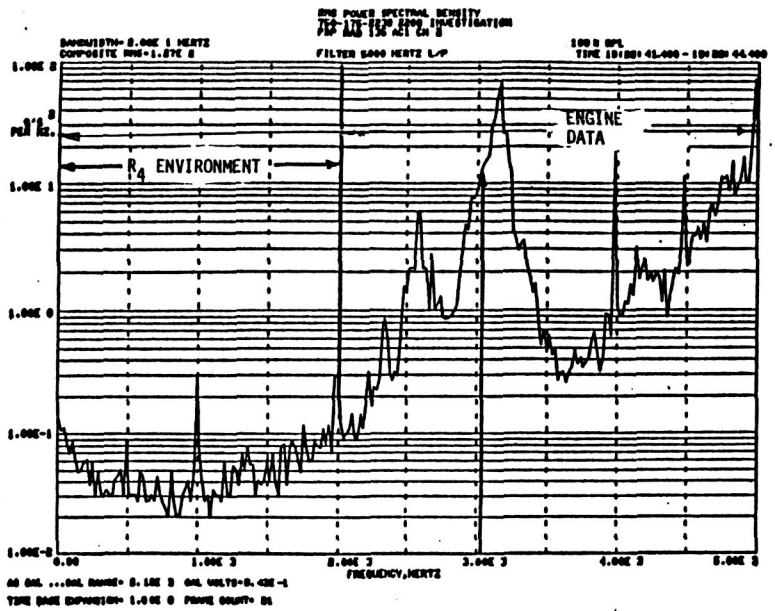

FIGURE E.5 HPOTPDD BASE VIBRATION ENVIRONMENT

E.6 Shock Transients

These loads are predicted from the actual engine firing test data from SSME. The primary shock transients occur at start and cutoff, and to a lesser extent, by preburner pops. The primary contributor to the start and cutoff transients is the nozzle side load caused by flow separation. During engine start and cutoff, the flow inside the SSME nozzle is constantly changing. Unsteady flow separation occurs in the nozzle during this time period. The axial location of this flow separation moves toward the exit of the nozzle as combustion chamber pressure is increased, and back into the nozzle as chamber pressure is decreased. Side loads are developed in the nozzle walls because the flow separation patterns are not symmetrical. The start transient is more severe than the cutoff transient due to comparatively longer cutoff time sequence as well as due to the higher altitude. The SSME shock spectra criteria was developed by enveloping a minimum of six starts and six cutoffs of engine data. A typical shock spectra is shown in Figure E.6 for Zone A and Zone G that govern the HPOTPDD environment. It must further be noted that the shock transients are not a strong function of the power level the engine is starting or that the cutoff is initiated from.

ZONE	AXIS
A	X, Y, Z
10 HZ @	1.0 g Peak
30 HZ @	40. g Peak
800 HZ @	60. g Peak
2000 HZ @	150. g Peak

ZONE	AXIS
G	X, Y, Z
10 @	2. g Peak
30 @	28. g Peak
60 @	53. g Peak
220 @	104. g Peak
320 @	200 g Peak
950 @	157 g Peak
2000 @	333 g Peak

FIGURE E.6 HPOTPDD ZONE A AND ZONE G SHOCK SPECTRUM

E.7 Dynamic Pressure Loads

The high frequency pressure measurement made just downstream of HPOTP discharge are used as a forcing function to the HPOTPDD duct. Power spectral density plots of engine tests at 100% and at 109% are presented in Figure E.7 and Figure E.8, respectively.

Primary characteristics are at rather flat low level power at about 1/3 psi^2/HZ from 0 to 10KHZ. Superimposed on this background are two characteristic signals, speed harmonics and a broad random hump in the 6000 to 9000 HZ range. At 100% power level the random hump and 16/rev harmonic are distinct, while at 109% they superimpose at 8KHZ. Total power (psi^2/HZ) at 109% is twice the 100% power level value.

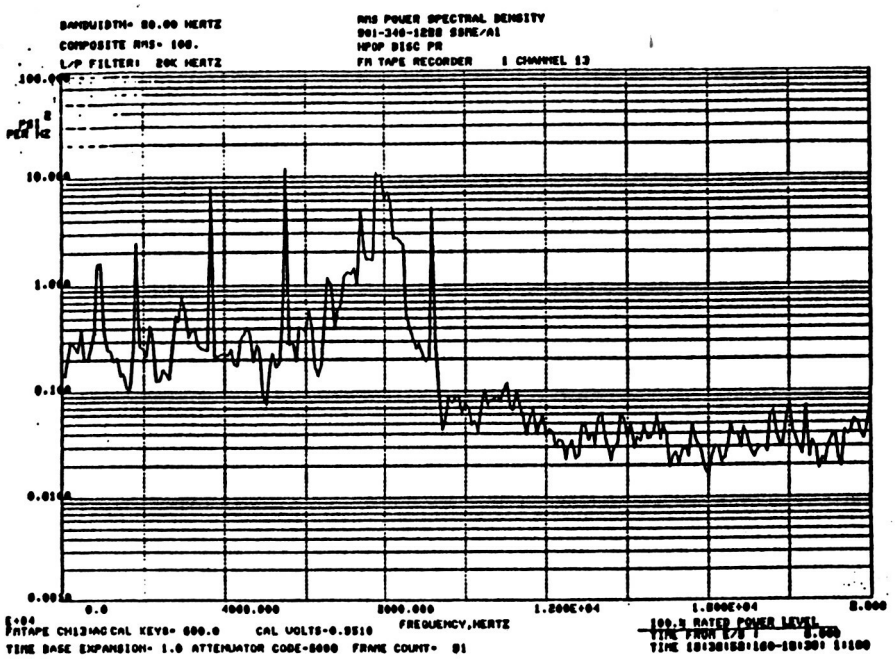

FIGURE E.7 HPOTP DISCHARGE PRESSURE PSD AT 100% POWER LEVEL

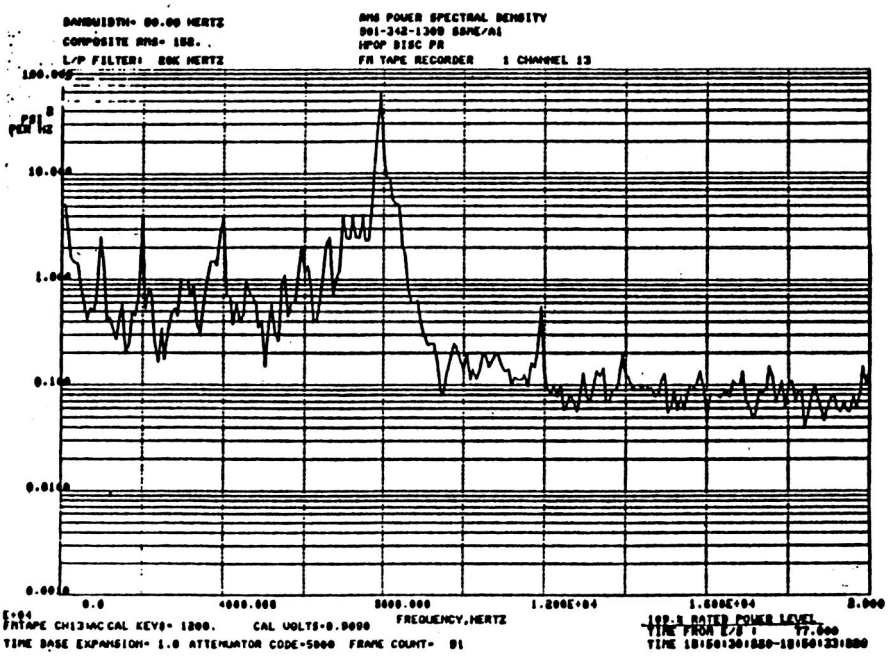

FIGURE E.8 HPOTP DISCHARGE PRESSURE PSD AT 109% POWER LEVEL

Speed harmonics have narrow power spikes typical of sinusoidal components. The fact that the first three or four multiples of 8/rev show an increase with frequency and then decrease indicate a wave form like positive-negative pulse with a duration of about 25% of the period between the 8/rev pulses. This type of excitation tends to propagate as a plane wave down the duct and would be attenuated by a reflection at the constriction formed by the main oxidizer valve.

The broad random hump is explained by the attenuated power radiated by lateral acoustics driven in the constant velocity pump volute by the blade wakes. The variable diameter volute causes local resonances at different frequencies with the broad hump being the sum of all components. As the power level is increased, local frequencies will remain the same, although the magnitude would increase. This tendency is seen in Figure E.8 and Figure E.9. The broad hump would tend to decrease with distance. However, data at these frequency ranges may have to be used when local shell modes are of concern, near the HPOTP discharge.

E.8 Misalignment Loads

The duct misalignment loads are considered in the design of rigid ducts. The design is based on worst case tolerance stackup in the duct assembly. The sequence of assembly of the ducts is tightly controlled through the specifications. The acceptable tolerances are specified in the form of interaction curves at flange joints. As examples, the interaction curves for high pressure oxidizer duct inlet and outlet are shown in Figure E.9 and Figure E.10. In general, only misalignment that fall outside the specification are recorded for MR action. One exception to the above rule is the ASI (Augmented Spark Igniter) fuel and LOX lines where the entire misalignment data is available. Shop experience indicates that due to the method for manufacture of larger ducts using jig fixtures, unacceptable misalignment (outside the specification) is very rarely encountered.

FIGURE E.9 ALLOWABLE MISALIGNMENT AT HPOD INLET

FIGURE E.10 ALLOWABLE MISALIGNMENTS AT HPOD OUTLET

Further, the misalignments found in practice in the large ducts are within the tolerances of the play in the bolt holes of the flanges and the large rigid ducts are not generally subjected to any significant preloads during assembly. The small ASI fuel and LOX lines are formed and any unacceptable misalignments in the flanges are first corrected by further forming the tube away from welded areas.

E.9 Gimbaling Loads

All lines which are subjected to deflections due to gimbaling have flex joints. The angulations at the joints are calculated using finite element analysis programs treating the ducts as a series of straight pipes and elbows. The maximum gimbal angle is 11° about any of the gimbaling axis. This maximum gimbaling occurs only in an abort cycle. In addition the joint angulations are also calculated for maximum torsional twist of 1° about the engine axis. The rigid ducts like HPOTPDD are not subjected to gimbaling deflections.

E.10 Acceleration Loads

Ducts are designed for acceleration loads due to gimbaling acceleration and vehicle acceleration. The gimbaling acceleration is bounded by calculating the maximum g load that it can produce at any point in the duct. This has been calculated to be 5g and this load is applied over the entire duct. The vehicle acceleration loads come from the SSME load criteria and is calculated to be 5g. Thus the ducts are designed for a total of 10g acceleration load subjected to on any axis. The fluid weight in the ducts must be considered in the analysis.

E.11 Flow Momentum Loads

The flow momentum loads are calculated using the flow rate of the fluid, density of the fluid at operating temperature and pressure, flow area and gravitational constant. The flow load calculated is applied as an axial load on the duct beam elements.

APPENDIX F SSME MAIN COMBUSTION CHAMBER LINER LOADS

F.1 Introduction

An assessment of the individual loads on the SSME MCC liner is furnished in this appendix. A summary is presented in section 11.3.6.

F.2 Temperature Loads

During an operational duty cycle (mission) the MCC liner is subjected to a thermal gradient approaching 1200°F. The peak SSME MCC heat flux region is located 1.22 inch upstream of the geometric throat. A two-dimensional thermal model is used to define the life cycle transient temperature history as a function of time. The MCC average axial thermal conditions are determined from hot-fire calorimeter chamber measured heat transfer rates. These type of measurements cannot distinguish circumferential heat transfer variations commonly associated with injection/combustion abnormalities. SSME MCC regenerative cooled cyclic life testing has shown that cracking occurs in local hot spot regions associated with the injector abnormalities. These hot spot regions are identified by hot-gas wall surface discoloration (blanching) and typically exist over a width of 5 to 10 channels.

F.3 Gas Side Heat Transfer.

The SSME MCC heat transfer rates are based on sub-scale 40K thrust calorimeter chamber testing. The sub-scale test article employed a staged combustion system and utilized main injector elements identical to the SSME. The combustor length (injector to throat) was identical to the SSME MCC. This water-cooled calorimeter chamber provided local axial heat flux measurements over a range of chamber pressure up to 1750 psia. Chamber pressure scaling criteria were attained from the 40K calorimeter MCC and subsequent testing on two 40K hydrogen cooled chambers up to 3000 psia chamber pressure. These hydrogen cooled chambers were configured of the SSME MCC channel geometry. Comparison of local heat flux measurements and total heat load data provided local heat transfer scaling to 3000 psia chamber pressure, which adhered to the classical scaling relationship of:

$$hg \propto (Pc)^{0.8}$$

Since the purpose of the two 40K hydrogen cooled chambers was a life demonstration, these combustion chambers utilized the identical SSME MCC throat region channel geometry and hot-gas wall contour. The local gas-side heat transfer conditions of the full-size SSME MCC were obtained by correcting for local hot-gas wall mass velocity ($hg \propto [\rho V]^{0.8}$) where the SSME MCC axisymmetric geometry differed from the 40K MCC. This correction is effectively attained by integrating the measured 40K calorimetric MCC heat transfer data with the Rocketdyne analytical boundary layer computer program. This allows evaluation of any chamber and nozzle geometry on an empirical basis. The injector and heat transfer conditions are based on experimental data. This empirical approach was subsequently verified by measured SSME MCC heat load measurements.

F.4 Coolant Heat Transfer

The hydrogen coolant coefficient is based on the Rocketdyne hydrogen coolant correlation as noted below:

$$hc = C_H \; G \; C_p \left(\frac{T_B}{T_W}\right) \phi_c$$

where

T_B = bulk temperature
T_W = wall temperature
C_p = heat capacity
G = mass flux
ϕ_c = curvature enhancement
C_H = $\dfrac{f/8}{0.92 + \sqrt{f/8}\;[g\,(\epsilon^*) - 8.48]}$
f = friction coefficient
$g(\epsilon^*)$ = $4.7\;\epsilon^{*0.2}$ for $\epsilon^* \geq 7.0$
$g(\epsilon^*)$ = $4.5 + 0.57\;\epsilon^{*0.75}$ for $\epsilon^* < 7.0$
ϵ^* = $Re\;(E/D)\quad F/8$
ϵ = surface roughness
D = hydraulic diameter

A coolant curvature enhancement (ϕ_c) of 1.4 is used in the life-limited throat region at X = -1.22 inch. This enhancement was experimentally evaluated by laboratory tests for the SSME MCC geometry.

The thermal computer-program/analysis logic diagram used in this study is shown in Figure F.1. Figure F.2 shows the analysis geometry.

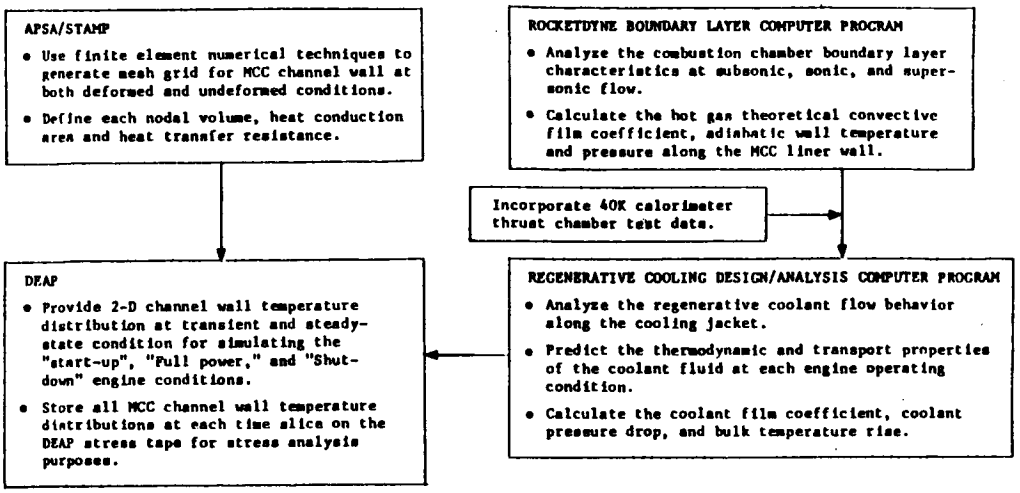

FIGURE F.1 THERMAL COMPUTER PROGRAMS FLOW CHART

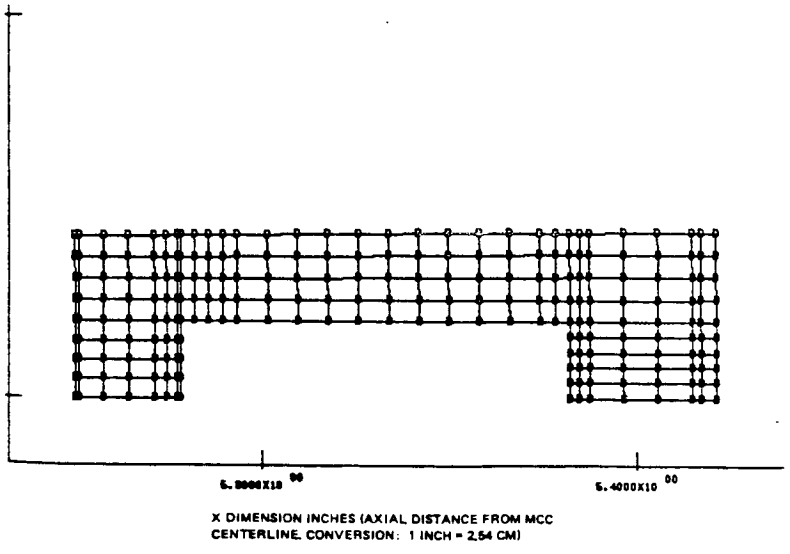

FIGURE F.2 SSME MCC COOLING CHANNEL GEOMETRY AND MODAL STRUCTURE

The temperature distribution of the coolant channel is determined by a 277 node grid model. The model uses a finite difference technique. The same nodal network was used for the thermal and structural analyses. The coolant channel thermal distribution is shown in Figure F.3 at 1.22 inch upstream of the geometric throat. The maximum hot gas wall temperature is 1100 F at steady-state FPL (100% hg) conditions. Temperatures throughout the duty cycle of key points in the model are shown in Figures F.4 through F.7.

The thermal analysis is performed for the overall liner structure for the detail liner analysis. A sensitivity analysis is also made to simulate hot spot conditions by increasing the convertive cooling film coefficient in a local zone of the liner analysis. This can drive the temperatures in the channels at a hot spot to a maximum of 1500°F. The structural analysis is also performed at this operating condition to estimate cycle life to cracking at hot spots.

F.5 Pressure Loads

The hot wall pressures on the liner are based on the MCC chamber pressure duty cycle. A typical engine measured trace is shown in Figure F.8.

STATION NO. 51 X = -1.23 RT = -.233

NUMBER OF ITERATIONS = 27
DIFFERENCE BETWEEN HEAT IN & HEAT OUT = .00999 PERCENT

HEAT INPUT = 131.519
2-D/1-D B/A = 1.03352

1355	1355	1355	1356	1356	1356	HOT GAS WALL
865	862	862	862	863	864	
566	563	563	562	573	672	
491	458	425	459	495	493	COOLANT WALL
253	237	155				
99	78	12				
-11	-25	-72				
-92	-95	-123				
-127	-134	-155				
-155	-160	-173				
-171	-175	-188				
-179	-182	-191	-199	-232	-203	CLOSE-OUT
-187	-188	-191	-193	-194	-196	
-189	-189	-191	-192	-192	-195	

COOLANT CHANNEL

S.I. Conversion
K = 5/9 (F + 460)

1. LAND WIDTH = .04571
2. CHANNEL WIDTH = .04000
3. HOT WALL THICKNESS = .02510
4. CHANNEL DEPTH = .13079
5. CLOSEOUT THICKNESS = .00300
6. TAU = 5325. DEG. F
7. XI = .3231033
8. TC = -211. DEG. F
9. REFERENCE HC = .1883722
10. HC FACTOR FOR UPPER WALL = 1.0330
11. HC FACTOR FOR LOWER WALL = 1.0330
12. PERIMETER = .4580
13-14. K OF REGION 1 = .004875 + (-.1870E-05) * T
15-16. K OF REGION 2 = .004875 + (-.1870E-06) * T
17-18. K OF REGION 3 = .021340 + (-.1393E-05) * T
19. CONVERGENCE CRITERION = .1000 DEG. F
20. COATING THICKNESS = 0.000300
21-22. COATING K = 0. + (0.) * T

100%

FIGURE F.3 COOLANT CHANNEL THERMAL DISTRIBUTION AT 100% FPL hg

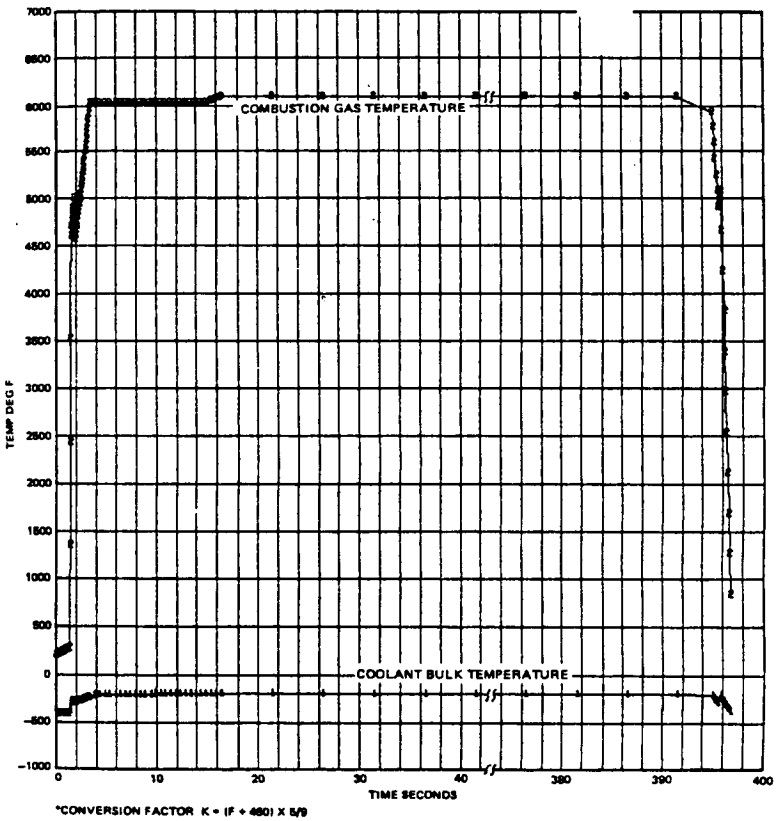

*CONVERSION FACTOR K = (F + 460) X 5/9

FIGURE F.4 COMBUSTION GAS TEMPERATURE & HYDROGEN COOLANT TEMPERATURE DUTY CYCLE PROFILES FOR SSME AT X=-3.1cm (X=-1.22 INCH)

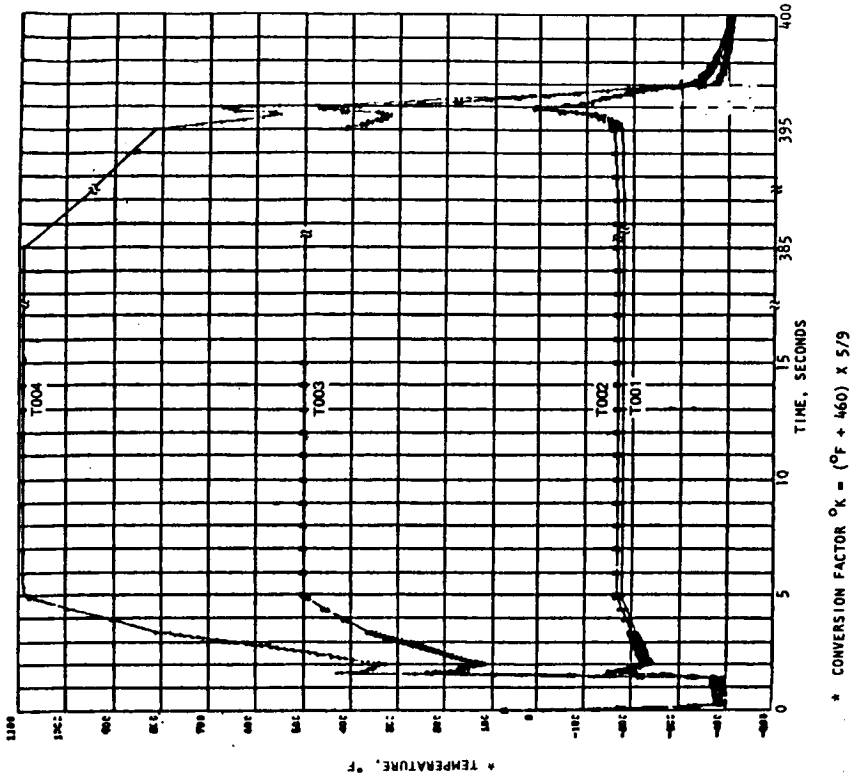

FIGURE F.6 SSME MCC LINER MIDCHANNEL TEMPERATURE RESPONSE AT X=-3.1cm (X=-1.22 INCH) AT FPL OPERATION (100% FPL hg)

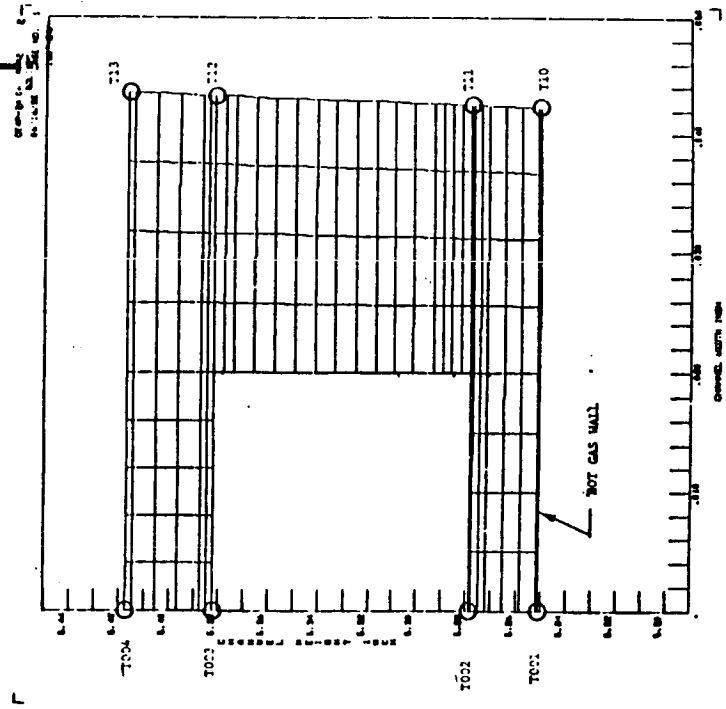

FIGURE F.5 SSME MCC COOLANT CHANNEL GEOMETRY AT X=-3.1cm (X=-1.22 INCH)

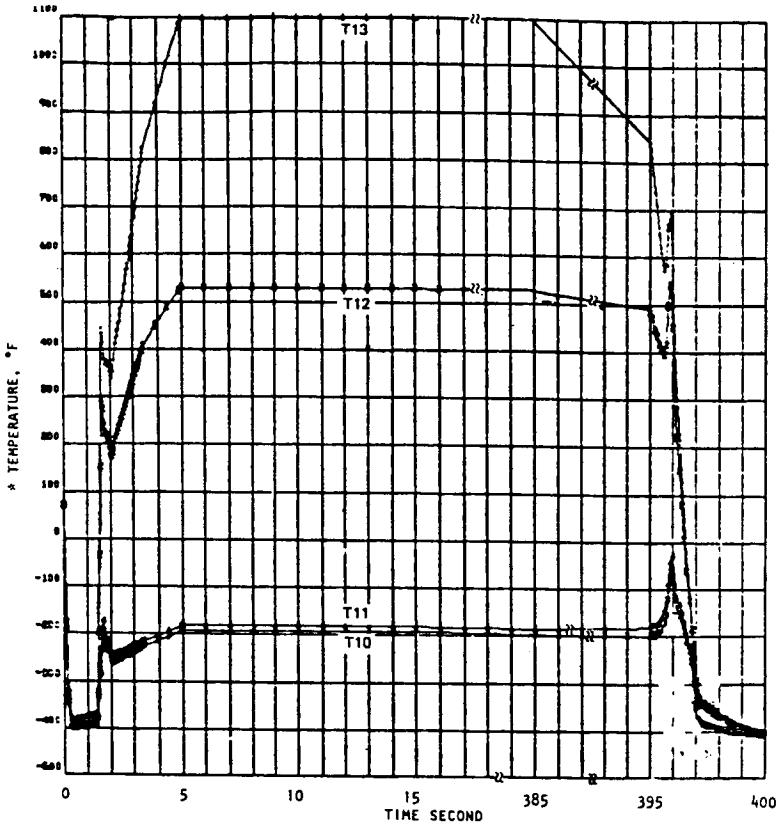

FIGURE F.7 SSME MCC LINER MIDLAND TEMPERATURE RESPONSE AT X=-3.1 cm (X=-1.22 INCH) AT FPL OPERATION (100% FPL hg)

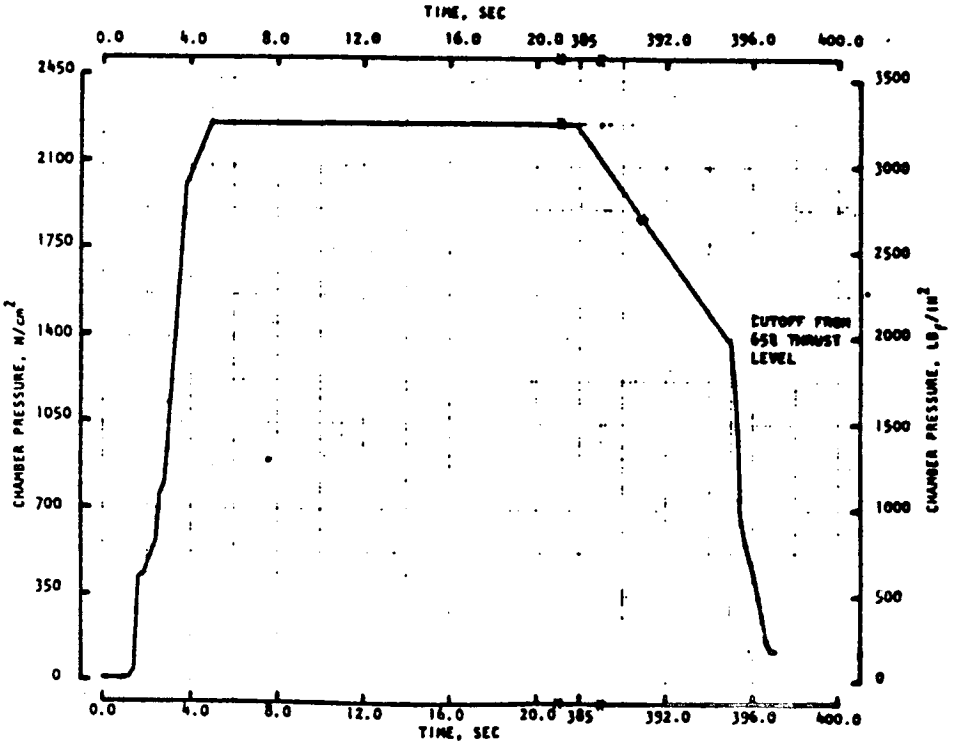

FIGURE F.8 SSME MCC CHAMBER PRESSURE PROFILE TO FPL OPERATIONS (100% hg)

The channel pressure is calculated as part of the regenerative cooling analysis program; see Figure F.1. The coolant pressure drop from the inlet, to along the liner to the exit, are inter-related to the detailed thermodynamic modeling. The duty cycle calculated is shown in Figure F.9.

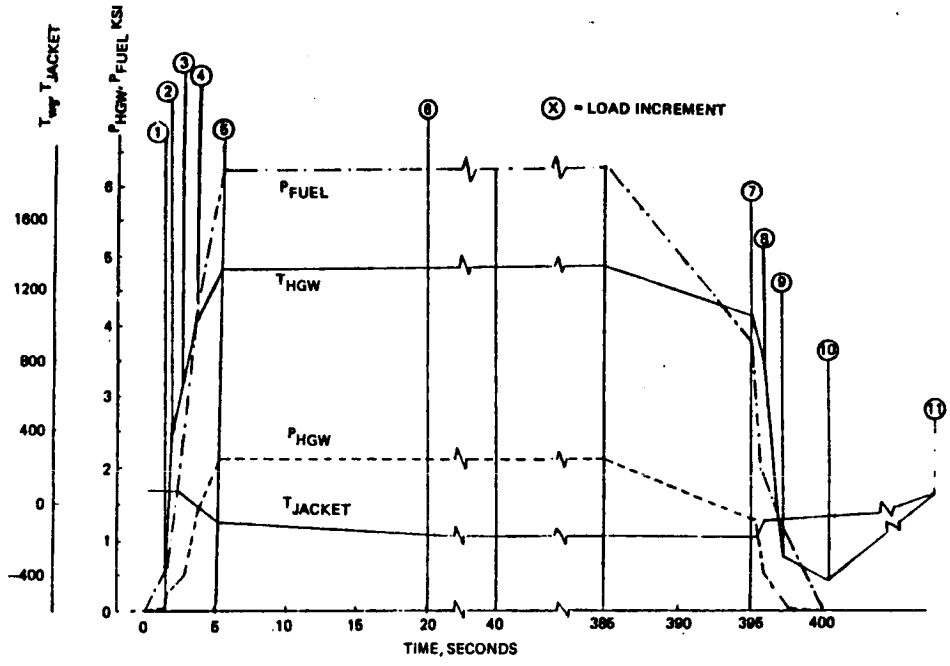

FIGURE F.9 SSME MCC LIFE ANALYSIS DUTY CYCLE & PRESSURE DISPLAY WITH TIME SLICES NOTED

SSME MCC Baseline Design. The selected baseline operating level was Full Power Level (FPL) with the heat transfer rates noted as 100± hg. This power level is 9% above the SSME rated power level (RPL). The FPL chamber pressure is 3250 psia and the MCC mixture ratio is 6.0 (oxygen/hydrogen). The SSME duty cycle, including the start and cutoff transient conditions, were used for all analyses.

Existing Structural Analysis Methodology. Channel wall combustion chambers are sized by hand solutions followed by local detailed finite-element analysis of a channel cross section. The finite-element analysis utilizes a duty cycle considering the prechill, start, mainstage, and cutoff conditions for temperature, pressure, and movement of any support jacket.

F.6 Radial and Axial Restraint

The affect of the other loads on the MCC are passed to the liner as a radial deflection or an axial displacement of the structural shell.

The MCC jacket motion was analyzed to establish radial displacement and axial strain influence coefficients for both combustion chamber pressure, average jacket temperature, and external load effects. Using heat transfer data generated from the 100% hg case FPL duty cycle run, compatible time slice values of jacket temperatures and combustion chamber pressure were established, which in turn were used to define the compatible radial displacements and axial strains of the jacket used for the liner cross section model boundary conditions.

A verbal description of the sequential events helps to understand the time-temperature-pressure relationships between the liner and jacket. The MCC as manufactured can have a maximum radial gap between the liner outer diameter and the structural jacket inner diameter of 0.5 mm (0.020 inch). During the start prechill, the cold hydrogen gas flowing through the liner coolant channels causes a thermal contraction of the liner which increases the liner/jacket radial gap. During this time, there is a negligible cooling effect on the jacket due to the cold radiation from the liner. Then, upon ignition, the combustion pressure increases and the weak liner expands radially, like an inner tube in a tire. At a fairly low pressure it contacts the jacket inner diameter. Once liner/jacket contact is made, the jacket mean temperature experiences a fairly rapid drop in temperature to approximately 100 F, while combustion pressure is increasing to its steady-state value. During this time, there is a net radial growth of the

jacket from the positive radial displacement of the jacket due to combustion pressure. This displacement is partially offset by the negative radial motion of the jacket as it drops in temperature. After steady-state combustion pressure is reached at 4.9 seconds, the jacket continues to get colder over the next 150 seconds, resulting in a decrease in the jacket radial displacement and axial strain.

At this point, pressure and thermal equilibrium loads in the jacket have been achieved. During shutdown, combustion pressure is throttled down to 65% of rated power level, and then the engine is shut down. During shutdown, the purge flow of hydrogen through the coolant channels rapidly chills the liner to -400 F, and the liner separates from the jacket. When combustion pressure reaches zero, the mean temperature of the jacket has warmed up to approximately -80 F. The jacket eventually warms back up to room temperature and returns to essentially a line-to-line contact position with the jacket.

APPENDIX G SSME NOZZLE FEEDLINE LOADS

G.1 INTRODUCTION

An assessment of the individual loads on the SSME nozzle feedline is furnished in this appendix. A summary is presented in section 11.4.3.

G.2 Static Pressure and Temperature

The internal pressure furnishes a high mean stress and is one of the primary loads on the line. The largest thermal gradient usually occurs during transient and can be of the order of 200°R. Temperature is not generally a significant load as it occurs during lower transient pressure values; however, the combination of temperature and pressure at transient must be considered for HEE (Hydrogen Embrittlement Effect) susceptibility.

Figure G.1 shows the inter-relation, of the pressure, temperature and HEE susceptibility. The line pressures are below 1000 psi in the HEE critical temperatures, and the resulting thermal and pressure stresses are low. Similar conditions exist during the cutoff conditions. Pressure decreases more rapidly than the thermal effects can follow.

Restraint. The feedline restraint load comes primarily from the differential thermal growth between the upper attach point and the 9th hat band fixed restraint. The other hat band supports are axially sliding joints. The thermal expansion loop accommodates the ≃.2" thermal motion in the line. The loads are calculated as part of a finite element model using average feedline and nozzle wall temperatures.

G.3 Steady State Random Vibration

During steady state operation when the nozzle is flowing full and there is no jet separation, the nozzle vibration loads are low. Typical hat band environment PSD loads are shown in Figure G.2. These loads are used as base inputs to a nozzle feedline line model to calculate the resulting vibration loads.

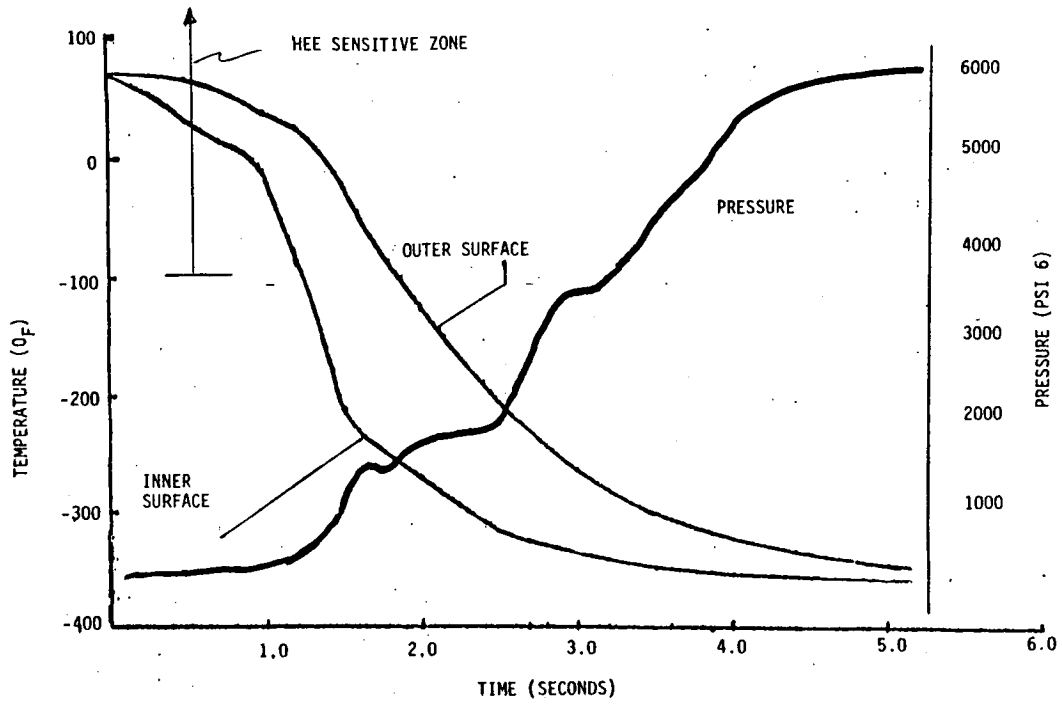

FIGURE G.1 NOZZLE FEEDLINE START TRANSIENT TEMPERATURE & PRESSURE PROFILE

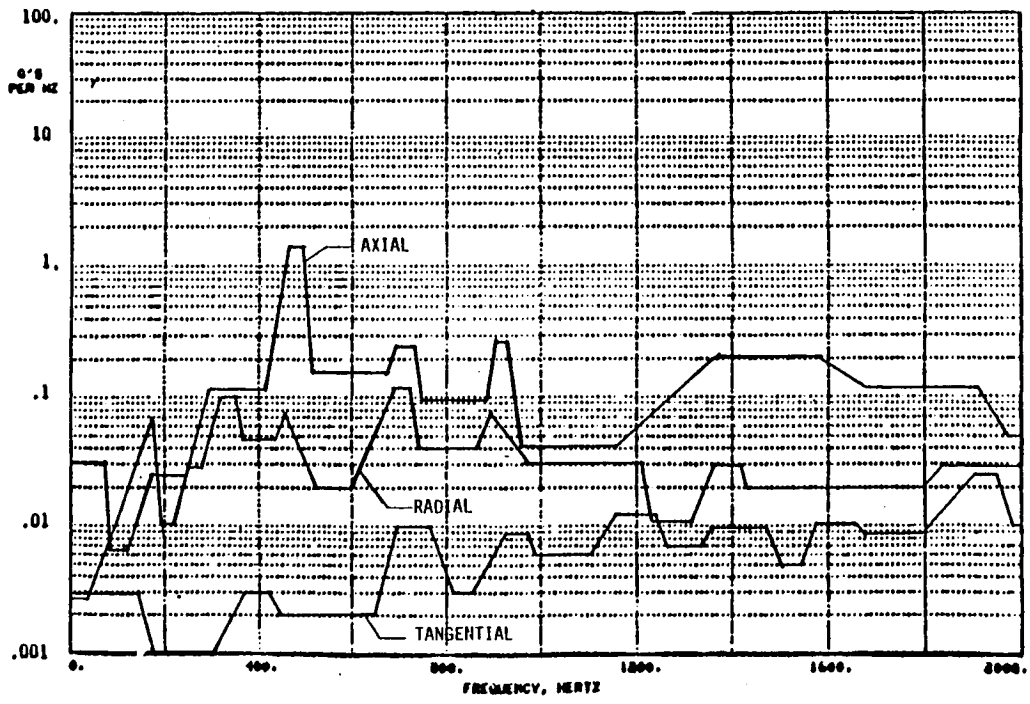

FIGURE G.2 RMS POWER SPECTRAL DENSITY PLOTS FOR ACCELERATION AT STEADY STATE AT HATBAND 9

G.4 Transient Loads - Mechanical

The other primary load is caused by the transient aerodynamic load on the whole aft section of the nozzle at start and cutoff. This plays a critical role in the nozzle feed line design. Early designs of SSME nozzle feedline did not consider the shock transient load in the 200 to 400 Hz regime.

The aerodynamic transient load is due to the unsteady flow separation effects. The different aspects of the flow separation is conveniently divided as sideloads, oscillating shock loads and breathing mode loads. Such a classification is made as their effects are in different frequency ranges.

Sideloads. Rocket engines incorporating high nozzle expansion ratios and operating in an environment wherein significant ambient pressure level exists, encounter a region of asymmetric flow during their start and cutoff transients as the nozzle fills or empties. This causes an imbalance of pressure forces in the nozzle wall and may result in side loads of significant magnitude. The effect of this side load can be seen by the pendulum mode deformation of the nozzle in SSME firings at transient. The engine start and cutoff sequences are planned to minimize the side loads. Dwelling at thrust levels where separation is expected will result in large side loads leading to structural damage to say actuator attach points as occurred on the J-2 engine early development cycle.

Exact theoretical evaluation of the side load, which is due to asymmetry flow, is beyond the scope of the current state-of-the-art. Hence, side load data is measured from many engine tests using load cells at the gimbal point or through strain gaged actuators or stiff arms. The strain gages measure the equilibrating forces, while the forces themselves are applied internally to the nozzle as a pressure gradient which varies with time. Dynamic pressure measurements of the nozzle wall pressure from actual engine firings are not available. However, nozzle pressure measurements from airflow tests on subscale models are used with appropriate scaling to obtain approximate oscillating engine pressure values. The magnitude of the side loads vary

significantly from test to test. This is illustrated by the statistical summary (Fig. G.3) of the maximum moment generated from 186 engine tests of the J-2 engine about the gimbal point. The J-2 engine which was an upper stage Saturn engine, encountered an overexpanded flow in the nozzle when fired during sea level. The results indicate a large spread in the measured magnitude of the side load and any realistic design must consider this inherent variation from firing to firing. Side load phenomenon is primarily a low frequency transient (up to 20 Hz) with oscillatory response due to ringing of the low damped structure. In the SSME engine, extensive analysis of strain gage measurements has indicated that side loads do not cause significant loading on the nozzle feed line itself. However, the effect of sideloads on nozzle and it's attachments must be considered in all over expanded nozzle designs.

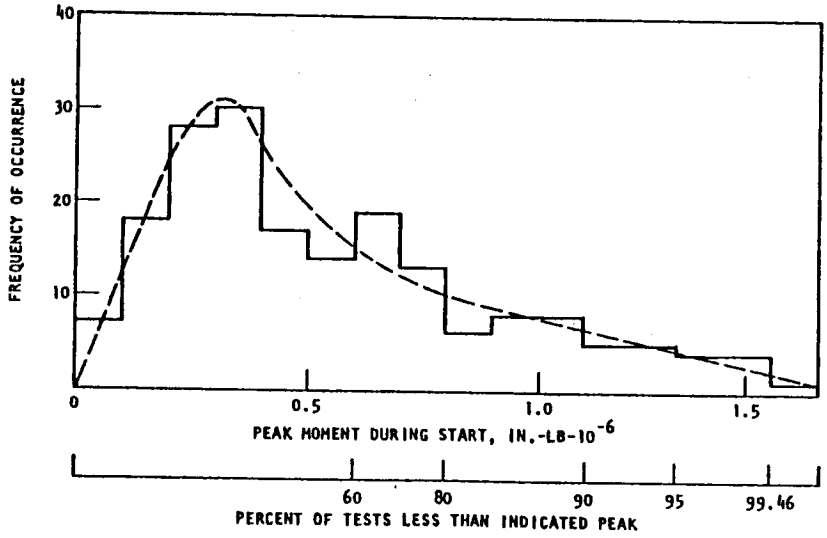

FIGURE G.3 DISTRIBUTION OF J-2 ENGINE SIDE LOAD MOMENTS ABOUT GIMBAL POINT (SUMMARY FROM 186 ENGINE TESTS)

Breathing Mode Loads. These loads also due to asymmetric flow separation effects and excites the nozzle in the low frequency range (<100 Hz). The presence of these loads can be seen in the motion pictures of engine firings near the exit of the nozzle as a flickering white band, referred to as "teepees". The dynamic nature of these shocks must be emphasized by their circumferential movement and appearing and disappearing at random intervals of time accompanied by inflow of ambient air at transient. Motion pictures of SSME firings will show a relatively large (2 inch or more) diametrical ovalization of the nozzle aft manifold due to the breathing mode. For the SSME nozzle feedline design, analysis and laboratory experiments have shown relatively low stresses are obtained in the critical areas of the feedline with this motion. Depending upon the feedline design, this mode has to be considered in the nozzle feed line designs.

Oscillatory Shock Transients. Shock transients are a higher frequency separated flow phenomena. The nozzle flow adjusts itself to the back pressure through oblique shocks near the wall and a normal shock in the interior flow. For large area expansion nozzles with shallow exit angles as is the case in SSME bell contour nozzle, this can result in large pressure fluctuations at the nozzle exit. This happens when separated free shear layer impinge on the nozzle at a steep angle (Fig. G.4). Due the steep impingement angle, more flow returns into the separated zone than that can be aspirated through mixing with the surrounding flow. Thus the pressure builds up and enlargement of the separation bubble occurs. As the separated region grows and reaches the nozzle exit, the accumulated gas is discharged to ambient with the free shear layer detaching from the nozzle.

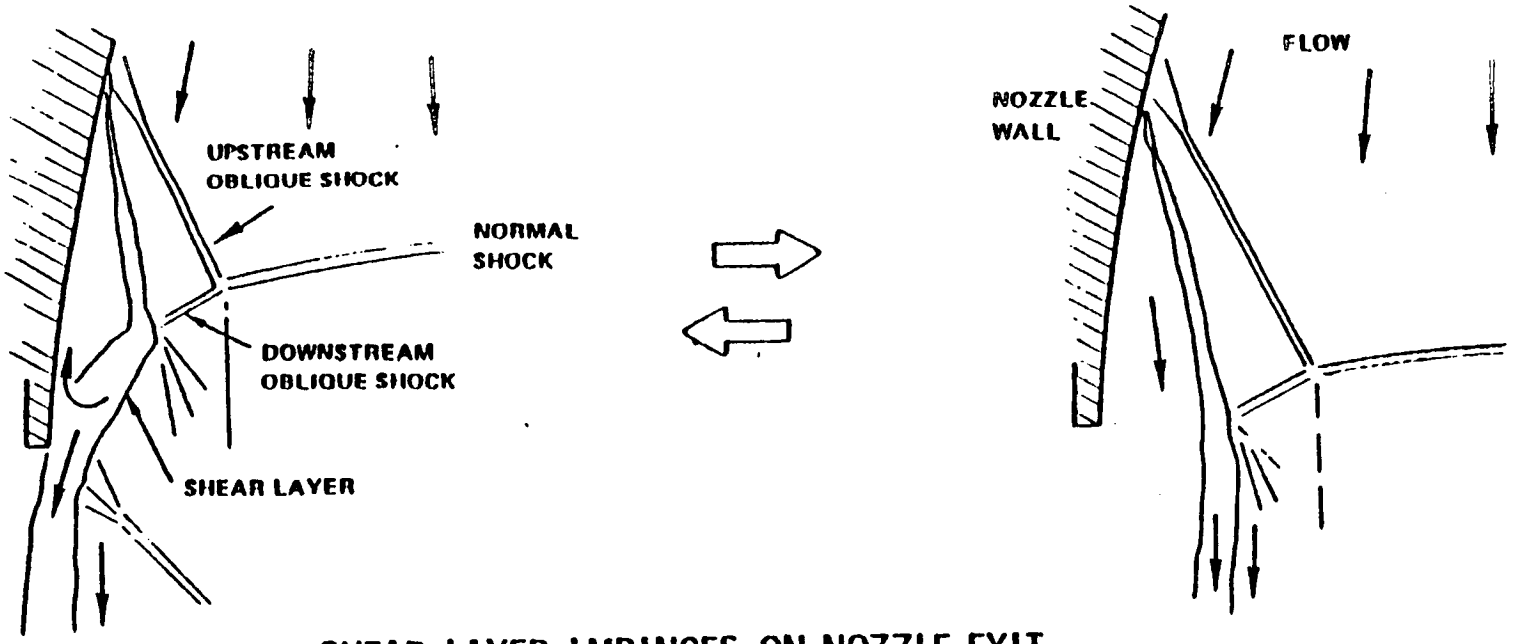

- SHEAR LAYER IMPINGES ON NOZZLE EXIT
- WALL PRESSURE INCREASES ABOVE AMBIENT
- SHEAR LAYER IS FORCED OFF NOZZLE WALL EXIT
- FREE JET PUMPING LOWERS WALL PRESSURE
- SHEAR LAYER IS PULLED BACK AGAINST WALL AND PROCESS REPEATS

Fig. G.4 Driver Mechanism for Oscillatory Pressure Pulse on the Nozzle

Free jet pumping of the region between the shear layer and the wall causes subambient pressures in the region. As a consequence, the shear layer is pushed back on the nozzle wall and the cycle continues. This explanation of the phenomenon is supported by air flow tests on scaled models where exit wall pressures as low as one fifth and as high as twice the ambient pressure has been seen in data. The frequency range of this transient in SSME is in the 100 to 500 Hz. The magnitude and shape of these loads are based on subscale air tests. The distribution of the peak magnitude of the load is infurred from the variation in nozzle feedline strain gage measurements.

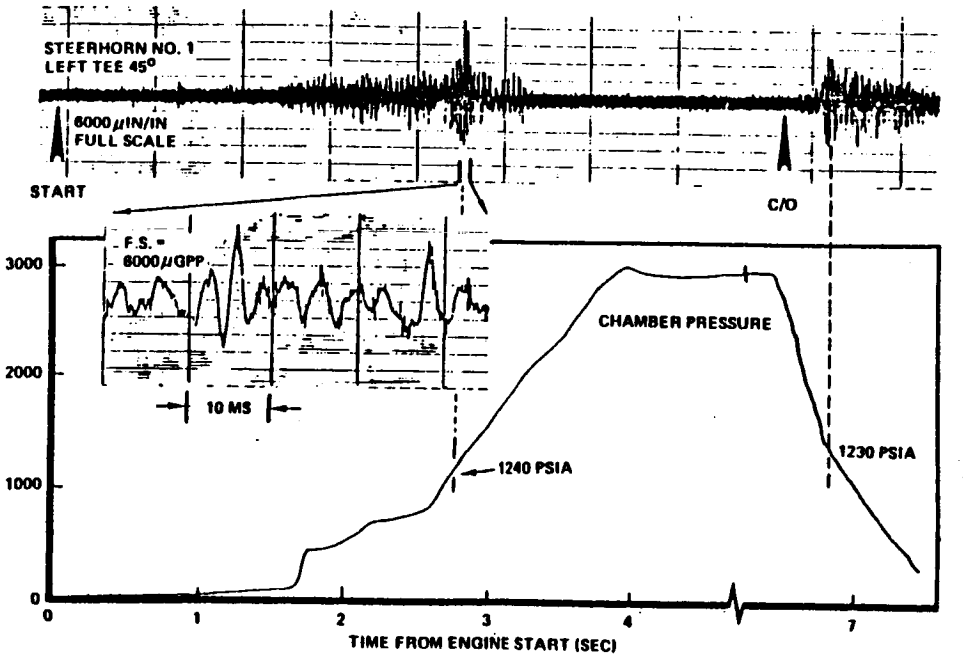

FIGURE G.5 STEERHORN STRAINS AT TEE IN TRANSIENT OPERATION

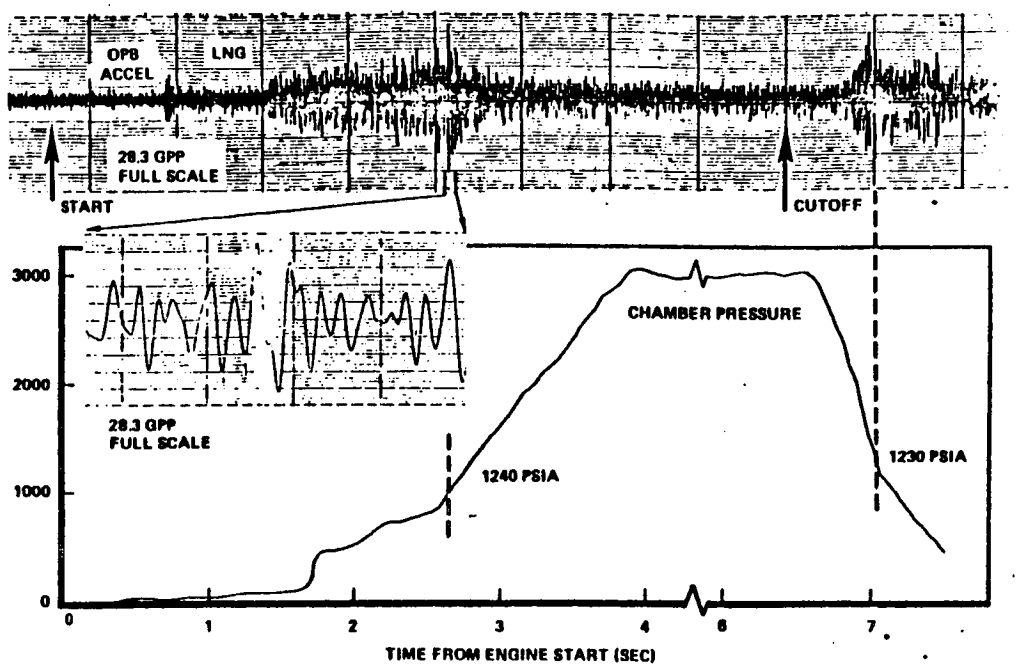

FIGURE G.6 OXIDIZER PREBURNER ACCELERATIONS IN TRANSIENT OPERATIONS

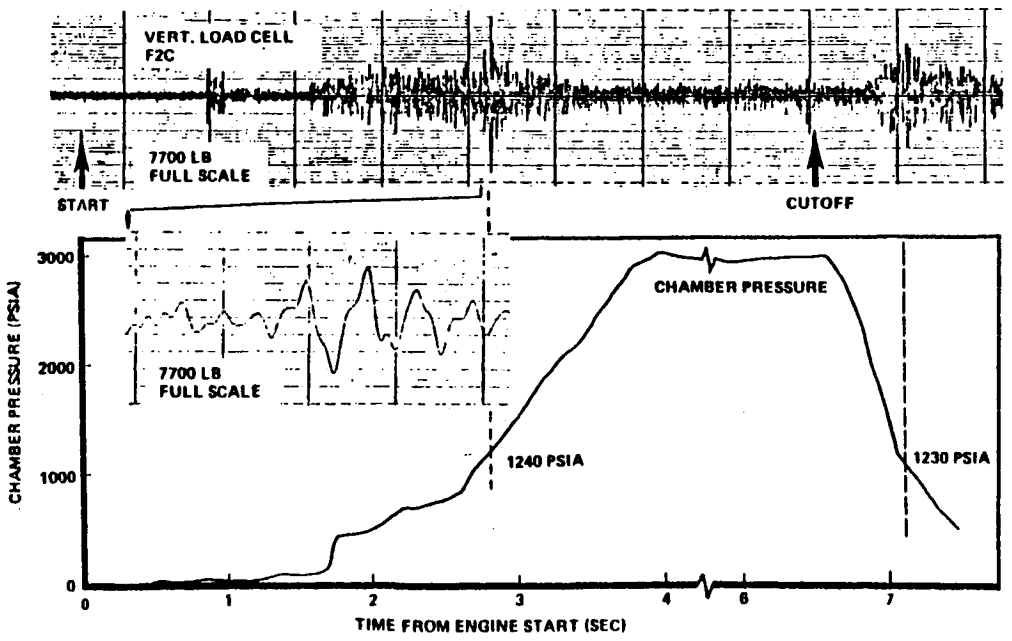

FIGURE G.7 VERTICAL LOAD CELLS IN TRANSIENT OPERATION

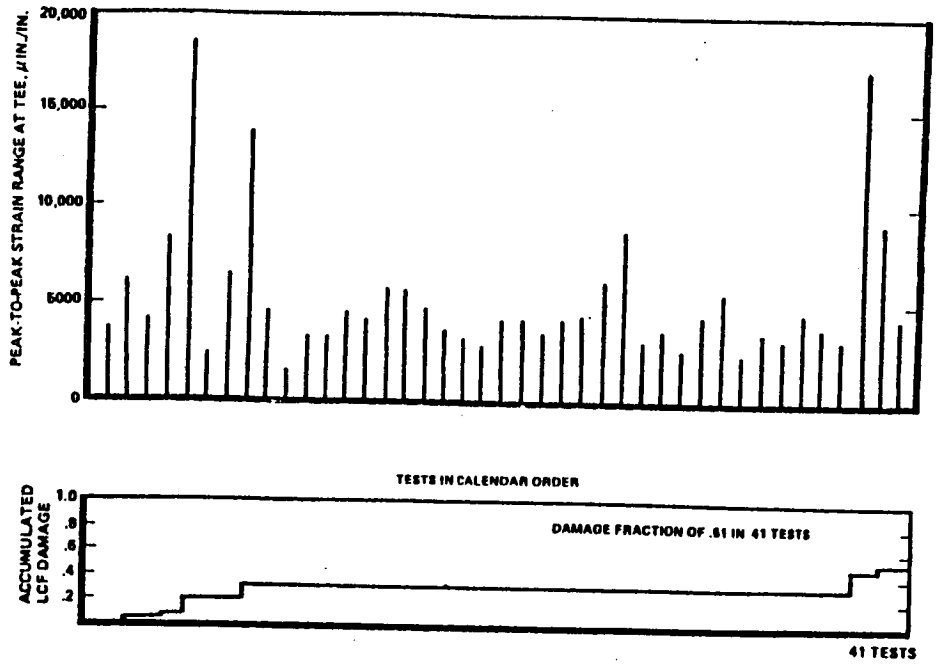

FIGURE G.8 HISTORY OF MAXIMUM STRAINS AT THE NOZZLE FEEDLINE TEE (SUMMARY OF 41 TESTS

Strain, microinch per inch	No. of Cycles
19,500	1
15,000	2
13,500	1
12,500	1
12,000	2
11,500	4
10,500	13
8,500	25
7,500	36

TABLE G.1 CUMULATIVE DAMAGE SPECTRUM (SUMMARY OF 41 TESTS)

The presence of high level transient spikes is supported by strain gage accelerometer and load cell data. The strain gage response on the nozzle feed line (Fig. G.5), and the accelerometer response mounted on the oxidizer preburner (Fig. G.6) show the maximum transient loads occur after few seconds of start or cutoff. These shock transients are seen by major components on a number of locations throughout the engine as evidenced by the test stand load cell response (Fig. G.7).

Experimental observations on strain gage readings mounted axially near the steerhorn tee and manifold show a considerable variation in the maximum strain gage from test to test (Fig. G.8). A typical spectrum is shown in Table G.1, and consists of listing of peak to peak strain levels and the corresponding number of cycles that were recorded at the indicated strain level. In this case, out of 41 tests, a total spectrum of 85 strain cycles above the range of 7000 microinches per inch was obtained.

An analysis of the observed maximum strain ranges can be used to provide a framework of probabilistically estimating future maximum strain ranges as well as load distribution. Kolmogorov-Smirnov goodness of fit test has indicated that the maximum strain range distribution do not deviate significantly from the lognormal distribution. Using the distribution information, the design maximum strain range for evaluating safety factors for 99% best estimate (the level exceeded once in 100 tests) and the 3σ level or 99.87% probability (the level exceeded once in 750 tests) as an upper limit that the hardware must survive without failure can be established.

The feedlines are considered as part of an overall nozzle model. The transient loads are input to the line through pressure loading the aft portion of the nozzle. The pressure pulse loading is essentially a transient phenomena, the characteristic pulse frequency, amplitude and number determined from a statistical survey of several test cycles on subscale model tests. A typical pressure pulse that is used is shown in Fig. G.9. The amplitude of the pulse is varied from a maximum at the nozzle

exit to zero approximately 30 inches upstream of the nozzle. For SSME, scaled results indicate pressure pulses as high as 38 psi at a frequency range of 100 Hz. The last 30 to 36 inches of the SSME nozzle experience approximately 7 pulses during start and 3 pulses during cutoff. This corresponds to an outward oscillating load on the structure of the order of 200,000 lbs.

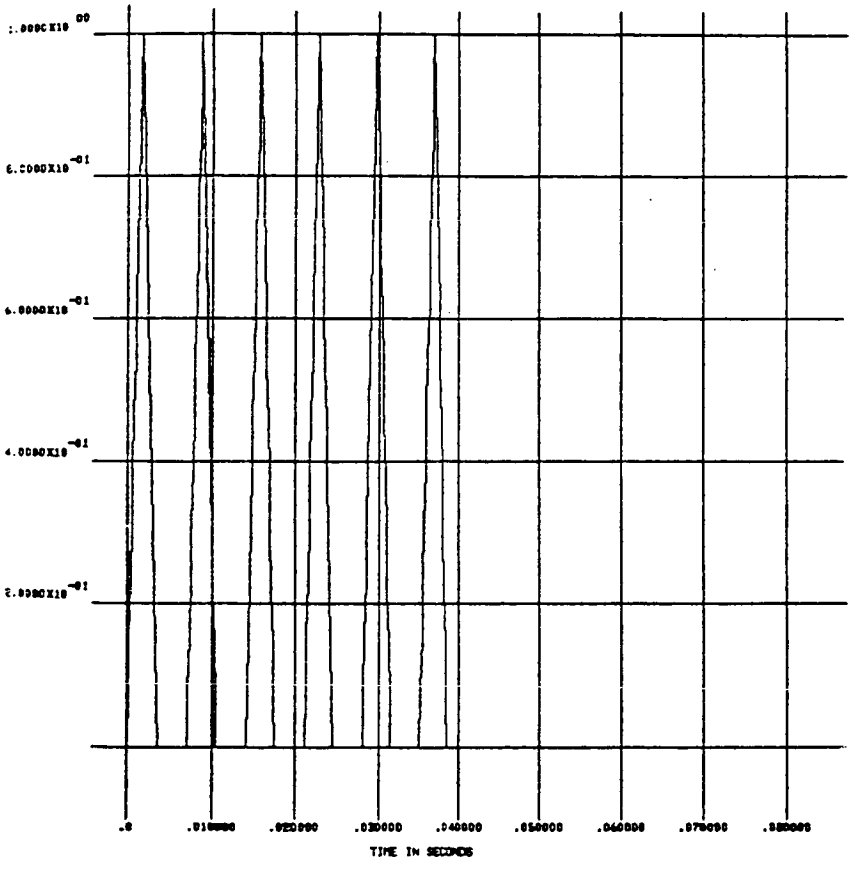

FIGURE G.9 A TYPICAL PULSE FORCING FUNCTION APPLIED ON THE NOZZLE

1. Report No.	2. Government Accession No.	3. Recipient's Catalog No.
NASA CR-179496		

4. Title and Subtitle	5. Report Date
Composite Load Spectra for Select Propulsion Components First Annual Report	March 1986
	6. Performing Organization Code 533-13-00
7. Author(s)	8. Performing Organization Report No.
J. F. Newell, R. E. Kurth, and H. Ho	RI/RD86-123
	10. Work Unit No.
9. Performing Organization Name and Address Rockwell International Rocketdyne Division 6633 Canoga Avenue Canoga Park, CA 91304	11. Contract or Grant No. NAS3-24382
	13. Type of Report and Period Covered First Annual Report
12. Sponsoring Agency Name and Address National Aeronautics and Space Administration Washington, DC 20546	14. Sponsoring Agency Code RTOP 553-13-00

15. Supplementary Notes

Project Manager - C. C. Chamis
NASA Lewis Research Center - MS 49-8
21000 Brookpark Road
Cleveland, OH 44135

16. Abstract

A multiyear program is performed with the objective to develop generic load models with multiple levels of progressive sophistication to simulate the composite (combined) load spectra that are induced in space propulsion system components, representative of Space Shuttle Main Engines (SSME), such as transfer ducts, turbine blades, and liquid oxygen (LOX) posts.

Progress of the first year's effort includes completion of a sufficient portion of each task -- probabilistic models, code development, validation, and an initial operational code. This code has from its inception an expert system philosophy that could be added to throughout the program and in the future. The initial operational code is only applicable to turbine blade type loadings. The probabilistic model included in the operational code has fitting routines for loads that utilize a modified Discrete Probabilistic Distribution termed RASCAL, a barrier crossing method and a Monte Carlo method. An initial load model was developed by Battelle that is currently used for the slowly varying duty cycle type loading. The intent is to use the model and related codes essentially in the current form for all loads that are based on measured or calculated data that have followed a slowly varying profile.

17. Key Words (Suggested by Author(s))	18. Distribution Statement
Probabilistic analyses, Computer code, Simulated loads, SSME, Discrete probability, Barrier crossing, Monte Carlo, RASCAL	Unclassified, unlimited

19. Security Classif. (of this report)	20. Security Classif. (of this page)	21. No. of pages	22. Price*
Unclassified	Unclassified		

*For sale by the National Technical Information Service, Springfield, Virginia 22161